Disturbance Feedback Control for Industrial Systems

Practical Design with Robustness

Kawai, Fukiko

DOI (link to publication from Publisher):
10.5278/vbn.phd.tech.00048

Publication date:
2018

Document Version
Publisher's PDF, also known as Version of record

DISTURBANCE FEEDBACK CONTROL FOR INDUSTRIAL SYSTEMS

PRACTICAL DESIGN WITH ROBUSTNESS

BY
FUKIKO KAWAI

DISSERTATION SUBMITTED 2018

AALBORG UNIVERSITY
DENMARK

Disturbance Feedback Control for Industrial Systems: Practical Design with Robustness

Ph.D. Dissertation

Fukiko Kawai

AALBORG UNIVERSITY
DENMARK

Dissertation submitted September 11, 2018

Dissertation submitted: September 11, 2018

PhD supervisor: Assoc. Prof. Jan D. Bendtsen
Aalborg University

Assistant PhD supervisor: Assoc. Prof. Palle Andersen
Aalborg University

PhD committee: Associate Professor Mohsen Soltani (chairman)
Aalborg University

Associate Professor Hans Henrik Niemann
Technical University of Denmark

Professor Shiro Masuda
Tokyo Metropolitan University

PhD Series: Technical Faculty of IT and Design, Aalborg University

Department: Department of Electronic Systems

ISSN (online): 2446-1628
ISBN (online): 978-87-7210-321-1

Published by:
Aalborg University Press
Langagervej 2
DK – 9220 Aalborg Ø
Phone: +45 99407140
aauf@forlag.aau.dk
forlag.aau.dk

Printed in Denmark by Rosendahls, 2018

Abstract

The Japanese company Fuji Electric Co., Ltd. (Fuji) first introduced and patented the concept of *Disturbance Feedback Control* (DFC) in 1980, for the purpose of attenuating drop impact disturbances in rolling mill processes at steel plants. Since then, DFC has been applied to dampen oscillations in electric motors with backlash, compensate for dead-time voltage errors in power electronics, as well as several other industrial applications.

A controller with DFC can be categorized as a two-degree-of-freedom controller, in the sense that one controller is designed as an ordinary reference-following controller, while the DFC itself is designed specifically to deal with unwanted disturbances, thus enhancing the performance of the overall control loop. Even though DFC as mentioned has been applied with success in various contexts, there are still some issues that remain to be resolved in a systematic way, in particular robustness guarantees, constraint handling, and anti-windup. The aim of the present study is thus to propose practical design methods using robust control theory in order to improve the stability and performance of existing industrial controllers.

To address this aim, a design methodology is proposed, in which the plant to be controlled, a nominal model of it, and the existing controller are considered together as an extended plant. The DFC is designed for this extended plant using robust control techniques such as optimization via Linear Matrix Inequalities (LMIs). Specifically, optimization problems are formulated to minimize the effect of disturbances while maintaining stability and performance for a range of model uncertainties.

Two very different case studies, refrigeration systems and gantry cranes, are chosen from Fuji's product portfolio for evaluating the feasibility of the design methodology.

In the first case study, a conventional controller for a commercial refrigeration system is designed, tested and then augmented with DFC. A two-step design procedure is proposed; first, a set of LMIs is solved to design a robust DFC without taking saturation into account, and then a second set of LMIs is solved to yield an anti-windup compensator to accommodate for actuator saturation. The proposed design is compared with the conventional control

system, both in simulation and through practical experiments. The results indicate that both robustness and performance can be improved in the presence of model uncertainties, and the proposed design is able to avoid wind-up phenomena when the control inputs are saturated.

The second case study considered in the thesis concerns gantry cranes, which are widely used in factory automation, construction and shipping contexts. For this case study, an anti-sway control scheme is proposed, in which a robust DFC is designed using the same fundamental approach as in the first case study to minimize the sway angle and trolley position errors via LMI optimization. The robust DFC is added to an existing crane control system composed of a feedforward and state feedback control. Both simulation and lab test results show improvements in control performance when the gantry load is subjected to impulse force disturbances for a wide range of rope lengths.

Resumé

Det japanske firma Fuji Electric Co., Ltd. (Fuji) indførte og patenterede begrebet Disturbance Feedback Control (DFC) i 1980 med det formål at dæmpe stød i forbindelse med afklipning af emner i stålvalseprocesser. Siden da har DFC været anvendt til at dæmpe oscillationer i elektriske motorer med hysterese, kompensere for spændingsafvigelser i effektelektronik, og forskellige andre industrielle applikationer.

En regulator med DFC kan kategoriseres som havende to frihedsgrader, i den forstand at den består af en almindelig reference-følgende regulator og en DFC-del. Den reference-følgende regulator kan designes efter klassiske principper, mens DFC-delen designes specifikt til at håndtere uønskede forstyrrelser, og dermed forbedre performance af den samlede kontrolsløjfe.

Selv om DFC som nævnt er blevet anvendt med succes i forskellige sammenhænge, er der stadig en række problemer der mangler at blive taget hånd om, såsom robusthedsgarantier, begrænsninger på tilstande og inputs, samt anti-windup.

Formålet med dette studie er således at foreslå praktiske designmetoder baseret på robust kontrolteori til at forbedre stabiliteten og ydeevnen hos eksisterende industrielle regulatorer.

For at opnå dette mål foreslås en designmetode, hvor den proces, der skal reguleres, en nominel model af samme, og den eksisterende regulator betragtes som et samlet system. DFC-delen designes derpå som en regulator til dette udvidede system ved hjælp af teknikker kendt fra robust kontrolteori, såsom optimering via lineære matrix-uligheder (LMI). Specifikt formuleres optimeringsproblemer med det formål at minimere virkningen af forstyrrelser, samtidig med at stabilitet og performance garanteres for afgrænsede model-usikkerheder.

To meget forskellige case-studier, kølesystemer og portalkraner udvælges fra Fujis produktportefølje til praktisk verifikation af designmetodens anvendelighed.

I det første case-studie designes og testes en konventionel regulator til et kommercielt kølesystem. Den udvides derefter med DFC, som designes ved hjælp af en to-trins designprocedure; Først løses et sæt LMI'er, som giver en robust DFC uden hensyntagen til mætning, og derefter løses et andet sæt LMI'er

for at opnå en anti-windup-kompensator til at håndtere aktuatormætning. Det foreslåede design sammenlignes med det konventionelle kontrolsystem, både i simulering og gennem praktiske forsøg. Resultaterne indikerer, at både robusthed og ydeevne kan forbedres på trods af modelusikkerheder, og det foreslåede design er i stand til at undgå wind-up mens styresignalerne er i mætning.

Det andet case-studie, der behandles i afhandlingen vedrører portalkraner, der er meget anvendt i automatiserings-, bygnings- og shipping-sammenhænge. Til denne case foreslås en anti-sway-regulering, hvor en robust DFC er designet ved hjælp af samme grundlæggende tilgang som i det første case-studie til at minimere udsvinget og positioneringsfejl af kranens bogie via LMI-optimering. Den robuste DFC føjes til et eksisterende kran-kontrolsystem, der består af en feed-forward og tilstandsfeedback-del. Det udvidede kontrolsystem udviser forbedret performance i både simulering og laboratorietest, når lasten udsættes for kortvarige forstyrrelser ved forskellige kabellængder.

Contents

Abstract **iii**

Resumé **v**

Preface and Acknowledgement **xi**

1 Introduction **1**
1.1 Background and Motivation 1
1.2 Fuji's Control 6
1.3 State of the Art 10
1.4 Research Objectives and Hypotheses 16
1.5 Summary of Contributions 18

2 Application 1: Refrigeration Systems **23**
2.1 Practical Design in Refrigeration Systems 23
2.2 Grid Search Optimization for SISO Systems 24
2.3 LMI Optimization for MIMO Systems 33
2.4 Experimental Results 43

3 Application 2: Crane Systems **57**
3.1 Crane System Model 57
3.2 Disturbance Feedback Control Design 59
3.3 Verification of Robustness against Internal Uncertainty in Frequency Domain 68
3.4 Comparison of Nonlinear Model and Linear Model 71
3.5 Lab Test at Fuji Electric 73

4 Closing Remarks **85**
4.1 Conclusion 85
4.2 Perspectives and Strategies 86

References **89**

I Papers **97**

A PID Control with Robust Disturbance Feedback Control **99**
1 Introduction . . . 101
2 Problem statement . . . 102
3 Uncertainty model . . . 103
4 Disturbance feedback function search algorithm . . . 106
5 Numerical examples . . . 109
6 Discussion and conclusions . . . 115
References . . . 116

B MIMO Robust Disturbance Feedback Control for Refrigeration Systems via an LMI Approach **121**
1 Introduction . . . 123
2 Problem Definition . . . 124
3 LMI Formulation for DFC Design . . . 127
4 Practical Example . . . 132
5 Discussion and Conclusions . . . 139
References . . . 140

C Robust & Anti-Windup Disturbance Feedback Control for Water Chiller Systems **143**
1 Introduction . . . 145
2 Problem Definition . . . 146
3 Disturbance Feedback Control Design . . . 148
4 Anti-Windup Control Design . . . 150
5 Numerical Examples . . . 154
6 Discussion and Conclusions . . . 158
References . . . 161

D Anti-windup Disturbance Feedback Control: Practical Design with Robustness **163**
1 Introduction . . . 165
2 DFC Design . . . 166
3 Experimental Results . . . 176
4 Conclusions . . . 191
References . . . 191

E Anti-Sway Control for Crane Systems: Robust Design with LMI Optimization **197**
1 Introduction . . . 199
2 Problem Definition . . . 202
3 Disturbance Feedback Control design . . . 204
4 Numerical Examples . . . 206

5 Discussion and Conclusions 212
References 212

F Robustness against Uncertainties in Frequency Domain for Crane Control Systems Designed by Polytopic Approach 215
1 Introduction 217
2 Problem Definition 219
3 Disturbance Feedback Control Design 222
4 Numerical Examples 224
5 Discussion and Conclusions 229
References 229

Preface and Acknowledgement

This thesis consists of contribution papers given by joint research between Aalborg University and Fuji Electric Co., Ltd. The collaboration work started from October 2013, then this PhD project began in February 2015. The project has been carried out for three and half years under the supervision of Associate Professor Jan Dimon Bendtsen and Associate Professor Palle Andersen.

Firstly, I would like to express my deepest gratitude to my supervisors, Jan and Palle. I'm so grateful for their guidance and support with passion. Their suggestions both from theoretical and practical aspects, can create new idea and innovations for industrial applications. In addition, their direction made it possible to produce results for the PhD project, and improved the quality of research and development. Through the collaboration with them, I really understood what is the Problem Based Learning (PBL).

Besides my supervisors, I would like to express my gratitude to Dr. Naoya Eguchi for allowing me to stay in Aalborg for three years. He always responded to my monthly report by e-mail from Japan, and gave helpful comments and suggestions. Further, I am very grateful to Mr. Yasuhiro Okuma for his support, encouragement, and consideration of my daily work and the PhD project balance. I would also like to express my sincere thanks to Dr. Kiyoaki Sasagawa and Dr. Yasushi Matsumoto for suggestions in regards to the PhD project, especially for crane control applications. Finally, I would like to thank Mr. Chikashi Nakazawa for his support of making a new proposal about collaboration with Aalborg University in 2012.

Regarding a lab test of a refrigeration system, I would like to thank Kasper Vinther, Tomasz Minko, Simon Jensen, and Rasmus Pedersen for technical supports to make an experiment at Aalborg University or even try it with remote control from Tokyo, Japan. For crane test in Fuji Electric, Mr. Xu Jinchi, Dr. Takashi Hayashi, and Dr. Takayuki Kaneko really helped the experimental test so that I can include the results in this thesis. Thank you!

Last but not least, I would like to thank my family for great support and all the help they have given me.

Fukiko Kawai (河合　富貴子)
Aalborg University, July 30, 2018

1 Introduction

This chapter first describes the background and motivation of the thesis. The motivation came from discussions at Fuji Electric(Fuji) in Japan, and the results brings a main concept of a proposed design method; robust Disturbance Feedback Control (DFC). Next, the state of the art mentions an outline of the history on traditional control in industry including Fuji's recent stage in the development of a product. Relevant works from academia are described as well, then our challenges are extracted for the thesis. After that, research objectives and hypotheses are given. Finally our compact summary of our contributions are presented.

1.1 Background and Motivation

What is the practical design method for industrial systems? Traditionally PID control has been widely used for industrial systems [Åström et al., 1993]. Besides of classical control, modern control had been introduced to numerous real applications [T. Samad and A.M. Annaswamy (eds.), 2014].

For instance, Smart Grid projects in Europe has been the mainstream of Research & Development to innovate new control algorithm and applications during the past decade [Gangale F., Vasiljevska J., Covrig F., Mengolini A., Fulli G, 2017]. Through the projects, advanced control methods have been applied in Smart Grid as integrated control [Farhangi, 2010; Covrig et al., 2014; Vardakas et al., 2015]. Regarding budget policy in United States at that time, Department of Energy in launched the Smart Grid Investment Grant program, funded by $ 3.4 billion invested through the American Recovery and Reinvestment Act of 2009 in order to *modernize* the electricity system in U.S. [U.S. Department of Energy, 2016].

For some years ahead, Internet of Things (IoT) and Industry 4.0 represent a new trend of technical development in industrial systems [Shrouf et al., 2014]. The German government proposed Industry 4.0, which has a concept with automated factory connected by a standard network. The scheme of Industry 4.0 can be a kind of firewall; which means a strategy against the American forces.

These trends mentioned above had been undertaken to develop the most advanced and large-scale systems with a huge sum of budget through the initiation of the government and major corporations. Now, one question arises:

The new solutions given by ideal concepts can be fit for small-scale industrial systems with tight budget?

In fact, engineers at site prefer to handle their control design with the several existing methods. If the existing control works reasonably, the engineers reluctant to introduce new control methods even though its advantage is clarified. Since control engineers must prevent any accidents related to their control design, they may choose a control design with low risk in order to fulfill their responsibility as control engineers.

1.1.1 Requests of Fuji's engineers

In order to bridge the gap between ideal concept and real demand, and barrier between academia and industry, the requests of Fuji's engineers were investigated. Based on the concept of "practical design that will be useful" derived from a reflection on past issues, R&D division in Fuji interviewed individual departments on-site.

The results of survey indicated "high engineering *cost* of *time*" as the most obstructive factor for control design. As a result, summarized needs are obtained as three points (Quality, Cost, and Delivery):

- Disturbance rejection performance must be good (Quality)
- The cost for implication should be kept to a minimum (Cost)
- Design methods should require as little tuning time as possible, regardless of system changes and products type (Delivery)

These requests can be translated into the control issues in theoretical approaches; robust control design, low order controller, and maintain the existing control and augment it with robust DFC.

1.1.2 Robust control design

Robust control is a theory, which introduces model uncertainty, and the robust control define a class of models $G = G_n + \Delta$, where G_n is the nominal model and the model uncertainty or perturbation Δ is bounded, but otherwise unknown [Skogestad and Postlethwaite, 2005].

Robustness can be defined as the ability of a system to continue to function more or less as intended in spite of external and internal disturbances

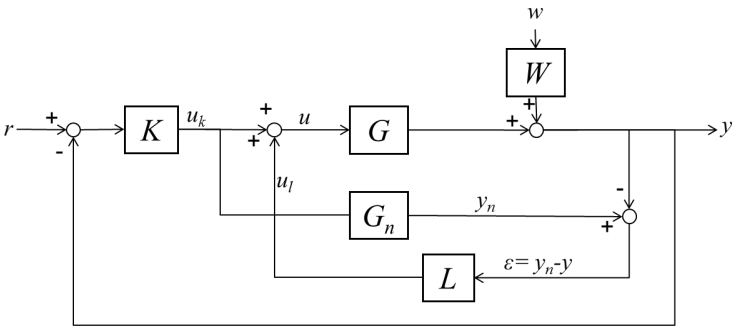

Figure 1.1: Block diagrams of disturbance feedback control.

and uncertainties. External disturbances can come in the form of noise, faults, changing references or changes in operating conditions, while internal disturbances typically arise from unmodeled dynamics or poorly estimated parameter values.

Responding the Fuji's engineers, to be strong against disturbance and system changes, the robust control could be reasonable choice from other control methods. Fuji had introduced H_∞ control in the 1990s, and the combination of observer and H_∞ control were applied in electric motor systems and rolling mill process [Kenichi Kurotani, Osamu Itoh, 1998].

In reality, however, robust control has never been popular in Fuji. Similar tendency was seen among the chemical industrial area as well in Japan [M. Kano, 2009].

This means that it may be difficult for engineers on site to handle robust control, but that it could be more widely applied in various industrial areas if simple, easy-to-use robust design methods were made available. A new concept is necessary to achieve this goal; practical design with robustness. We assumed that two concepts, low order control, and maintaining the existing control and make it robust with DFC, are key to apply the robust design to real systems.

1.1.3 Maintain the existing control, and augment it with robust DFC

The main concept of the thesis is mentioned as follows. Fig. 1.1 shows block diagrams of disturbance feedback control. The figure indicates that the control structure of DFC is categorized as two-degree-of-freedom (2DOF) controllers, and DFC is originally developed by Fuji [Fuji Electric Co., Ltd., 1981].

This control structure has an additional *feedback* loop L to compensate for disturbance and model uncertainties as shown in Fig. 1.1.

We focused on the control structure of DFC, and defined the concept of

control design;

An existing single DOF controller K is designed to stabilize the plant, and another controller L is designed to augment the existing control system.

Fig. 1.2 shows a general closed-loop system with two input, two output formulation (left) and the closed-loop system for DFC (right). In general, robust controller is designed using the left formulation with the transfer function T from w to z, where z is the output for evaluating the performance of the controlled systems and y are the measurements. Note that the motivation of the DFC design is to improve the existing system. We assume that the existing controller K is fixed, meaning we can handle K as a part of the plant P. Therefore, P includes G, G_n, W, and K in the robust DFC design. While K determines the response from reference, the disturbance feedback controller L is designed to improve disturbance rejection also facing model uncertainty.

Keeping the existing controller K would be useful for engineers considering that know-how of their design, and requirements specification from customers can be retained, and engineering and design periods may be shortened. This light reformulation of existing systems is expected to be positively received by both engineers and customers.

To design the robust DFC L, the robust control theory and H_∞ control scheme are introduced. We defined model uncertainties to guarantee the robust stability when *internal* system change, model perturbation, or disturbance are obtained. In addition, H_∞ control scheme is introduced to minimize the effect of *external* disturbance to guarantee the robust performance.

The effectiveness of proposed methods was demonstrated by related products or systems of Fuji. We applied the robust DFC in two applications; refrigeration systems and crane systems were chosen from the main products of Fuji. Fig. 1.3 shows overview of PhD thesis.

For the first application of refrigeration systems, two different concept is proposed for robust DFC design. One concept is presented for edge devices such as PLC for introducing the grid search optimization.Other concept is proposed for more systematic design with modern robust control using LMI optimization.

For the second application of crane systems, anti-sway control scheme is presented to robust DFC designed to minimize the sway angle and trolley position errors via LMI. The robust DFC is added to an existing crane control system composed of a feed forward and state feedback control.

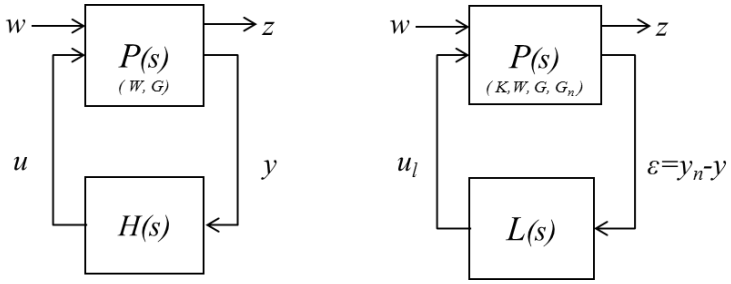

Figure 1.2: A closed-loop system for design of an H_∞ controller $H(s)$ (left), and a closed-loop system for design of DFC $L(s)$ (right).

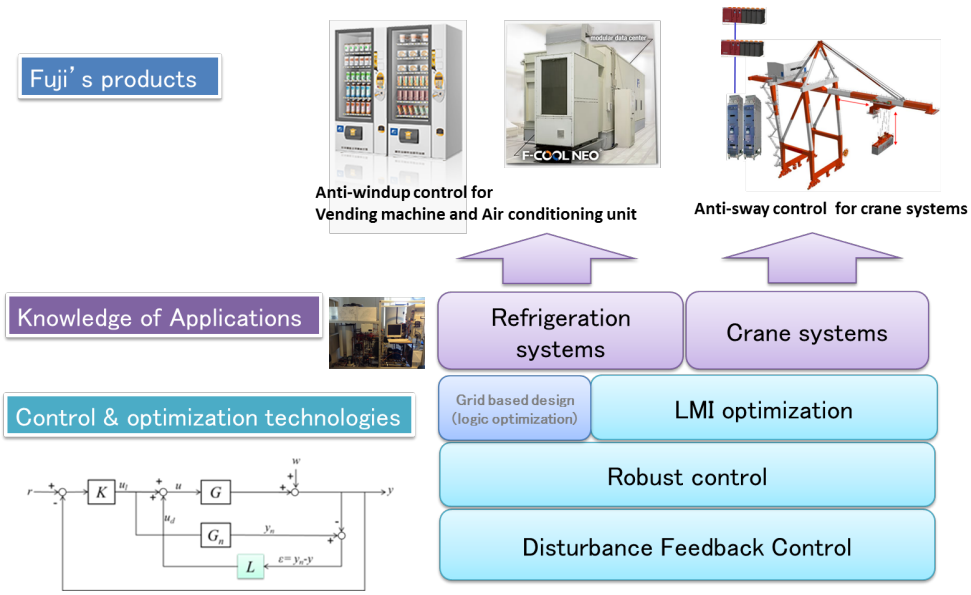

Figure 1.3: Overview of PhD thesis.

1.2 Fuji's Control

Throughout its history, Fuji has developed control systems and products for various industrial fields. The overview of Fuji's control history is described in this section including DFC and its application. After that, the issues on conventional design are indicated, and the weaker points will be underpinning motivation for the research objectives.

1.2.1 Overview of control applications in Fuji

Fuji started research and development for control area in 1970s. Fig. 1.4 shows trends of control technologies and Fuji's applications from 1980.

In water treatment research, which is one of the process control fields, Model Predictive Control (MPC) and fuzzy control were applied in flocculation process control of water treatment plants. In addition, optimization-based control schemes were introduced to water distribution systems and water pressure control for pump systems. To this time, no robust control has been introduced in the water treatment fields by Fuji's research.

Regarding applications using electromotive power drives, observer based control and H_∞ control were applied in anti-sway control for crane systems and torsional vibration reducing device of shaft systems. As for steel plants in industry fields, H_∞ control was introduced in 1980s. However, these control design using H_∞ control can be applied for SISO system only, and no systematic control design, such as LMIs or other control design based on optimization, have been introduced so far. Moreover, internal uncertainties, i.e., model uncertainties, are not explicitly taken into account.

With respect to power system control, control system for self-commutated static var compensators was developed for unbalanced-load compensation [Eguchi et al., 1994; Hirakawa et al., 1995]. Multivariable optimal control of generator excitation and speed governor system was proposed in 1980s [Otsuka et al., 1984]. For predicting service for power systems, peak load forecasting system using neural networks and fuzzy theory was developed [Ueki et al., 1996]. Fuji has introduced new technologies for electric power system applications over the years, however, no robust control has been applied in power systems yet.

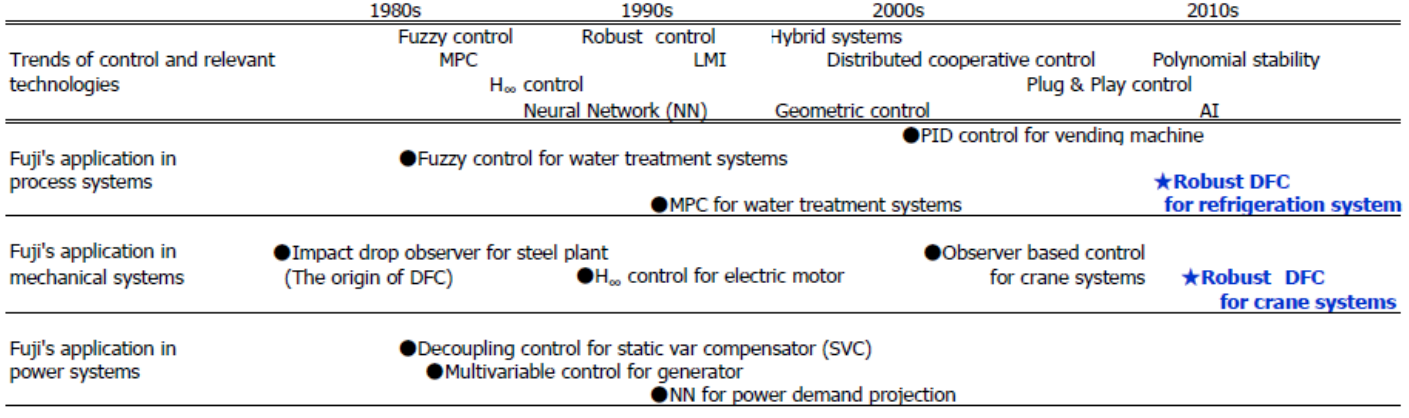

Figure 1.4: Trends of control technologies and Fuji's applications.

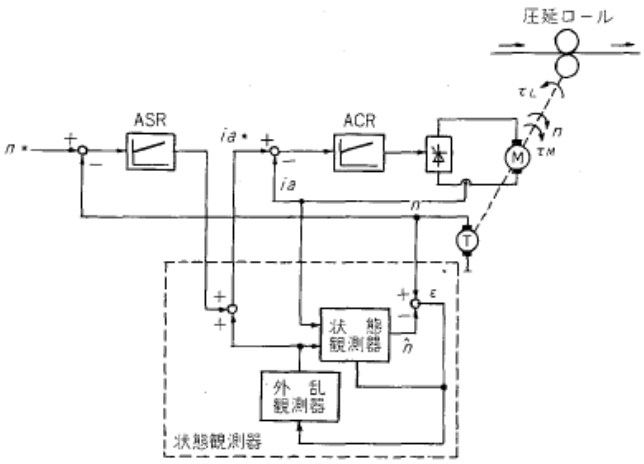

第 25 図　状態観測器を使用した速度制御系

Figure 1.5: Origin of DFC, then denoted impact drop observer [Fuji Electric Co., Ltd., 1981].

1.2.2 Origin of DFC

DFC was developed in 1980, then called "impact drop observer" or "disturbance observer" for rolling mill process at steel plants [Fuji Electric Co., Ltd., 1981]. The original block diagram is shown in Fig. 1.5, copied from the original Japanese source.

In addition, this control scheme has been applied in winch of coal mine plants, and a electric motor [Tsutomu Miyashita and Hideyuki Nishida and Shinichi Ito, 2000]. H_∞ control idea was considered for the DFC design around 2000, however, it was not systematic design, for the idea did not explicitly define the model uncertainties and not applied optimization techniques to solve the control parameters. Furthermore, the above application was applied to SISO systems. The appropriate introduction of robust control theory was necessary in order to improve that DFC design.

Recently we changed the name to DFC based on the control structure because DFC is not categorized as observer in the theoretical point of view [Kawai et al., 2014]. In stead, DFC plus existing controller can be classified as 2DOF controllers as we mentioned above.

1.2.3 Control on refrigeration systems

Fuji's market share of the vending machines has acquired with about 50 % of the total domestic production. Fuji's efforts will include developing more energy-efficient, environmentally friendly vending machines in response to the market environment, which has changed greatly since the Great East Japan Earthquake in 2011 [Fuji Electric Co., Ltd., 2011].

The On-Off controllers were traditionally implemented in the refrigeration cycle inside of vending machines, and then PID controllers was introduced to avoid hunting phenomena of evaporating temperature by electronic expansion valve [Fuji Electric Co., Ltd., 2012].

The PID controllers contributed a stabilization of the refrigeration systems, however, some issues for control design still remained for more practical methods. The robustness against external and internal uncertainties is necessary to meet the needs of engineers on-site.

1.2.4 Control on crane systems

Over the years, Fuji Electric has developed various anti-sway control schemes for crane systems, including an observer based control scheme. Application of fuzzy control to automatic crane operation was proposed in order to improve tracking control and anti-sway control performance [Itoh et al., 1993].

Subsequently, this anti-sway control scheme was further improved to combine feed forward control and state feedback control, and applied in commercial gantry cranes. In addition, Anti-sway crane control based on dual state observer with sensor-delay correction was proposed for more practical control design [Sano et al., 2010].

This controller exhibits sufficient performance in terms of tracking control; however, better stability and performance could be obtained if robustness against external disturbances and model parameter uncertainties were taken into account.

1.3 State of the Art

This section mentions firstly an outline of the history on control applications in industry. Next, Japanese history and trends on control technology is also described to specify real issues in industry area. After that, previous researches related to the thesis are described by literature searching. Finally shortcoming of conventional control technologies is pointed out, and then it leads to the research objective in section 1.4 to address the issues.

1.3.1 Control Applications in industry

Impact of control technologies reviews a number of control technology accomplishments and presents prospects for future opportunities for the field [T. Samad and A.M. Annaswamy (eds.), 2014]. This report describes success stories of deployed products and solutions that have been enabled by advanced control. Especially, all of the developments featured in this category have gone beyond simulation or laboratory demonstration and have achieved "real-world" impact. The research challenges that outline new opportunities for control technology toward future impact. The challenges were described for both societal and industry need, not control theory gaps, and point out the field' s promise and potential for real applications.

Robust control techniques such as H_∞ / H_2 have been successfully applied to deal with complex architectures such as large flexible appendages (solar arrays and deployable reflectors) and requirements such as tight pointing stability performance, while reducing development cost and time.

For example, the Linear Quadratic Gaussian controller applied in the atmospheric flight phase of the Ariane 5 launcher was replaced by a H_∞-based controller for the Ariane 5 Evolution [Pignié, 2002]. This change seems to be necessary to optimize the control design trade-off between the low-frequency performance requirements, such as load reduction and tracking of the attitude setpoint, and the attenuation of the low-frequency structural bending and fuel sloshing modes.

Other application for telecommunication satellites, a robust control approach through a loop-shaping H_∞ design has been introduced [Frapard and Champetier, 1997]. The control approach achieved a 10 % reduction in propellant mass consumption during station-keeping maneuvers.

Regarding process control area, applications of multivariable decoupling control solutions have become standard in many pulp and paper mills [Stewart et al., 2003]. Plant wide model-based optimization of paper mills has also been reported. In an application of robust multivariable control design to the cross-direction control of paper machines, an approximately 80 % reduction in control tuning time and up to 50% higher performance have been reported.

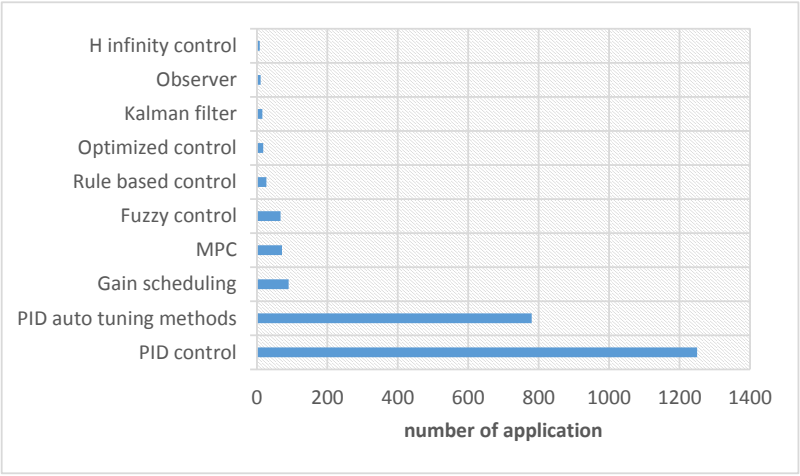

Figure 1.6: Control methods applied in industrial process systems, results of survey in 1997, Japan.

1.3.2 History and Trends of Control in Japan

In 1990s, industrial trends of control technologies in Japan were surveyed. Two questionnaire surveys were investigated, one for process control systems, the another one for mechanical control systems.

The survey results of process control systems is written by [Haruo Takatsu and Toshiaki Ito, 1997]. As expected, PID control has been the most widely used in process control systems. More than 1000 control system using PID or Two degree of freedom PID control were applied by 110 industrial companies in Japan as shown in Fig. 1.7. Gain schedule control had 90 applications, which was the second largest values on the survey.

Another survey results of mechanical control systems is presented by [Yoshiro Tsuruhara and Naotoshi Iwasawa, 1999]. The results showed that industrial systems introduced PID control for more than 40 %, and H_∞ control is selected to the second largest applications from control methods.

About ten years after, survey about process control has been investigated by one Japanese control committee [M. Kano, 2009]. The survey results described that classical control still has been widely used application in 2000s. As for model based control, Model Predictive Control (MPC) has been made use as an advanced control, particularly, for of-refining/petrochemical plants. The

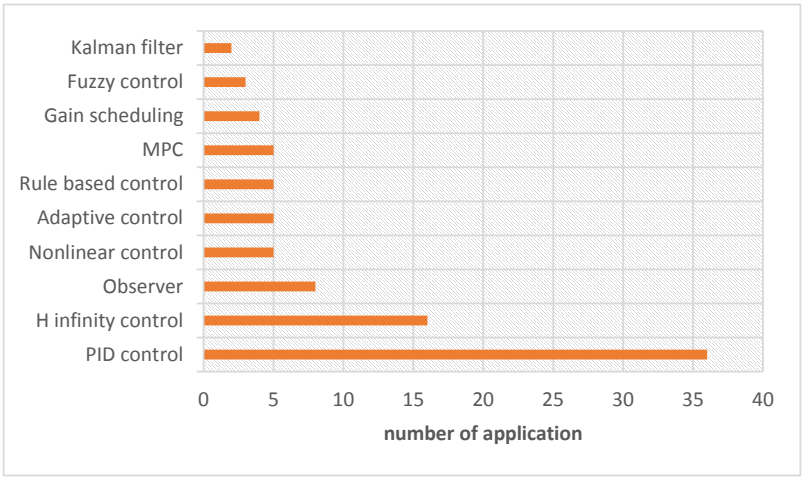

Figure 1.7: Control methods applied in industrial mechanical systems, results of survey in 1998, Japan

survey pointed out the control issues in industry that the shortage of skilled person who can handle these advanced control methods. Moreover, the results also noted that the cost of designing and maintenance should be reduced for spreading the modern control technologies.

As the results of trend survey of industrial control in Japan, typically classical PID control is still widely used as well in process control as in mechanical control systems. At the same time, engineers in industry have tried to introduce modern control theory such as H_∞, MPC, and other control methods.

However, both classical control and modern control methods have shortcoming that conventional classical control cannot achieve sufficient operation performance, on the other hand, modern control methods faced engineering and maintenance costs, and shortage of skilled engineers. These issues of industrial fields in Japan still remain even though new technologies has been developed.

1.3.3 Optimization technologies for robust control design

LMI design can handle advantagegeously MIMO system, and systematic designs of robust control are presented in previous studies [Scherer et al., 1997; Chesi et al., 2005; Peaucelle and Fradkov, 2008; Rosa et al., 2014; Adegas and Stoustrup, 2014; Boyd et al., 2016].

For output feedback controllers using LMI based design, Robust static output feedback controller LMI based design via elimination has been proposed [Veselý et al., 2011].

Regarding PID control design, robust control is introduced in previous researches. Many researchers have proposed robust PID control or low order robust controllers, for satisfying stability and robustness of systems, e.g., see [Sivrioglu and Nonami, 1996; Ge et al., 2002; Sadabadi and Karimi, 2013]. As for MIMO design, MIMO PID tuning by an iterative LMI procedure has been proposed as a new challenge by [Boyd et al., 2015].

Recently, an automatic loop-shaping method for designing robust PID controller [Mercader et al., 2017]. Criteria in this paper are given for load disturbance attenuation, measurement noise injection, set-point response and robustness to model uncertainties. In addition, a modified proportional-integral derivative (PID)-type controller that contains a distributed delay term to Euler-Lagrange systems with an unknown constant input delay [Alibeji and Sharma, 2017].

Previous researches above have presented new theory or practical methods for robust control design using LMI-based approach. However, *no* methodology has been proposed with a concept as in this thesis:

- Maintaining existing control
- Augmented the existing system

1.3.4 Anti-windup control for robust control design

Anti-windup control scheme for robust design is necessary if existing control system consists of integrator and limiter.

A tutorial on modern anti-windup design can be found in on Modern Anti-windup Design [2009], in which two approaches, namely direct linear anti-windup and model recovery anti-windup, are presented. In addition, the authors state that most anti-windup designs can be formulated by LMIs. LMI-based anti-windup synthesis methods have been proposed for robust control of linear systems [Grimm et al., 2004]. Another approach in which a dead-zone is introduced for anti-windup control design, and a local control design technique is proposed, is presented in Wasiwitono and Saeki [2011]. Anti-windup schemes for discrete time system using LMI based design were proposed by Rohman et al [Syaichu-Rohman and Middleton, 2004] in order to address the issues of the algebraic loops of anti-windup controllers.

Time-response shaping using output to input saturation transformation is proposed [Chambon et al., 2018]. The transformation convert prescribed bounds on an output variable into time-varying saturations on the synthesised linear scalar control law.

As for dynamic control design, dynamic anti-windup design for a class of nonlinear systems is proposed [da Silva Jr. et al., 2016]. This design method addresses the dynamic anti-windup design problem for a class of nonlinear systems subject to an actuator saturation. The class regards the systems which can be cast in a differential algebraic representation such as rational and polynomial systems.

Previous researches above have presented something new theory or practical methods for robust control design including anti-windup controllers. However, *no* methodology has proposed such a concept in this thesis:

- Maintaining existing control
- Augmented the existing control system using DFC with anti-windup controller

1.3.5 Anti-sway control design for crane systems

Gantry cranes are of immense importance in shipping applications and can be found in container harbors all over the world. Traditionally, gantry crane systems have been controlled by means of feedforward control, taking motor torque and trolley speed limitations into account [Ackermann, 2002; Ahmad et al., 2009]. Feedback control is also necessary to remove errors between references and measurement values; this is typically achieved by PID control of the gantry crane trolley [Jaafar et al., 2012].

Several results on robust gantry crane control have been published in the literature. For example, a robust iterative learning control scheme is proposed and validated experimentally in [Son et al., 2014]. A Linear Matrix Inequality (LMI)-based H_∞ design was proposed in [Tumari et al., 2012], and a robust fuzzy H_∞ control scheme for nonlinear systems was presented in [Lee et al., 2001].

As for offshore boom crane, adaptive repetitive learning control is proposed [Qian et al., 2017]. This work considers the periodic property of sea waves as disturbances, then an adaptive repetitive learning control strategy containing a learning law to deal with practical problems such as disturbances and unknown system parameters.

Regarding overhead cranes, nonlinear control for underactuated multi-rope cranes is proposed [Lu et al., 2018]. This work presented firstly dynamic model for multi-rope cranes using utilizing Lagrangian modeling method. Next, a nonlinear controller is further proposed, which incorporates more swing-related information into the control law so that the proposed method guarantees the robustness and swing suppression performance of the closed-loop system.

Previous researches above have presented something new theory or practical methods for anti-sway control design for crane systems. However, *no* methodology has proposed such a concept in this thesis:

- Maintaining existing anti-sway control
- Augmented the existing anti-sway control system using DFC

1.3.6 Shortcoming of conventional approaches

The aforementioned robust designs are all constructed as one-degree-of freedom (1DOF) controllers, in which case the existing controllers already in place have to be removed and replaced by the new, more advanced controllers.

However, many industrial practitioners prefer to keep existing controllers, because they embody extensive tuning and domain-specific know-how by customers and experienced engineers. In case a new control design for a system that has already been commissioned is desired, for example for improved closed-loop performance, it is thus often advantageous to maintain the original controller [Stoustrup, 2009].

Moreover, 2DOF controllers are used for many industrial applications because the systems need to guarantee both set point following and disturbance rejection responses.

Therefore, it could be useful for industrial applications to find a design methods for robust 2DOF controllers for discrete time systems. In addition, numerical analysis including experimental test is necessary to find out whether the previous studies can be applied for 2DOF systems as well.

1.4 Research Objectives and Hypotheses

As mentioned in the preceding section, shortcoming and defect of previous works are revealed. The practical design method for industrial systems is proposed in order to address the design issues. Research objectives in this thesis are described, then the objectives lead to three hypotheses which will be the main challenges of the PhD research.

Augmentation of existing systems

Augmentation of existing systems is the main objective of our research. We define *practical design* as keeping the existing systems and augmented by a reasonable controller instead of replacing high-end controllers.

Low order control design with robustness

Next we define *reasonable control* which is described above, that is a control represented by low order systems, and less parameters of the systems can be easily handled for industrial engineers. At the same time, we challenged low order control design which can guarantee the *robustness* against various uncertainties. This approach is challenging in that the system should maintain the existing systems and achieve the robust design with limited control structures. Our challenges is to present a design method which is easy to be accepted by the industrial engineers.

Robustness against internal and external uncertainties

For industrial systems, robustness is necessary to guarantee the quality and their systems even though the internal model is shifting and external disturbances are adding to the systems. We proposed robust control design in order to maintain the stability of the systems and minimize the degradation from these uncertainties. Moreover, specific control challenges are defined, anti-windup control for refrigeration systems and gantry crane systems.

The research objectives which comes from background, motivation, and state-of-the-art lead to three hypotheses. The following hypotheses are given in terms of *Quality, Cost, and Delivery (QCD)* for industrial systems.

Hypothesis 1. The robust DFC can augment the robust stability and robust performances against both internal and external uncertainties. The proposed method can made the improvement of *Quality* in industrial systems.

Hypothesis 2. The proposed method can be added in the existing systems. Since the proposed the existing system can be maintained, only small-scale modification of software is necessary to update the system. The method can made the improvement of both *Cost* and *Delivery* in industrial systems.

Hypothesis 3. The proposed method can be designed as low order controller with guarantee of the robustness against uncertainties. In addition, the robust DFC can be implemented in the low spec controller such as PID controller. The method can made the improvement of both *Quality* and *Cost* in industrial systems.

1.5 Summary of Contributions

To reply the research objectives and hypotheses mentioned above, the following outlines the contributions of this thesis.

1.5.1 Lists of contributions

Contribution papers with short summary are listed, and the main content and relationship between each contribution are described.

- **PID control with robust disturbance feedback control (Paper A)**

  In this work, we analyze the robustness and performance of a PID-based control system with DFC. A multiplicative uncertainty model is used to represent mismatch between a nominal model and the actual plant, and expressions for robust stability, nominal and robust performance are derived. We propose a simple grid-based search algorithm that can be used to find DFC gains to achieve robust stability and performance (if such gains exist). Finally, two different simulation case studies are evaluated and compared. Our numerical studies indicate that better performance can be achieved with the proposed method compared with a conservatively tuned PID controller and comparable performance can be achieved when compared with an H-infinity controller. This work is published as [Kawai et al., 2015]

- **MIMO Robust Disturbance Feedback Control for Refrigeration Systems Via an LMI Approach (Paper B)**

  This paper presented robust DFC design using LMIs for Multi Input and Multi Output systems. The extended state space representation of the overall system is considered with parametric model uncertainties. LMIs are formulated to solve the optimization problem such that the DFC satisfies Lyapunov stability and robust performance. DFC was applied in the superheat control and the suction pressure control for a refrigeration system, and experimental results show that DFC improves disturbance rejection compared to conventional PI controllers. This work is published as [Kawai et al., 2017]

- **Robust & Anti-Windup Disturbance Feedback Control for Water Chiller Systems (Paper C)**

  We have extended the work presented in Paper B. This paper proposed a robust DFC including the anti-windup controllers for process control systems. The proposed method is designed in two steps; firstly, the robust DFC without saturation is designed by LMI approach, and then LMI

technique are used again for stabilizing the closed loop system with anti-windup compensator. The simulation results for the water chiller system shows the improvements of control performances, and keeps stability of the system when the saturation blocks are introduced. This work is published as [Kawai, Fukiko and Vinther, Kasper and Anderson, Palle and Bendtsen, Jan Dimon, 2017].

- **Anti-windup Disturbance Feedback Control: Practical Design with Robustness (Paper D)**

  We have further extended the work presented in Paper C, where the practical test is demonstrated to examine the effectiveness of proposed methods. This paper introduced an anti-windup compensator for 2DOF controllers, one for an existing controller and another for DFC, in a discrete time systems. The test results indicate that both robustness and performance can be improved in the presence of model uncertainties, and the proposed method can avoid wind-up phenomena when the control inputs are saturated. This work is published as [Kawai et al., 2018a].

- **Anti-Sway Control for Crane Systems: Robust Design with LMI Optimization (Paper E)**

  We challenged one more application from FA area, and crane systems were chosen for robust design. Fuji had designed the anti-sway control system for crane systems, and the control system consists of feed forward control and state feedback control. Sufficient control performance to tracking control can be obtained by conventional Fuji's controllers, however, improvements are necessary on regulation control with disturbance. For this reason, this paper proposes an anti-sway control scheme for crane systems using robust DFC designed to minimize the sway angle and trolley position errors via LMI optimization. The robust DFC is added to an existing crane control system composed of a feed forward and state feedback control. Simulation results for the gantry crane system shows improvements in control performance when the gantry load is subjected to impulse force disturbances. This work is published as [Kawai et al., 2018b].

- **Anti-Sway Control for Crane Systems: Robust Design with LMI Optimization (Paper F)**

  We have extended the work presented in Paper E. This paper examined additional model uncertainties in frequency domain for robust DFC which was designed with parametric uncertainties for crane control systems. Robust stability of the robust DFC in frequency domain is analyzed in order to verify the robustness against uncertainties in frequency domain. The results of analysis show that the proposed method can cut off the

uncertainties in high frequency domain. This work is published as [Kawai, Fukiko and Anderson, Palle and Bendtsen, Jan Dimon, 2018].

Chapter 2 and 3 will describe detail of the research results which were briefly summarized above. Chapter 2 presents a design method for refrigeration systems and demonstrated the lab test to evaluate the feasibility of proposed method. Chapter 3 proposes a design method for crane systems. Chapter 4 gives closing remarks and perspectives for future works.

1.5.2 Additional Publications

Additional contributions, which are not included in the thesis, are mentioned in this subsections. Three papers in total were excluded.

- **An Industrial Model Based Disturbance Feedback Control Scheme (Excluded paper 1)**

  Basic features of DFC are presented in this paper [Kawai et al., 2014], this paper presented the main concept of DFC, however, the DFC was not designed by robust control theory. In addition, this works proposed stability condition for SISO systems based on characteristic equation of closed loop systems.

- **Design method for low-order disturbance feedback control (Excluded paper 2)**

  This paper presented SISO robust control design with grid search optimization. Besides of LMI approach, the logic based optimization for robust DFC was introduced. This contribution was reedited using the results of Paper A [Kawai et al., 2015], and it can be available *in Japanese* [Kawai, 2016].

- **An LMI Approach for Robust Design of Disturbance Feedback Control (Excluded paper 3)**

  This paper proposed robust DFC design with LMI optimization. In the numerical examples, simple SISO model was chosen to examine the advantage of proposed method. Simulation results show that the robust DFC improve the both setpoint response and disturbance response compared to the conventional control. Details of the contribution can be available at [Kawai, Fukiko and Vinther, Kasper and Anderson, Palle and Bendtsen, Jan Dimon, 2017].

1.5.3 Patents

Three patents has been filed as research contributions, and two of them are granted patents.

- **Design method and a control device of the control device**
  Application Number: JP5817940B2
  Status: Grant
  This patent claims the control design method for SISO DFC systems, and a design for PI control with DFC is proposed by using one parameter DFC gain L. This research output is obtained by a relevant work in [Kawai et al., 2014].

- **Control system, method for designing control system, and program**
  Application Number: JP2017027570A
  Status: Application
  This patent claims the design method and system for robust DFC, and the DFC is tuned by logic based optimization. This research output is obtained by a relevant work in [Kawai et al., 2015]

- **Power stabilization system and a control device**
  Application Number: JP6032365B2
  Status: Grant
  This patent claims the DFC application for power systems, especially frequency control on micro grid where photovoltaic power generation systems are introduced. Note that I am not the first inventor of this patent, therefore, this contribution is excluded from the thesis.

2 Application 1: Refrigeration Systems

This chapter describes contributions of the first application, refrigeration systems. Each contribution paper that composes the thesis is presented. Mainly two different concept is proposed for robust DFC design. One concept is presented for edge devices such as PLC [Greg Gorbach, ARC Advisory Group, 2016], where the tuning and control process can be implemented. Other concept is presented for more systematic design with modern robust control using LMI.

2.1 Practical Design in Refrigeration Systems

Table 2.1 shows two concepts of robust DFC design. Concept No.1 can be implemented in PLC, focusing on the edge devised implementation for all control design processes including tuning DFC parameters. The concept can follow the edge heavy computing, however, which can be only applied for SISO system, and the risk of local minimum in the optimization problems.

On the other hand, concept No.2 addresses the short coming of the concept No.1 using LMI, which can be designed for MIMO system using mathematical programming. In this case, additional PC is necessary to design the robust DFC.

Table 2.1: Two concepts of robust DFC design

No.	Tuning process at	Control device	Extend-ability	Optimized by	Robust control
1	PLC	PC or PLC	SISO	Grid search	Classical
2	PC	PC or PLC	MIMO	LMI	Modern & Classical

2.2 Grid Search Optimization for SISO Systems

In the following, we propose a simple search algorithm for tuning of the disturbance feedback function L. The concept of the algorithm is that it shapes "two peaks" in the frequency domain by tuning L.

One peak appears due to Nominal Performance (NP) and the other due to Robust Stability (RS). Each peak has a relationship to a trade off; if one peak gets smaller, the other peak gets larger. Therefore shaping the two peaks can achieve a minimization of both peaks and a balancing of the trade off.

Here are explanation of Nominal stability (NS), Nominal Performance (NP), Robust stability (RS), Robust performance (RP) [Skogestad and Postlethwaite, 2005].

Nominal stability (NS). The system is stable with no model uncertainty.

Nominal Performance (NP). The system satisfies the performance specifications with no model uncertainty.

Robust stability (RS). The system is stable for all perturbed plants about the nominal model up to the worst-case model uncertainty.

Robust performance (RP). The system satisfies the performance specifications for all perturbed plants about the nominal model up to the worst-case model uncertainty.

More precisely, definition is given as follows [Zhou et al., 1996]:

Definition: Given the description of an uncertainty model set Π and a set of performance objectives, suppose $P \in \Pi$ is the nominal design model and K is the resulting controller. Then the closed-loop feedback system is said to have

Nominal Stability (NS): if K internally stabilizes the nominal model P.

Robust Stability (RS): if K internally stabilizes every plant belong to Π.

Nominal Performance (NP): if the performance objectives are satisfied for the nominal plant P.

Robust Performance (RP): if the performance objectives are satisfied for every plant belong to Π.

If the function L is chosen as a simple gain, then it can be tuned by gradually increasing the gain, while making a robust performance (RP) check. The largest gain that still achieves RP can be chosen as the disturbance feedback gain L. If RP cannot be achieved using a simple gain function, then L can be tuned as a filter which is expressed by a first order transfer function with gain k_L and time constant τ_L. Fig. 2.1 shows the proposed search algorithm for disturbance feedback control and the algorithm consist of 5 steps. The detail of the algorithm is as follows:

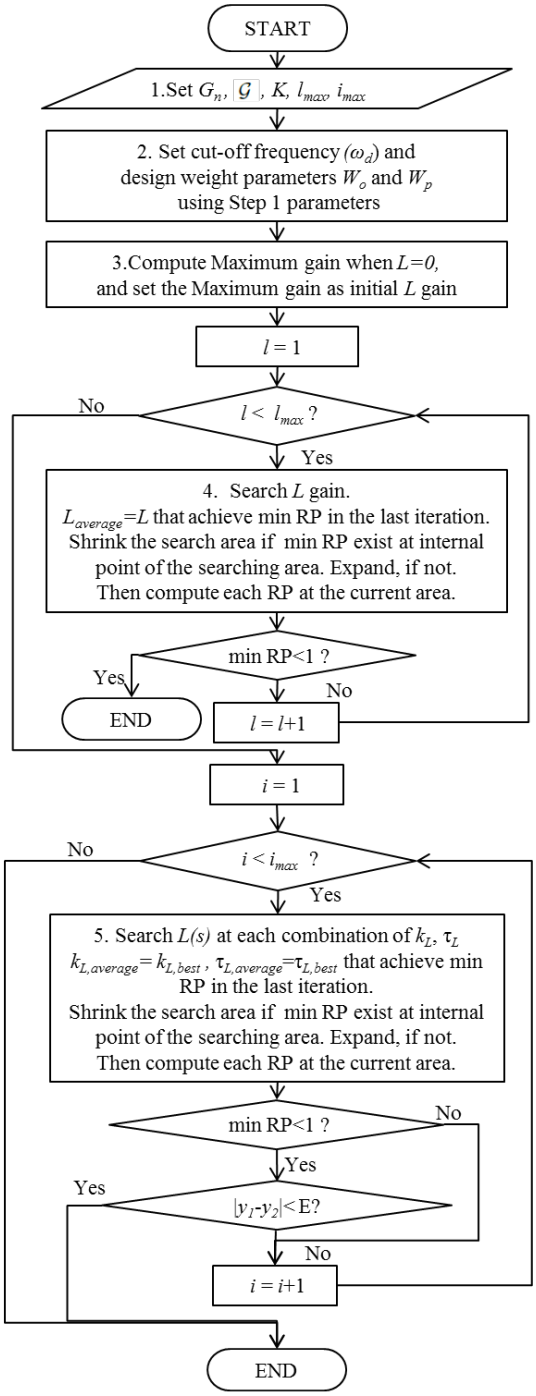

Figure 2.1: Disturbance feedback function search algorithm for disturbance feedback control. l and i are iteration counters.

Step 1: Set the nominal model G_n, the uncertainty description $\mathcal{G}$, the controller K, and the range of frequency for evaluation, where

$$\begin{aligned}\mathcal{G} &= \{G_\Delta | G_\Delta(j\omega) = G(j\omega)(1+\Delta_m(j\omega))\} \\ &= G(j\omega)(1+W_o(\omega)\Delta(j\omega)), |\Delta(j\omega)| \leq 1\},\end{aligned} \tag{2.1}$$

and Δ_m and Δ are the complex perturbation.

Step 2: Set the cut-off frequency ω_d, then design weight parameters W_o and W_p using parameters at Step 1.

$$W_o = \frac{b_1 s + b_0}{a_1 s + a_0}, W_p = \frac{b_0}{a_n s^n + a_{n-1} s^{n-1} + ... + a_0} \tag{2.2}$$

where $a_n, a_{n-1}...a_1$, and a_0 are the parameters of denominator, and b_1 and b_0 are the parameters of numerator.

Step 3: Compute the peak gain when $L = 0$ and call the peak gain L_{max0}. The L_{max0} is applied as an initial value for L gain search.

Step 4: Search for an L gain. Make the L gain larger gradually, for example ($L = L_{max0} \times 10^{a-1}, a = 1, 2, 3, ..., n$), and compute and save RP for each L. After that, compute RP for each L gain within the searching area. The minimum value of RP for all RPs is found and the minimum spot is used as middle point for next iteration. In addition, the minimum RP is saved and if the minimum RP is located on the boundary of the L parameter searching area at last iteration, then expand the searching area, and if not, shrink. **Step 5**: Search for an L transfer function which is represented by a first order time constant as follows:

$$\begin{aligned}L(s) &= \frac{k_L}{1+\tau_L s} \\ k_{Lmin} &< k_L < k_{Lmax} \\ \tau_{Lmin} &< \tau_L < \tau_{Lmax}\end{aligned} \tag{2.3}$$

Where k_L is the gain, k_{Lmin} and k_{Lmax} is the lower and upper limit of k_L, τ_L is the time constant, τ_{Lmin} and τ_{Lmax} is the lower and upper limit of τ_L. The two dimensional area, which is defined by k_L and τ_L, is divided by log scale and to make a searching mesh. After that, compute RP for each combination of k_L and τ_L within the searching area. The minimum value of RP for all RPs is found and the minimum spot is used as middle point for next iteration.

$$k_{L,average} = k_{L,best} \tag{2.4}$$

$$\tau_{L,average} = \tau_{L,best} \tag{2.5}$$

where $k_{L,average}$ is the middle point of k_L for next iteration, $k_{L,best}$ is the gain that achieves minimum RP in the search area, $\tau_{L,average}$ is the middle point

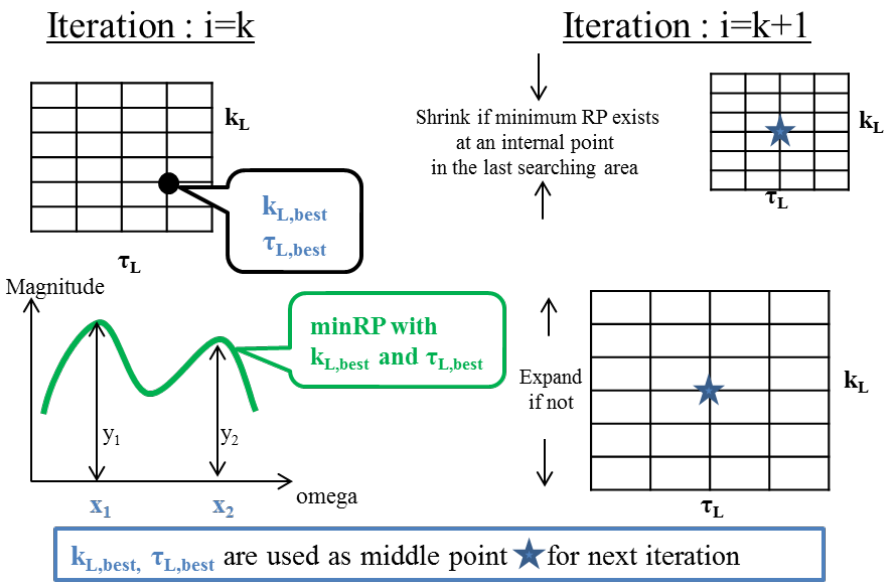

Figure 2.2: A conceptual diagram of Step 5.

of τ_L for next iteration, x_1 is the angular frequency of the one peak gain y_1 with the best $L(s)$ that achieves minimum RP in the search area, and x_2 is the angular frequency of the other peak gain y_2 with the best $L(s)$ that achieves minimum RP in the search area. In addition, the minimum RP is saved and if the minimum RP is located on the boundary of the L parameter searching area at last iteration, then expand the searching area, and if not, shrink, as shown in Fig. 2.2.

This algorithm breaks and terminates if an iteration reaches i_{max} or following condition:

$$|y_1 - y_2| < E \tag{2.6}$$

where E is the user-specified margin of error between y_1 and y_2.

2.2.1 Evaporator superheat control for a refrigeration system.

This example considers superheat control for a refrigeration system [Larsen, 2005]. Fig. 2.3 shows a layout of the refrigeration system with basic control structure. The system includes four components, a compressor, a condenser, an expansion valve, and an evaporator. In a typical refrigeration system, one loop control device is installed for each component as shown in Fig. Fig. 2.3. These

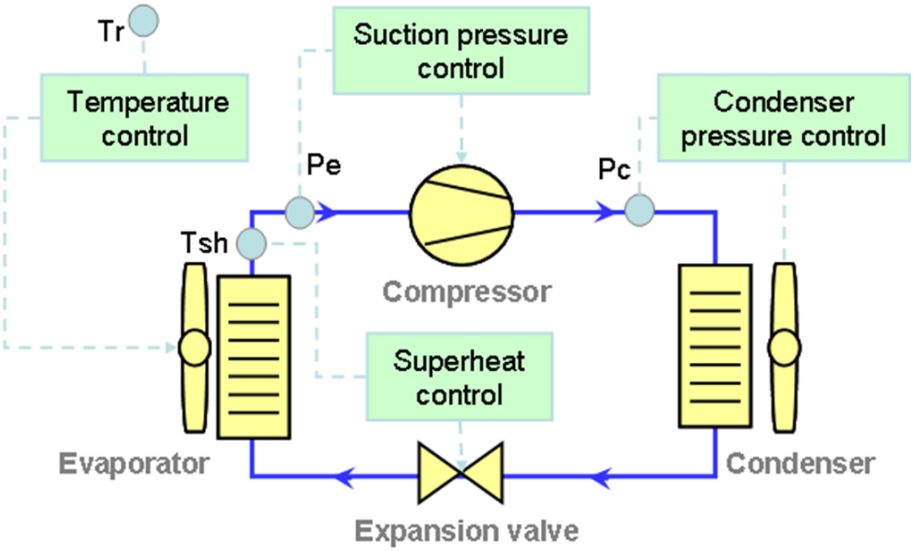

Figure 2.3: A layout of the refrigeration system with basic control structure.

controllers regulate a pressure or a temperature based on operating conditions. For instance, the compressor controls the rotational speed so that the controller keeps the pressure of suction refrigerant P_e constant. It is called a suction pressure control. The electronic expansion valve controls the open degree of the valve so that the controller keeps the superheat T_{sh} (difference between the temperature at the outlet of the evaporator and the evaporation temperature inside the evaporator) constant. The speed of the evaporator fan is controlled so as to keep the temperature on the load side T_r constant. The speed of the condenser fan is controlled so as to keep the condensing pressure P_c constant.

Now consider a simple superheat model described by a first order plus dead time system [Izadi-Zamanabadi et al., 2012]. The model for superheat control is created using experimental data obtained from step response tests conducted at different operating conditions.

$$\mathcal{G} = \frac{k}{1+\tau s} e^{-\theta s}; \tag{2.7}$$
$$k \in [k_{min}, k_{max}], \tau \in [\tau_{min}, \tau_{max}], \theta \in [\theta_{min}, \theta_{max}]$$

with $k_{min} = -41.6, k_{max} = -26.6, \tau_{min} = 39.8, \tau_{max} = 49.2, \theta_{min} = 20.9$, and $\theta_{max} = 30$.

Next, the nominal model is computed using average parameter values of $\mathcal{G}$.

$$G_n = \frac{k_n}{1+\tau_n s} e^{-\theta_n s} \tag{2.8}$$

with $k_n = -34.1, \tau_n = 44.5, \theta_n = 25.45$.

A multiplicative uncertainty weight W_o is designed by over-approximating the gain characteristics of $\mathcal{G}$, see e.g. [Skogestad and Postlethwaite, 2005].

$$W_o = \frac{17s + 0.6}{5.667s + 1} \tag{2.9}$$

The performance demands is expressed by a weight function.

$$W_p = \frac{1}{91s + 1} \tag{2.10}$$

A PI controller K is designed using the Chien–Hrones–Reswick (CHR) method [Chien et al., 1952] with the parameters of $\mathcal{G}$. The PI parameters are tuned using the worst case, where the gain and the time delay are maximum and the time constant is minimum, so that the PI controller is the most conservative to ensure stability.

$$K = \frac{0.35\tau_{min}}{k_{max}\theta_{max}}(1 + \frac{1}{1.17\tau_{min}s}) \tag{2.11}$$

2.2.2 NP, RS, and RP Measures for DFC.

The performance measures for DFC are given by as follows, and see more details in section 3 of Paper A:

Nominal Stability (NS):

$$N \text{ is internally stable.} \tag{2.12}$$

Robust Stability (RS):

$$\|-W_o(j\omega)(T(j\omega) + T_L(j\omega)S(j\omega))\| < 1, \forall\omega \in \mathbf{R}, \text{ and NS.} \tag{2.13}$$

Nominal Performance (NP):

$$\|-W_p(j\omega)S(j\omega)S_L(j\omega)\| < 1, \forall\omega \in \mathbf{R}, \text{ and NS.} \tag{2.14}$$

Robust performance (RP) is explained using NP with the worst case, which means that the uncertainty is maximum $|\Delta_{max}| = 1$, that is

$$RP \Leftrightarrow \sup\|-W_pSS_L\| < 1$$
$$\Leftrightarrow \frac{\|-W_p\|}{\|1 + G_nK\| - \|W_oG_nK\|}\frac{1}{\|1 + G_nL\| - \|W_oG_nL\|} < 1$$

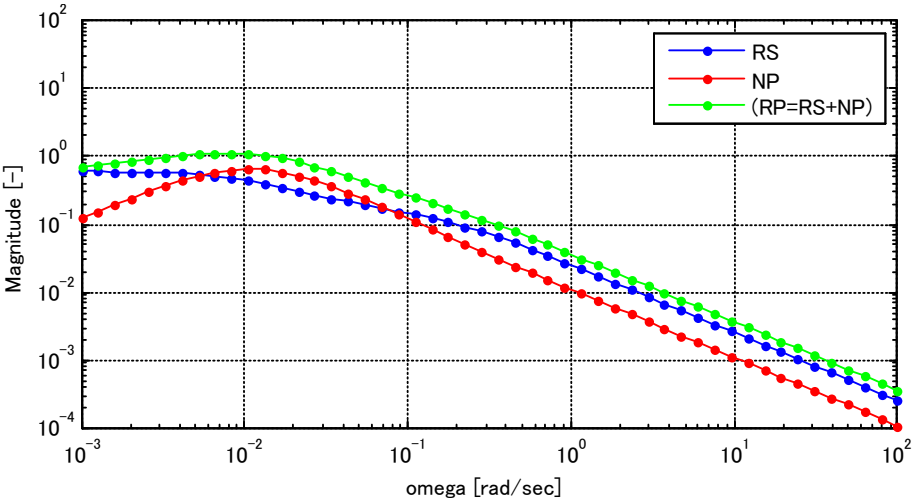

Figure 2.4: RS, NP, and RP for system with only PI control ($L = 0$).

$$\Leftrightarrow \|-W_o T - W_o(1-T)T_L\| + \|-W_p S S_L\| < 1 \tag{2.15}$$

Then we derive the robust performance as follows:

Robust Performance (RP):

$$\begin{aligned} &\|-W_o(j\omega)(T(j\omega) + T_L(j\omega)S(j\omega))\| + \\ &\|-W_p(j\omega)S(j\omega)S_L(j\omega)\| < 1, \forall\omega \in \mathbf{R}, \\ &\qquad\qquad \text{and NS.} \end{aligned} \tag{2.16}$$

Fig. 2.4 shows *RS*, *NP*, and *RP* for the system with only PI control when $L = 0$. The figure indicates that the PI control satisfies both the *RS* demand and the *NP* demand. However, the controller cannot satisfy the *RP* demand.

Fig. 2.5 shows *RS*, *NP*, and *RP* for system with PI control and DFC where L is tuned by the search algorithm. The figure confirms that the DFC can satisfy the RP demand and that one peak when PI control is applied almost disappears due to the L function, which flattens the peak. In the calculation, the maximum value of the RP shows 0.8314 at 0.004095 [rad/sec] as shown in Table 2.2.

Fig. 2.6 shows a set point response and a disturbance response of an evaporator superheat control. PI control with DFC shows better disturbance rejection compared to PI control. Average Integral Absolute Error (IAE) for nine simulations with PI and PI + DFC give 255.74, 200.01, respectively.

Table 2.2 shows a summary of the results using either PI or PI with DFC. The table indicates that PI control alone cannot satisfy RP. However, adding DFC yields both satisfactory robustness and performance.

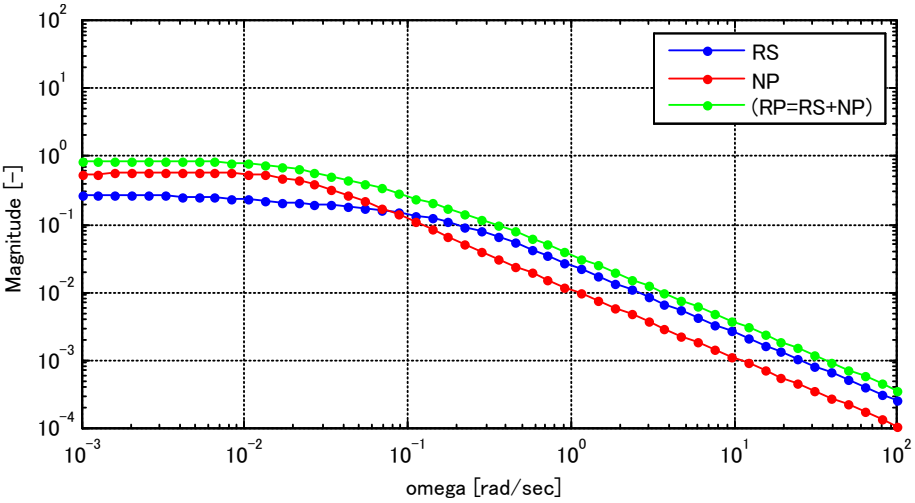

Figure 2.5: RS, NP, and RP for system with PI control and DFC (L is tuned by search algorithm).

2.2.3 Discussions

This section proposed PID based control with robust DFC for SISO systems. A simple search algorithm was presented such that the DFC can satisfy robust performance. Numerical examples showed the effectiveness of the proposed method compared with the conventional PID controller.

However, the search algorithm has risk for convergence of local minimum values. Moreover, the algorithm can be applied only in SISO systems. Therefore, more systematic design is necessary to guarantee the robust performances for target systems.

For this reasons, LMI optimization approach is introduced for more practical design on MIMO systems in the next section.

Table 2.2: results using either PI or PI with DFC.

Evaluation	PI	PI + DFC
Maximum magnitude of RP	1.1140	0.8314
NP	0.6313	0.5729
RS	0.4827	0.2585
Frequency of largest peak in RP [rad/sec]	0.008286	0.004095
L function	$L = 0$	$L = \frac{-0.0293}{1 + 150.8s}$

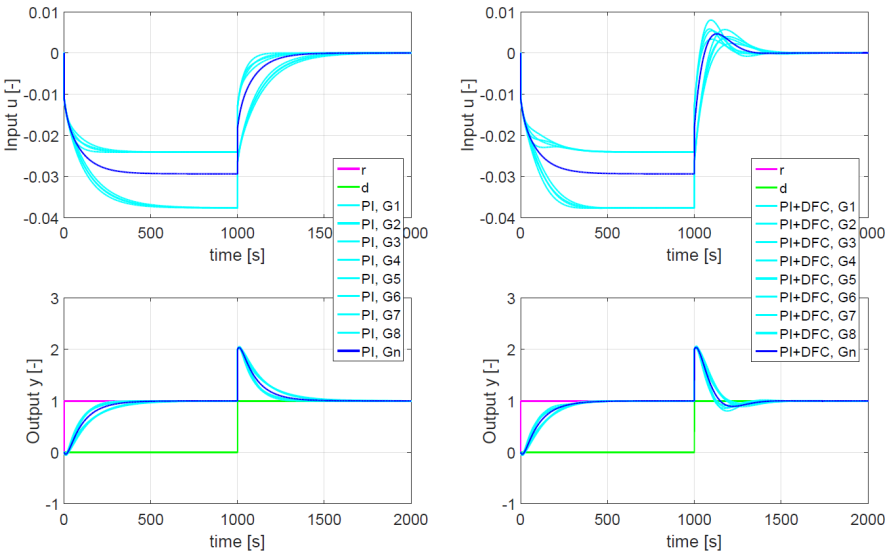

Figure 2.6: A set point response and a disturbance response of an evaporator superheat control. $G_1 - G_8$: Combinations of plant parameters, k_{min}/k_{max}, τ_{min}/τ_{max}, $\theta_{min}/\theta_{max}$. G_n: Nominal model.

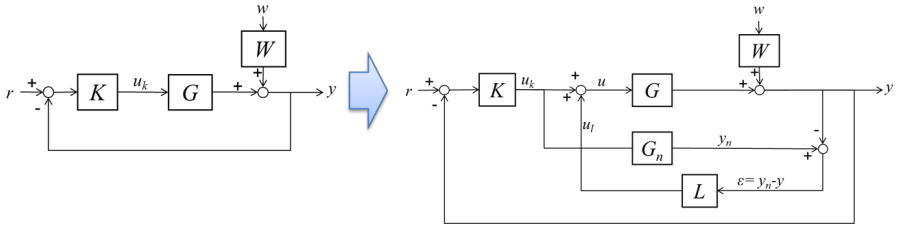

Figure 2.7: Block diagrams of existing control systems(Left), and the existing control with DFC(Right).

2.3 LMI Optimization for MIMO Systems

2.3.1 DFC Design

Fig. 2.7 shows block diagrams of an existing control system (Left) and the same system augmented with DFC (Right). The existing controller K is assumed to be a 1DOF controller, a PID controller for instance, and it may be designed by traditional methods; IMC, pole placement, or similar. W is a disturbance weighting transfer matrix.

On the right side, DFC is added to the existing control system to improve the robustness against disturbances. In addition, DFC can work to compensate for model uncertainties if there are modeling errors between the nominal model G_n and the actual plant G. Notice how the DFC control signal is added to the existing control signal after the u_k branch; this configuration makes DFC different from IMC [Rivera et al., 1986].

Other variations of DFC can be described as shown in Fig. 2.8. In one variant, the existing controller is composed of a feedback and a feedforward part. In another variant, a weighting function W places more emphasis on certain disturbance frequency ranges. The method presented in the following applies to these variants as well with minor modifications.

This section presents a method to design the DFC to meet certain stability and robustness requirements. Firstly, the existing control systems are defined. Next, LMIs for the DFC synthesis are presented, and finally the controller is discretized and augmented with anti-windup.

2.3.2 Existing Control Systems

The plant model G in Fig. 2.7 is assumed given as a time domain representation in state space;

$$\begin{aligned} \dot{x} &= Ax + Bu \\ y - d &= Cx, \end{aligned} \tag{2.17}$$

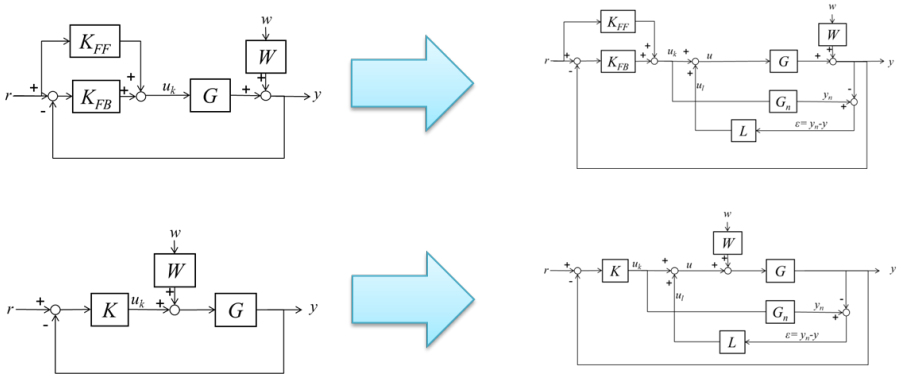

Figure 2.8: Block diagrams of other variations about existing control systems(Left), and the existing control with DFC(Right).

where $A \in \mathbb{R}^{n\times n}$, $B \in \mathbb{R}^{n\times m}$, and $C \in \mathbb{R}^{m\times n}$ are real constant matrices. $x \in \mathbb{R}^n$ is the plant state, $u \in \mathbb{R}^m$ is the control input and $y \in \mathbb{R}^m$ is the output. The plant parameters are affected by parametric uncertainties [Carsten Scherer and Siep Weiland, 2004] expressed by

$$
\begin{aligned}
A &= A_n + \sum_{i=1}^{p} \delta_{a,i} A_i, \quad \delta_{a,i} \in [-1, +1], \\
B &= B_n + \sum_{i=1}^{q} \delta_{b,i} B_i, \quad \delta_{b,i} \in [-1, +1], \\
C &= C_n + \sum_{i=1}^{r} \delta_{c,i} C_i, \quad \delta_{c,i} \in [-1, +1],
\end{aligned}
\tag{2.18}
$$

where $\delta_a = (\delta_{a,1}, \ldots, \delta_{a,p})$, $\delta_b = (\delta_{b,1}, \ldots, \delta_{b,q})$, $\delta_c = (\delta_{c,1}, \ldots, \delta_{c,r})$ are unknown vectors, which express the ensemble of all uncertainty quantities in a given dynamics, A_n, B_n, and C_n are the nominal state space representation corresponding to G_n, and A_i, B_i, and C_i describe the uncertainties.

The existing control K is given by

$$
\begin{aligned}
\dot{x}_k &= A_k x_k + B_k (r - y), \\
u_k &= C_k x_k + D_k (r - y),
\end{aligned}
\tag{2.19}
$$

where $r \in \mathbb{R}^m$ is a reference signal, and $A_k \in \mathbb{R}^{n_K \times n_K}$, $B_k \in \mathbb{R}^{n_K \times m}$, $C_k \in \mathbb{R}^{m \times n_K}$, and $D_k \in \mathbb{R}^{m\times m}$ comprise the state space representation of K.

The weighting function W for the disturbance d is defined as

$$
\begin{aligned}
\dot{x}_w &= A_w x_w + B_w w, \\
d &= C_w x_w + D_w w,
\end{aligned}
\tag{2.20}
$$

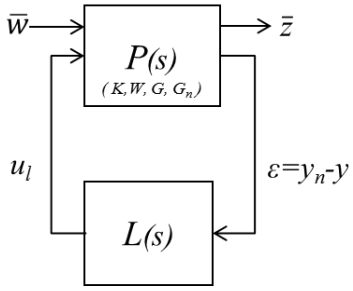

Figure 2.9: A closed-loop system for design of DFC $L(s)$.

where $A_w \in \mathbb{R}^{n_W \times n_W}$, $B_w \in \mathbb{R}^{n_W \times m}$, $C_w \in \mathbb{R}^{m \times n_W}$, and $D_w \in \mathbb{R}^{m \times m}$ are the state space representation of the weighting function. $w \in \mathbb{R}^m$ is an external bounded signal. Note that this weight function W is designed as weighting filter using classical H_∞ theory [Skogestad and Postlethwaite, 2005].

2.3.3 DFC Design for Existing Control Systems

We now consider adding the DFC block L in the right part of Fig. 2.7. This is done using the well-known configuration shown in Fig. 2.9, where the vector signal $\bar{w}$ contains the external inputs, disturbance w and measurement noise w_n, and $\bar{z}$ denotes outputs for evaluating performance. Note that the motivation of the DFC design is to improve the disturbance rejection of existing system since the existing controller already stabilizes the plant and is tuned to give a satisfactory response from reference changes. Therefore, r is disregarded as an external input, and removed away from DFC design.

We assume that the existing controller K is fixed, meaning we can deal with K as a part of the plant P. Thus, P includes G, G_n, W, and K in the DFC design.

The DFC is designed by classical and modern robust control theory, where W is chosen with weighting filter scheme of classical H_∞ theory, and the robust DFC is designed via LMI optimization using modern robust control theory.

The Disturbance Feedback Controller (DFC) is chosen as

$$\begin{aligned} \dot{x}_{ul} &= A_l x_{ul} + B_l \epsilon \\ u_l &= C_l x_{ul} + D_l \epsilon, \end{aligned} \tag{2.21}$$

where $A_l \in \mathbb{R}^{(2n+n_K+n_W)\times(2n+n_K+n_W)}$, $B_l \in \mathbb{R}^{(2n+n_K+n_W)\times m}$, $C_l \in \mathbb{R}^{m\times(2n+n_K+n_W)}$, and $D_l \in \mathbb{R}^{m\times m}$.

Note that DFC, as presented here, is a full order output feedback controller, and thus the scheme proposed in [Scherer et al., 1997], can be applied in the DFC design. Firstly, the closed loop transfer matrix $T(s) : \bar{w} \mapsto \bar{z}$ is obtained

by way of an extended state space representation. Next, two constraints are introduced in order to design L. Here, we make use of the Bounded Real Lemma and regional pole placement for continuous time systems [Scherer et al., 1997; Chilali et al., 1999]. The Bounded Real Lemma is used to guarantee robust performance, and regional pole placement is introduced to specify the control performance. Then, a linearizing change of variable is needed to formulate the problem in terms of LMIs.

The extended state space representation of the overall system shown in Fig. 2.10, can be written as follows;

$$\begin{aligned} \dot{x}_p &= A_p x_p + B_{pw}\bar{w} + B_p u_l \\ \bar{z} &= C_z x_p + D_z u_l \\ \epsilon &= C_p x_p + D_{pw}\bar{w}, \end{aligned} \tag{2.22}$$

where

$$x_p = \begin{pmatrix} x^{\mathrm{T}} & {x_n}^{\mathrm{T}} & {x_k}^{\mathrm{T}} & {x_w}^{\mathrm{T}} \end{pmatrix}^{\mathrm{T}},$$

$$A_p = \begin{pmatrix} A - BD_kC & 0 & BC_k & -BD_kC_w \\ -B_nD_kC & A_n & B_nC_k & -B_nD_kC_w \\ -B_kC & 0 & A_k & -B_kC_w \\ 0 & 0 & 0 & A_w \end{pmatrix},$$

$$B_{pw} = \left(\begin{array}{cccc} 0 & 0 & 0 & 0 \\ \hline -(BD_kD_w)^{\mathrm{T}} & -(B_nD_kD_w)^{\mathrm{T}} & -(B_kD_w)^{\mathrm{T}} & {B_w}^{\mathrm{T}} \end{array}\right)^{\mathrm{T}},$$

$$B_p = \begin{pmatrix} B^{\mathrm{T}} & 0 & 0 & 0 \end{pmatrix}^{\mathrm{T}},$$

$$C_z = \left(\begin{array}{cccc} -C & C_n & 0 & -C_w \\ \hline 0 & 0 & 0 & 0 \end{array}\right),$$

$$C_p = \begin{pmatrix} -C & C_n & 0 & -C_w \end{pmatrix},$$

$$D_z = \left(\begin{array}{c} 0 \\ \hline \rho_z I \end{array}\right), \quad D_{pw} = \left(\begin{array}{c|c} \rho_w I & 0 \end{array}\right),$$

In the above, ρ_z and ρ_w are small scalars which are introduced to maintain full rank and to avoid numerical issues if D_z and D_{pw} are zero matrices. Note that $\bar{z} = (\epsilon_z{}^{\mathrm{T}}, (\bar{D}_z u_l)^{\mathrm{T}})^{\mathrm{T}}$ where $\epsilon_z = y_n - (Cx + C_w x_w)$, $\bar{D}_z = \rho_z I$, and $\bar{D}_{pw} = \rho_w I$.

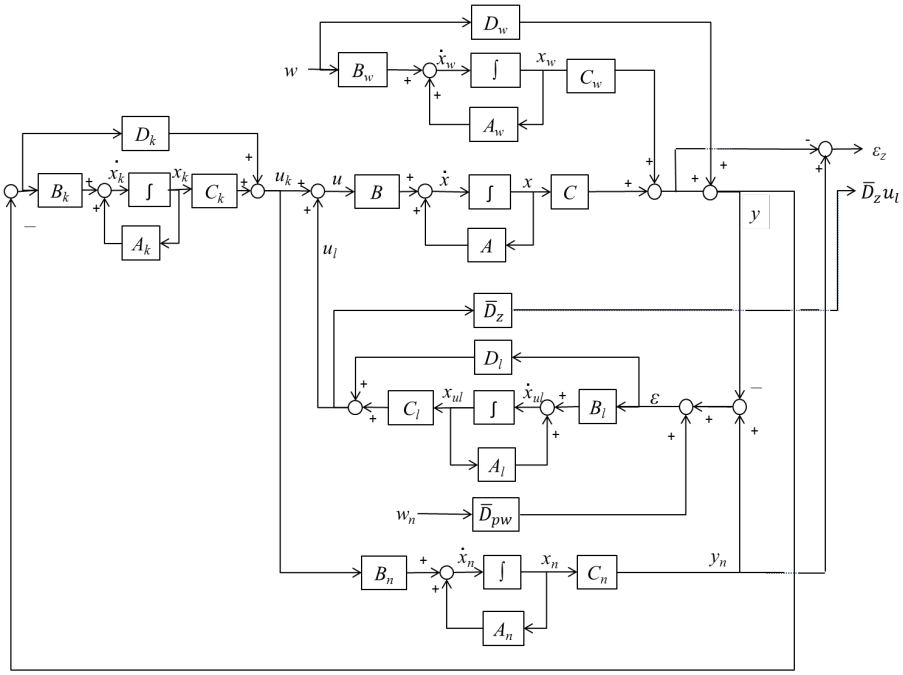

Figure 2.10: State space representation of the DFC design.

The closed loop transfer function $T(s)$ from $\bar{w}$ to $\bar{z}$ becomes;

$$\begin{aligned} \dot{x_{cl}} &= \mathcal{A}x_{cl} + \mathcal{B}\bar{w} \\ \bar{z} &= \mathcal{C}x_{cl} + \mathcal{D}\bar{w}, \end{aligned} \tag{2.23}$$

where

$$\left(\begin{array}{c|c} \mathcal{A} & \mathcal{B} \\ \hline \mathcal{C} & \mathcal{D} \end{array}\right) = \left(\begin{array}{cc|c} A_p + B_p D_l C_p & B_p C_l & B_{pw} + B_p D_l D_{pw} \\ B_l C_p & A_l & B_l D_{pw} \\ \hline C_z + D_z D_l C_p & D_z C_l & D_z D_l D_{pw} \end{array}\right),$$

which has to be stabilized for all possible values of $\delta_{a,i}$, $\delta_{b,i}$, $\delta_{c,i}$. Using the Bounded Real Lemma [Scherer et al., 1997] and regional pole placement [Chilali et al., 1999], we formulate the following optimization problem.

$$\underset{X,Y,\hat{A},\hat{B},\hat{C},\hat{D}}{\text{minimize}} \quad \gamma_1, \tag{2.24}$$

subject to;

$$\left(\begin{array}{ccc} \hat{\mathcal{A}_\circ}^{\mathrm{T}}\hat{\mathcal{P}} + \hat{\mathcal{P}}\hat{\mathcal{A}_\circ} & \hat{\mathcal{P}}\hat{\mathcal{B}_\circ} & \hat{\mathcal{C}_\circ}^{\mathrm{T}} \\ \hat{\mathcal{B}_\circ}^{\mathrm{T}}\hat{\mathcal{P}} & -\gamma_1 I & \hat{\mathcal{D}}^{\mathrm{T}} \\ \hat{\mathcal{C}} & \hat{\mathcal{D}} & -\gamma_1 I \end{array}\right) < 0, \quad \gamma_1 > 0,$$

$$\hat{\mathcal{P}} = \left(\begin{array}{cc} X & I \\ I & Y \end{array}\right), \quad \hat{\mathcal{P}} > 0,$$

$$2\alpha\hat{\mathcal{P}} + \hat{\mathcal{A}_\circ}^{\mathrm{T}}\hat{\mathcal{P}} + \hat{\mathcal{P}}\hat{\mathcal{A}_\circ} < 0,$$

where

$$\hat{\mathcal{A}_\circ}^{\mathrm{T}}\hat{\mathcal{P}} + \hat{\mathcal{P}}\hat{\mathcal{A}_\circ} = \left(\begin{array}{c} A_p X + X A_p^{\mathrm{T}} + B_p\hat{C} + (B_p\hat{C})^{\mathrm{T}} \\ \hat{A} + (A_p + B_p\hat{D}C_p)^{\mathrm{T}} \end{array} \right.$$
$$\left. \begin{array}{c} \hat{A}^{\mathrm{T}} + (A_p + B_p\hat{D}C_p) \\ A_p^{\mathrm{T}}Y + YA_p + \hat{B}C_p + (\hat{B}C_p)^{\mathrm{T}} \end{array}\right)_\delta,$$

$$\hat{\mathcal{P}}\hat{\mathcal{B}_\circ} = \left(\begin{array}{c} B_c + B_p\hat{D}F_c \\ YB_c + \hat{B}F_c \end{array}\right)_\delta,$$

$$\hat{\mathcal{C}_\circ} = \left(\begin{array}{cc} C_c X + E_c\hat{C} & C_c + E_c\hat{D}C_p \end{array}\right)_\delta,$$

$$\hat{\mathcal{D}} = E_c\hat{D}F_c,$$

$$B_c := B_{pw}R_c, \quad C_c := N_c C_z,$$

$$E_c := N_c D_z, \quad F_c := D_{pw}R_c,$$

In the above, the subscript δ notation should be understood as requiring the LMIs to be satisfied for all extremal points of δ as defined in (2.18). That is, the LMIs must be satisfied everywhere on the convex hull defined by the permissible values of the uncertainties; i.e., one LMI has to be solved for every vertex of the hypercube $(\delta_a, \delta_b, \delta_c) \in [-1, 1]^{p+q+r}$ to yield one common $\hat{\mathcal{P}}$. The scaling parameter $\alpha > 0$ is included to provide extra tuning freedom; essentially, the permitted pole locations are to the left of $s = -\alpha$. N_c, R_c are given input/output channel maps for $T(s)$ from $\bar{w}$ to $\bar{z}$;

$$T_c = N_c T R_c. \tag{2.25}$$

2.3.4 Disctretization and Anti-windup Control

Assuming the minimization problem (2.24) can be solved, this section describes an anti-windup control design for the discretized PI controller K and the robust DFC L for practical implementation. The anti-windup control design for discrete time systems proposed by Syaichu-Rohman and Middleton [Syaichu-Rohman and Middleton, 2004], and was originally derived for 1DOF control systems. As mentioned in Section 1, DFC is categorized as a 2DOF controller, and therefore, the method will be reshaped for DFC.

Firstly, discretization of the closed loop system including G, G_n, W, and L is done by bilinear method [Oppenheim and Schafer, 1989]. With $H_c(s)$ denoting the continuous time transfer function and $H(z)$ the discrete time transfer function, the bilinear transformation corresponds to replacing s by

$$s = \frac{2}{T_d}\left(\frac{1 - z^{-1}}{1 + z^{-1}}\right), \tag{2.26}$$

that is,

$$H_z = H_c\left[\frac{2}{T_d}\left(\frac{1 - z^{-1}}{1 + z^{-1}}\right)\right], \tag{2.27}$$

where T_d is a sampling time.

Next, the extended state space representation including the anti-windup controllers in Fig. 2.11 is considered. Unit delay blocks for wind-up gains Λ_{k2} and Λ_{l2} are introduced to avoid algebraic loops.

The vector $v(k)$, the saturation function Φ, and the dead zone function Ψ can be described by

$$v(k) = \tilde{u}(k) - u(k) = \tilde{u}(k) - \Phi(\tilde{u}(k)) \tag{2.28}$$

$$\Psi(\tilde{u}(k)) = I - \Phi(\tilde{u}(k)) \tag{2.29}$$

where $\tilde{u}$ is a control output before a saturation block, $\Phi : \mathbb{R}^m \to \mathbb{R}^m$ is a saturation function, $\Psi : \mathbb{R}^m \to \mathbb{R}^m$ is a deadzone function, and $\tilde{u}(k)$ is a control

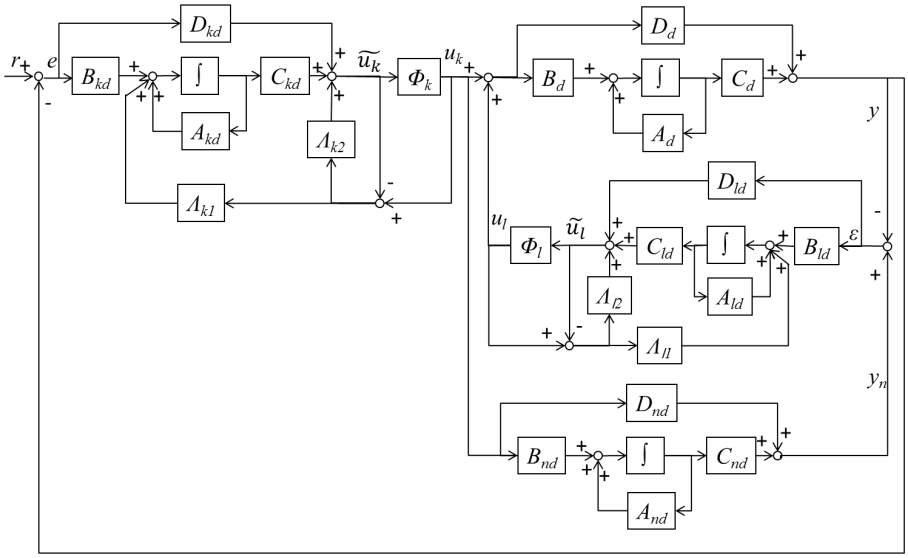

Figure 2.11: A state space representation of the PI control with robust DFC including the anti-windup controllers.

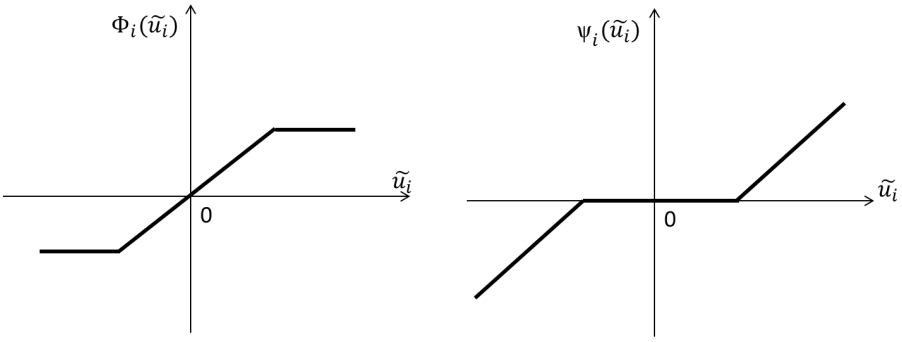

Figure 2.12: A saturation function (left) and a dead zone function (right).

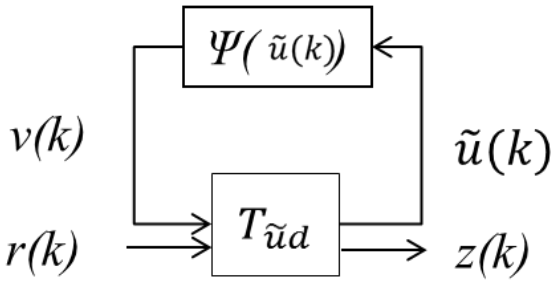

Figure 2.13: A simplified feedback system for anti-windup control design.

output vector before saturation block. These two functions are illustrated in Fig. 2.12. PI control is discretized with bilinear method, and the anti-windup gains Λ_{k1} and Λ_{k2} for discrete PI control are described as follows:

$$\begin{aligned} x_k(k+1) &= A_{kd}x_k(k) + B_{kd}(r(k) - y(k)) - \Lambda_{k1}(\tilde{u}_k(k) - u_k(k)) \\ \tilde{u}_k(k) &= C_{kd}x_k(k) + D_{kd}(r(k) - y(k)) + x_{ek}(k) \\ x_{ek}(k+1) &= -\Lambda_{k2}(\tilde{u}_k(k) - u_k(k)). \end{aligned} \tag{2.30}$$

Similarly, the anti-windup gains Λ_{l1} and Λ_{l2} for the discrete DFC are included in the controller equations as follows:

$$\begin{aligned} x_l(k+1) &= A_{ld}x_l(k) + B_{ld}(r(k) - y(k)) - \Lambda_{l1}(\tilde{u}_l(k) - u_l(k)) \\ \tilde{u}_l(k) &= C_{ld}x_k(k) + D_{ld}(r(k) - y(k)) + x_{el}(k) \\ x_{el}(k+1) &= -\Lambda_{l2}(\tilde{u}_l(k) - u_l(k)). \end{aligned} \tag{2.31}$$

The last terms of the controller equations in (2.30) and (2.31), $(\tilde{u_k}(k) - u_k(k))$ and $(\tilde{u_l}(k) - u_l(k))$ can be seen as a disturbance in terms of stability and performance. The system in Fig. 2.11 can be simplified in Fig. 2.13, giving rise to the system equations

$$\begin{aligned} \tilde{x}(k+1) &= \tilde{\mathcal{A}}\tilde{x}(k) + \tilde{\mathcal{B}}v(k) + \tilde{\mathcal{B}}_r r(k) \\ \tilde{u}(k) &= \tilde{\mathcal{C}}_u\tilde{x}(k) + \tilde{\mathcal{D}}_u v(k) + \tilde{\mathcal{D}}_{ur} r(k) \\ z(k) &= \tilde{\mathcal{C}}_z\tilde{x}(k) + \tilde{\mathcal{D}}_z v(k) + \tilde{\mathcal{D}}_{zr} r(k) \end{aligned} \tag{2.32}$$

where

$$\begin{pmatrix} v_1(k) \\ v_2(k) \end{pmatrix} = \begin{pmatrix} \tilde{u}_k(k) \\ \tilde{u}_l(k) \end{pmatrix} - \begin{pmatrix} u_k(k) \\ u_l(k) \end{pmatrix}, \tag{2.33}$$

$$
\begin{aligned}
\tilde{x}(k) &= \begin{pmatrix} x(k)^{\mathrm{T}} & x_n(k)^{\mathrm{T}} & x_k(k)^{\mathrm{T}} & x_{ek}(k)^{\mathrm{T}} & x_l(k)^{\mathrm{T}} & x_{el}(k)^{\mathrm{T}} \end{pmatrix}^{\mathrm{T}}, \\
\tilde{\mathcal{A}}_\delta &= \begin{pmatrix} A_d - B_d D_{kd} C_d - B_d D_{ld} C_d & B_d D_{ld} C_{nd} & B_d C_{kd} & B_d & B_d C_{ld} & B_d \\ -B_{nd} D_{kd} C_d & A_{nd} & B_{nd} C_{kd} & B_{nd} & 0 & 0 \\ -B_{kd} C_d & 0 & A_{kd} & 0 & 0 & 0 \\ 0 & 0 & 0 & 0 & 0 & 0 \\ -B_{ld} C_d & B_{ld} C_{nd} & 0 & 0 & A_{ld} & 0 \\ 0 & 0 & 0 & 0 & 0 & 0 \end{pmatrix}_\delta, \\
\tilde{\mathcal{B}}_\delta &= \begin{pmatrix} -B_d & -B_d \\ -B_{nd} & 0 \\ -\Lambda_{k1} & 0 \\ -\Lambda_{k2} & 0 \\ 0 & -\Lambda_{l1} \\ 0 & -\Lambda_{l2} \end{pmatrix}_\delta, \tilde{\mathcal{B}}_{v,\delta} = \begin{pmatrix} -B_d & -B_d \\ -B_{nd} & 0 \\ 0 & 0 \\ 0 & 0 \\ 0 & 0 \\ 0 & 0 \end{pmatrix}_\delta, \\
\tilde{\mathcal{B}}_e &= \begin{pmatrix} 0 & 0 \\ 0 & 0 \\ I & 0 \\ I & 0 \\ 0 & I \\ 0 & I \end{pmatrix}, \tilde{\mathcal{B}}_{r,\delta} = \begin{pmatrix} -B_d D_{kd} \\ -B_{nd} D_{kd} \\ B_{kd} \\ 0 \\ 0 \\ 0 \end{pmatrix}_\delta, \\
\tilde{\mathcal{C}}_{u,\delta} &= \begin{pmatrix} -D_{kd} C_d & 0 & C_{kd} & I & 0 & 0 \\ -D_{ld} C_d & D_{ld} C_{nd} & 0 & 0 & C_{ld} & I \end{pmatrix}_\delta, \\
\tilde{\mathcal{C}}_{z,\delta} &= \begin{pmatrix} -C_d & 0 & 0 & 0 & 0 & 0 \end{pmatrix}_\delta, \\
\tilde{\mathcal{D}}_u &= \begin{pmatrix} 0 \\ 0 \end{pmatrix}, \tilde{\mathcal{D}}_{ur} = \begin{pmatrix} D_k \\ 0 \end{pmatrix}, \tilde{\mathcal{D}}_z = \begin{pmatrix} 0 & 0 \end{pmatrix}, \tilde{\mathcal{D}}_{zr} = I.
\end{aligned}
\tag{2.34}
$$

The explicit static anti-windup scheme proposed by Rohman [Syaichu-Rohman and Middleton, 2004] is reshaped for conventional controller K and DFC L as follows:

$$
\begin{aligned}
&\underset{\tilde{Q},V,M,\kappa}{\text{minimize}}\ \gamma_2 \\
&\text{subject to;} \\
&\begin{pmatrix} \tilde{Q} & * & * & * & * & * \\ 0 & -\gamma_2 I & * & * & * & * \\ \tilde{\mathcal{C}}_{u,\delta}\tilde{Q} & \tilde{\mathcal{D}}_{ur} & -2M & * & * & * \\ \tilde{\mathcal{C}}_{z,\delta}\tilde{Q} & \tilde{\mathcal{D}}_{zr} & 0 & -\gamma_2 I & * & * \\ \tilde{\mathcal{A}}_\delta\tilde{Q} & \tilde{\mathcal{B}}_{r,\delta} & \tilde{\mathcal{B}}_{r,\delta}M - \tilde{\mathcal{B}}_e V & 0 & -\tilde{Q} & * \\ 0 & 0 & M & 0 & 0 & \kappa I \end{pmatrix} \leq 0, \\
&\tilde{Q} = \tilde{Q}^{\mathrm{T}} > 0, \quad \gamma_2 > 0, \quad \kappa > 0,
\end{aligned}
\tag{2.35}
$$

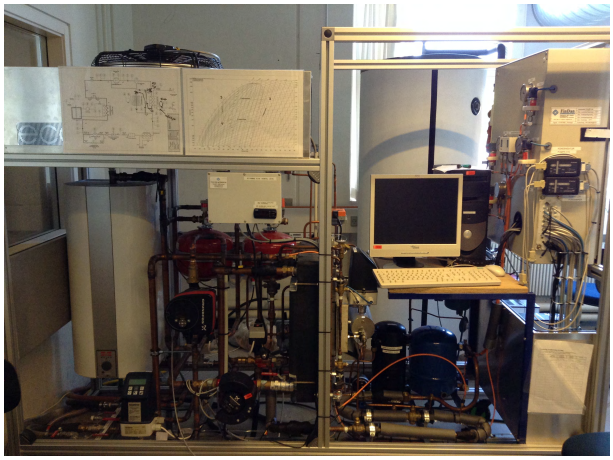

Figure 2.14: The refrigeration system test setup at Aalborg University.

where $M > 0 \in \mathbb{R}^{2m \times 2m}$ is a diagonal matrix, $V := \Lambda M \in \mathbb{R}^{2m \times 2m}$ is an arbitrary matrix, γ_2 and κ are scalars.

Similarly to (2.24), subscript $(\cdot)_\delta$ in (2.35) indicates that one LMI has to be solved for every extremal point of $(\delta_a, \delta_b, \delta_c) \in [-1, 1]^{p+q+r}$ to yield one common $\tilde{\mathcal{Q}}$.

2.4 Experimental Results

This section demonstrates the proposed design on a model of a MIMO water chiller system at Aalborg University (AAU) shown in Fig. 2.14. The system is challenging to control due to model uncertainties, changing system gains, and time delays. Conventional control designs tend to exhibit poor performance away from nominal operating conditions due to these effects.

Especially the superheat control is challenging to design, because the refrigerant exhibits strong nonlinear characteristics due to the two-phase (vapor-liquid) state in the evaporator. Due to nonlinearities, the gains of linearizations in different operating points vary significantly, for instance.

These model variations are dealt with in the following by means of robust design. The application is inspired by Fuji Electric's business case of refrigerant applications such as vending machine and air conditioning units (two examples are shown in Fig. 2.15). These applications exhibit the same control issues as the laboratory system, and the applications need robustness against changes in heat load and outside air temperature.

Figure 2.15: The refrigeration applications by Fuji Electric, Vending machines (Left), and Hybrid indirect air conditioning unit F-COOL NEO (Right).

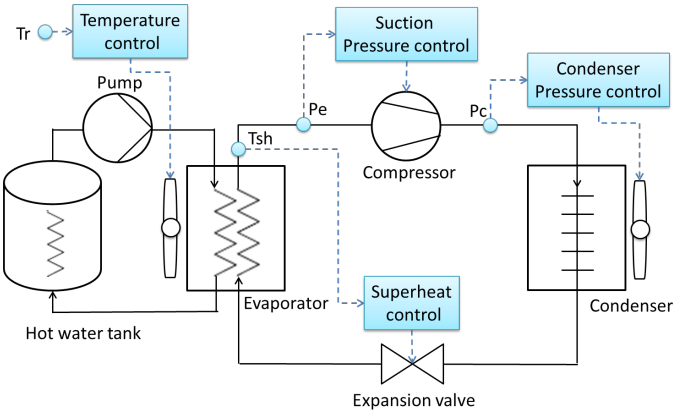

Figure 2.16: A layout of the water chiller system with basic control structure.

2.4.1 Lab system setup

The lab system includes four main components; a compressor, a condenser, an expansion valve, and an evaporator. In a basic refrigeration system, one control device is installed for each component as shown in Fig. 2.16. These controllers regulate pressure or temperature to maintain specified operating conditions. For example, the rotational speed of the compressor is controlled to keep a constant refrigerant suction pressure P_e. The opening degree of the expansion valve maintains a suitable refrigerant superheat T_{sh} (difference between the temperature at the outlet of the evaporator and the evaporation temperature inside the evaporator). The speed of the evaporator fan is controlled to keep the temperature on the load side T_r constant. The speed of the condenser fan is controlled in order to keep the condensing pressure P_c constant. A hot water tank is set as heat load.

2.4.2 Model

In the following, a simple 2 input and 2 output model is considered for MIMO control design of the water chiller system. A simple superheat model and a suction pressure model is chosen for the MIMO control design, and these models can be described by a first order plus dead time system, see e.g., [Izadi-Zamanabadi et al., 2012]. Practical results in previous studies furthermore also indicate that the dominant uncertainty is the gain of the superheat model [Kawai et al., 2017; Vinther et al., 2015].

The model is created using experimental data obtained from step-up and step-down responses conducted at two operating conditions, which means that four sets of step responses are used for model identification.

We assume a model of the form as follows:

$$\begin{pmatrix} y_1(s) \\ y_2(s) \end{pmatrix} = \begin{pmatrix} G_{11}(s) & G_{12}(s) \\ G_{21}(s) & G_{22}(s) \end{pmatrix} \begin{pmatrix} u_1(s) \\ u_2(s) \end{pmatrix}, \tag{2.36}$$

where y_1 is a superheat temperature, y_2 is a suction pressure of the compressor, G_{11}, G_{12}, G_{21}, G_{22} are subsystems of the 2 input 2 output system, u_1 is the opening degree of the expansion valve, and u_2 is a compressor speed.

That is, scalar gains k_{ij}, time constants τ_{ij}, and time delay θ_{ij} in the following first-order plus time delay models are fitted to measurement data using straightforward least-squares methods.

$$\begin{aligned} G_{ij} &= \frac{k_{ij}}{1+\tau_{ij}s} e^{-\theta_{ij}s}; \\ k_{ij} &\in [k_{min,ij}, k_{max,ij}], \tau_{ij} \in [\tau_{min,ij}, \tau_{max,ij}], \\ \theta_{ij} &\in [\theta_{min,ij}, \theta_{max,ij}], \\ i &= 1,2, j = 1,2. \end{aligned} \tag{2.37}$$

Next, the nominal model is computed using average parameter values of $\mathcal{G}$, i.e.,

$$G_{n,ij} = \frac{k_{n,ij}}{1+\tau_{n,ij}s} e^{-\theta_{n,ij}s}. \tag{2.38}$$

where

$$k_{n,ij} = \frac{k_{max,ij}+k_{min,ij}}{2}, \tau_{n,ij} \quad = \frac{\tau_{max,ij}+\tau_{min,ij}}{2}, \theta_{n,ij} = \frac{\theta_{max,ij}+\theta_{min,ij}}{2},$$

We focus on the worst case of model, which is the corner points of the model sets. That is the reason why average values of minimum and maximum parameters are used for nominal model. To keep the design simple, the time delay is approximated by a first order filter. In addition, only one parameter,

k_{11}, is considered uncertain because it represents the strongest uncertainty (nonlinearity). Therefore, G and G_n are approximated as follows:

$$G_{11} = \frac{k_{11}}{(1+\tau_{n,11}s)(1+\theta_{n,11}s)}; \quad k_{11} \in [-10.64, -8.71], \tag{2.39}$$

and the rest of the subsystems are expressed by the nominal model.

$$G_{ij} = \frac{k_{n,ij}}{(1+\tau_{n,ij}s)(1+\theta_{n,ij}s)}; \quad i = 1,2, j = 1,2, except \;\; ij = 11. \tag{2.40}$$

and nominal parameters of the subsystems are shown in Table 2.3.

Table 2.3: Nominal parameters of the subsystems.

	k	τ	θ
$g_{n,11}$	-9.68	44.83	20.50
$g_{n,21}$	0.28	10.32	5.50
$g_{n,12}$	0.74	42.03	18.50
$g_{n,22}$	-0.046	7.20	4.0

2.4.3 Control Design

This subsection demonstrates the robust DFC with anti-windup control by two types of LMIs. First, the robust DFC without saturation are designed, and then the anti-windup controllers are solved for both of the PI and robust DFC controllers.

The PI controllers are tuned based on the parameters of each corner point of the plant of the subsystems in order to maintain nominal stability for all parameter values. Each corner point was chosen from largest absolute gain, minimum time constant, and largest time delay respectively. In addition, Betraqs method proposed by Fuji Electric, was chosen for PI control design [Mitsuhashi Shigetaka and Tatsuo Inoue, 1965].

$$K = \begin{pmatrix} K_{11}(s) & 0 \\ 0 & K_{22}(s) \end{pmatrix}, \tag{2.41}$$

where

$$K_{11} = \frac{-0.0675s - 0.00229}{s}, \; K_{22} = \frac{-6.439s - 0.7013}{s}.$$

The disturbance weight function is chosen as a first order system, and designed using the nominal time constants $\tau_{n,11}, \tau_{n,22}$. In addition, the weight of superheat W_{11} is given priority in terms of disturbance rejection.

$$W = \begin{pmatrix} W_{11}(s) & 0 \\ 0 & W_{22}(s) \end{pmatrix}. \tag{2.42}$$

where

$$W_{11} = \frac{1}{14.95s + 1},\ W_{22} = \frac{0.1}{7.208s + 1}. \tag{2.43}$$

The artificial parameters in (2.22) for DFC are chosen as follows:

$$\rho_z = 10^{-1},\ \ \rho_w = 10^{-6}. \tag{2.44}$$

The optimal H_∞ performance obtained by solving the first LMIs in (2.24) was $\gamma_1 = 0.4000$ with full order DFC without saturation, and the DFC was a 20th order system because $dim(A_l) = 2n + n_K + n_W, n = 8, n_K = 2, n_W = 2$. It would be more useful for industrial systems if a lower order DFC can be obtained. Therefore, model reduction is applied to reduce the DFC to a simple gain. The Matlab command `modred` yields

$$D_l = \begin{pmatrix} -0.2835 & 0.2860 \\ 1.6681 & -7.0684 \end{pmatrix}. \tag{2.45}$$

Fig. 2.17 shows bode-plots in comparison with DFCs before/after the model reduction. The figure indicates that the DFC gain matrix can maintain the response of the original DFC in the frequency range of interest.

Note that this reduced order DFC can satisfy the requirements specification in the frequency domain. However, other examples may not achieve the sufficient performance with a simple gain DFC. Thus, it needs to be examined how much orders can be reduced for each case study through simulation analysis.

Fig. 2.18 shows a pole-zero map in the s-plane of closed loop system with DFC gain matrix. The mapping shows that all the poles for all model corner points are in the left half plane, and therefore the system with DFC gain matrix guarantees the stability. In addition, the norm γ_1 with DFC gain was 0.7960. Thus the system can maintain $\gamma_1 < 1$.

Next, discrete anti-windup controllers are designed for the PI controller. Solving (2.35), from which we obtained the results

$$\Lambda_{k1} = \begin{pmatrix} -0.8546 & -0.0288 \\ -0.3146 & -0.0575 \end{pmatrix}, \tag{2.46}$$

$$\Lambda_{k2} = \begin{pmatrix} 0.1136 & 0.0678 \\ -2.9893 & -0.1257 \end{pmatrix}.$$

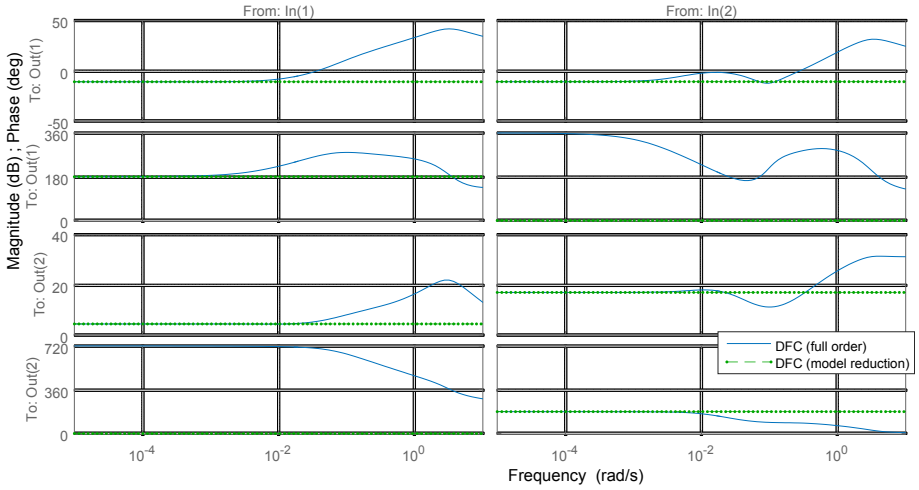

Figure 2.17: Bode plots of DFC from ϵ to u_l, before and after model reduction.

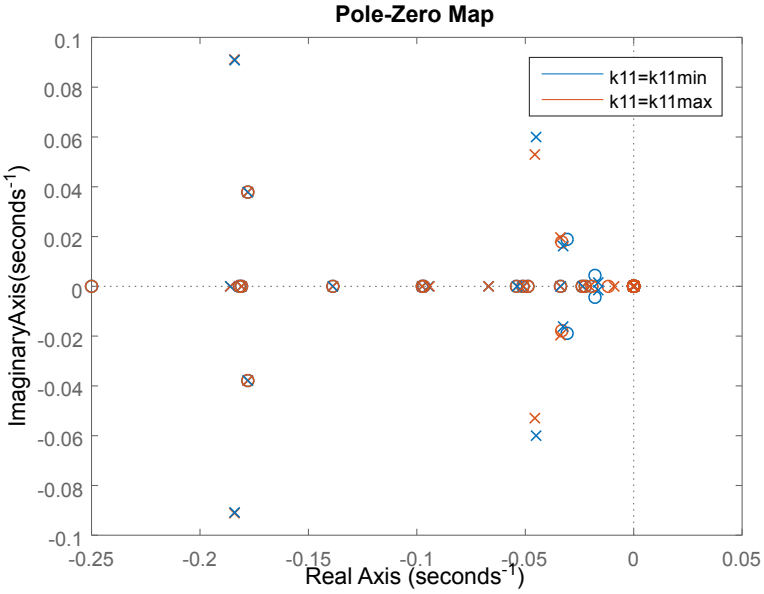

Figure 2.18: Pole-zero map of closed loop system with DFC gain matrix.

Table 2.4: Simulation conditions.

Items	Values	Unit	Remarks
Set point r_1	5.0	[C]	
Set point r_2	0.0	[bar]	
Disturbance w_1	$16.0\sin(\frac{\pi}{400})t$	[C]	
Disturbance w_2	0.0	[bar]	
Step time of set points	1.0	[sec]	
Step time of disturbances	600	[sec]	
Simulation time T	1600	[sec]	
Control output u_{k1}	[-4.0, 4.0]	[-]	input constraint
Control output u_{l1}	[-1.0, 1.0]	[-]	input constraint
Control output u_{k2}	[-10.0, 15.0]	[Hz]	input constraint
Control output u_{l2}	[-5.0, 5.0]	[Hz]	input constraint

2.4.4 Simulation Results

Now simulation tests are examined on simulation conditions in Table 2.4. The simulation results are obtained with linear transfer function models, which are identified from experimental data. Step response and load disturbance response are evaluated for PI with/without robust DFC and with/without anti-windup controller as shown as Fig. 2.19 and Fig. 2.20 . Each design method is evaluated for three cases, where the actual superheat gain is set to $k_{min} = -10.64$ as case 1, $k_{max} = -8.71$ as case 2, $k_n = -9.68$ as case 3.

The results show that both sets of limiters, Λ_{k1} and Λ_{k2}, work correctly and wind-up phenomena can be avoided with the proposed method, PI+DFC with anti-windup control. In addition, the proposed method can follow the no saturation behaviour whenever the signals are unsaturated. In other word, the proposed method can achieve improved performance compared to the controller with saturation block only.

It can also be confirmed that DFC yields the intended disturbance attenuation, even after the system is discretized and anti-windup gains are introduced.

Table 2.5 shows the evaluation results of each design. Five designs are examined, and then evaluated by four performance items. Item number 1 and 2 evaluate the robustness against model uncertainties δ. For these items, we compute the performances $\max_{t\in[0,T]} |y_{case_i}(t) - y_{case_j}(t)|,\ i = 1,2,3, j = 1,2,3$ as shown in Fig. 2.21. Items number 3 and 4 are simply the maximum values of y_1 and y_2 to evaluate the wind-up phenomena. Design number one, PI + robust DFC with anti-windup controller obtains the best values (minimum values) for all items within the control limiters. On the other hand, design number two, PI + robust DFC *without* anti-windup exhibits worse the performance due to the windup phenomena as shown in Table 2.5 and Fig. 2.19.

Design number three, PI + robust DFC with no saturation obtains smaller values than design number one. However, design number three does not take saturation into account, which means that this design will not work in many real applications.

In design numbers four and five, the PI control alone shows poorer control performance compared to the PI + robust DFC. To conclude, the proposed design, PI control + robust DFC with anti-windup controller, exhibits the best simulation performance while respecting the input constraints.

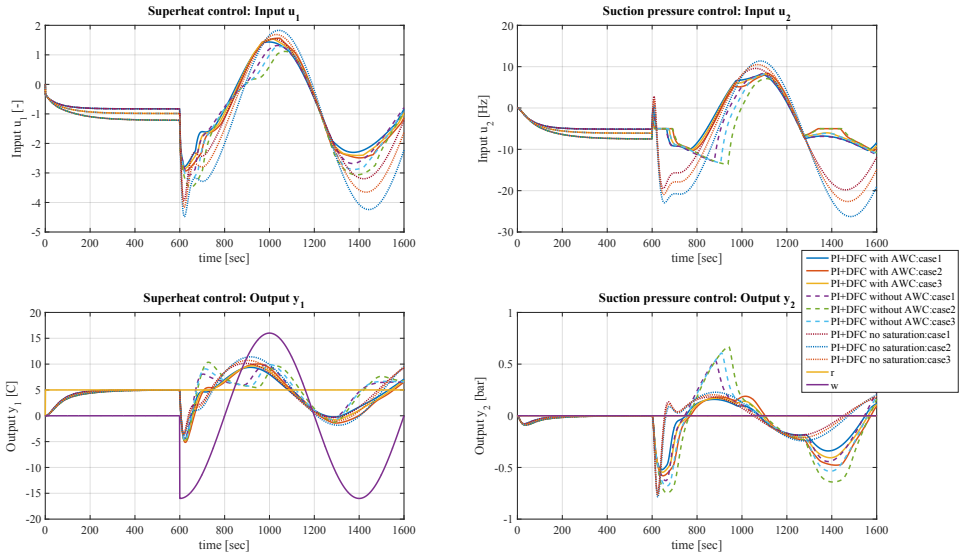

Figure 2.19: Simulation results of the PI control + robust DFC.

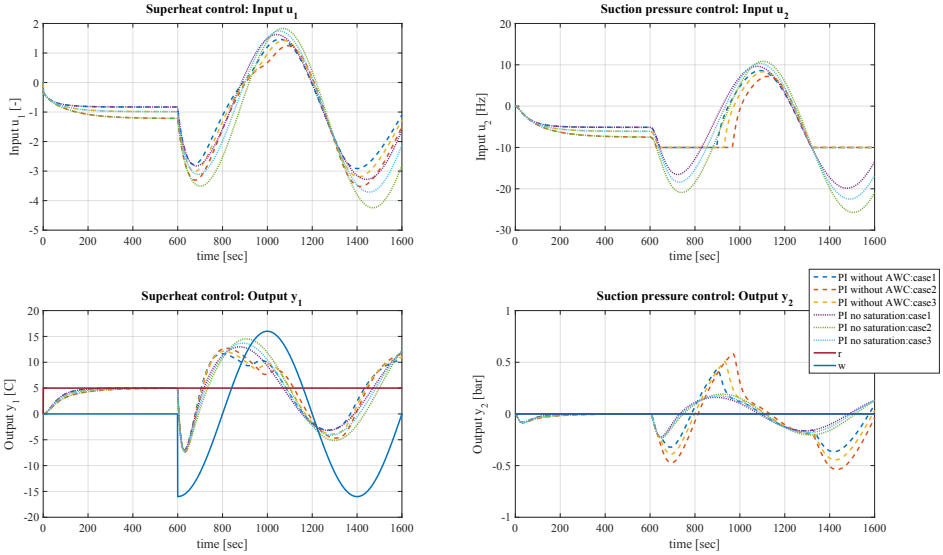

Figure 2.20: Simulation results of the PI control.

Table 2.5: Evaluations of each control design.

	Design method number	1	2	3	4	5
Item number	Description	PI + Robust DFC with AW	PI + Robust DFC without AWC	PI + Robust DFC no saturation	PI control without AWC	PI control no saturation
1	Robustness from δ_{y_1}	**1.9114**	3.6732	*1.8311*	2.5681	2.8069
2	Robustness from δ_{y_2}	**0.3405**	0.4905	*0.1016*	0.4365	*0.0565*
3	Maximum value y_1	**10.0221**	10.3608	11.4051	12.7000	14.5240
4	Maximum value y_2	**0.1887**	0.6709	0.2278	0.5811	0.1915

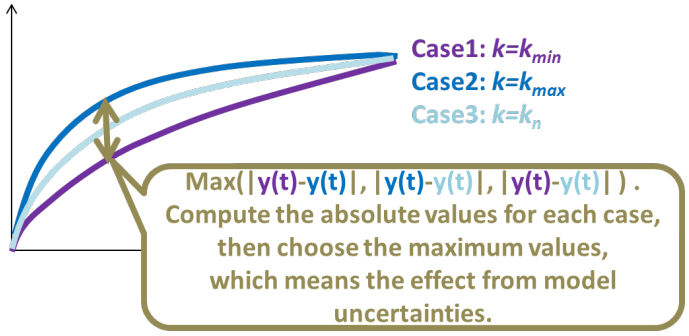

Figure 2.21: An explanation of the item number 1 and 2, the robustness of controllers from model uncertainties.

2.4.5 Experimental Results

Table 2.6 and 2.7 show set point values of the test system and the experimental conditions, respectively. The temperature of the water tank is set at 14 degrees for the initial condition. Then the set point is changed to 15.0 degrees, and kept there for the first 500 seconds for making a load disturbance response. Next, the set point is changed to 16.0 degrees from 501 to 1000 seconds in order to test that the anti-windup controllers work correctly. The set point is changed back to 14 degrees after 1000 seconds, and kept there for additional 1000 seconds. Experimental data is sampled each second, and the data is evaluated for 2000 seconds in total.

Fig. 2.22 shows PI control without anti-windup controllers. Fig. 2.23 and 2.24 show a disturbance response of PI control + robust DFC with/without anti-windup controllers. The test results show that both control configurations, PI+DFC with and without anti-windup, can improve the performance of the superheat control.

In addition, PI control + robust DFC with anti-windup can avoid wind-up phenomena from 1000 - 1200 seconds, and demonstrates more accurate regulation compared to PI control + robust DFC without anti-windup controllers.

We also confirmed that the windup phenomenon during 1000-1200 seconds affects the cross-coupled output (superheat y_1), when the suction pressure speed (u_2) is saturated in the design without anti-windup controller. This result indicates that the anti-windup design is also effective for MIMO systems.

Table 2.8 shows Integral Absolute Error (IAE) of the superheat control and suction pressure control for the three control design methods. The IAE of suction pressure with PI + robust DFC without anti-windup obtained 104.9,

which was a poorer performance than the PI without anti-windup, IAE=84.2, due to the lower priority of the weighting function W. However, the IAE of proposed method, PI + robust DFC with anti-windup, amounted to 89.7, which means that the proposed method can recover the performance.

The superheat control with PI + DFC with/without anti-windup control obtained IAE=1966.4 and IAE=2220.5 respectively. The IAE of PI control without anti-windup control amounted to 3472.7, which means that the proposed method achieved 43 % better performance than only PI control alone without anti-windup.

Table 2.6: Set point values of the test system.

Set point	Value	Controlled by
Superheat	10.0 [C]	PI with/without DFC
Suction pressure	2.8 [*bar*]	PI with/without DFC
Condenser	9.0 [*bar*]	PI
Water tank (initial condition)	14.0 [C]	PI

Table 2.7: Experimental conditions.

Items	Values	Unit	Remarks
Load disturbance by changing	14.0 $\rightarrow$ 15.0	[C]	
the setpoint of water tank w_1	$\rightarrow$ 16.0 $\rightarrow$ 14.0		
Experimental time T	2000	[sec]	
Control output u_{k1}	[-5.0, 5.0]	[-]	input constraint
Control output u_{l1}	[-2.5, 2.5]	[-]	input constraint
Control output u_{k2}	[-10.0, 15.0]	[Hz]	input constraint
Control output u_{l2}	[-5.0, 7.5]	[Hz]	input constraint

Table 2.8: IAE of the experimental results.

	PI + robust DFC with AWC	PI + robust DFC without AWC	PI without AWC
The superheat control	1966.4	2220.5	3472.7
The suction pressure control	89.7	104.9	84.2

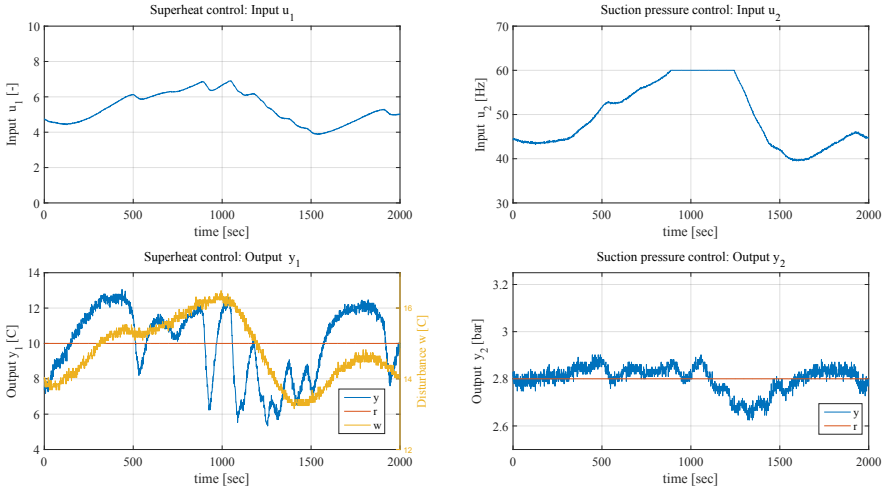

Figure 2.22: Experimental results of PI control without anti-windup controllers.

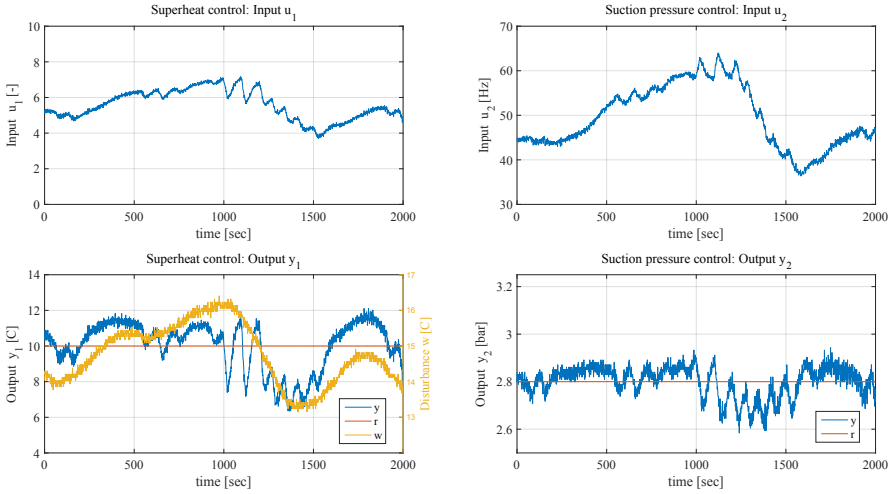

Figure 2.23: Experimental results of PI control + robust DFC without anti-windup controllers.

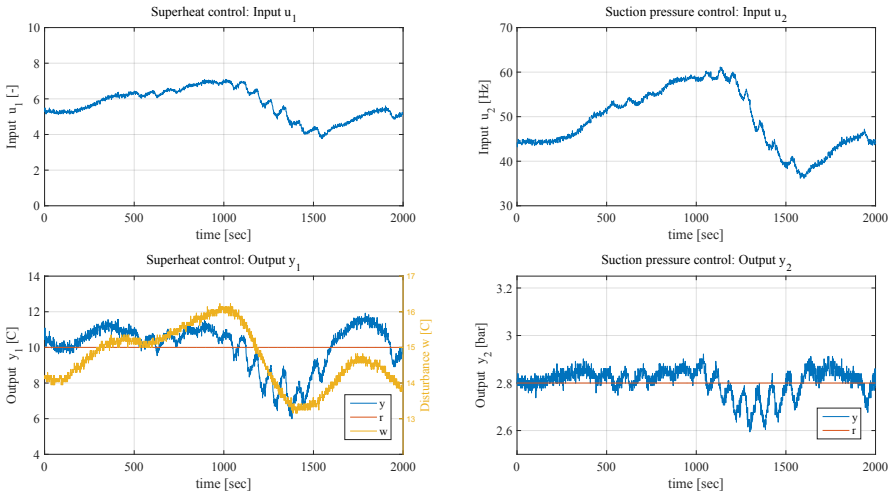

Figure 2.24: Experimental results of PI control + robust DFC with anti-windup controllers.

3 Application 2: Crane Systems

This chapter presents an anti-sway control scheme for crane systems using robust DFC designed to minimize the sway angle and trolley position errors via LMI. The robust DFC is added to an existing crane control system composed of a feed forward and state feedback control. Both simulation and test results for the crane system shows improvements in control performance when the gantry load is subjected to impulse force disturbances.

3.1 Crane System Model

The crane system model considered in this work is taken from [Ackermann, 2002]. It is described by the nonlinear coupled differential equations

$$(m_T + m_L)\ddot{x}_T + m_L l\ddot{\theta}\cos\theta - m_L l\dot{\theta}^2 \sin\theta = F \tag{3.1}$$

$$\ddot{x}_T \cos\theta + l\ddot{\theta} + g\sin\theta = 0 \tag{3.2}$$

where m_T and m_L are masses of trolley and load, x_T is the trolley position along the supporting rail, θ is the angle of the load from vertical, l is the length of the suspension rope, g is the gravitational acceleration and F is the force applied to the trolley via the drive train (command input); see also Fig. 3.1.

For the sake of both the conventional design and the subsequent LMI-based DFC design, the model has to be linearized in an operating point. Assuming θ to be small, we can make the simplifications

$$\sin\theta \approx \theta,\ \cos\theta \approx 1,\ \sin^2\theta \approx 0,\ \dot{\theta}^2 \approx 0 \text{ , and } x \approx l\theta$$

where x is the position of the load along the x_T-axis. These approximations yield the linear model

$$m_T\ddot{x} = F + m_L g\theta \tag{3.3}$$

$$m_L(\ddot{x}_T + \ddot{x}) = -m_L g\theta, \tag{3.4}$$

which will be used for control design.

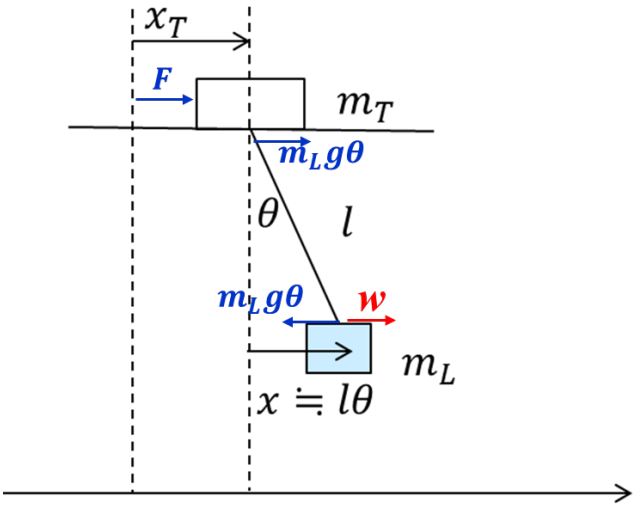

Figure 3.1: A crane model for control design.

The motor force to the trolley F is given by a inverter, which regulates the trolley speed:

$$F = G_{asr}(u_T - \dot{x}_T), \tag{3.5}$$

where G_{asr} is the Auto Speed Regulator (ASR) gain, u_T is the reference of trolley speed, and $\dot{x}_T$ is the trolley speed.

Equations (3.3)–(3.5) are combined into the LTI description

$$\dot{x}_p = Ax_p + B_2 u_T,$$

where $x_p = (\dot{x}_T \quad \dot{x} \quad x_T \quad x)^{\mathrm{T}}$ is the state vector, and

$$A = \begin{pmatrix} \frac{-G_{ASR}}{m_T} & 0 & 0 & \frac{g}{l}(\frac{m_L}{m_T}) \\ \frac{G_{ASR}}{m_T} & 0 & 0 & \frac{-g}{l}(\frac{m_L}{m_T}+1) \\ 1 & 0 & 0 & 0 \\ 0 & 1 & 0 & 0 \end{pmatrix}, \tag{3.6}$$

$$B_2 = \begin{pmatrix} \frac{G_{ASR}}{m_T} \\ \frac{-G_{ASR}}{m_T} \\ 0 \\ 0 \end{pmatrix} \tag{3.7}$$

are the system dynamics and input matrices, respectively.

3.1.1 Existing controller

The feedforward controller K_{FF} is designed by reference data set based on the oscillation cycle of hoisting loads. The data set of acceleration and deceleration was obtained from measurements of the trolley speed carried out on an actual gantry crane [MIYOSHI et al., 1998]. A reference trajectory for the trolley velocity $\dot{x_T}$ was designed to avoid oscillations in the load to the greatest degree possible. The rest of the state variable trajectories, i.e., trolley position x_T, load position $x = l\theta$, and horizontal load velocity $\dot{x}$, are calculated with control input data $u_T = x_T$.

The state feedback control K_{FB} is defined as

$$u_k = K_{FB} x_p, \tag{3.8}$$

where $K_{FB} \in \mathbb{R}^{m \times n}$ is a standard state feedback gain matrix, in this case designed via pole placement.

3.2 Disturbance Feedback Control Design

This section presents a robust DFC design method for state feedback control using LMI optimization.

The bottom diagram in Fig. 3.2 shows the closed-loop system with DFC, where r is the reference input, $u_T = u_k + u_l$ is the control input, w is the disturbance, B_1 is a gain matrix for w, A and B_2 are matrices of the plant model. The existing controller is specified by a feedforward term K_{FF} and a feedback term K_{FB}. The DFC comprises a nominal plant model specified by parameter matrices A_n and B_{2n} along with the disturbance feedback L. The true states of the plant are denoted x_p, while x_{pn} contains the state values of the nominal plant.

Fig. 3.3 shows a general closed-loop system in a two input, two output formulation (left) and the closed-loop DFC design configuration (right). As per usual, the design consists of choosing L such that the transfer function T from w to z, where z is the output for evaluating the performance of the controlled systems, becomes small in some sense. We assume that K_{FF} and K_{FB} are fixed; that is, the existing controller is considered as part of the plant P. Thus, P includes the true plant G, the nominal model G_n, and the existing controller K in the robust DFC design setup.

3.2.1 Parametric Uncertainty Model

To achieve a robust design, parametric uncertainties in the crane system model must be considered. Let the true plant be

$$\dot{x}_p = A x_p + B_2 u_T, \tag{3.9}$$

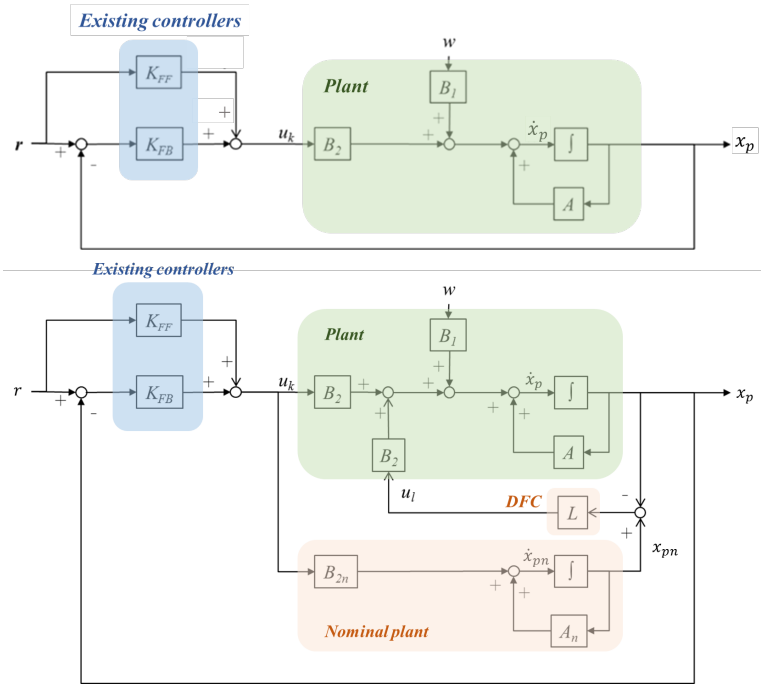

Figure 3.2: Top: Block diagram of an existing crane control system. Bottom: The control system augmented with Disturbance Feedback Control.

with the plant parameters $A \in \mathbb{R}^{n\times n}$ being affected by parametric uncertainties of the form, which is the same description as (2.18) in Chapter 2.

The Disturbance Feedback Controller (DFC) is chosen as

$$u_l = L\epsilon, \tag{3.10}$$

where $L \in \mathbb{R}^{m\times n}$ is the disturbance feedback gains, $\epsilon = x_{pn} - x_p$, and $x_{pn} = \begin{pmatrix} \dot{x}_{Tn} & \dot{x}_n & x_{Tn} & x_n \end{pmatrix}^{\mathrm{T}} \in \mathbb{R}^{n\times 1}$ is the state vector of the nominal plant model.

The extended state space representation of the overall system can be written as follows;

$$\begin{aligned} \dot{x}_{pp} &= A_{pp}x_{pp} + B_{pp1}w + B_{pp2}u_l \\ z &= C_z x_{pp} + D_z u_l \end{aligned} \tag{3.11}$$

where

$$x_{pp} = \begin{pmatrix} \dot{x}_T & \dot{x} & x_T & x & \dot{x}_{Tn} & \dot{x}_n & x_{Tn} & x_n \end{pmatrix}^{\mathrm{T}},$$

$$A_{pp} = \begin{pmatrix} A_\delta - B_2K_{FB} & 0 \\ 0 & A_n - B_2K_{FB} \end{pmatrix},$$

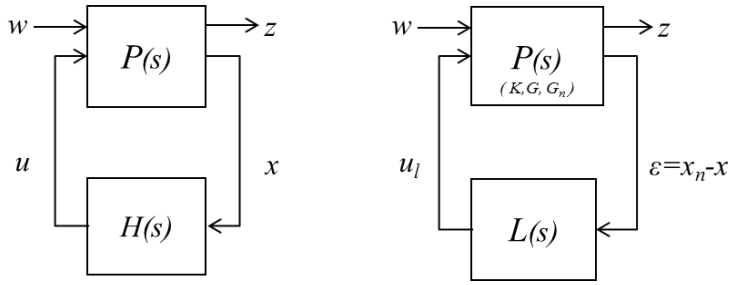

Figure 3.3: Closed-loop setup for design of an H_∞ controller $H(s)$ (Left), and the corresponding setup for design of DFC $L(s)$ (Right).

$$B_{pp1} = \begin{pmatrix} B_1 \\ 0 \end{pmatrix}, B_{pp2} = \begin{pmatrix} B_2 \\ 0 \end{pmatrix},$$
$$C_z = \begin{pmatrix} -I & 0 \end{pmatrix}, D_z = 0,$$

and w is an input disturbance, and A_δ can be any extremal value of A in (**??**).

The closed loop transfer function T from w to z is computed as follows:

$$\begin{aligned} \dot{x}_{pp} &= \mathcal{A}_\delta x_{pp} + \mathcal{B} w \\ z &= \mathcal{C} x_{pp} + \mathcal{D} w, \end{aligned} \tag{3.12}$$

where

$$\left(\begin{array}{c|c} \mathcal{A}_\delta & \mathcal{B} \\ \hline \mathcal{C} & \mathcal{D}, \end{array}\right) = \left(\begin{array}{cc|c} A_\delta - B_2 K_{FB} - B_2 L & B_2 L & B_1 \\ 0 & A_n - B_2 K_{FB} & 0 \\ \hline -I & 0 & 0 \end{array}\right).$$

3.2.2 Optimization Problem of robust DFC Design

The optimization problem of robust DFC design is given as follows:

$$\underset{X_1, X_2, Y, W}{\text{minimize}} \quad \gamma, \tag{3.13}$$

$$\text{subject to;} \tag{3.14}$$

$$\begin{pmatrix} \mathcal{A}_\delta{}^{\mathrm{T}} \mathcal{X} + \mathcal{X} \mathcal{A}_\delta & \mathcal{B} & \mathcal{X} \mathcal{C}^{\mathrm{T}} \\ \mathcal{B}^{\mathrm{T}} & -\gamma I & \mathcal{D}^{\mathrm{T}} \\ \mathcal{C} \mathcal{X} & \mathcal{D} & -\gamma I \end{pmatrix} < 0,$$

$$\mathcal{X} = \begin{pmatrix} X_1 & 0 \\ 0 & X_2 \end{pmatrix}, \quad \mathcal{X} > 0, \quad \gamma > 0,$$

$$\begin{pmatrix} X_1 & Y \\ Y & \mu^2 I \end{pmatrix} > 0, \begin{pmatrix} X_2 & W \\ W & \mu^2 I \end{pmatrix} > 0,$$

where $Y := LX_1$, $W := LX_2$, and μ is the upper limit of the control signal, i.e., the trolley velocity. In the above, the subscript-δ notation should as usual be understood as requiring the LMIs to be satisfied for all extremal points of δ_a to yield one common $\mathcal{X}$.

3.2.3 Numerical Examples

This subsection demonstrates the robust DFC design for an example gantry crane system.

3.2.4 Modeling of the Crane Systems

The nonlinear system (3.1)–(3.2) is simulated in Matlab using the built-in fixed-step `automatic solver selection` solver with the parameter values given in Table 1. The existing controller and the DFC are designed based on the linearized model with parameter matrices (3.6)-(3.7). The DFC is furthermore allowed knowledge about the permitted changes in the parameter l (shown in the table). The nominal model G_n is thus given by

$$A_n = \begin{pmatrix} -6.25 & 0 & 0 & 1.960 \\ 6.25 & 0 & 0 & -2.352 \\ 1.00 & 0 & 0 & 0 \\ 0 & 1.0 & 0 & 0 \end{pmatrix}, B_{2n} = \begin{pmatrix} 6.25 \\ -6.25 \\ 0 \\ 0 \end{pmatrix}$$

where A_n is the nominal model with rope length set to 25 m.

Fig. 3.4 shows the reference data set r for state $\dot{x}_T$, $\dot{x}$, x_T, and x. This data set is created in advance according to the following rules:

- The acceleration/deceleration of the trolley should be piecewise constant.
- The trolley position profile must match the fundamental load oscillation period.
- The angle θ and $\dot{\theta}$ should be zero when the acceleration and deceleration phases are finished.

The state feedback controller K_{FB} is designed by standard pole placement:

$$K_{FB} = \begin{pmatrix} 3.8708 & 3.5494 & 1.5625 & -0.6732 \end{pmatrix}. \tag{3.15}$$

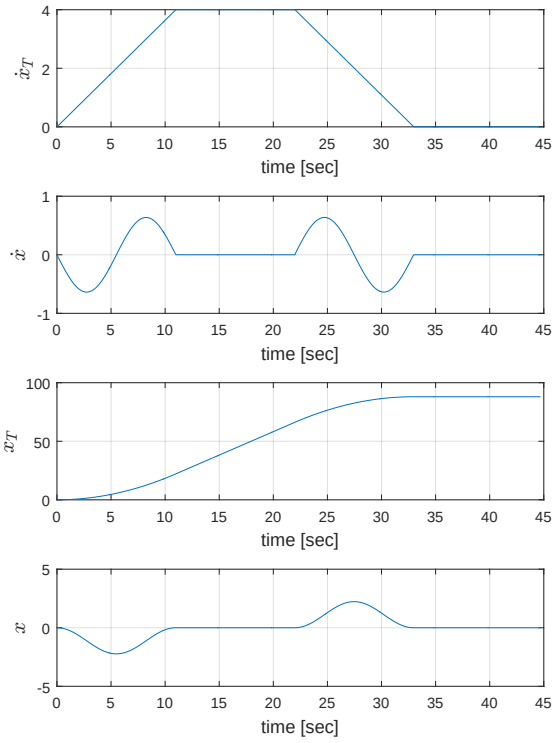

Figure 3.4: A reference data set r for state $\dot{x}_T$, $\dot{x}$, x_T, and x ($x := \theta l$).

3.2.5 Robust DFC Design

The optimal H_∞ performance achieved by solving the optimization problem in (3.13) was $\gamma = 0.5052$, and the robust DFC gain is obtained as follows,

$$L = \begin{pmatrix} 14.2388 & 11.9464 & 2.5123 & -10.7141 \end{pmatrix}. \tag{3.16}$$

The design may for example be analyzed in the frequency domain. Bode plots of T are shown in Fig. 3.5, where it is seen that the proposed design is able to achieve better disturbance attenuation for all state variables than the conventional control, especially for frequencies less than 20 [rad/sec].

Table 3.1: Parameter values of the crane system model.

Parameter	Value	Unit
m_T	10×10^3	kg
m_L	50×10^3	kg
l	[5, 45]	m
g	9.8	m/s^2
G_{asr}	62.5	-

3.2.6 Simulation Results

The system's response to position set point changes and disturbances are then examined to compare the conventional control and proposed control. A summary of the simulation conditions are shown in Table 3.2.

Fig. 3.6 and Fig. 3.7 show simulation results of Fuji's existing control (left), and Fuji's control with robust DFC (right). The robust DFC did not disturb the original control during the set point change, and thus $\dot{x}_T$, $\dot{x}$, x_T, and x, are almost identical for both control methods for the first minute. On the other hand, as can be seen, the robust DFC went into action to attenuate the load sway when an impulse force was applied to the load. Impulse disturbances could for instance represent sudden gusts of wind or collisions during the operation of the gantry crane system.

The simulation in case 3, which has the shortest rope length with l=5m, exhibits the worst sway for both control methods. Here, the proposed method shows noticeably better performance than the conventional method, but in fact one can notice better attenuation in all three cases. Table 3.3 shows evaluation values in simulation results of the disturbance responses. The proposed method improved the maximum and minimum load angle θ by 0.04 and 0.08 radians, respectively, which means DFC decreased the sway by 4.58 degrees in total. In addition, the settling time was improved by between 1.22 seconds (case 2, l = 45m) and 2.07 seconds (case 3, l = 5m). As a result, the proposed method demonstrated the improvement of anti-sway control when an impulse disturbance is applied. Also, while 4.6 degrees may not sound like much, it is worth noting that the simulation considers a 50-ton load.

Table 3.2: Simulation conditions.

Item	Value	Unit
Sampling time	10^{-3}	s
Set point of trolley	88	m
Upper limit of trolley velocity	6.0	m/s
Simulation time	100	s
Time of impulse disturbance	60	s
Pulse width of disturbance	2	s
Pulse amplitude of disturbance	2×10^5	N

Table 3.3: Simulation results of the disturbance responses.

Item	Conventional method $(K_{FF} + K_{FB})$	Proposed method $(K_{FF} + K_{FB} + DFC)$
Maximum angle	0.68 rad	0.64 rad
Minimum angle	-0.16 rad	-0.12 rad
Maximum settling time	89.49 s	88.27 s
Minimum settling time	66.12 s	64.04 s

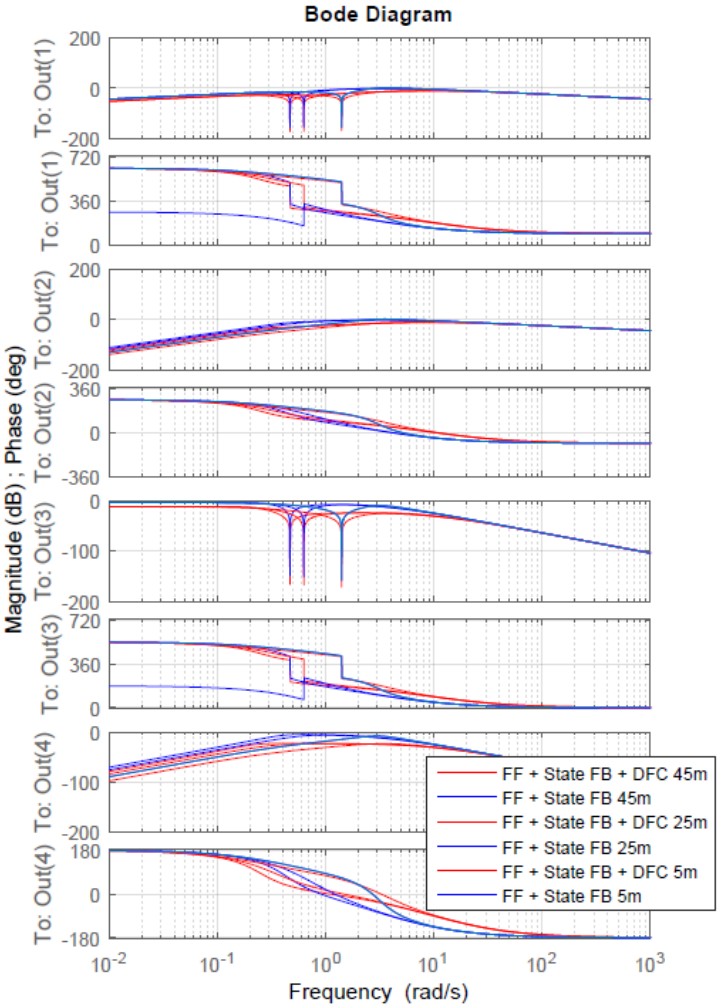

Figure 3.5: Bode plots of closed loop system transfer function from w to z.

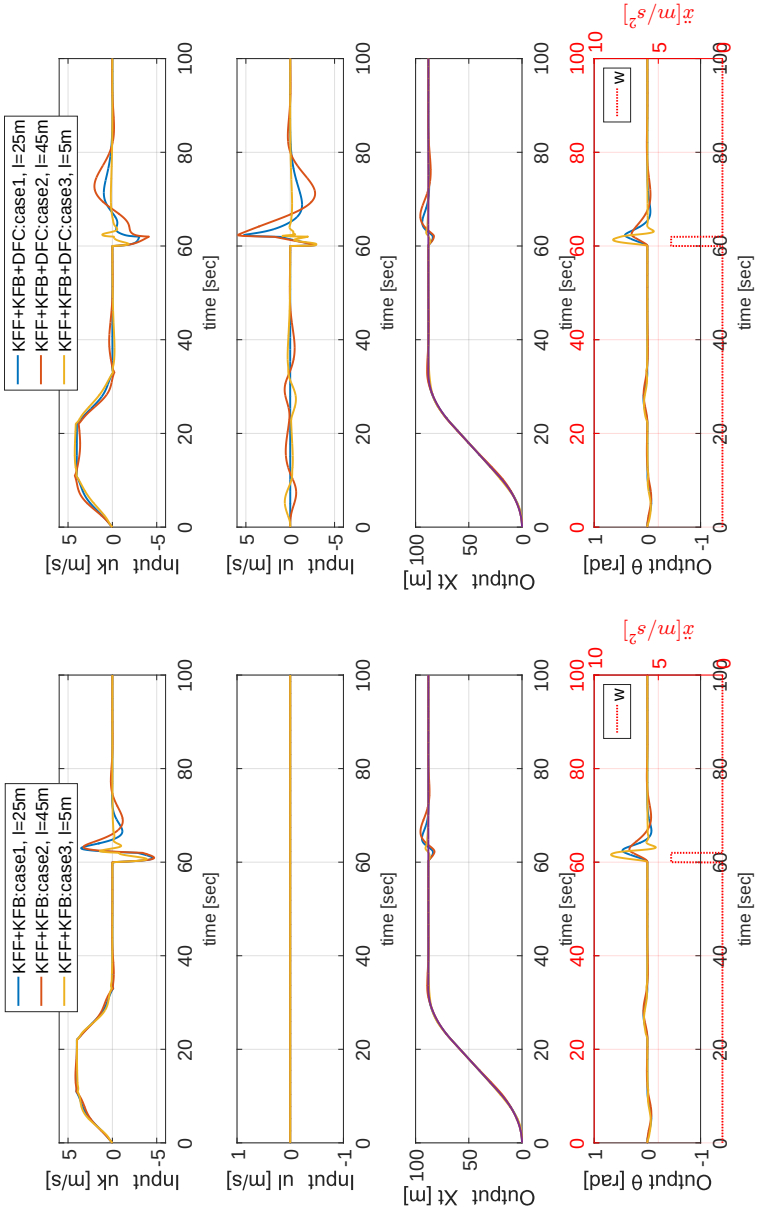

Figure 3.6: Simulation results of Fuji's conventional control (left), and Fuji's control with robust DFC (right).

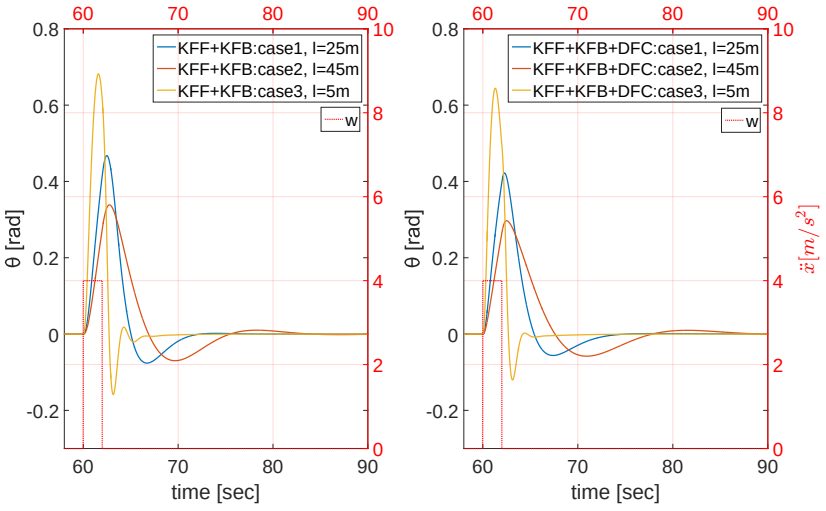

Figure 3.7: Zoom on the sway angle in the disturbance responses.

3.3 Verification of Robustness against Internal Uncertainty in Frequency Domain

Robust stability against internal uncertainties in frequency domain is considered for robust DFC L which was solved in 4.2. Multiplicative uncertainties Δ and its weight function W_u are added to the plant model set G which includes the parametric uncertainties in 2.3. Transfer function from u to $\tilde{u}$ in Fig. 3.8 is represented by

$$T_{\tilde{u}u} = -(LG_nK_{FB}G + LG + K_{FB}G) \tag{3.17}$$

where G is plant model set, G_n is nominal plant model represented by transfer function, K_{FB} is state feedback controller which is given in (3.15), and L is robust DFC which is solved in (3.16).

The model of weight function W_u is chosen as first order systems.

$$W_u = \kappa\frac{s+\beta}{s+\alpha} \tag{3.18}$$

where κ, α, and β are tuning parameters in order to find the worst case of $|W_u||T_{\tilde{u}u}| < 1$

An example of the worst case of W_u is given with κ=2.27210523, α=1000, and β=0.0001. W_u gives magnitude more than 0 [dB] in the high frequency area 500-10000 [rad/sec]. The peak gain of $W_uT_{\tilde{u}u}$ gives -0.975 [dB] at 0.457 [rad/sec].

The figure shows that the optimized DFC L including parametric uncertainties can be robust against the high frequency domain.

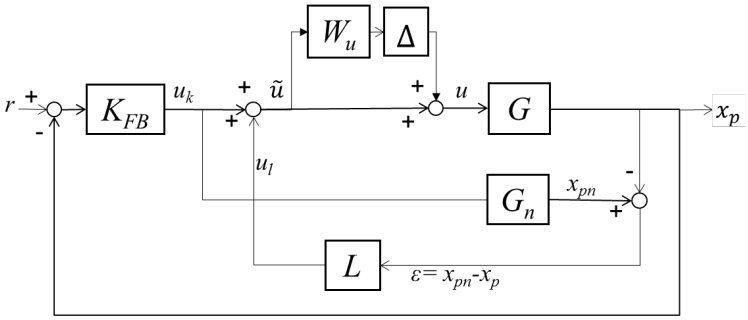

Figure 3.8: Block diagrams of a crane control system with DFC, and multiplicative uncertainty $W_u\Delta$ is added to the plant set G.

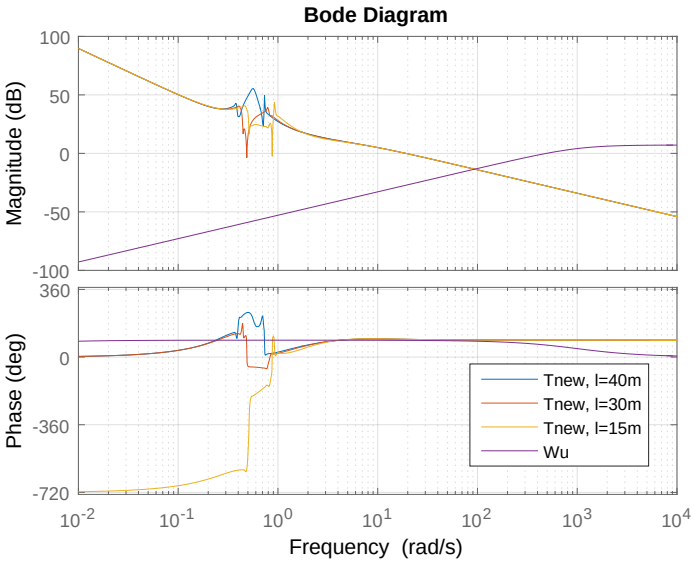

Figure 3.9: Bode diagram of weight function W_u, and transfer function from $\tilde{u}$ to u, $T_{\tilde{u}u}$ with each corner points of parametric uncertainties.

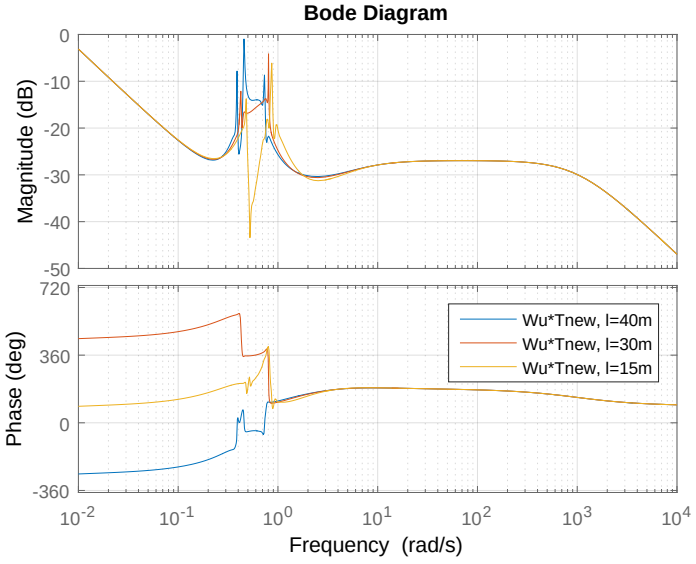

Figure 3.10: Bode diagram of $W_u T_{\tilde{u}u}$ for verification of the robustness against additional frequency domain uncertainties.

3.4 Comparison of Nonlinear Model and Linear Model

Paper E evaluated the robustness against the disturbance only with nonlinear model. Here, a comparison of nonlinear and linear models is undertaken to evaluate how the model differences are effected against disturbances.

Fig. 3.11 and Fig. 3.12 show impulse disturbance responses, where Fuji's existing control is shown on the left, and Fuji's control with robust DFC is shown on the right.

Basically, the linear model shows similar behavior as the nonlinear model, however, the nonlinear model has larger load sway than linear model for all three cases. Regarding robsut DFC, both models show that existing controllers with DFC can attenuate the load sway compared to the existing controller by itself.

In addition, difference between nonlinearites and linearities occurs biggest when rope length is shortest in case 3. The reason is that the case 3 has the biggest sway so that approximation error in $\sin\theta \approx \theta$ gets the largest as well.

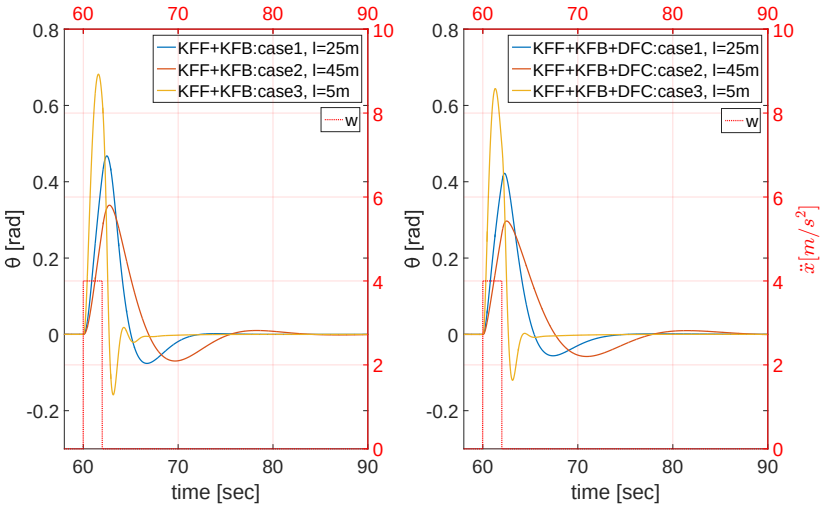

Figure 3.11: Zoom on the sway angle with *nonlinear* model in the disturbance responses.

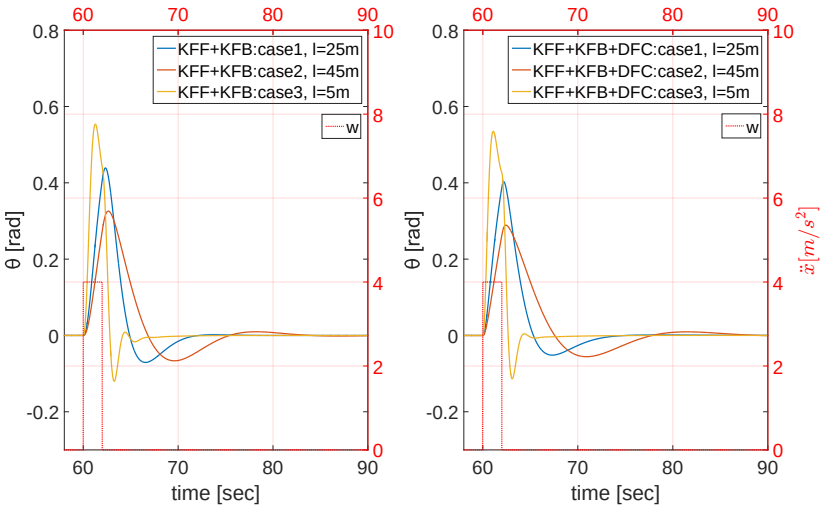

Figure 3.12: Zoom on the sway angle with *linear* model in the disturbance responses.

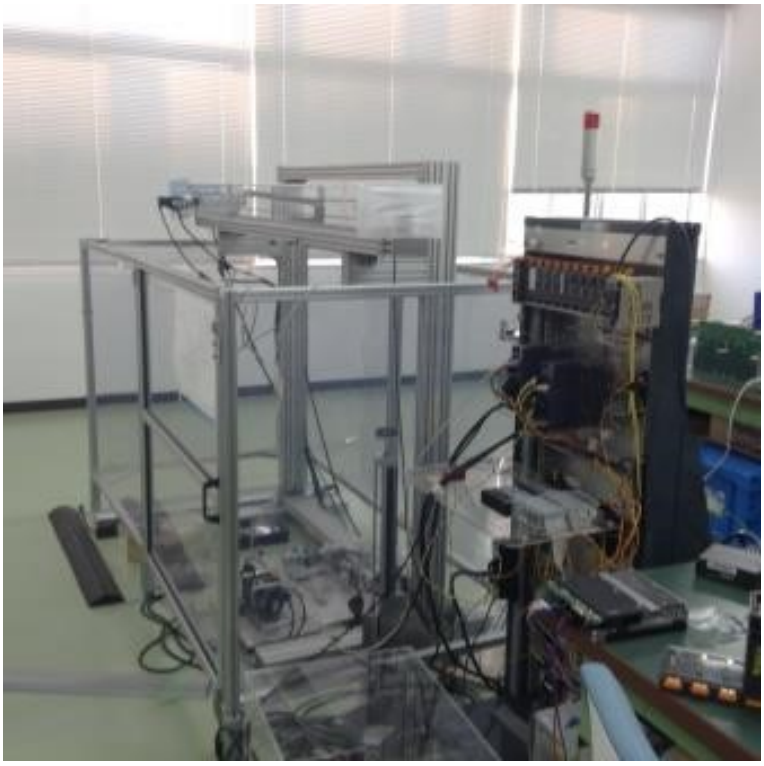

Figure 3.13: Crane system setup at Fuji' s laboratory in Japan.

3.5 Lab Test at Fuji Electric

Lab test of crane system is carried out at Fuji Electric for verification of proposed method. The system is scaled down from the huge harbor gantry crane to a laboratory scale, but the crane model (with different parameters) is reused to emphasize that the proposed model and design methodology can be feasible when the size of system is changed.

The lowest-spec PLC in Fuji's lineup, the SPH200 shown in Fig. 3.14, is chosen from Fujis's CPU module lists. For comparison of CPU modules, the highest spec module, which is SPH3000MG, carries out ultra-high-speed processing with 6 nanosecond(ns). On the other hands, SPH200 takes 70 ns for the same processing. The reason to choose SPH200 is that it is necessary to examine whether the proposed method can be available on such a cheep device implementation.

Figure 3.14: A picture of SPH200, CPU module of Fuji Electric.

Table 3.4: Parameter values of the lab system model.

Parameter	Value	Unit
m_T	2.01	kg
m_L	0.43	kg
l	[0.8 1.0]	m
g	9.8	m/s^2
G_{asr}	57.43	-

3.5.1 System Parameters

This subsection demonstrates the robust DFC design for an lab test of crane system.

3.5.2 Modeling of the Crane Systems

The crane system is controlled by PLC, which calculates the fixed-step with the parameter values given in Table 3.4. The existing controller and the DFC are designed based on the linearized model using LMI optimization.

For existing control, the state feedback controller K_{FB} is designed by standard pole placement:

$$K_{FB} = \begin{pmatrix} 0.2072 & 0.1860 & 7.1429 & -0.2504 \end{pmatrix}. \tag{3.19}$$

The optimal H_∞ performance achieved by solving the optimization problem was $\gamma = 2.4024$, and the robust DFC gain is obtained as follows,

$$L = \begin{pmatrix} 0.5346 & 0.5051 & -0.0002 & -1.0188 \end{pmatrix}. \tag{3.20}$$

Table 3.5: Test conditions.

Item	Value	Unit
Sampling time	2×10^{-3}	sec
Set point of trolley	0.9	m
Upper limit of trolley speed	0.3	m/sec
Pulse width of input disturbance	1.0	sec
Pulse Amplitude of input disturbance	0.1	m/sec

Table 3.6: Test results of the disturbance responses.

Item	Conventional method ($K_{FF} + K_{FB}$)	Proposed method ($K_{FF} + K_{FB} + DFC$)
Maximum angle	2.36 $\times 10^{-2}$ rad	1.82$\times 10^{-2}$ rad
Minimum angle	-2.77$\times 10^{-2}$ rad	-2.12$\times 10^{-2}$ rad
Maximum settling time	10.8 sec	7.8 sec
Minimum settling time	10.6 sec	6.1 sec

The robust DFC design may be analyzed in the frequency domain. Bode plots of T are shown in Fig. 3.15, where it is seen that the proposed design is able to achieve better disturbance attenuation for all state variables than the conventional control, especially for frequencies around angular velocity $\omega = \sqrt{\frac{g}{l}}$, about 3.0 [rad/sec].

3.5.3 Test Results

Fig. 3.16, Fig. 3.17, and Fig. 3.18 show test results of Fuji's existing control with or without robust DFC. Regarding set point response, the robust DFC did not disturb the original control during the set point change. Fuji's existing control control with robust DFC improve the disturbance rejection, which means that less sway angle and shorten the settling time as well as shown in table 3.6. These improvement are shown for all rope length at 0.8 m, 0.9 m, 1.0 m respectively. The average improvement of sway angle was 29.5 %, and the robust DFC improves settling time by 3.9 seconds.

As results, the advantage of proposed method are verified thorough the lab test of crane systems. The results also indicated that the design method can be feasible when system scale is changed.

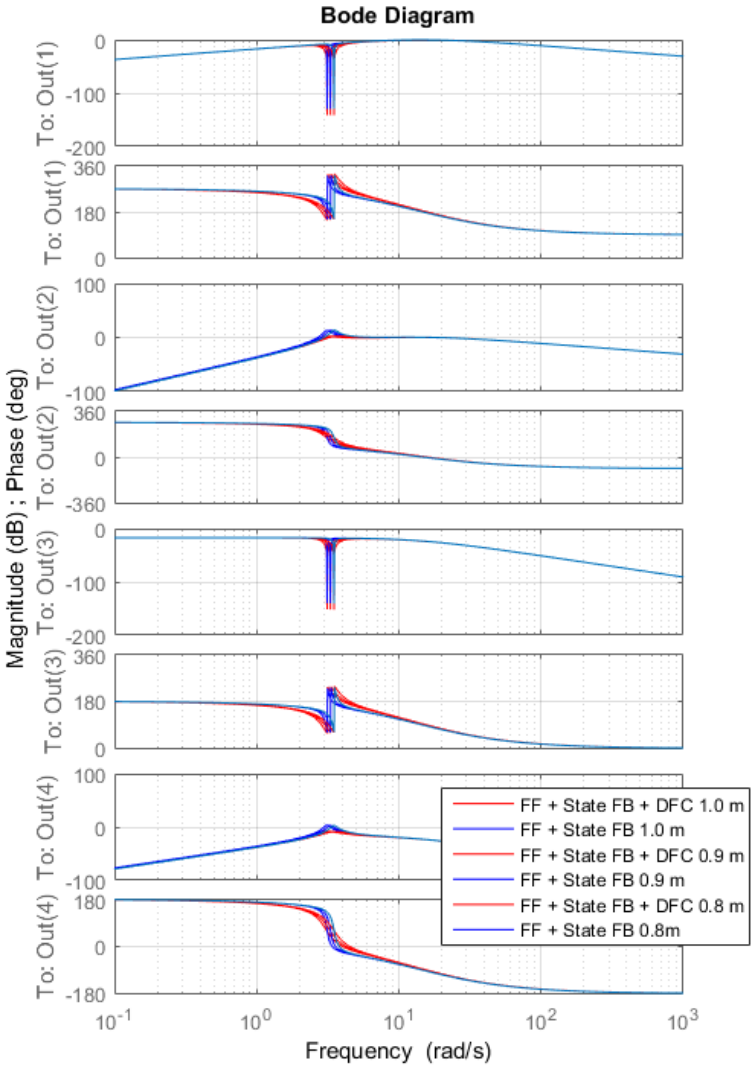

Figure 3.15: Bode plots of closed loop system transfer function from w to z for the lab system.

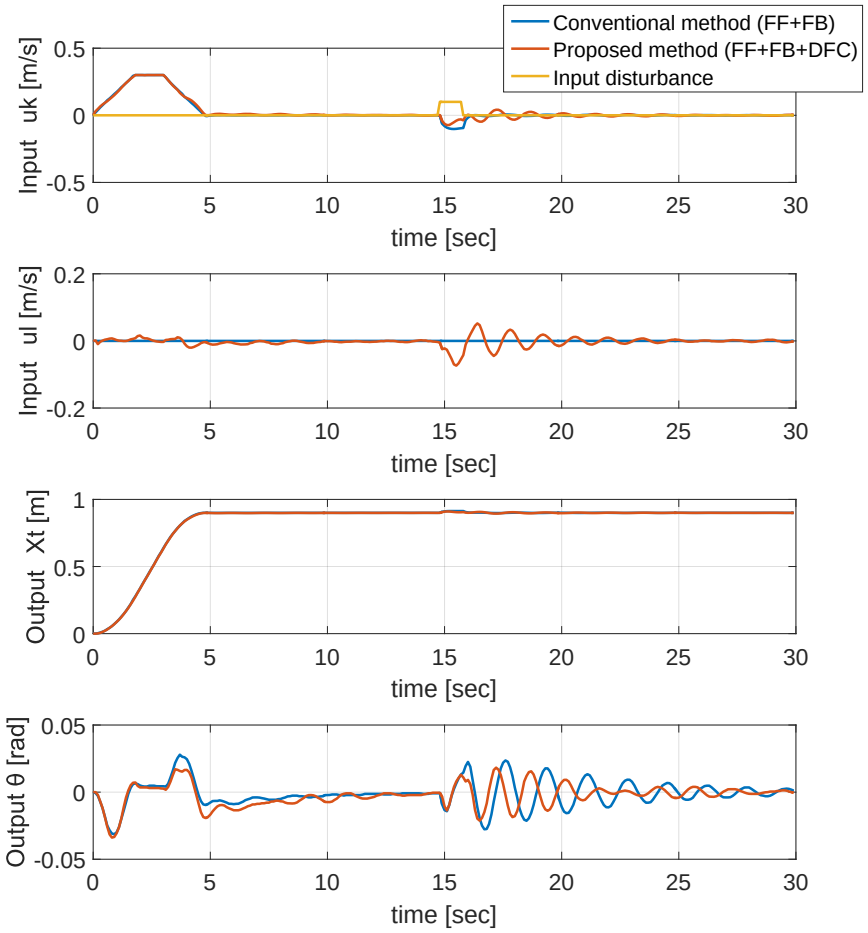

Figure 3.16: Test results of Fuji's conventional control with or without DFC at rope length 0.8 m.

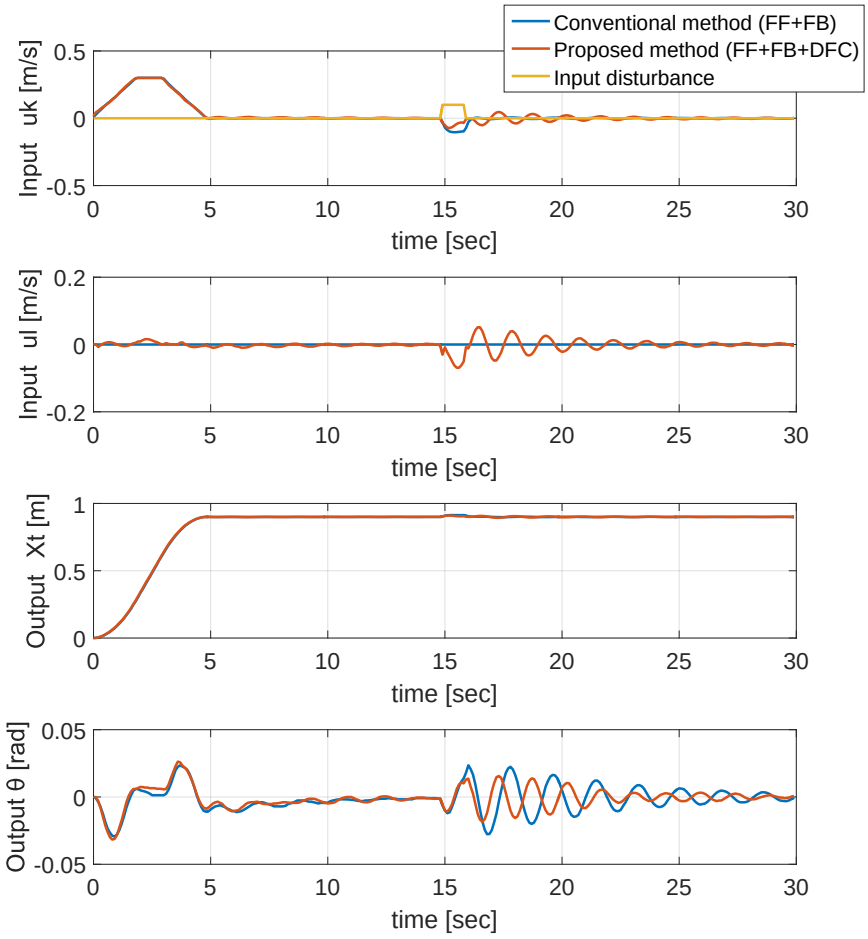

Figure 3.17: Test results of Fuji's conventional control with or without DFC at rope length 0.9 m

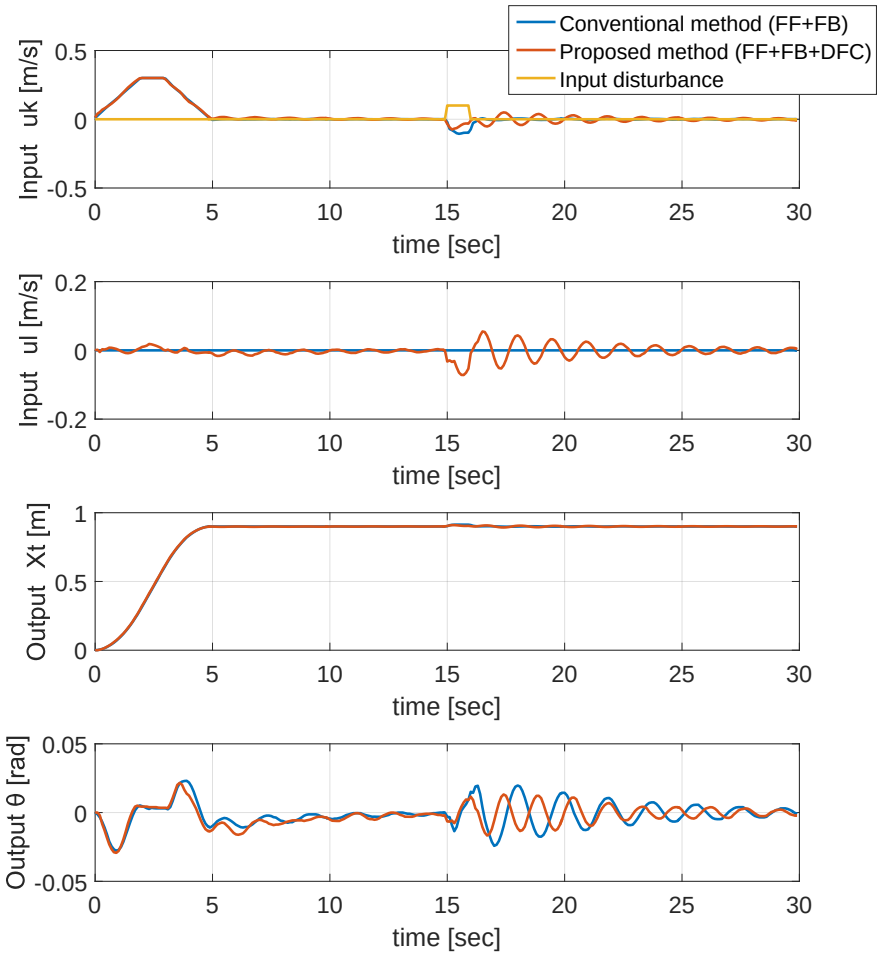

Figure 3.18: Test results of Fuji's conventional control with or without DFC at rope length 1.0 m

Table 3.7: Test results of the disturbance responses with additional load math.

Item	Conventional method ($K_{FF} + K_{FB}$)	Proposed method ($K_{FF} + K_{FB}$ $+DFC$)
Maximum angle	2.41×10^{-2} rad	1.74×10^{-2} rad
Minimum angle	-2.87×10^{-2} rad	-1.97×10^{-2} rad
Maximum settling time	12.4 sec	7.9 sec
Minimum settling time	11.9 sec	6.2 sec

3.5.4 Test Results of Robustness against Load Mass and Rope Length

Now the lab test is repeated again with additional load mass, which is a 100 g magnet attached to the original iron load. The test is made in order to validate the robustness against model uncertainty, 100 g load mass. Note that the robust DFC was designed with uncertainty of rope length only; the mass in the model was set to nominal parameter value of 250 g.

Fig. 3.20, Fig. 3.21, and Fig. 3.22 show test results of Fuji's existing control with or without robust DFC adding a100g magnet. Similarly to the test results without the magnet, the robust DFC did not disturb the original control during the set point change. Fuji's existing control control with robust DFC improve the disturbance rejection, which means that less sway angle and shorten the settling time as well as shown in table 3.7.

Robust DFC improves the sway angle for all rope length at 0.8 m, 0.9 m, 1.0 m respectively. The average improvement of sway angle was 33 %, and the robust DFC improves settling time by 4.9 seconds. Compared to the results without a 100 g magnet, the results shows less sway angle for all rope length due to the increase of total load mass.

In addition, comparing table 3.6 and table 3.7, the robust DFC did not get worse settling time after adding the magnet, however, the existing controller takes 1 second longer to settle with the additional load mass.

As results, the advantage of proposed method are verified thorough the lab test of crane systems with parametric uncertainties by additional load math. Moreover, the results demonstrated that the proposed method can be implemented on the cheapest PLC available.

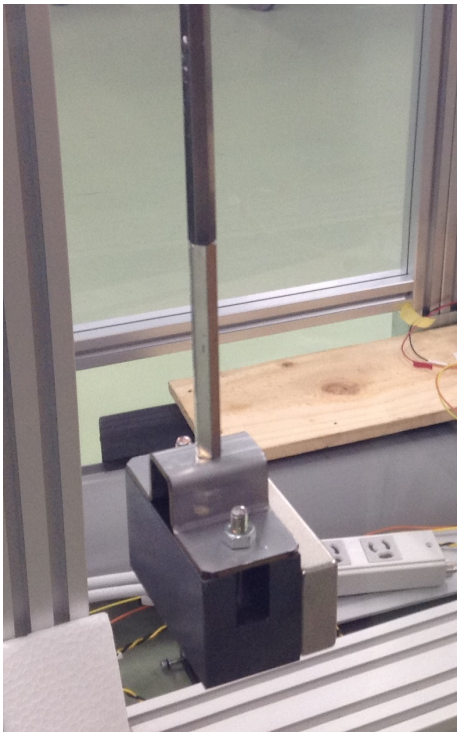

Figure 3.19: Additional load math (a 100 g magnet, which is attracted to the main load math).

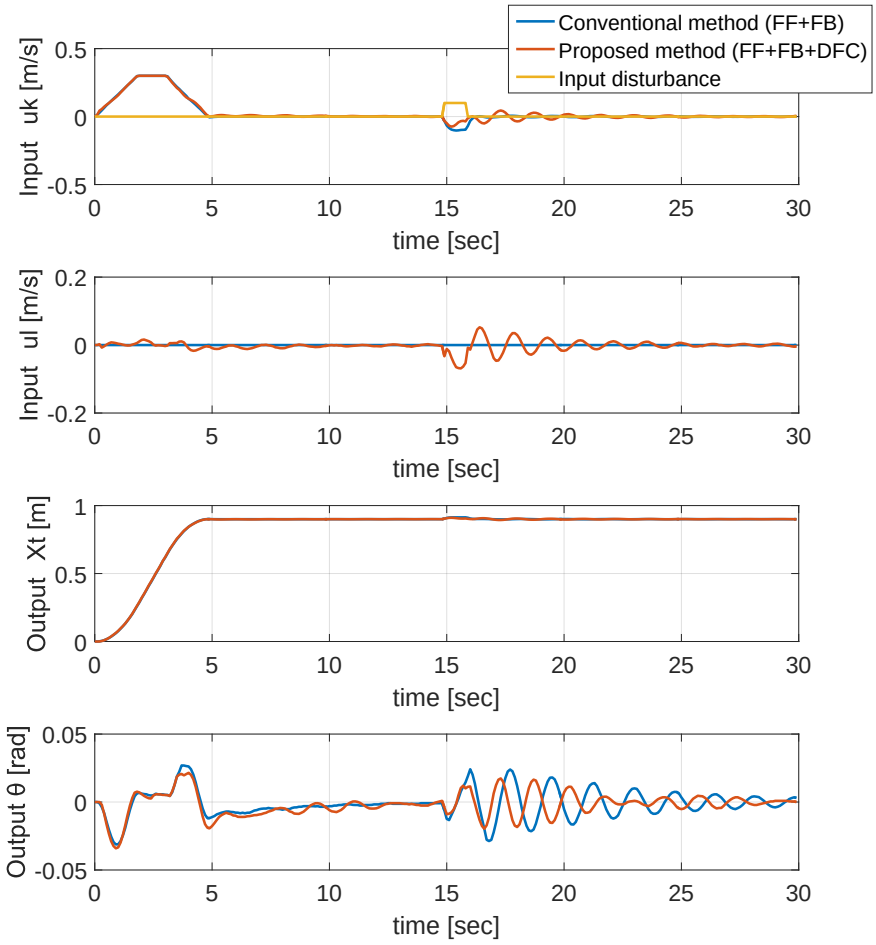

Figure 3.20: Test results of Fuji's conventional control with or without DFC at rope length 0.8 m, adding a 100 g magnet.

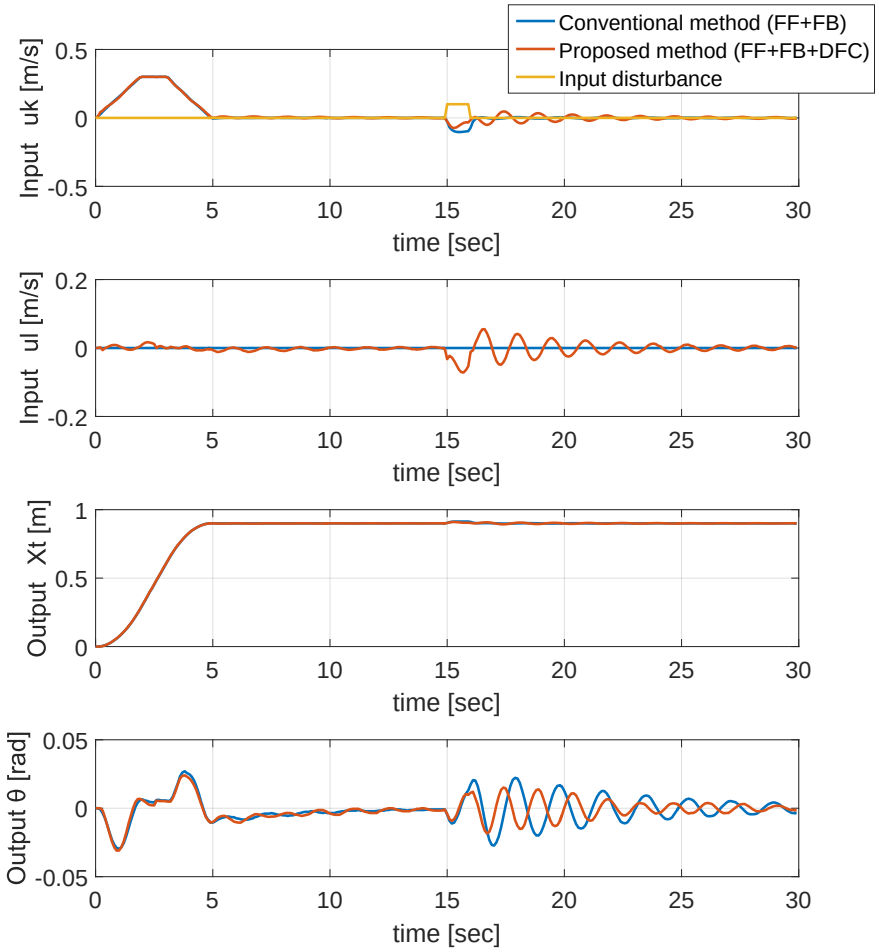

Figure 3.21: Test results of Fuji's conventional control with or without DFC at rope length 0.9 m, adding a 100 g magnet.

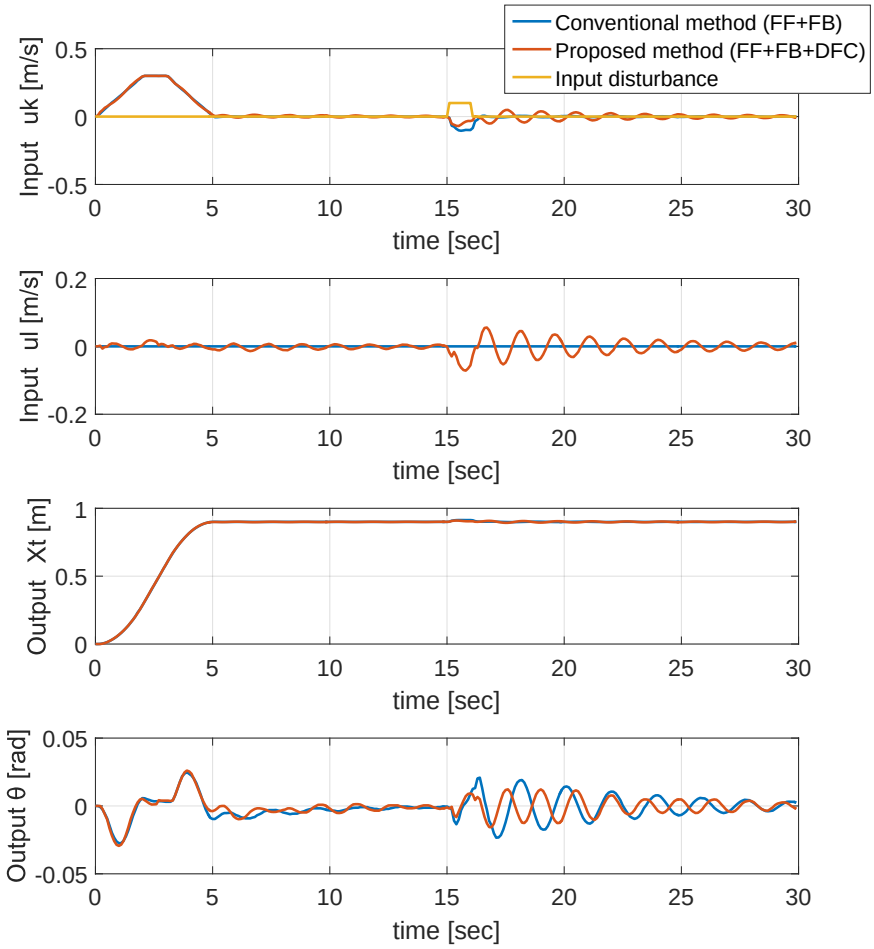

Figure 3.22: Test results of Fuji's conventional control with or without DFC at rope length 1.0 m, adding a 100 g magnet.

4 Closing Remarks

This chapter mentions the conclusion of the thesis. Furthermore, perspectives and strategies is described for future research & development in Fuji electronic, and possibility of new collaboration with Aalborg university.

4.1 Conclusion

The purpose of the present study has been to propose practical design methods using robust control theory in order to improve the stability and performance of existing industrial controllers.

To address this aim, a design methodology has been proposed in Chapter 2 and Chapter 3, in which the plant to be controlled, a nominal model of it, and the existing controller were considered together as an extended plant. The DFC is designed for this extended plant using robust control techniques such as LMI optimization. Specifically, optimization problems were formulated to minimize the effect of disturbances while maintaining stability and performance for a range of model uncertainties.

Two different case studies, refrigeration systems and gantry cranes, have been chosen from Fuji's product portfolio for evaluating the feasibility of the design methodology.

In the first case study in Chapter 2, a conventional controller for a commercial refrigeration system was designed, tested and then augmented with DFC. A two-step design procedure was proposed; first, a set of LMIs is solved to design a robust DFC without taking saturation into account, and then a second set of LMIs is solved to yield an anti-windup compensator to accommodate for actuator saturation. The proposed design is compared with the conventional control system, both in simulation and through practical experiments. The results indicated that both robustness and performance can be improved in the presence of model uncertainties, and the proposed design is able to avoid wind-up phenomena when the control inputs are saturated.

The second case study in Chapter 3 considered in the thesis concerns gantry cranes for an application of factory automation, construction, and shipping contexts. For this case study, an anti-sway control scheme has been proposed,

in which a robust DFC is designed using the same fundamental approach as in the first case study to minimize the sway angle and trolley position errors via LMI optimization. The robust DFC is added to an existing crane control system composed of a feedforward and state feedback control. Simulation results using a realistic gantry crane model show improvements in control performance when the gantry load is subjected to impulse force disturbances for a wide range of rope lengths. Further, lab test of a crane system has been demonstrated, and the results shows that the robust DFC can decrease the sway angle of a hoisting load which is caused by input disturbance.

4.2 Perspectives and Strategies

This section describes perspectives and strategies for future research & development in Fuji electronic, and possibility of new collaboration with Aalborg university.

4.2.1 Short Term Perspectives

Sensor-less Control

Anti-sway control for crane systems in this thesis assumed that all state variables can be measured correctly without sensor error. However, real systems have issues of adverse influence by measurement error which causes degradation in control performance. Furthermore, the angle sensor is not mounted on some crane systems such as overhead crane systems.

For refrigeration systems, robust DFC was designed under the assumption that a suction pressure of compressor can be measured correctly without sensor error as well. However, the pressure sensor is not mounted on commercial vending machine for reducing the cost.

To solve the problems in that, observer based control could address the control issues, and the observer may be introduced into two case studies in industrial systems.

From Lab Systems to Real Systems

In this study, refrigeration systems and crane systems have been chosen from Fuji's product portfolio for evaluating the feasibility of the proposed methodology. Test results of both systems indicated that proposed method is industrially feasible, and is thus practical design. For more practical usability, demonstration using real products and systems will be necessary for future research.

From One Researcher to All Engineers in Fuji

One more future work, a software of robust DFC design using Graphical User Interface (GUI) may be necessary to deploy the design methodology. The software will be developed for industrial engineers who are not familiar with LMI and robust control theory. In addition, the software could be used for a training tool, for instance, two case studies in this thesis will be chosen when trainees learn robust DFC and try exercises at Fuji.

4.2.2 Long Term Perspectives

Robust Plug & Play Control

The motivation of the thesis is to augment the existing systems. This concept has the same motivations as the Plug & Play Control scheme. Thus, combination of robust DFC by Fuji and Plug & Play Control by AAU may be new control methodology to address the auto tuning problem at engineers on site.

For new research project, collaboration, productive sparring, and fruitful discussion between AAU and Fuji will be continued to make it real, more practical design with robustness as industrial systems.

References

J. Ackermann, *Robust Control The Parameter Space Approach*. Springer, 2002.

F. D. Adegas and J. Stoustrup, "Linear Matrix Inequalities for Analysis and Control of Linear Vector Second-Order Systems," *International Journal of Robust and Nonlinear Control*, vol. 25, no. 16, pp. 2939–2964, 2014.

M. Ahmad, R. Raja Ismail, M. Ramli, N. Abd Ghani, and N. Hambali, "Investigations of feed-forward techniques for anti-sway control of 3-d gantry crane system," in *Proc. 2009 IEEE Symposium on Industrial Electronics & Applications*, Kuala Lumpur, Malaysia, Oct. 2009, pp. 265–270.

N. Alibeji and N. Sharma, "A pid-type robust input delay compensation method for uncertain euler x2013;lagrange systems," *IEEE Transactions on Control Systems Technology*, vol. 25, no. 6, pp. 2235–2242, Nov 2017.

K. Åström, T. Hägglund, and W. H. CC Hang, "Automatic tuning and adaptation for PID controllers-a survey," *Control Engineering Practice*, vol. 1, no. 4, pp. 699–714, 1993.

S. Boyd, M. Hast, and K. J. Åström, "MIMO PID Tuning via Iterated LMI Restriction," *International Journal of Robust and Nonlinear Control, DOI: 10.1002/rnc.3376*, 2015.

S. Boyd, M. Hast, and K. J. Åström, "MIMO PID tuning via iterated LMI restriction," *MIMO PID tuning via iterated LMI restriction*, vol. 26, no. 8, pp. 1718–1731, 2016.

Carsten Scherer and Siep Weiland. (2004) Linear matrix inequalities in control. [Online]. Available: http://www.dcsc.tudelft.nl/~cscherer/lmi/notes05.pdf

E. Chambon, L. Burlion, and P. Apkarian, "Time-response shaping using output to input saturation transformation," *International Journal of Control*, vol. 91, no. 3, pp. 534–553, 2018. [Online]. Available: https://doi.org/10.1080/00207179.2017.1286043

G. Chesi, A. Garulli, A. Tesi, and A. Vicino, "Polynomially parameter-dependent lyapunov functions for robust stability of polytopic systems: an lmi approach," *IEEE Transactions on Automatic Control*, vol. 50, no. 3, pp. 365–370, March 2005.

K. Chien, J. A. Hrones, and J. B. Reswick, " On the automatic control of generalized passive systems," *Transactions of the American Society of Mechanical Engineers,*, vol. 74, pp. 175–185, 1952.

M. Chilali, P. Gahinet, and P. Apkarian, "Robust pole placement in LMI regions ," *IEEE Transactions on Automatic Control*, vol. 44, no. 12, pp. 2257 – 2270, 1999.

C. F. Covrig, M. Ardelean, J. Vasiljevska, A. Mengolini, G. Fulli, and E. Amoiralis, *Smart Grid Projects Outlook 2014*. a Science and Policy Report by the Joint Research Centre of the European Commission, 2014.

J. M. G. da Silva Jr., M. B. Longhi, and M. Z. Oliveira, "Dynamic anti-windup design for a class of nonlinear systems," *International Journal of Control*, vol. 89, no. 12, pp. 2406–2419, 2016. [Online]. Available: https://doi.org/10.1080/00207179.2016.1159731

N. Eguchi, M. Yamamoto, K. Endo, S. Konishi, and T. Morita, "Control system for self-commutated static var compensators with unbalanced-load compensation," *IEEJ Transactions on Industry Applications*, vol. 114, no. 4, pp. 444–450, 1994.

H. Farhangi, "The path of the smart grid," *IEEE Power and Energy Magazine*, vol. 8, no. 1, pp. 18–28, January 2010.

B. Frapard and C. Champetier, "H∞ techniques: From research to industrial applications," vol. 381, p. 231, 01 1997.

Fuji Electric Co., Ltd. (2012) Hybrid heat pump beverage vending machines, fuji electric journal 85, (5), pp.33 in industry application, *in Japanese*,. [Online]. Available: https://www.fujielectric.co.jp/about/company/gihou_2012/pdf/85-05/FEJ-85-05-345-2012.pdf

Fuji Electric Co., Ltd. (1981) Fuji electric journal 54, (1), pp.33 in industry application, *in Japanese*,. [Online]. Available: http://www.fujielectric.co.jp/company/jihou_archives/pdf/54-01/FEJ-54-01-024-1981.pdf

Fuji Electric Co., Ltd. (2011) Vending machines, *in Japanese*,. [Online]. Available: https://www.fujielectric.com/ir/management/business_segments/vending_machines.html

Gangale F., Vasiljevska J., Covrig F., Mengolini A., Fulli G. (2017) Smart grid projects outlook 2017: facts, figures and trends in europe, eur 28614 en, doi:10.2760/701587,. [Online]. Available: https://ses.jrc.ec.europa.eu/sites/ses.jrc.ec.europa.eu/files/u24/2017/sgp_outlook_2017-online.pdf

M. Ge, M.-S. Chiu, and Q.-G. Wang, "Robust PID controller design via LMI approach," *Journal of Process Control*, vol. 12, no. 1, pp. 3–13, 2002.

Greg Gorbach, ARC Advisory Group. (2016) The power of the industrial edge, industrial iot/industrie 4.0 viewpoints,. [Online]. Available: https://industrial-iot.com/2016/11/4006/

G. Grimm, A. R. Teel, and L. Zaccarian, "Robust linear anti-windup synthesis for recovery of unconstrained performance," *Int. J. Robust Nonlinear Control,*, vol. 14, no. 13-14, pp. 1133—1168, 2004.

Haruo Takatsu and Toshiaki Ito, "制御技術動向調🄵報告-プロセス装置産業における制御技術の適用状🄵-," 計測と制御, vol. 36, no. 4, pp. 238–244, 1997.

M. Hirakawa, N. Eguchi, M. Yamamoto, S. Konishi, and Y. Makino, "Self-commutated svc for electric railways," in *Proceedings of 1995 International Conference on Power Electronics and Drive Systems. PEDS 95*, Feb 1995, pp. 732–737 vol.2.

O. Itoh, H. Migita, J. Itoh, and Y. Irie, "Application of fuzzy control to automatic crane operation," in *Industrial Electronics, Control, and Instrumentation, 1993. Proceedings of the IECON '93., International Conference on*, Nov 1993, pp. 161–164 vol.1.

R. Izadi-Zamanabadi, K. Vinther, H. Mojallali, H. Rasmussen, and J. Stoustrup, "Evaporator unit as a benchmark for plug and play and fault tolerant control," in *Proc. 8th IFAC Symposium on Fault Detection, Supervision and Safety of Technical Processes*, Mexico City, Mexico, 2012, pp. 701–706.

H. I. Jaafar, Z. Mohamed, A. F. Z. Abidin, and Z. A. Ghani, "Pso-tuned pid controller for a nonlinear gantry crane system," in *Proc. 2012 IEEE International Conference on Control System, Computing and Engineering*, Penang, Malaysia, Mar. 2012, pp. 515–519.

F. Kawai, "Design method for low-order disturbance feedback control," *IEEJ Transactions on Electronics, Information and Systems*, vol. 136, no. 5, pp. 690–696, 2016.

F. Kawai, C. Nakazawa, K. Vinther, H. Rasmussen, P. Andersen, and J. Stoustrup, "An industrial model based disturbance feedback control scheme," in *Proc. The 19th World Congress of the International Federation of Automatic Control (IFAC 2014)*, Cape Town, 2014, pp. 804–809.

F. Kawai, K. Vinther, P. Andersen, and J. D. Bendtsen, "Pid control with robust disturbance feedback control," in *The 2015 IEEE Multi-Conference on Systems and Control (MSC)*, Sydney, 2015, pp. 1223–1229.

F. Kawai, K. Vinther, P. Anderson, and J. D. Bendtsen, "Mimo robust disturbance feedback control for refrigeration systems via an lmi approach," in *Proc. IFAC 2017*, Toulouse, Jul. 2017, pp. 14 525 – 14 532.

F. Kawai, T. Hayashi, T. Kaneko, P. Andersen, and J. D. Bendtsen, "Anti-sway control for crane systems: Robust design with lmi optimization," in *Proc. IEEE Conference on Control Technology and Applications (CCTA).*, Copenhagen, Denmark, Aug. 2018.

F. Kawai, K. Vinther, P. Andersen, and J. D. Bendtsen, "Anti-windup Disturbance Feedback Control: Practical Design with Robustness," *Journal of Process Control*, vol. 69, no. 9, pp. 30–43, 2018.

Kawai, Fukiko and Anderson, Palle and Bendtsen, Jan Dimon, "Robustness against uncertainties in frequency domain for crane control systems designed by polytopic approach," in *Submitted to 2018 57th Annual Conference of the Society of Instrument and Control Engineers of Japan (SICE)*, Nara, Japan, 2018.

Kawai, Fukiko and Vinther, Kasper and Anderson, Palle and Bendtsen, Jan Dimon, "Robust and anti-windup disturbance feedback control for water chiller systems," in *Proc. 2017 IEEE Conference on Control Technology and Applications (CCTA2017)*, Hawaii, United States, Aug. 2017, pp. 1472 – 1479.

Kawai, Fukiko and Vinther, Kasper and Anderson, Palle and Bendtsen, Jan Dimon, "An lmi approach for robust design of disturbance feedback control," in *Proc. 2017 56th Annual Conference of the Society of Instrument and Control Engineers of Japan (SICE)*, Kanazawa, Japan, 2017, pp. 1447 – 1452.

Kenichi Kurotani, Osamu Itoh. (1998) Fuji electric journal 71, (3), pp.149–152, *in Japanese*),. [Online]. Available: https://www.fujielectric.co.jp/company/jihou_archives/pdf/71-03/FEJ-71-03-0000-1998.pdf

L. F. S. Larsen, "Model based control of refrigeration systems," Ph.D. dissertation, Aalborg University, Fredrik Bajers Vej 7C, DK-9220 Aalborg Ø, Denmark, 2005. [Online]. Available: http://www.control.aau.dk/~jakob/phdStudents/lfslThesis.pdf

K. R. Lee, E. T. Jeung, and H. B. Park, "Robust fuzzy H∞ control for uncertain nonlinear systems via state feedback: an LMI approach," *Fuzzy Sets and Systems*, vol. 120, pp. 123–134, 2001.

B. Lu, Y. Fang, and N. Sun, "Nonlinear control for underactuated multi-rope cranes: Modeling, theoretical design and hardware experiments," *Control Engineering Practice*, vol. 76, pp. 123 – 132, 2018. [Online]. Available: http://www.sciencedirect.com/science/article/pii/S0967066118300741

M. Kano. (2009) Jsps pse143 workshop no.27 report *in Japanese*. [Online]. Available: http://ws27.pse143.org/files/WS27_APCsurvey2009_public.pdf

P. Mercader, K. J. Åström, A. Baños, and T. Hägglund, "Robust pid design based on qft and convex x2013;concave optimization," *IEEE Transactions on Control Systems Technology*, vol. 25, no. 2, pp. 441–452, March 2017.

Mitsuhashi Shigetaka and Tatsuo Inoue. (1965) Fuji electric journal 38, (4), pp.257-266 , *in Japanese*),. [Online]. Available: https://www.fujielectric.co.jp/company/jihou_archives/pdf/38-04/FEJ-38-04-257-1965.pdf

T. MIYOSHI, K. TERASHIMA, and M. MORITA, "Study of Feedforward Control Input without Residual Vibration for the Time-Variant Vibration Mechanism and Its Application to the Crane System," *Transactions of the Japan Society of Mechanical Engineers Series C*, vol. 64, no. 624, pp. 2859–2866, 1998.

A. T. on Modern Anti-windup Design, "Automatic tuning and adaptation for PID controllers-a survey," *European Journal of Control*, vol. 15, no. 3-4, pp. 418–440, 2009.

A. V. Oppenheim and R. W. Schafer, *Discrete-time signal processing.* Englewood Cliffs, N.J. : Prentice Hall, 1989.

F. K. Otsuka, U. Chikasa, and N. Katsuyoshi, "Multivariable optimal control of generator excitation and speed governor system," *Electrical Engineering in Japan*, vol. 104, no. 6, pp. 79–87, 1984. [Online]. Available: https://onlinelibrary.wiley.com/doi/abs/10.1002/eej.4391040611

D. Peaucelle and A. Fradkov, "Robust adaptive L 2 -gain control of polytopic MIMO LTI systems —LMI results," *Systems Control Letters*, vol. 57, no. 11, pp. 881–887, 2008.

G. Pignié, "Ariane 5 and Ariane 5 Evolution GNC Overview," in *IAF abstracts, 34th COSPAR Scientific Assembly*, 2002, p. 6.

Y. Qian, Y. Fang, and B. Lu, "Adaptive repetitive learning control for an offshore boom crane," *Automatica*, vol. 82, pp. 21 – 28, 2017. [Online]. Available: http://www.sciencedirect.com/science/article/pii/S0005109817301759

D. E. Rivera, M. Morari, and S. Skogestad, "Internal model control: PID controller design," *Industrial & engineering chemistry process design and development*, vol. 25, no. 1, pp. 252–265, 1986.

P. Rosa, G. J. Balas, C. Silvestre, and M. Athans, "A synthesis method of lti mimo robust controllers for uncertain lpv plants," *IEEE Transactions on Automatic Control*, vol. 59, no. 8, pp. 2234–2240, Aug 2014.

M. Sadabadi and A. Karimi, "An lmi formulation of fixed-order h infinity and h2 controller design for discrete-time systems with polytopic uncertainty," in *Proc. Decision and Control (CDC), 2013 IEEE 52nd Annual Conference*, Firenze, 2013, pp. 2453 – 2458.

H. Sano, K. Ohishi, T. Kaneko, and H. Mine, "Anti-sway crane control based on dual state observer with sensor-delay correction," in *Proc. Advanced Motion Control, 2010 11th IEEE International Workshop*, Niigata, Japan, March 2010, pp. 679 – 684.

C. Scherer, P. Gahinet, and M. Chilali, "Multiobjective Output-Feedback Control via LMI Optimization," *IEEE Transactions on Automatic Control*, vol. 42, no. 7, pp. 896–911, 1997.

F. Shrouf, J. Ordieres, and G. Miragliotta, "Smart factories in industry 4.0: A review of the concept and of energy management approached in production based on the internet of things paradigm," in *2014 IEEE International Conference on Industrial Engineering and Engineering Management*, Dec 2014, pp. 697–701.

S. Sivrioglu and K. Nonami, "Lmi approach to gain scheduled h_∞ control beyond pid control for gyroscopic rotor-magnetic bearing system," in *Proc. Decision and Control (CDC), 1996 IEEE 35th Annual Conference*, Kobe, Japan, 1996, pp. 3694–3699.

S. Skogestad and I. Postlethwaite, *Multivariable Feedback Control*. John Wiley & Sons, Ltd, 2005.

T. D. Son, G. Pipeleers, and J. Swevers, "Experimental validation of robust iterative learning control on an overhead crane test setup," in *Proc. IFAC 2014*, Cape Town, Aug. 2014, pp. 5981 – 5986.

G. E. Stewart, D. M. Gorinevsky, and G. A. Dumont, "Feedback controller design for a spatially distributed system: the paper machine problem," *IEEE Transactions on Control Systems Technology*, vol. 11, no. 5, pp. 612–628, Sept 2003.

J. Stoustrup, "Plug Play Control: Control Technology towards new Challenges," *European Journal of Control*, vol. 15, no. 3-4, pp. 311–330, 2009.

A. Syaichu-Rohman and R. Middleton, “Anti-windup schemes for discrete time systems: an lmi-based design,” in *Proc. 5th Asian Control Conference*, Melbourne, 2004, pp. 554 – 561.

T. Samad and A.M. Annaswamy (eds.). (2014) The impact of control technology, 2nd edition. [Online]. Available: http://ieeecss.org/general/IoCT2-report

Tsutomu Miyashita and Hideyuki Nishida and Shinichi Ito. (2000) Fuji electric journal 73, (11), pp.600-605, *in Japanese*),. [Online]. Available: https://www.fujielectric.co.jp/company/jihou_archives/pdf/73-11/FEJ-73-11-600-2000.pdf

M. Z. M. Tumari, M. S. Saealal, M. R. Ghazali, and Y. A. Wahab, “H∞ controller with graphical lmi region profile for gantry crane system,” in *Proc. SCIS-ISIS 2012*, Kobe, Japan„ Nov. 2012, pp. 1398 – 1402.

Y. Ueki, T. Matsui, H. Endo, T. Kato, and R. Araya, “Development of peak load forecasting system using neural networks and fuzzy theory,” *Electrical Engineering in Japan*, vol. 117, no. 3, pp. 41–51, 1996. [Online]. Available: https://onlinelibrary.wiley.com/doi/abs/10.1002/eej.4391170304

U.S. Department of Energy. (2016) Smart grid investment grant (sgig) program final report,. [Online]. Available: http://www.tealgroup.com.

J. S. Vardakas, N. Zorba, and C. V. Verikoukis, “A survey on demand response programs in smart grids: Pricing methods and optimization algorithms,” *IEEE Communications Surveys Tutorials*, vol. 17, no. 1, pp. 152–178, Firstquarter 2015.

V. Veselý, D. Rosinová, and V. Kučera, “Robust static output feedback controller lmi based design via elimination,” *Journal of the Franklin Institute*, vol. 348, no. 9, pp. 2468 – 2479, 2011. [Online]. Available: http://www.sciencedirect.com/science/article/pii/S0016003211001840

K. Vinther, R. J. Nielsen, K. M. Nielsen, P. Andersen, T. S. Pedersen, and J. D. Bendtsen, “Absorption Cycle Heat Pump Model for Control Design,” in *2015 European Control Conference (ECC)*, 2015.

U. Wasiwitono and M. Saeki, “Fixed-Order Output Feedback Control and Anti-Windup Compensation for Active Suspension Systems,” *Journal of System Design and Dynamics*, vol. 5, no. 2, pp. 264–278, 2011.

Yoshiro Tsuruhara and Naotoshi Iwasawa, “メカニカルシステムにおける制御技術動向,” 計測と制御, vol. 38, no. 1, pp. 23–30, 1999.

K. Zhou, J. C. Doyle, and K. Glover, *Robust and Optimal Control*. Upper Saddle River, NJ, USA: Prentice-Hall, Inc., 1996.

Part I

Papers

Paper A

PID Control with Robust Disturbance Feedback Control

Fukiko Kawai, Kasper Vinther, Palle Andersen, and Jan D. Bendtsen

The paper has been published in the
Proceedings of the 2015 IEEE Conference on Control Applications, IEEE Computer Society Press, 2015, p. 1223 - 1229.

Abstract

Disturbance Feedback Control (DFC) is a technique, originally proposed by Fuji Electric, for augmenting existing control systems with an extra feedback for attenuation of disturbances and model errors. In this work, we analyze the robustness and performance of a PID-based control system with DFC. A multiplicative uncertainty model is used to represent mismatch between a nominal model and the actual plant, and expressions for robust stability, nominal and robust performance are derived. We propose a simple grid-based search algorithm that can be used to find DFC gains to achieve robust stability and performance (if such gains exist). Finally, two different simulation case studies are evaluated and compared. Our numerical studies indicate that better performance can be achieved with the proposed method compared with a conservatively tuned PID controller and comparable performance can be achieved when compared with an H-infinity controller.

1 Introduction

PID controllers have been widely applied during the past hundred years and many tuning methods have been developed [1], [2]. Internal Model Control (IMC) is an example of model based controller tuning that focuses on the plant model [3]. Other references have introduced robust control tuning methods based on frequency responses for PID or low order controllers [4], [5], [6], [7]. These controllers take into account both stability and performance. Moreover, combinations of robust control and IMC have been proposed as new challenges in the literature [8].

Motivated by the same objectives as the above researchers the objective in this paper is to augment existing control in a closed-loop system, with a new Disturbance Feedback Control (DFC) to compensate for model uncertainty and to guarantee stability of the closed-loop system while keeping high performance. In addition, by using the DFC, which can improve disturbance attenuation, it is possible to keep the existing PID controller and its parameters unchanged, This is not the case using the modified Smith predictor [9], [10], which has similar control structure. Moreover, the modified Smith predictor only improves the performance in cases where the system has time delay.

Previous research has suggested that DFC can be converted equivalently to two-degrees-of-freedom PID and stability conditions involving a disturbance feedback factor L and a controller K were analyzed in [11]. This paper proposes a parameter tuning method for DFC. In order to attenuate the impact of disturbances and model errors, a simple search algorithm is proposed, which finds an L such that robust performance is guaranteed.

The rest of the paper describes the problem statement in Section 2 and

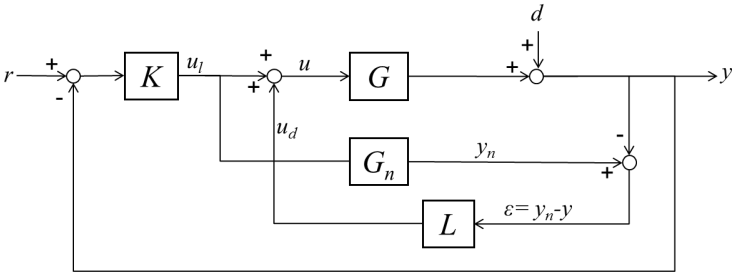

Fig. 1: A block diagram of the closed-loop system with the addition of disturbance feedback control.

the uncertainty model is defined in Section 3. Section 4 presents the L search algorithm. Section 5 shows numerical examples and finally discussion and conclusion are made in Section 6. Note that all signals are scalar, unless explicitly stated; transfer functions are written with capital letters.

2 Problem statement

A block diagram of DFC is shown in Fig. 1, where r is the reference input, u is the control input ($u = u_1 + u_d$), y is the control output, d is the disturbance, G is the plant, K is the feedback controller, G_n is the nominal plant model, L is the transfer function of the disturbance feedback, y_n is the output of the nominal plant, $\epsilon = y_n - y$ is the error between y_n and y. The block diagram shows that the proposed method compensates for the disturbance using u_d.

Note that this control method is not the same as IMC because DFC has two feedbacks signals, which means two degrees of freedom. Basic IMC has only one feedback signal, which will be zero when there is no modeling error. This control method compensates for the error between y_n and y including the effect of disturbances and mutual interference. For this reason, the proposed method is an effective technique to handle disturbances, mutual interference and model error for various systems. The closed loop transfer function is obtained as follows:

$$y = \frac{GK(1+G_nL)}{(1+GK)+GL(1+G_nK)}r + \frac{1}{(1+GK)+GL(1+G_nK)}d \tag{1}$$

When $G = G_n$, i.e., the plant model is equal to the nominal plant model, then Equation (1) can be reduced to

$$y = \frac{GK}{(1+GK)}r + \frac{1}{(1+GK)(1+GL)}d \tag{2}$$

Equation (2) shows that L can attenuate the disturbance without affecting the transfer function from r to y. That is, L can be tuned independently and L will have no impact on the set-point response.

3 Uncertainty model

We now consider disturbance feedback control in an output multiplicative uncertainty framework [12], [13]. As indicated by Fig. 2, each transfer function of the ΔPL structure becomes

$$y' = -KG_n(u_\Delta + d + y') + G_n u_d. \tag{3}$$

where y' is the signal from output of G_n. A signal y_Δ can be written to

$$y_\Delta = \frac{-KG_nW_o}{1+KG_n}(u_\Delta + d) + \frac{G_nW_o}{1+KG_n}u_d \tag{4}$$

where

$$y_\Delta = W_o y' \tag{5}$$

and W_o is the output multiplicative uncertainty. The control output u is a summation of the disturbance feedback output u_d and the output of the controller u_l.

$$u = \frac{-K}{1+KG_n}(u_\Delta + d) + \frac{1}{1+KG_n}u_d. \tag{6}$$

Since $u = u_d + u_l$, we get

$$u_l = \frac{-K}{1+KG_n}(u_\Delta + d) - \frac{KG_n}{1+KG_n}u_d. \tag{7}$$

The input u_l can be defined by Ke and $e' = W_p e$ giving

$$e' = W_p \frac{1}{K}u_l \tag{8}$$

where W_p is the performance weight. The model error ε is described by

$$\varepsilon = y_n - y. \tag{9}$$

Equation (9) can be rewritten to

$$\varepsilon = G_n u_l - (d + u_\Delta + y'). \tag{10}$$

Substituting (3) and (7) into (10) then yield

$$\varepsilon = -G_n u_d - d - u_\Delta. \tag{11}$$

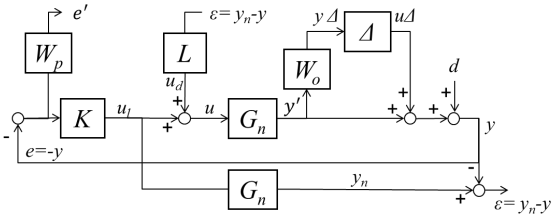

Fig. 2: A block diagram of the disturbance feedback control with output multiplicative uncertainty.

Now consider the ΔPL structure and the ΔN structure as shown in Fig. 3. First, we can formulate the ΔPL structure by combining Equations (4), (7), (8), and (11):

$$\begin{bmatrix} y_\Delta \\ e' \\ \hline \varepsilon \end{bmatrix} = \left[\begin{array}{ccc} \frac{-W_o K G_n}{1+KG_n} & \frac{-W_o K G_n}{1+KG_n} & \frac{W_o G_n}{1+KG_n} \\ \frac{-W_p}{1+KG_n} & \frac{-W_p}{1+KG_n} & \frac{-W_p G_n}{1+KG_n} \\ \hline -1 & -1 & -G_n \end{array}\right] \begin{bmatrix} u_\Delta \\ d \\ \hline u_d \end{bmatrix} \tag{12}$$

Let the transfer matrix in (12) be denoted by P, and let P be partitioned as

$$P = \begin{bmatrix} P_{11} & P_{12} \\ P_{21} & P_{22} \end{bmatrix} \tag{13}$$

with $P_{22} = -G_n$. Assuming $1 + G_n L$ is invertible, it is then possible to recast the ΔPL structure in the right block diagram in Fig. 3 as the ΔN structure shown to the left, using Linear Fractional Transformation [12]:

$$\begin{aligned} N &= P_{11} + P_{12} L (1 - P_{22} L)^{-1} P_{21} \\ &= \begin{bmatrix} \frac{-W_o K G_n}{1+KG_n} & \frac{-W_o K G_n}{1+KG_n} \\ \frac{-W_p}{1+KG_n} & \frac{-W_p}{1+KG_n} \end{bmatrix} + \\ &\quad \begin{bmatrix} \frac{W_o G_n}{1+KG_n} \\ \frac{-W_p G_n}{1+KG_n} \end{bmatrix} L (1 + G_n L)^{-1} \begin{bmatrix} -1 & -1 \end{bmatrix}. \end{aligned} \tag{14}$$

The matrix N can be rewritten as follows:

$$\begin{aligned} N &= \begin{bmatrix} -W_o T & -W_o T \\ -W_p S & -W_p S \end{bmatrix} + T_L \begin{bmatrix} -W_o S & -W_o S \\ W_p S & W_p S \end{bmatrix} \\ &= \begin{bmatrix} -W_o (T + T_L S) & -W_o (T + T_L S) \\ -W_p (S - T_L S) & -W_p (S - T_L S) \end{bmatrix} \end{aligned} \tag{15}$$

where

$$S + T = \frac{1}{1 + KG_n} + \frac{KG_n}{1 + KG_n} = 1 \tag{16}$$

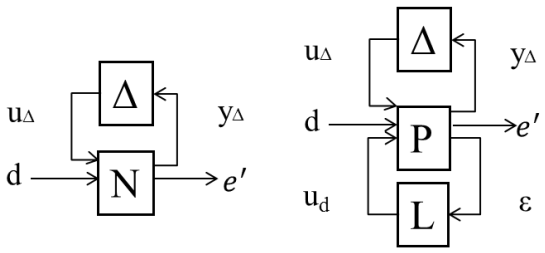

Fig. 3: ΔN structure for robust performance (left) and ΔPL structure for control configuration (right).

$$S_L + T_L = \frac{1}{1 + LG_n} + \frac{LG_n}{1 + LG_n} = 1 \tag{17}$$

Since robust stability is equivalent to $\|N_{11}\| < 1$ and nominal performance is equivalent to $\|N_{22}\| < 1$, this leads to the following performance measures for disturbance feedback control:

Nominal Stability (NS):

$$N \text{ is internally stable.} \tag{18}$$

Robust Stability (RS):

$$\|-W_o(j\omega)(T(j\omega) + T_L(j\omega)S(j\omega))\| < 1, \forall\omega \in \mathbf{R}, \text{ and NS.} \tag{19}$$

Nominal Performance (NP):

$$\|-W_p(j\omega)S(j\omega)S_L(j\omega)\| < 1, \forall\omega \in \mathbf{R}, \text{ and NS.} \tag{20}$$

Robust performance (RP) is explained using NP with the worst case, which means that the uncertainty is maximum $|\Delta_{max}| = 1$, that is

$$\begin{aligned} RP &\Leftrightarrow \sup\|-W_pSS_L\| < 1 \\ &\Leftrightarrow \frac{\|-W_p\|}{\|1 + G_nK\| - \|W_oG_nK\|}\frac{1}{\|1 + G_nL\| - \|W_oG_nL\|} < 1 \\ &\Leftrightarrow \|-W_oT - W_o(1-T)T_L\| + \|-W_pSS_L\| < 1 \end{aligned} \tag{21}$$

Then we derive the robust performance as follows:

Robust Performance (RP):

$$\|-W_o(j\omega)(T(j\omega) + T_L(j\omega)S(j\omega))\| + \|-W_p(j\omega)S(j\omega)S_L(j\omega)\| < 1, \forall\omega \in \mathbf{R},$$

and NS. (22)

An output multiplicative uncertainty is also applied in H-infinity control. In this case, we consider the ΔPK structure and we derive P and N as follows:

$$\left[\begin{array}{c} y_\Delta \\ \hline e' \\ e \end{array}\right] = \left[\begin{array}{cc|c} 0 & 0 & W_o G_n \\ -W_p & -W_p & -W_p G_n \\ \hline -1 & -1 & -G_n \end{array}\right] \left[\begin{array}{c} u_\Delta \\ \hline d \\ u \end{array}\right] \tag{23}$$

$$N = \left[\begin{array}{cc} -W_o T & -W_o T \\ -W_p S & -W_p S \end{array}\right] \tag{24}$$

4 Disturbance feedback function search algorithm

In the following, we propose a simple search algorithm for tuning of the disturbance feedback function L. The concept of the algorithm is that it shapes "two peaks" in the frequency domain by tuning L. One peak appears due to Nominal Performance (NP) and the other due to Robust Stability (RS). Each peak has a relationship to a trade off; if one peak gets smaller, the other peak gets larger. Therefore shaping the two peaks can achieve a minimization of both peaks and a balancing of the trade off. If the function L is chosen as a simple gain, then it can be tuned by gradually increasing the gain, while making a robust performance (RP) check. The largest gain that still achieves RP can be chosen as the disturbance feedback gain L. If RP cannot be achieved using a simple gain function, then L can be tuned as a filter which is expressed by a first order transfer function with gain k_L and time constant τ_L. Fig. 4 shows the proposed search algorithm for disturbance feedback control and the algorithm consist of 5 steps. The detail of the algorithm is as follows:

4. Disturbance feedback function search algorithm

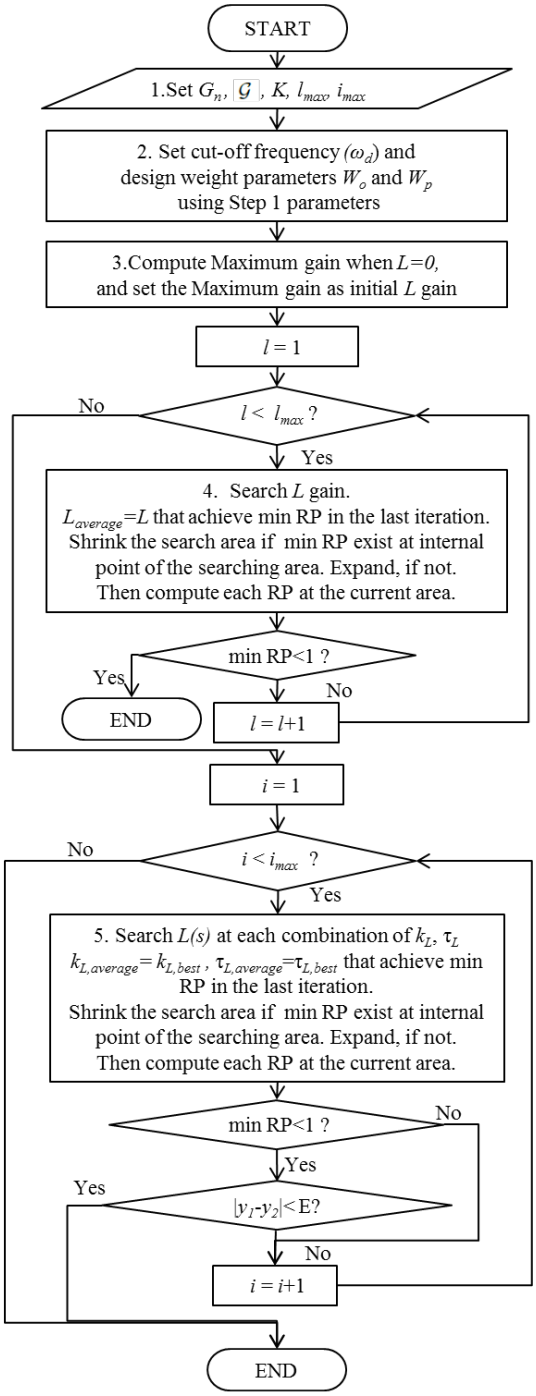

Fig. 4: Disturbance feedback function search algorithm for disturbance feedback control. l and i are iteration counters.

Step 1: Set the nominal model G_n, the uncertainty description $\mathcal{G}$, the controller K, and the range of frequency for evaluation, where

$$\begin{aligned}\mathcal{G} &= \{G_\Delta | G_\Delta(j\omega) = G(j\omega)(1+\Delta_m(j\omega))\} \\ &= G(j\omega)(1+W_o(\omega)\Delta(j\omega)), |\Delta(j\omega)| \leq 1\},\end{aligned} \tag{25}$$

and Δ_m and Δ are the complex perturbation.

Step 2: Set the cut-off frequency ω_d, then design weight parameters W_o and W_p using parameters at Step 1.

$$W_o = \frac{b_1 s + b_0}{a_1 s + a_0}, W_p = \frac{b_0}{a_n s^n + a_{n-1} s^{n-1} + ... + a_0} \tag{26}$$

where $a_n, a_{n-1}...a_1$, and a_0 are the parameters of denominator, and b_1 and b_0 are the parameters of numerator.

Step 3: Compute the peak gain when $L = 0$ and call the peak gain L_{max0}. The L_{max0} is applied as an initial value for L gain search.

Step 4: Search for an L gain. Make the L gain larger gradually, for example ($L = L_{max0} \times 10^{a-1}, a = 1, 2, 3, ..., n$), and compute and save RP for each L. After that, compute RP for each L gain within the searching area. The minimum value of RP for all RPs is found and the minimum spot is used as middle point for next iteration. In addition, the minimum RP is saved and if the minimum RP is located on the boundary of the L parameter searching area at last iteration, then expand the searching area, and if not, shrink.

Step 5: Search for an L transfer function which is represented by a first order time constant as follows:

$$\begin{aligned}L(s) &= \frac{k_L}{1+\tau_L s} \\ k_{Lmin} &< k_L < k_{Lmax} \\ \tau_{Lmin} &< \tau_L < \tau_{Lmax}\end{aligned} \tag{27}$$

Where k_L is the gain, k_{Lmin} and k_{Lmax} is the lower and upper limit of k_L, τ_L is the time constant, τ_{Lmin} and τ_{Lmax} is the lower and upper limit of τ_L. The two dimensional area, which is defined by k_L and τ_L, is divided by log scale and to make a searching mesh. After that, compute RP for each combination of k_L and τ_L within the searching area. The minimum value of RP for all RPs is found and the minimum spot is used as middle point for next iteration.

$$k_{L,average} = k_{L,best} \tag{28}$$

$$\tau_{L,average} = \tau_{L,best} \tag{29}$$

where $k_{L,average}$ is the middle point of k_L for next iteration, $k_{L,best}$ is the gain that achieves minimum RP in the search area, $\tau_{L,average}$ is the middle point

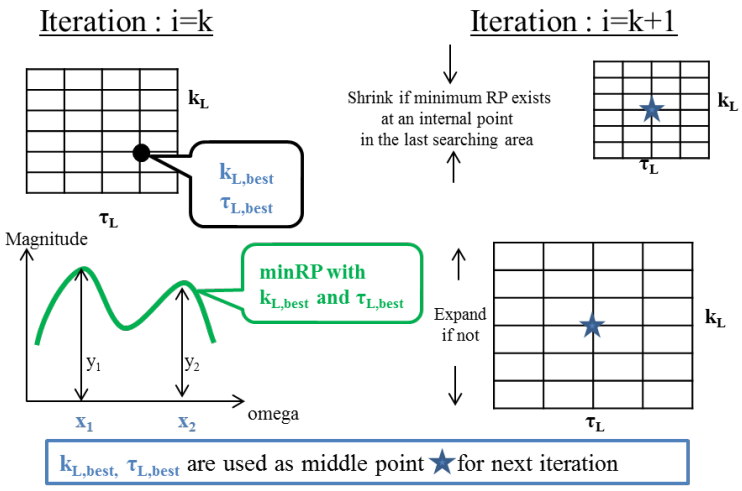

Fig. 5: A conceptual diagram of Step 5.

of τ_L for next iteration, x_1 is the angular frequency of the one peak gain y_1 with the best $L(s)$ that achieves minimum RP in the search area, and x_2 is the angular frequency of the other peak gain y_2 with the best $L(s)$ that achieves minimum RP in the search area. In addition, the minimum RP is saved and if the minimum RP is located on the boundary of the L parameter searching area at last iteration, then expand the searching area, and if not, shrink, as shown in Fig. 5.

This algorithm breaks and terminates if an iteration reaches i_{max} or following condition:

$$|y_1 - y_2| < E \tag{30}$$

where E is the user-specified margin of error between y_1 and y_2.

5 Numerical examples

5.1 Focus control in a CD-player.

This example considers focus control in a CD-player [14] and Fig. 6 shows the optical system of a CD-player. Laser light is emitted from the laser diode and passes through the diffraction grating where it is divided into the main beam and sub-beams. These laser beams are converted by the polarizing beam splitter and reach to the pit of CD media through the collimator lens, the 1/4-wave plate, and the focusing lens. A pick-up unit for a CD player consists of a tracking-control and a focus-control.

Tracking-control: If the CD-media has an eccentricity, the pit of the CD media sways to the left and/or right. Tracking-control moves the focusing lens to the left and/or right in order to follow the sway of the media. It compensates the lens such that the laser beam hits the pit correctly.

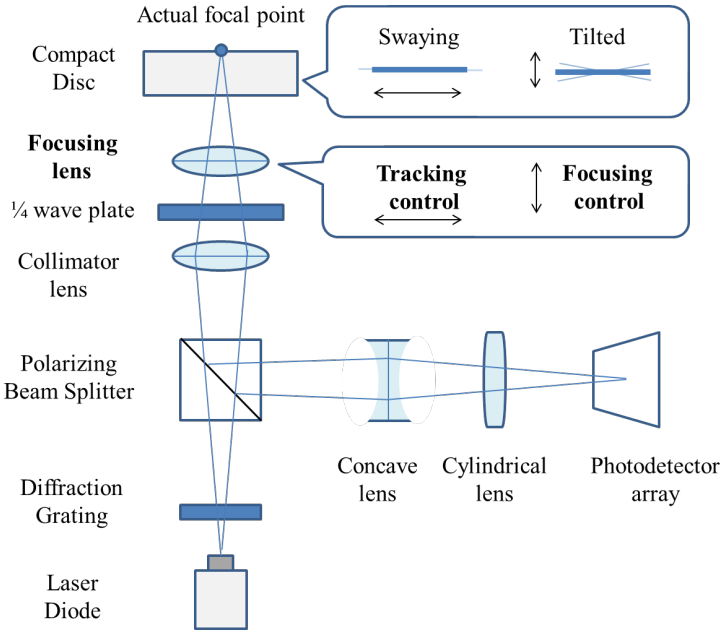

Fig. 6: An optical system of a CD-player.

Focus-control: If the CD-Media is tilted, the pit of the CD media moves up and down. Focus-control moves the focusing lens up and down in order to follow the "surge" of the surface. It focuses the lens on the pit correctly.

The motion of the pick-up for the focus-control is modelled using a mass, spring, and damper equivalent. This results in the following model for the pick-up [15]:

$$G_n(s) = \frac{\frac{Bl}{mr}}{s^2 + (\frac{(Bl)^2}{mr} + \frac{b}{m})s + \frac{k}{m}} \tag{31}$$

with the coil resistance $r = 18\Omega$, the magnetic flux density B, the effective length l, $Bl = 0.25N/A$, the mass $m = 5.2 \times 10^{-4}kg$, the spring modulus $k = 18.6N/m$, and the viscosity coefficient $b = 0.0074N/(m/s)$. The model has some uncertainty which is partly an uncertainty in the gain and partly in the high frequency range. The uncertainty can be modelled by a multiplicative

uncertainty of the form

$$W_o(s) = l_{mo}\frac{\frac{s}{\omega_{s1}}+1}{\frac{s}{\omega_{s2}}+1} \tag{32}$$

with $l_{mo} = 0.3, \omega_{s1} = 1000, \omega_{s2} = 100000$. The performance demands may be expressed by a weight function

$$W_p(s) = \frac{K_d}{(\frac{s}{\omega_d}+1)^3} \tag{33}$$

with $K_d = 15000, \omega_d = 10$. Let K be a PID controller parametrized with the (approximate) crossover frequency ω_c as a parameter

$$K(s) = 0.01\omega_c^2\frac{(\frac{4}{\omega_c}s+1)^2}{\frac{4}{\omega_c}s(\frac{1}{4\omega_c}s+1)} \tag{34}$$

It is found that $\omega_c = 2370$ can stabilize the system.

Fig. 7 shows RS, NP, and RP for the system with only PID control (without DFC). The Figure indicates that the PID control satisfies the RS demand. However, the controller cannot satisfy the NP demand due to a peak at 6.551 [rad/sec], therefore RP, which is a summation of RS and NP, also cannot satisfy the demand.

Fig. 8 shows RS, NP, and RP for system with PID control and DFC where L is tuned by the search algorithm.The figure confirms that the DFC can satisfy the RP demand and that one peak gain shows 0.9992 at 6.551 [rad/sec] and the other shows 0.9995 at 2947 [rad/sec].

Fig. 9 shows the best result in terms of the magnitude of the maximum peak (H_∞) at each iteration when the L search algorithm is applied. The value of RP converges quickly and almost reaches its lowest value at the third iteration.

Fig. 10 shows RS, NP, and RP for the example system without DFC and with the PID control replaced by an H-infinity control which is derived using the robust control toolbox in Matlab. The control can satisfy RP by H-infinity optimal control synthesis.

Table 1 shows a summary of the results using either PID, DFC, or H-infinity control. The table indicates that PID control alone cannot satisfy RP. However, DFC and H-infinity control satisfy both robustness and performances. In addition, DFC and H-infinity control have almost the same peak value of RP . Remember that DFC is added in addition to the existing PID control with the L feedback transfer function represented by first order filter.

A low order DFC can show almost the same robust performance compared to a high order controller such as H-infinity control. Therefore, these results show the advantage of DFC when a robust control strategy is considered.

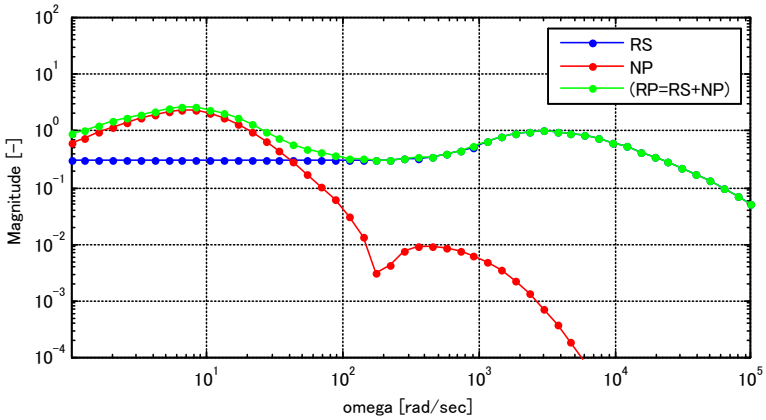

Fig. 7: RS, NP, and RP for system with only PID control (L=0).

5.2 Evaporator superheat control for a refrigeration system.

This example considers superheat control for a refrigeration system [16]. Fig. 11 shows a layout of the refrigeration system with basic control structure. The system includes four components, a compressor, a condenser, an expansion valve, and an evaporator. In a typical refrigeration system, one loop control device is installed for each component as shown in Fig. 11. These controllers regulate a pressure or a temperature based on operating conditions. For instance, the compressor controls the rotational speed so that the controller keeps the pressure of suction refrigerant P_e constant. It is called a suction pressure control. The electronic expansion valve controls the open degree of the valve so that the controller keeps the superheat T_{sh} (difference between the temperature at the outlet of the evaporator and the evaporation temperature inside the evaporator) constant. The speed of the evaporator fan is controlled so as to keep the temperature on the load side T_r constant. The speed of the condenser fan is controlled so as to keep the condensing pressure P_c constant.

Now consider a simple superheat model described by a first order plus dead time system [17]. The model for superheat control is created using experimental data obtained from step response tests conducted at different operating conditions.

$$\mathcal{G} = \frac{k}{1+\tau s} e^{-\theta s}; \tag{35}$$
$$k \in [k_{min}, k_{max}], \tau \in [\tau_{min}, \tau_{max}], \theta \in [\theta_{min}, \theta_{max}]$$

with $k_{min} = -41.6, k_{max} = -26.6, \tau_{min} = 39.8, \tau_{max} = 49.2, \theta_{min} = 20.9$, and $\theta_{max} = 30$.

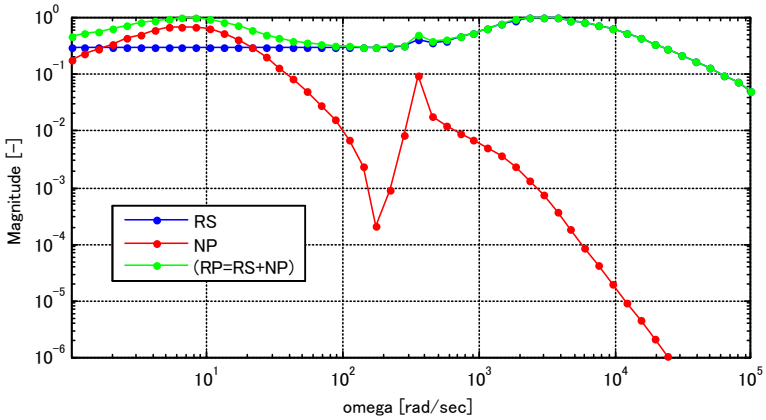

Fig. 8: RS, NP, and RP for system with PID control and DFC (L is tuned by the search algorithm).

Next, the nominal model is computed using average parameter values of $\mathcal{G}$.

$$G_n = \frac{k_n}{1+\tau_n s} e^{-\theta_n s} \tag{36}$$

with $k_n = -34.1, \tau_n = 44.5, \theta_n = 25.45$.

A multiplicative uncertainty weight W_o is designed by over-approximating the gain characteristics of $\mathcal{G}$, see e.g. [**?**].

$$W_o = \frac{17s + 0.6}{5.667s + 1} \tag{37}$$

The performance demands is expressed by a weight function.

$$W_p = \frac{1}{91s + 1} \tag{38}$$

A PI controller K is designed using the CHR method with the parameters of $\mathcal{G}$. The PI parameters are tuned using the worst case, where the gain and the time delay are maximum and the time constant is minimum, so that the PI controller is the most conservative to ensure stability.

$$K = \frac{0.35\tau_{min}}{k_{max}\theta_{max}}(1 + \frac{1}{1.17\tau_{min}s}) \tag{39}$$

Fig. 12 shows RS, NP, and RP for the system with only PI control when $L = 0$. The figure indicates that the PI control satisfies both the RS demand and the NP demand. However, the controller cannot satisfy the RP demand.

Fig. 13 shows RS, NP, and RP for system with PI control and DFC where L is tuned by the search algorithm. The figure confirms that the DFC can

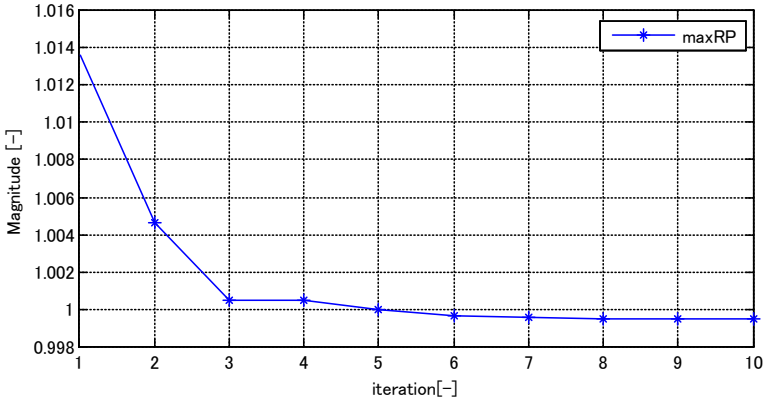

Fig. 9: Best result in terms of magnitude of maximum peak in RP at each iteration with the L search algorithm.

satisfy the RP demand and that one peak when PI control is applied almost disappears due to the L function, which flattens the peak. In the calculation, the maximum value of the RP shows 0.8314 at 0.004095 [rad/sec] as shown in Table 2.

Fig. 14 shows a set point response and a disturbance response of an evaporator superheat control. PI control with DFC shows better disturbance rejection compared to PI control. Average Integral Absolute Error (IAE) for nine simulations with PI and PI + DFC give 255.74, 200.01, respectively.

Table 2 shows a summary of the results using either PI or PI with DFC. The table indicates that PI control alone cannot satisfy RP. However, adding DFC yields both satisfactory robustness and performance.

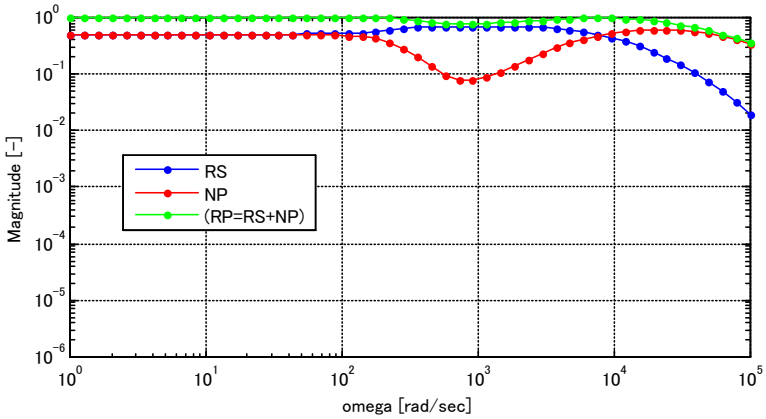

Fig. 10: RS, NP, and RP for the system without DFC and with the PID control replaced by an H-infinity control.

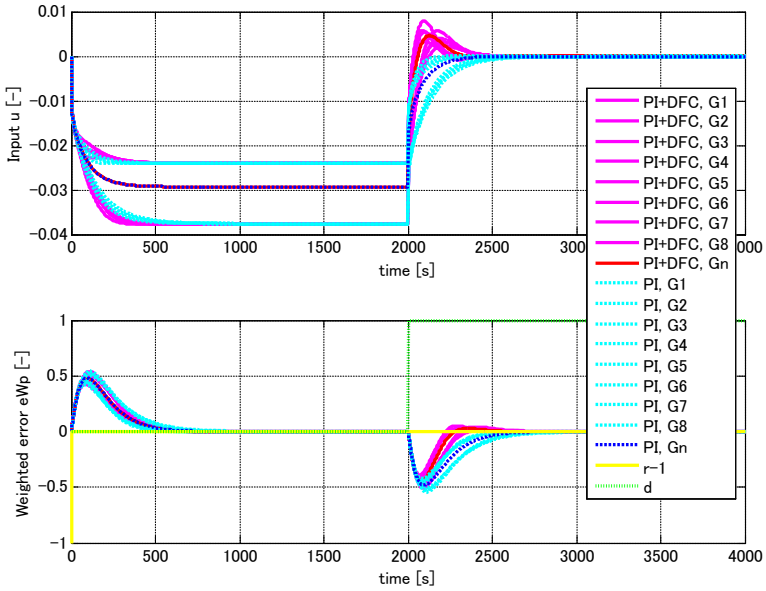

Fig. 14: A set point response and a disturbance response of an evaporator superheat control. $G_1 - G_8$: Combinations of plant parameters, k_{min}/k_{max}, τ_{min}/τ_{max}, $\theta_{min}/\theta_{max}$. G_n: Nominal model.

6 Discussion and conclusions

This paper presents PID based control with robust Disturbance Feedback Control (DFC) method. The authors propose a simple search algorithm such that

Table 1: results using either PID, PID with DFC, or H-infinity control.

Evaluation	PID	PID + DFC	H-infinity control
Maximum magnitude of RP	2.611	0.9995	0.9998
NP	2.311	7.359×10^{-04}	0.4889
RS	0.300	0.9988	0.5109
Frequency of largest peak in RP [rad/sec]	6.551	2947	1.00
L function	$L = 0$	$L = \frac{3084}{1 + 2.558 \times 10^{-04} s}$	none

the DFC can satisfy robust performance by ΔPL structure instead of ΔPK structure. Simulation results on two examples show the effectiveness of the proposed method compared with the conventional PID controller and H-infinity control. As future work, we will examine DFC for MIMO systems.

References

[1] K. Åström, T. Hägglund, and W. H. CC Hang, "Automatic tuning and adaptation for PID controllers-a survey," *Control Engineering Practice*, vol. 1, no. 4, pp. 699–714, 1993.

[2] K. Åström and T. Hägglund, *Advanced PID Control. 2005, The Instrumentation, Systems, and Automation Society.* Research Triangle Park, NC 27709, 2005.

[3] D. E. Rivera, M. Morari, and S. Skogestad, "Internal model control: PID controller design," *Industrial & engineering chemistry process design and development*, vol. 25, no. 1, pp. 252–265, 1986.

[4] V. M. Alfaro and R. Vilanova, "Model reference based robust tuning of five-parameter 2dof pid controllers for first-order plus dead-time models," in *Proc. European Control Conference (ECC2013)*, Zurich, Switzerland, 2013, pp. 3931–3936.

[5] T. Emami and R. J. Hartnett, "Discrete time robust stability design of pid

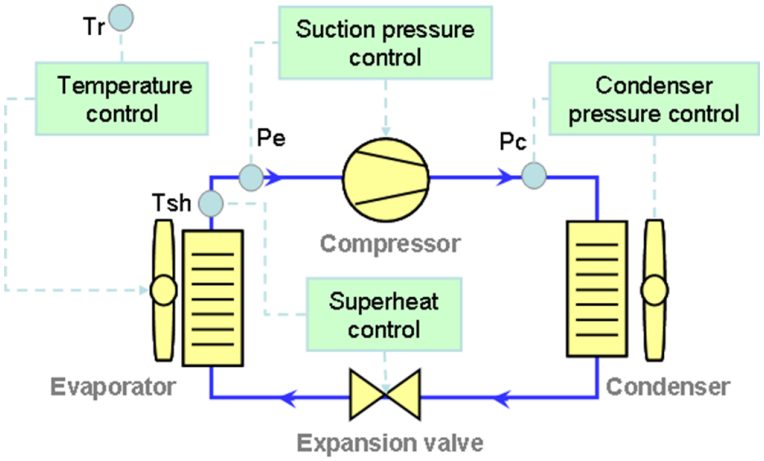

Fig. 11: A layout of the refrigeration system with basic control structure.

controllers autonomous sailing vessel application," in *Proc. the American Control Conference (ACC2014)*, Portland, OR, 2014, pp. 1993–1998.

[6] M. Saeki and M. Ogawa, "Partial numerical optimization of low order h inf controller on the frequency domain," in *Proc. IEEE International Conference on Control Applications*, San Antonio, TX, 2008, pp. 804–809.

[7] H. Bevrani, T. Hiyama, and H. Bevrani, "Robust PID based power system stabiliser: Design and real-time implementation," *International Journal of Electrical Power and Energy Systems*, vol. 33, no. 2, pp. 179–188, 2011.

[8] S. Alcantara, W. Zhang, C. Pedret, R. Vilanova, and S. Skogestad, " IMC-like analytical H inf design with S/SP mixed sensitivity consideration: Utility in PID tuning guidance," *Process Control*, vol. 21, no. 4, pp. 554–563, 2011.

[9] K. Åström, C. Hang, and B. Lim, "A New Smith Predictor for Controlling a Process with an Integrator and Long dead -Time," *IEEE Transaction on Automatic Control*, vol. 39, no. 2, pp. 343–345, 1994.

[10] W. D. Zhang and Y. X. Sun, "Modified Smith Predictor for Controlling Integrator/Time Delay Processes," *Industrial and Engineering Chemistry Research*, vol. 35, no. 8, pp. 2769—2772, 1996.

[11] F. Kawai, C. Nakazawa, K. Vinther, H. Rasmussen, P. Andersen, and J. Stoustrup, "An industrial model based disturbance feedback control scheme," in *Proc. The 19th World Congress of the International Federation of Automatic Control (IFAC 2014)*, Cape Town, 2014, pp. 804–809.

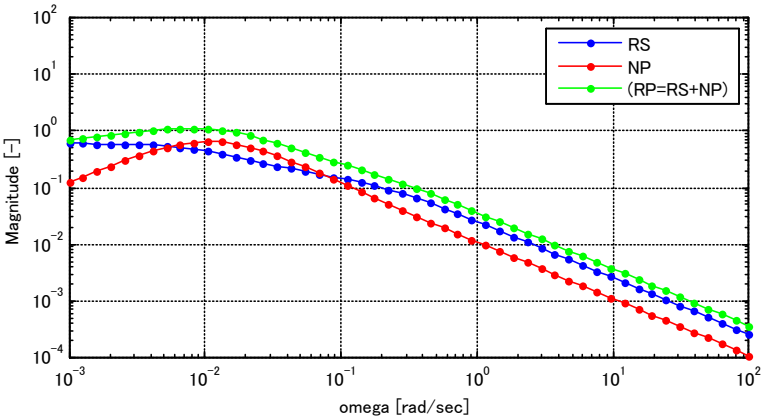

Fig. 12: RS, NP, and RP for system with only PI control ($L = 0$).

Table 2: results using either PI or PI with DFC.

Evaluation	PI	PI + DFC
Maximum magnitude of RP	1.1140	0.8314
NP	0.6313	0.5729
RS	0.4827	0.2585
Frequency of largest peak in RP [rad/sec]	0.008286	0.004095
L function	$L = 0$	$L = \frac{-0.0293}{1 + 150.8s}$

[12] S. Skogestad and I. Postlethwaite, *Multivariable Feedback Control*. John Wiley & Sons, Ltd, 2005.

[13] K. Zhou, J. C. Doyle, and K. Glover, *Robust and Optimal Control*. Upper Saddle River, NJ, USA: Prentice-Hall, Inc., 1996.

[14] P. Crowley, *CD and DVD Forensics*. Syngress, 2006.

[15] P. F. Odgaard, "Feature based control of compact disc players," Ph.D. dissertation, Aalborg University, Fredrik Bajers Vej 7C, DK-9220 Aalborg Ø, Denmark, 2004. [Online]. Available: http://www.control.aau.dk/~jakob/phdStudents/pfoThesis.pdf

[16] L. F. S. Larsen, "Model based control of refrigeration systems,"

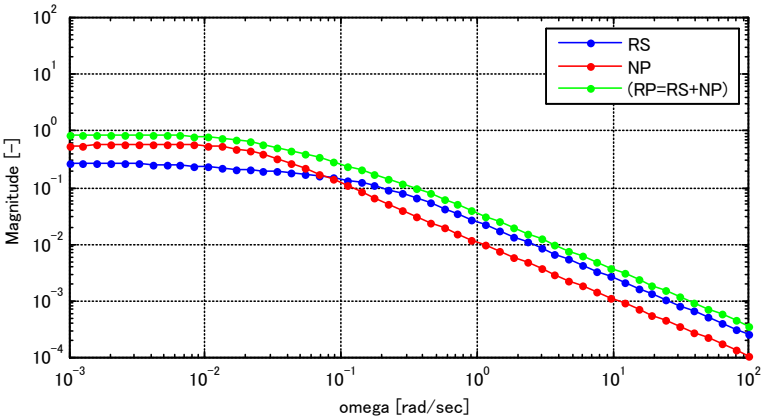

Fig. 13: RS, NP, and RP for system with PI control and DFC (L is tuned by search algorithm).

Ph.D. dissertation, Aalborg University, Fredrik Bajers Vej 7C, DK-9220 Aalborg Ø, Denmark, 2005. [Online]. Available: http://www.control.aau.dk/~jakob/phdStudents/lfslThesis.pdf

[17] R. Izadi-Zamanabadi, K. Vinther, H. Mojallali, H. Rasmussen, and J. Stoustrup, "Evaporator unit as a benchmark for plug and play and fault tolerant control," in *Proc. 8th IFAC Symposium on Fault Detection, Supervision and Safety of Technical Processes*, Mexico City, Mexico, 2012, pp. 701–706.

Paper B

MIMO Robust Disturbance Feedback Control for Refrigeration Systems via an LMI Approach

Fukiko Kawai, Kasper Vinther, Palle Andersen, and Jan D. Bendtsen

The paper has been published in the
IFAC-PapersOnLine, Vol. 50, No. 1, 07.2017, p. 14525-14532.

The layout has been revised.

Abstract

This paper proposes Multi Input and Multi Output (MIMO) robust Disturbance Feedback Control (DFC) design using Linear Matrix Inequalities (LMIs). DFC can be added to existing controllers as an additional control loop, to attenuate disturbances and model uncertainties. The extended state space representation of the overall system is considered with parametric model uncertainties. LMIs are formulated to solve the optimization problem such that the DFC satisfies Lyapunov stability and robust performance. DFC was applied in the superheat control and the suction pressure control for a refrigeration system, and experimental results shows that DFC improves disturbance rejection compared to conventional PI controllers.

1 Introduction

PID control has been widely adopted in industrial control systems due to its simplicity and low cost, e.g., see [1]. Conventional PID control has only been designed for Single-input and Single-output (SISO) systems , and the design is typically based on a linear time invariant (LTI) system description without model uncertainties, which means the classical PID controllers do not consider the modeling error and mutual interactions for Multi-input and Multi-output (MIMO) systems explicitly.

Robust control design is a method to guarantee stability and performance of systems with model uncertainty. In addition, the robust control design can be extended easily to MIMO control systems using state-space representation. Therefore, the robust control design method can be a powerful tool to address the issue of the conventional PID control. Moreover, the robust control design can be formulated using LMIs as Semi Definite Programming (SDP), and the SDP can be solved systematically with an optimization solver such as CVX by [2].

Many researchers have proposed robust PID control or low order robust controllers, for satisfying stability and robustness of systems, e.g., see [3], [4], [5]. As for MIMO design, MIMO PID tuning by an iterative LMI procedure has been proposed as a new challenge by [6].

The authors of this paper suggests to improve the existing control in closed-loop systems using Disturbance Feedback Control (DFC) as shown in Fig. 1. We have proposed simple grid-based DFC design using robust control theory for industrial control devices such as Programmable Logic Controllers (PLCs), for more detail see [7]. This method is for SISO systems, and it could be improved if the DFC applies systematic design methods using LMIs for MIMO systems.

One of the industrial companies in Japan, Fuji Electric has applied control

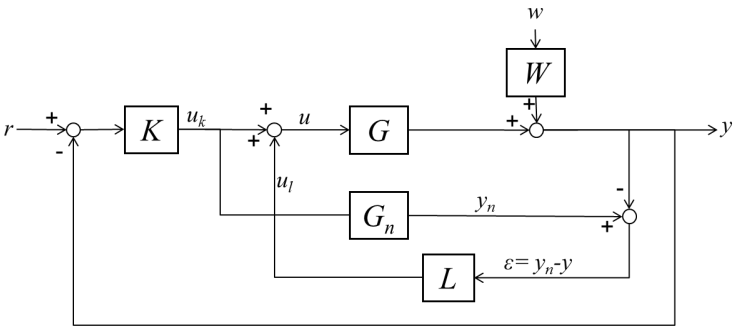

Fig. 1: Block diagrams of disturbance feedback control.

to V/f (motor voltage/output frequency) using a similar control structure, which is called "disturbance observer" proposed by Ohnishi [8], to compensate for the dead-time voltage error ([9]). This design method has important issues to guarantee the robustness for variation of the motor parameters.

DFC is applied in the superheat control and the suction pressure control for the refrigeration system, and the effectiveness against the heat load disturbances using PI with/without DFC is examined.

The rest of the paper first describes the problem definition and the parametric uncertainty model in Section 2. Next, Section 3 then shows the LMIs formulations for DFC design. After that, practical examples are demonstrated in Section 4 using the refrigeration system as shown in Fig. 8. Finally, discussion and conclusions are described in Section 5.

2 Problem Definition

Fig. 1 shows a block diagram of a closed-loop system with DFC (L block), where r is the reference input, $u = u_k + u_l$ is the control input, y is the plant output, w is the disturbance, W is a weighting function, G is the plant, G_n is the nominal plant model, K is an existing feedback controller, L is the transfer function of the disturbance feedback, y_n is the output of the nominal plant, and ϵ is the error between y_n and y. The block diagram indicates that the DFC compensates for the disturbance using u_l. Furthermore, DFC does not add anything to the control input if the plant has no model uncertainty, or disturbance. Therefore, the basic features and performance of the existing system can be maintained with DFC. For this reason, the proposed method is an effective technique to handle disturbances and model uncertainty for various systems. Note that, although superficially similar, this configuration is not identical to model reference control.

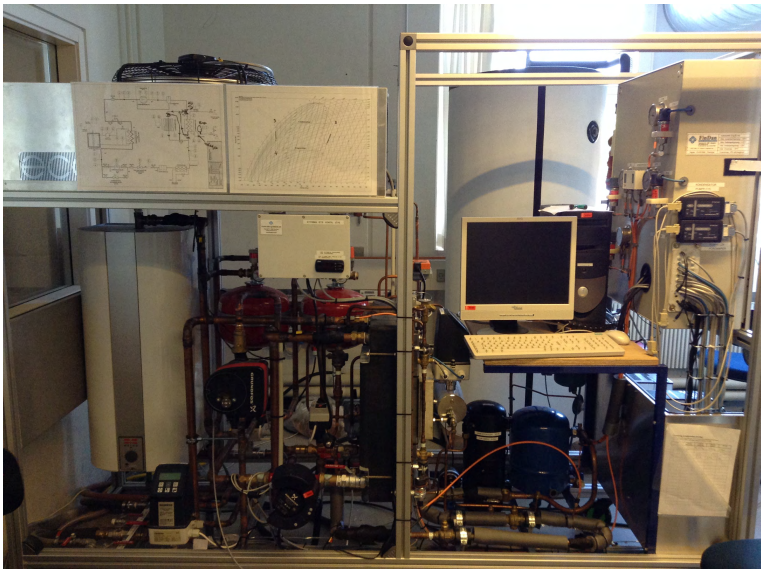

Fig. 2: The refrigeration system test setup at Aalborg University.

2.1 Design Concepts for Disturbance Feedback Control

Fig. 4 shows a general closed-loop system with two input, two output formulation (left) and the closed-loop system for DFC $L(s)$ (Right). In general, when designing controllers, the transfer function T from w to z, where z is the output for evaluating the performance of the controlled systems and y are the measurements.

Note that the motivation of the DFC design is to improve the existing system. We assume that the existing controller K is fixed, meaning we can deal with K as a part of the plant P. Thus, P includes G, G_n, W, and K in the DFC design.

2.2 Parametric Uncertainty Model

Fig. 4 shows a block diagram of the closed-loop system with the addition of DFC. The plant model is transformed from the s-domain shown in Fig. 1 to a time domain representation;

$$\begin{aligned} \dot{\boldsymbol{x}} &= \boldsymbol{A}\boldsymbol{x} + \boldsymbol{B}\boldsymbol{u} \\ \boldsymbol{y} &= \boldsymbol{C}\boldsymbol{x}, \end{aligned} \tag{1}$$

where $\boldsymbol{A} \in \mathbb{R}^{n\times n}$, $\boldsymbol{B} \in \mathbb{R}^{n\times m}$, $\boldsymbol{C} \in \mathbb{R}^{m\times n}$.We assume that the plant model has no direct feed through $\boldsymbol{D}$ because most real thermo dynamical systems have

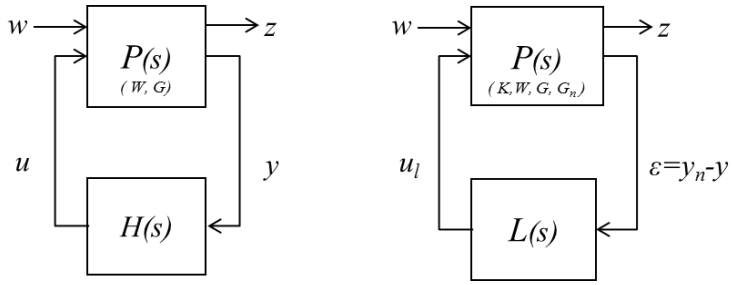

Fig. 3: A closed-loop system for design of an H_∞ controller $H(s)$ (Left), and a closed-loop system for design of Disturbance Feedback Control $L(s)$ (Right).

relative degree at least one. The plant parameters are affected by parametric uncertainties ([10]) expressed by

$$\boldsymbol{A} = \boldsymbol{A_n} + \sum_{i=1}^{p} \delta_{a,i} \boldsymbol{A_i}, \quad \delta_{a,i} \in [-1, +1], \tag{2}$$

$$\boldsymbol{B} = \boldsymbol{B_n} + \sum_{i=1}^{q} \delta_{b,i} \boldsymbol{B_i}, \quad \delta_{b,i} \in [-1, +1], \tag{3}$$

$$\boldsymbol{C} = \boldsymbol{C_n} + \sum_{i=1}^{r} \delta_{c,i} \boldsymbol{C_i}, \quad \delta_{c,i} \in [-1, +1], \tag{4}$$

where $\boldsymbol{\delta_a} = (\delta_{a,i}, \ldots, \delta_{a,p})$, $\boldsymbol{\delta_b} = (\delta_{b,i}, \ldots, \delta_{b,q})$, $\boldsymbol{\delta_c} = (\delta_{c,i}, \ldots, \delta_{c,r})$ are unknown vectors, which express the ensemble of all uncertainty quantities in a given dynamics and $\boldsymbol{A_n}$, $\boldsymbol{B_n}$, and $\boldsymbol{C_n}$ are the nominal state space representation using G_n and $\boldsymbol{A_i}$, $\boldsymbol{B_i}$, and $\boldsymbol{C_i}$ describe the uncertainty.

2.3 PI Controller

We consider PI controllers as the existing controller $\boldsymbol{K}$;

$$\begin{aligned} \dot{\boldsymbol{x}}_{\boldsymbol{k}} &= \boldsymbol{A_k x_k} + \boldsymbol{B_k}(\boldsymbol{r} - \boldsymbol{y}), \\ \boldsymbol{u_k} &= \boldsymbol{C_k x_k} + \boldsymbol{D_k}(\boldsymbol{r} - \boldsymbol{y}), \end{aligned} \tag{5}$$

where $\boldsymbol{A_k} \in \mathbb{R}^{m \times m}$, $\boldsymbol{B_k} \in \mathbb{R}^{m \times m}$, $\boldsymbol{C_k} \in \mathbb{R}^{m \times m}$, and $\boldsymbol{D_k} \in \mathbb{R}^{m \times m}$ are the state space representation of $\boldsymbol{K}$. If SISO system with a PI controller is considered, then $A_k = 0, B_k = 1, C_k = k_i$, and $D_k = k_p$, where k_p is a proportional gain, and k_i is an integral gain.

2.4 Disturbance Weighting Function

We consider a disturbance weighting function. The weighting function for the disturbance $\boldsymbol{w}$ is defined as

$$\begin{aligned} \dot{\boldsymbol{x}}_{\boldsymbol{w}} &= \boldsymbol{A}_{\boldsymbol{w}}\boldsymbol{x}_{\boldsymbol{w}} + \boldsymbol{B}_{\boldsymbol{w}}\boldsymbol{w}, \\ \boldsymbol{y}_{\boldsymbol{w}} &= \boldsymbol{C}_{\boldsymbol{w}}\boldsymbol{x}_{\boldsymbol{w}} + \boldsymbol{D}_{\boldsymbol{w}}\boldsymbol{w}, \end{aligned} \tag{6}$$

where $\boldsymbol{A}_{\boldsymbol{w}} \in \mathbb{R}^{m_w \times m_w}$, $\boldsymbol{B}_{\boldsymbol{w}} \in \mathbb{R}^{m_w \times m_w}$, $\boldsymbol{C}_{\boldsymbol{w}} \in \mathbb{R}^{m_w \times m_w}$, and $\boldsymbol{D}_{\boldsymbol{w}} \in \mathbb{R}^{m_w \times m_w}$ are the state space representation of the weighting function. Note that this choice of order s may depend on the given application. Here, we simply chose $m_w = m$

2.5 Disturbance Feedback Controller

The Disturbance Feedback Controller (DFC) is chosen as

$$\begin{aligned} \dot{\boldsymbol{x}}_{\boldsymbol{ul}} &= \boldsymbol{A}_{\boldsymbol{l}}\boldsymbol{x}_{\boldsymbol{ul}} + \boldsymbol{B}_{\boldsymbol{l}}\boldsymbol{\epsilon} \\ \boldsymbol{u}_{\boldsymbol{l}} &= \boldsymbol{C}_{\boldsymbol{l}}\boldsymbol{x}_{\boldsymbol{ul}} + \boldsymbol{D}_{\boldsymbol{l}}\boldsymbol{\epsilon}, \end{aligned} \tag{7}$$

where $\boldsymbol{A}_{\boldsymbol{l}} \in \mathbb{R}^{2n+m+m_w \times 2n+m+m_w}$, $\boldsymbol{B}_{\boldsymbol{l}} \in \mathbb{R}^{2n+m+m_w \times m}$, $\boldsymbol{C}_{\boldsymbol{l}} \in \mathbb{R}^{m \times 2n+m+m_w}$, and $\boldsymbol{D}_{\boldsymbol{l}} \in \mathbb{R}^{m \times m}$ are the state space representation of the DFC. Note that the DFC is defined as full order controller because the dimension of the plant P in Fig. 3 is $dim(G) + dim(G_n) + dim(K) + dim(W) = n + n + m + m_w$.

3 LMI Formulation for DFC Design

In this section, we present a MIMO robust DFC design method based on output feedback control via an LMI approach. Firstly, the closed loop system $T(s)$ is obtained by the extended state space representation. Next, two constraints are introduced to design DFC. Here, we make use of the Bounded Real Lemma and regional pole placement for continuous time systems [11]. The Bounded Real Lemma is used to guarantee a robust performance, and regional pole placement is introduced to specify the control performance. Moreover, a linearizing change of variables is introduced to design DFC. The DFC is categorized as an output feedback control. Therefore, a linearizing change of variable is needed to formulate the problem in terms of LMI.

3.1 The Extended State Space Representation

If the setpoint $r = 0$, the extended state space representation of the overall system in Fig. 4 can be written as follows [1];

$$\begin{aligned} \dot{\boldsymbol{x_p}} &= \boldsymbol{A_p x_p} + \boldsymbol{B_{w1} w} + \boldsymbol{B_p u_l} \\ \boldsymbol{z} &= \boldsymbol{C_z x_p} + \boldsymbol{D_z u_l} \\ \boldsymbol{\epsilon} &= \boldsymbol{C_p x_p} + \boldsymbol{D_{w1} w}, \end{aligned} \tag{8}$$

where

$$\boldsymbol{x_p} = \begin{pmatrix} \boldsymbol{x}^{\mathrm{T}} & \boldsymbol{x_n}^{\mathrm{T}} & \boldsymbol{x_k}^{\mathrm{T}} & \boldsymbol{x_w}^{\mathrm{T}} \end{pmatrix}^{\mathrm{T}},$$

$$\boldsymbol{A_p} = \begin{pmatrix} \boldsymbol{A - BD_k C} & \boldsymbol{0} & \boldsymbol{BC_k} & \boldsymbol{-BD_k C_w} \\ \boldsymbol{-B_n D_k C} & \boldsymbol{A_n} & \boldsymbol{B_n C_k} & \boldsymbol{-B_n D_k C_w} \\ \boldsymbol{-B_k C} & \boldsymbol{0} & \boldsymbol{A_k} & \boldsymbol{-B_k C_w} \\ \boldsymbol{0} & \boldsymbol{0} & \boldsymbol{0} & \boldsymbol{A_w} \end{pmatrix},$$

$$\boldsymbol{B_{w1}} = \left(\begin{array}{cccc} \boldsymbol{0} & \boldsymbol{0} & \boldsymbol{0} & \boldsymbol{0} \\ \hline \boldsymbol{-(BD_k D_w)^{\mathrm{T}}} & \boldsymbol{-(B_n D_k D_w)^{\mathrm{T}}} & \boldsymbol{-(B_k D_w)^{\mathrm{T}}} & \boldsymbol{(B_w)^{\mathrm{T}}} \end{array} \right)^{\mathrm{T}},$$

$$\boldsymbol{B_p} = \begin{pmatrix} \boldsymbol{B}^{\mathrm{T}} & \boldsymbol{0} & \boldsymbol{0} & \boldsymbol{0} \end{pmatrix}^{\mathrm{T}},$$

$$\boldsymbol{C_z} = \left(\begin{array}{cccc} \boldsymbol{-C} & \boldsymbol{C_n} & \boldsymbol{0} & \boldsymbol{-C_w} \\ \hline \boldsymbol{0} & \boldsymbol{0} & \boldsymbol{0} & \boldsymbol{0} \end{array} \right),$$

$$\boldsymbol{C_p} = \begin{pmatrix} \boldsymbol{-C} & \boldsymbol{C_n} & \boldsymbol{0} & \boldsymbol{-C_w} \end{pmatrix},$$

$$\boldsymbol{D_z} = \left(\begin{array}{c} \boldsymbol{0} \\ \hline \boldsymbol{\rho_z I} \end{array} \right), \quad \boldsymbol{D_{w1}} = \left(\begin{array}{c|c} \boldsymbol{\rho_w I} & \boldsymbol{0} \end{array} \right),$$

w is an output disturbance, and ρ_z and ρ_w are a small numbers which are introduced to maintain full rank and to avoid numerical issues if $\boldsymbol{D_z}$ and $\boldsymbol{D_{w1}}$ are zero matrices.

The closed loop transfer function $T(s)$ from $\boldsymbol{w}$ to $\boldsymbol{z}$ is defined as follows;

$$\begin{aligned} \dot{\boldsymbol{x_{cl}}} &= \boldsymbol{\mathcal{A} x_{cl}} + \boldsymbol{\mathcal{B} w} \\ \boldsymbol{z} &= \boldsymbol{\mathcal{C} x_{cl}} + \boldsymbol{\mathcal{D} w}, \end{aligned} \tag{9}$$

where

$$\left(\begin{array}{c|c} \boldsymbol{\mathcal{A}} & \boldsymbol{\mathcal{B}} \\ \hline \boldsymbol{\mathcal{C}} & \boldsymbol{\mathcal{D}}, \end{array} \right) =$$

$$\left(\begin{array}{cc|c} \boldsymbol{A_p + B_p D_l C_p} & \boldsymbol{B_p C_l} & \boldsymbol{B_{w1} + B_p D_l D_{w1}} \\ \boldsymbol{B_l C_p} & \boldsymbol{A_l} & \boldsymbol{B_l D_{w1}} \\ \hline \boldsymbol{C_z + D_z D_l C_p} & \boldsymbol{D_z C_l} & \boldsymbol{D_z D_l D_{w1}} \end{array} \right).$$

[1] Corrigendum corrected in (8) compared to original publication

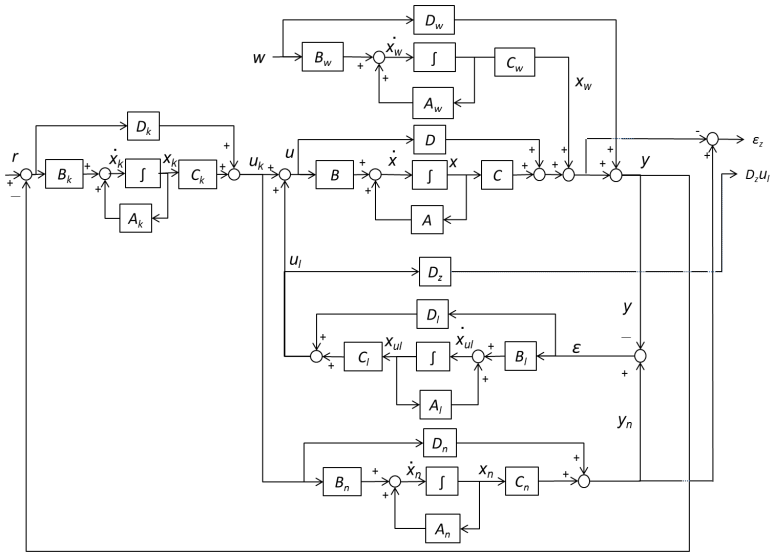

Fig. 4: State space representation of the DFC design.

Note that $\boldsymbol{z} = (\boldsymbol{\epsilon_z}, \boldsymbol{D_z u_l})^{\mathrm{T}}$ is defined in order to distinguish each performance, where $\boldsymbol{\epsilon_z} = \boldsymbol{y_n} - (\boldsymbol{y} - \boldsymbol{D_w w})$, and $\boldsymbol{\epsilon_z}$ is defined without the direct-thorough of disturbance $\boldsymbol{D_w w}$.

3.2 Bounded Real Lemma

The Bounded Real Lemma is used for the constraints in the DFC design. $\boldsymbol{\mathcal{A}}$ is stable and the H_∞ norm of $T(s)$ is smaller than γ if and only if there exists a Lyapunov matrix $\boldsymbol{\mathcal{P}}$, which satisfies the following two lemmas ([12, 13]).

Lemma1: *The LMI*

$$\begin{pmatrix} \boldsymbol{Q(x)} & \boldsymbol{S(x)} \\ \boldsymbol{S(x)} & \boldsymbol{R(x)} \end{pmatrix} > 0, \tag{10}$$

where $\boldsymbol{Q(x)} = \boldsymbol{Q(x)}^{\mathrm{T}}$, $\boldsymbol{R(x)} = \boldsymbol{R(x)}^{\mathrm{T}}$, *and* $\boldsymbol{S(x)}$ *depend affinely on x, is equivalent to*

$$\boldsymbol{R(x)} > 0, \tag{11}$$

$$\boldsymbol{Q(x)} - \boldsymbol{S(x)R(x)^{-1}S(x)}^{\mathrm{T}} > 0. \tag{12}$$

Lemma2: *Consider a continuous-time transfer function* $T(s)$ *of realizations* $T(s) = \boldsymbol{\mathcal{D}} + \boldsymbol{\mathcal{C}}(s\boldsymbol{I} - \boldsymbol{\mathcal{A}})^{-1}\boldsymbol{\mathcal{B}}$. *The following statements are equivalent:*

1. $\|\boldsymbol{\mathcal{D}} + \boldsymbol{\mathcal{C}}(s\boldsymbol{I} - \boldsymbol{\mathcal{A}})^{-1}\boldsymbol{\mathcal{B}}\|_\infty < \gamma$ (13)

and $\boldsymbol{\mathcal{A}}$ *is stable in the continious-time sense* $(Re(\lambda_i(\boldsymbol{\mathcal{A}})) < 0)$.

2. *There exist a symmetric positive definite solution* $\boldsymbol{\mathcal{P}}$ *to the LMI:*

$$\begin{pmatrix} \boldsymbol{\mathcal{A}}^{\mathrm{T}}\boldsymbol{\mathcal{P}} + \boldsymbol{\mathcal{P}}\boldsymbol{\mathcal{A}} & \boldsymbol{\mathcal{P}}\boldsymbol{\mathcal{B}} & \boldsymbol{\mathcal{C}}^{\mathrm{T}} \\ \boldsymbol{\mathcal{B}}^{\mathrm{T}}\boldsymbol{\mathcal{P}} & -\gamma \boldsymbol{I} & \boldsymbol{\mathcal{D}}^{\mathrm{T}} \\ \boldsymbol{\mathcal{C}} & \boldsymbol{\mathcal{D}} & -\gamma \boldsymbol{I} \end{pmatrix} < 0. \tag{14}$$

3.3 Regional Pole Placement

The Regional Pole Placement is used to stabilize the control systems in the DFC design ([14]). The regional pole constraints is introduced with Theorem 1 as follows.

Theorem 1: The matrix $\boldsymbol{\mathcal{A}}$ has all its eigenvalues in the LMI region $\{z \in C : f_{\mathcal{D}}(z) < 0\}$ with $f_{\mathcal{D}} : \mathbb{C} \to \mathbb{R}$:

$$\begin{aligned} f_{\mathcal{D}}(z) &= \boldsymbol{\alpha} + z\boldsymbol{\beta} + \bar{z}\boldsymbol{\beta}^{\mathrm{T}} \\ &= [\alpha_{ij} + \beta_{ij} z + \beta_{ji}\bar{z}]_{1 \le i,j \le l}, \end{aligned} \tag{15}$$

where $\boldsymbol{\alpha} = [\alpha_{ij}] \in \mathbb{R}^{l \times l}$ and $\boldsymbol{\beta} = [\beta_{ij}] \in \mathbb{R}^{l \times l}$ are symmetric matrices, and if and only if there exists a symmetric Lyapunov matrix $\boldsymbol{\mathcal{P}}$ such that

$$[\alpha_{ij}\boldsymbol{\mathcal{P}} + \beta_{ij}\boldsymbol{\mathcal{A}}^{\mathrm{T}}\boldsymbol{P} + \beta_{ji}\boldsymbol{\mathcal{P}}\boldsymbol{\mathcal{A}}]_{i,j} < 0, \quad \boldsymbol{\mathcal{P}} > 0. \tag{16}$$

Note that the left hand side of the first inequality in (15) is given in terms of the Kronecker product, which for any two matrices, e.g., $\boldsymbol{A}$ and $\boldsymbol{B}$, is defined as

$$\boldsymbol{A} \otimes \boldsymbol{B} = [\boldsymbol{A}_{ij}\boldsymbol{B}]_{ij}. \tag{17}$$

In addition, the function $f_{\mathcal{D}}$ takes values in the space of $l \times l$ Hermitian matrices.

3.4 Linearizing Change of Variables

As we described, DFC is categorized as an output-feedback case and a linearizing change of variables can therefore be used to design DFC. The Lyapunov matrix $\boldsymbol{\mathcal{P}}$ is partitioned, for more detail see [11], as follows;

$$\boldsymbol{\mathcal{P}} = \begin{pmatrix} \boldsymbol{Y} & \boldsymbol{N} \\ \boldsymbol{N}^{\mathrm{T}} & \star \end{pmatrix}, \boldsymbol{\mathcal{P}}^{-1} = \begin{pmatrix} \boldsymbol{X} & \boldsymbol{M} \\ \boldsymbol{M}^{\mathrm{T}} & \star \end{pmatrix}, \tag{18}$$

$$\boldsymbol{\mathcal{P}}\boldsymbol{\Pi_1} = \boldsymbol{\Pi_2}, \tag{19}$$

where

$$\boldsymbol{\Pi_1} := \begin{pmatrix} \boldsymbol{X} & \boldsymbol{I} \\ \boldsymbol{M}^{\mathrm{T}} & \boldsymbol{0} \end{pmatrix}, \boldsymbol{\Pi_2} := \begin{pmatrix} \boldsymbol{I} & \boldsymbol{Y} \\ \boldsymbol{0} & \boldsymbol{N}^{\mathrm{T}} \end{pmatrix},$$

and $\boldsymbol{X}$ and $\boldsymbol{Y}$ are symmetric matrices. Then we define the change of the variables as follows;

$$\begin{aligned} \hat{\boldsymbol{A}} :=& \boldsymbol{N}\boldsymbol{A}_l\boldsymbol{M}^{\mathrm{T}} + \boldsymbol{N}\boldsymbol{B}_l\boldsymbol{C}_p\boldsymbol{X} + \boldsymbol{Y}\boldsymbol{B}_p\boldsymbol{C}_l\boldsymbol{M}^{\mathrm{T}} \\ &+ \boldsymbol{Y}(\boldsymbol{A}_p + \boldsymbol{B}_p\boldsymbol{D}_l\boldsymbol{C}_p)\boldsymbol{X}, \end{aligned} \tag{20}$$

$$\hat{\boldsymbol{B}} := \boldsymbol{N}\boldsymbol{B}_l + \boldsymbol{Y}\boldsymbol{B}_p\boldsymbol{D}_l, \tag{21}$$

$$\hat{\boldsymbol{C}} := \boldsymbol{C}_l\boldsymbol{M}^{\mathrm{T}} + \boldsymbol{D}_l\boldsymbol{C}_p\boldsymbol{X}, \tag{22}$$

$$\hat{\boldsymbol{D}} := \boldsymbol{D}_l. \tag{23}$$

The LMI optimization finds $\hat{\boldsymbol{A}}, \hat{\boldsymbol{B}}, \hat{\boldsymbol{C}}, \hat{\boldsymbol{D}}, \boldsymbol{X}, \boldsymbol{Y}$ instead of $\boldsymbol{A}_l, \boldsymbol{B}_l, \boldsymbol{C}_l, \boldsymbol{D}_l$, and $\boldsymbol{\mathcal{P}}$. After that, the DFC is given by the results of the optimization problem;

$$\boldsymbol{D}_l := \hat{\boldsymbol{D}}, \tag{24}$$

$$\boldsymbol{C}_l := (\hat{\boldsymbol{C}} - \boldsymbol{D}_l\boldsymbol{C}_p\boldsymbol{X})\boldsymbol{M}^{-\mathrm{T}}, \tag{25}$$

$$\boldsymbol{B}_l := \boldsymbol{N}^{-1}(\hat{\boldsymbol{B}} - \boldsymbol{Y}\boldsymbol{B}_p\boldsymbol{D}_l), \tag{26}$$

$$\begin{aligned} \boldsymbol{A}_l :=& \boldsymbol{N}^{-1}(\hat{\boldsymbol{A}} - \boldsymbol{N}\boldsymbol{B}_l\boldsymbol{C}_p\boldsymbol{X} - \boldsymbol{Y}\boldsymbol{B}_p\boldsymbol{C}_l\boldsymbol{M}^{\mathrm{T}} \\ &- \boldsymbol{Y}(\boldsymbol{A}_p + \boldsymbol{B}_p\boldsymbol{D}_l\boldsymbol{C}_p)\boldsymbol{X})\boldsymbol{M}^{-\mathrm{T}}. \end{aligned} \tag{27}$$

3.5 Optimization Problem for DFC Design

Now, we summarize the conditions, which are described in subsections 3.1 to 3.4. The optimization problem after the change of variables is given by

$$\text{minimize } \gamma, \tag{28}$$

$$\text{subject to;} \tag{29}$$

$$\begin{pmatrix} \hat{\boldsymbol{\mathcal{A}}}^{\mathrm{T}}\hat{\boldsymbol{\mathcal{P}}} + \hat{\boldsymbol{\mathcal{P}}}\hat{\boldsymbol{\mathcal{A}}} & \hat{\boldsymbol{\mathcal{P}}}\hat{\boldsymbol{\mathcal{B}}} & \hat{\boldsymbol{\mathcal{C}}}^{\mathrm{T}} \\ \hat{\boldsymbol{\mathcal{B}}}^{\mathrm{T}}\hat{\boldsymbol{\mathcal{P}}} & -\gamma\boldsymbol{I} & \hat{\boldsymbol{\mathcal{D}}}^{\mathrm{T}} \\ \hat{\boldsymbol{\mathcal{C}}} & \hat{\boldsymbol{\mathcal{D}}} & -\gamma\boldsymbol{I} \end{pmatrix} < 0, \quad \gamma > 0,$$

$$\hat{\boldsymbol{\mathcal{P}}} = \begin{pmatrix} \boldsymbol{X} & \boldsymbol{I} \\ \boldsymbol{I} & \boldsymbol{Y} \end{pmatrix}, \quad \hat{\boldsymbol{\mathcal{P}}} > 0,$$

$$[\alpha_{ij}\boldsymbol{\mathcal{P}} + \beta_{ij}\boldsymbol{\mathcal{A}}^{\mathrm{T}}\boldsymbol{P} + \beta_{ji}\boldsymbol{\mathcal{P}}\boldsymbol{\mathcal{A}}]_{i,j} < 0,$$

where

$$\hat{\boldsymbol{\mathcal{A}}}^{\mathrm{T}}\hat{\boldsymbol{\mathcal{P}}} + \hat{\boldsymbol{\mathcal{P}}}\hat{\boldsymbol{\mathcal{A}}} =$$

$$\begin{pmatrix} \boldsymbol{A}_p\boldsymbol{X} + \boldsymbol{X}\boldsymbol{A}_p{}^{\mathrm{T}} + \boldsymbol{B}_p\hat{\boldsymbol{C}} + (\boldsymbol{B}_p\hat{\boldsymbol{C}})^{\mathrm{T}} \\ \hat{\boldsymbol{A}} + (\boldsymbol{A}_p + \boldsymbol{B}_p\hat{\boldsymbol{D}}\boldsymbol{C}_p)^{\mathrm{T}} \end{pmatrix}$$

$$\begin{pmatrix} \hat{A}^{\mathrm{T}} + (A_p + B_p\hat{D}C_p) \\ A_p{}^{\mathrm{T}}Y + YA_p + \hat{B}C_p + (\hat{B}C_p)^{\mathrm{T}} \end{pmatrix},$$

$$\hat{\mathcal{P}}\hat{\mathcal{B}} = \begin{pmatrix} B_j + B_p\hat{D}F_j \\ YB_j + \hat{B}F_j \end{pmatrix},$$

$$\hat{\mathcal{C}} = \begin{pmatrix} C_jX + E_j\hat{C} & C_j + E_j\hat{D}C_p \end{pmatrix},$$

$$\hat{\mathcal{D}} = E_j\hat{D}F_j,$$

$$B_j := B_wR_j, \quad C_j := L_jC_z,$$

$$E_j := L_jD_z, \quad F_j := D_wR_j,$$

and L_j, R_j are input/output channel for $T(s)$ from w to z;

$$T_j = L_jTR_j. \tag{30}$$

4 Practical Example

4.1 Refrigeration System

The system includes four main components; a compressor, a condenser, an expansion valve, and an evaporator. In a basic refrigeration system, one control device is installed for each component as shown in Fig. 5. These controllers regulate pressure or temperature based on operating conditions. A hot water tank is set as heat load. For example, the rotational speed of the compressor is controlled to keep a constant refrigerant suction pressure P_e. The opening degree of the expansion valve maintains a suitable refrigerant superheat T_{sh} (difference between the temperature at the outlet of the evaporator and the evaporation temperature inside the evaporator). The speed of the evaporator fan is controlled to keep the temperature on the load side T_r constant. The speed of the condenser fan is controlled in order to keep the condensing pressure P_c constant.

4.2 Modeling

Now 2 input and 2 output modeling for MIMO control design is considered. A simple superheat model and a suction pressure model is chosen for the MIMO control design and these models can be described by a first order plus dead time system, e.g., see [15]. The model is created using experimental data obtained from step response tests conducted at different operating conditions.

$$\mathcal{G}_{ij} = \frac{k_{ij}}{1 + \tau_{ij}s}e^{-\theta_{ij}s}; \tag{31}$$

$$k_{ij} \in [k_{min,ij}, k_{max,ij}], \tau_{ij} \in [\tau_{min,ij}, \tau_{max,ij}],$$

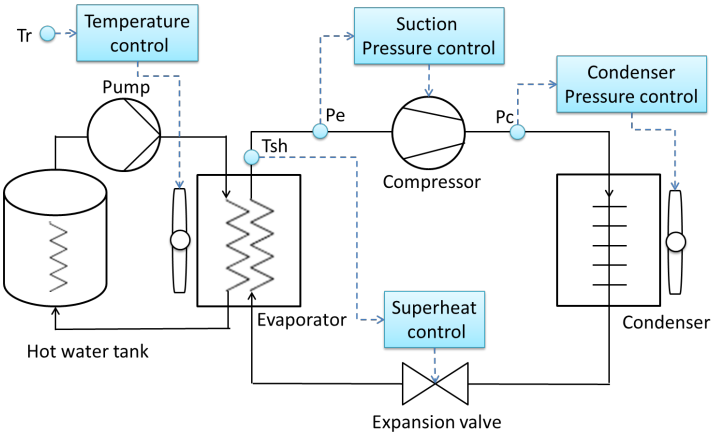

Fig. 5: A layout of the refrigeration system with basic control structure.

$$\theta_{ij} \in [\theta_{min,ij}, \theta_{max,ij}],$$
$$i = 1,2, j = 1,2.$$

Next, the nominal model is computed using average parameter values of $\mathcal{G}$.

$$G_{n,ij} = \frac{k_{n,ij}}{1 + \tau_{n,ij}s} e^{-\theta_{n,ij}s}. \tag{32}$$

The data for estimation was sampled by the open loop step up/down responses. These tests were repeated twice for two conditions, one for low refrigerant flow and low load conditions, and one for high refrigerant flow and high load conditions. In all modeling situations, the condenser pressure is fixed at 9 bar as shown in Table 1.

Table 1: Modeling conditions.

Set point	Condition 1	Condition 2	PI or fixed
Superheat	10.0 [C]	10.0 [C]	PI
Compressor speed	40 [Hz]	50 [Hz]	fixed
Condenser pressure	9.0 [bar]	9.0 [bar]	PI
Water tank	14.0 [C]	16.0 [C]	PI

Fig. 6 shows the input and output data, where operating point values are subtracted, and the data is analyzed for parameter estimation of the superheat control. Input data is OD, and output data is superheat.

Fig. 7 shows comparison of the estimation results and real data for subsystem g_{11} using the Matlab system identification toolbox. The fitness was 85.01

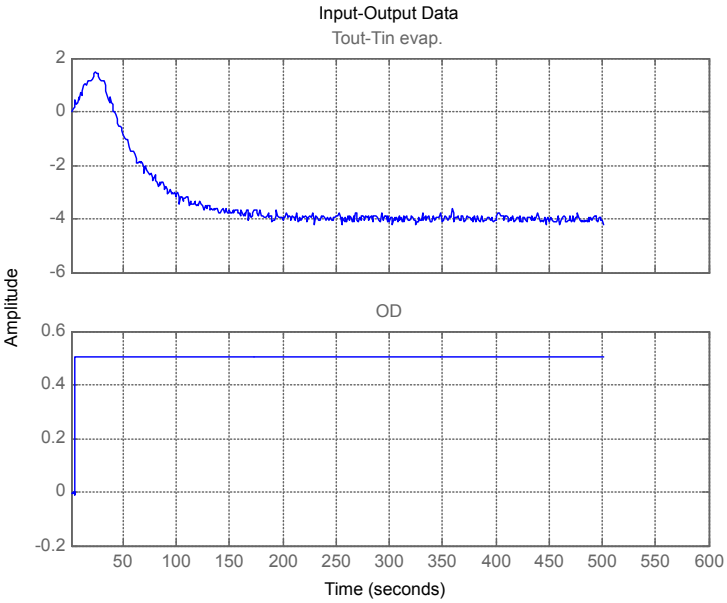

Fig. 6: Input-output data for superheat control design.

%. The other subsystems were estimated by the same procedures, and finally the parameter space for the MIMO system is obtained as shown in Table 1.

For more simple DFC design, the time delay is approximated by a first order system. In addition, only one parameter k_{11} is chosen as main uncertainty because a plant gain of the superheat k_{11} is the most dominant part of the uncertainty and nonlinearity, shown in Table 1. Therefore, G and G_n are approximated as follows:

$$\begin{aligned} \mathcal{G}_{11} &= \frac{k_{11}}{(1+\tau_{n,11}s)(1+\theta_{n,11}s)}; \\ k_{11} &\in [k_{min,11}, k_{max,11}], \end{aligned} \tag{33}$$

and the rest of the subsystems are expressed by the nominal model.

$$\begin{aligned} \mathcal{G}_{ij} &= \frac{k_{n,ij}}{(1+\tau_{n,ij}s)(1+\theta_{n,ij}s)}; \\ i &= 1,2, j = 1,2, except \quad ij = 11. \end{aligned} \tag{34}$$

These parameter values are shown in Table 2.

endfigure

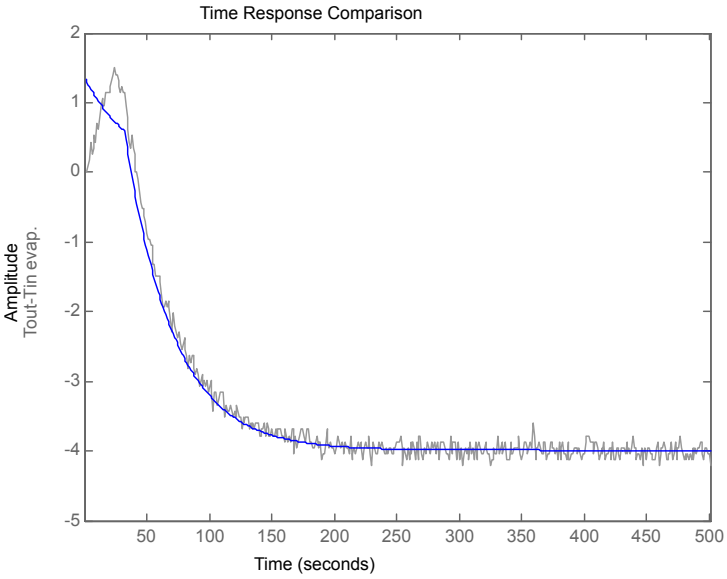

Fig. 7: Plots of the parameter estimation and real data.

4.3 Tuning parameters

The PI controllers are designed using the parameters of each corner point of the $\mathcal{G}$ space to maintain the nominal stability.

$$\boldsymbol{K} = \begin{pmatrix} K_{11} & 0 \\ 0 & K_{22} \end{pmatrix}, \tag{35}$$

$$\textit{where} \quad K_{11} = \frac{\tau_{11min}}{1.52 k_{11min} \theta_{11max}} (1 + \frac{1}{\tau_{11min} s}),$$

$$K_{22} = \frac{\tau_{22min}}{2.50 k_{22min} \theta_{22max}} (1 + \frac{1}{\tau_{22min} s}).$$

Note that the plant gain k_{11} and k_{22} have negative sign, thus we should chose *minimum* value as the worst case.

Table 2: Estimation results of parameter uncertainty corresponding to $-1 < \delta < 1$.

	k	τ	θ
g_{11}	[-10.65 -8.72]	[29.48 60.19]	[14 27]
g_{21}	[0.097 0.47]	[6.38 14.26]	[0 11]
g_{12}	[0.72 0.77]	[21.77 62.30]	[10 27]
g_{22}	[-0.071 -0.021]	[9.18 5.23]	[0 8]

The disturbance weight function is chosen as a first order system, and designed by the nominal time constant $\tau_{n,11}, \tau_{n,22}$. In addition, the weight of superheat W_{11} is given a priority for a disturbance rejection.

$$\boldsymbol{W} = \begin{pmatrix} W_{11} & 0 \\ 0 & W_{22} \end{pmatrix}. \tag{36}$$

$$\textit{where} \quad W_{11} = \frac{1}{1 + \frac{\tau_{n,11}}{3}s}, \; W_{22} = \frac{0.1}{1 + \tau_{n,22}s}.$$

The artificial parameters in (8) for DFC are chosen as follows:

$$\rho_z = 10^{-1}, \quad \rho_w = 10^{-6}. \tag{37}$$

4.4 DFC Design

The optimal H_∞ performance was $\gamma = 0.3940$ with full order DFC, and the DFC was a 20th order system because $A_l = 2n + m + m_w, n = 8, m = 2, m_w = 2$. It could be more useful for industrial applications if a lower order DFC can be obtained. For this reason, model reduction of DFC is considered, and the DFC gain $\boldsymbol{L}$ is obtained with the Matlab command `modred`.

$$\boldsymbol{L} = \begin{pmatrix} -0.3492 & 0.5071 \\ 1.393 & -6.533 \end{pmatrix}. \tag{38}$$

Fig. 11 shows a comparison of DFCs before/after the model reduction. The figure indicates that the DFC gain can keep the main feature of the original DFC in the low frequency area. Table 2 and Fig. 9 to Fig. 11 show the simulation results for comparing PI control with full order DFC or DFC gain. The set-point and disturbance were changed for the superheat control. These results indicate that DFC gain can improve the disturbance rejection more than 40 %. In addition, the DFC gain shows robustness against model uncertainties for the step response simulation as well as full order DFC. From these results, we can choose the DFC gain instead of the full order DFC.

Table 3: Primary parameter uncertainty and nominal parameters for LMI design.

	k	τ	θ
g_{11}	[-10.65 -8.72]	[44.84]	[20.50]
$g_{n,21}$	[0.29]	[10.32]	[5.50]
$g_{n,12}$	[0.75]	[42.03]	[18.50]
$g_{n,22}$	[-0.046]	[7.21]	[4.00]

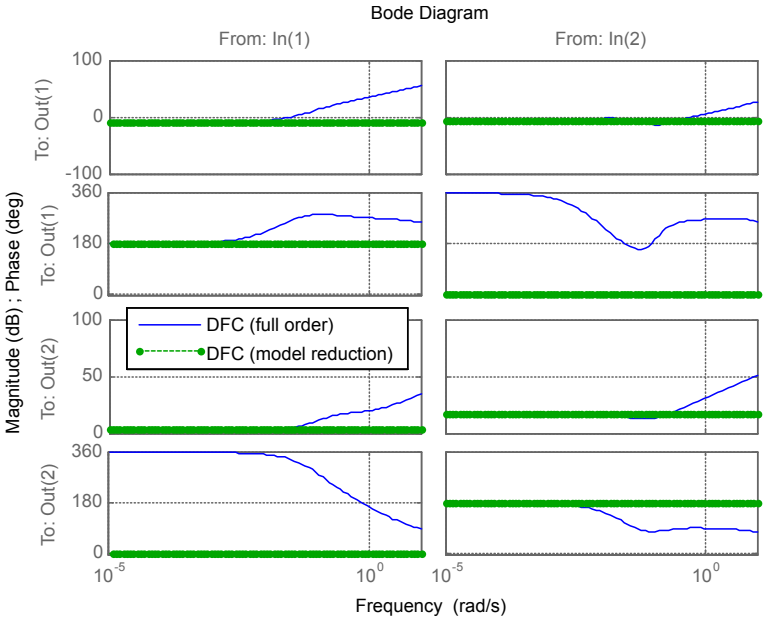

Fig. 8: Bode plots of DFC from ϵ to u_l, before and after model reduction.

4.5 Experimental Results

Table 5 shows the experimental condition for each component. Each set point follows the modeling condition in section 4.2 to examine the $\mathcal{G}$ space. Superheat control and suction pressure control are examined by PI with/without DFC for MIMO control systems. The temperature of the water tank is set at 14 degree for the initial condition. Then the set point is changed to 13.5 degree, and kept there for the first 500 seconds for making swing load disturbance response. The set point is changed to 14 degree again after the first 500 seconds, and kept there for additional 500 seconds. Experimental data is sampled each second, and the data is evaluated for 1000 seconds in total.

Fig. 18 and 19 show swing disturbance response of PI control with/without

Table 4: IAE of the simulation results.

	PI	PI + DFC (full order)	PI + DFC (gain)
The superheat control	464.76	260.00	263.67
The suction pressure control	8.97	11.94	14.94

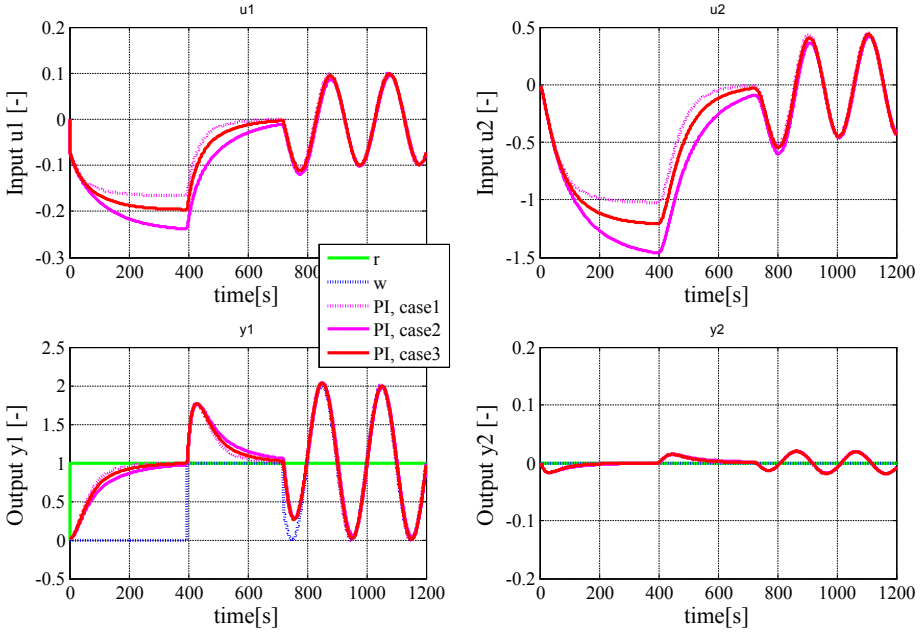

Fig. 9: Simulation results using PI control without DFC.

DFC. The PI control received the effects of the load disturbance, and then the superheat controller cannot regulate the set point around 10 degree. On the other hand, the proposed method can track the set point even though the load change disturbed the regulation. The suction pressure control for compressor with DFC gets worse slightly, however both controllers can keep the set point 2.5 ± 0.15 [bar] and maintain the stability.

Table 7 shows IAE of the superheat control and suction pressure control with/without DFC. IAE of the suction pressure control gets worse by 18.12. On the other hand, superheat control with DFC obtained IAE=640.23 and improved 52.43 % compared to only PI control (IAE=1345.80).

Table 5: Experimental conditions.

Set point	Value	Controlled by
Superheat	10.0 [C]	PI + DFC
Suction pressure	2.5 [bar]	PI + DFC
Condenser	9.0 [bar]	PI
Water tank	14.0 [C]	PI

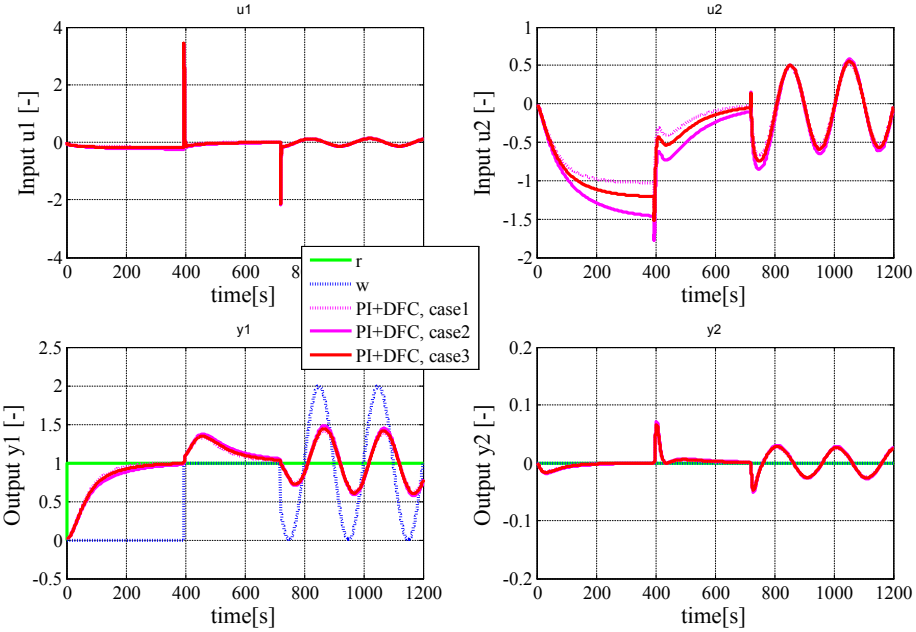

Fig. 10: Simulation results using PI control with full order DFC.

Table 6: IAE of the experimental results.

	PI	PI + DFC (gain)
The superheat control	1345.80	640.23
The suction pressure control	26.89	45.01

5 Discussion and Conclusions

This paper presents MIMO robust Disturbance Feedback Control using an LMI approach. The experimental results of the refrigeration system demonstrated the robustness of the proposed DFC. As future work, we will consider input constraints for this method, and we may also examine fixed order DFC design.

Acknowledgment

The authors wish to thank the anonymous reviewers for constructive comments.

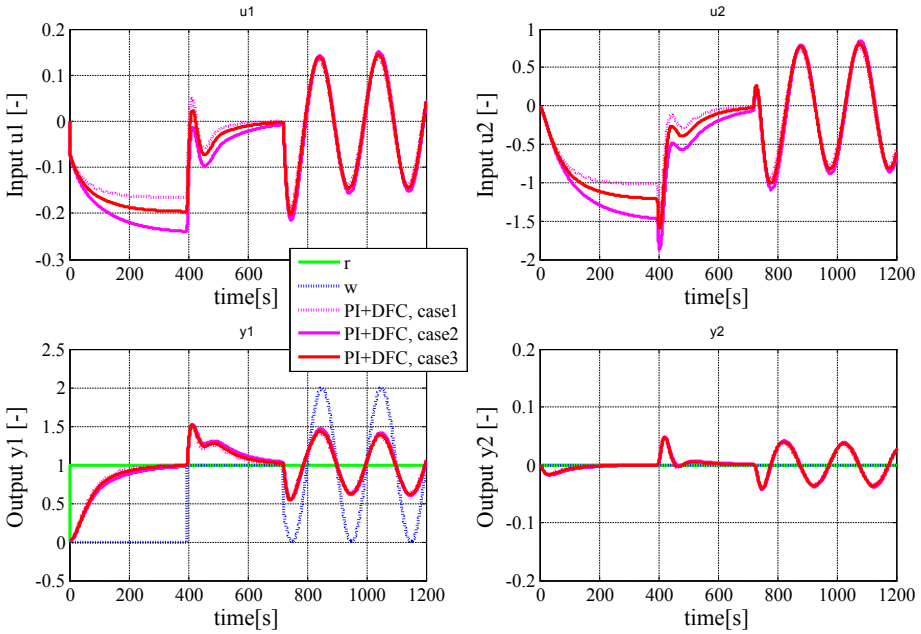

Fig. 11: Simulation results using PI control with DFC gain.

References

[1] K. Åström and T. Hägglund, *Advanced PID Control. 2005, The Instrumentation, Systems, and Automation Society.* Research Triangle Park, NC 27709, 2005.

[2] Michael Grant and Stephen Boyd. (2014) CVX: Matlab software for disciplined convex programming, version 2.1, build 1107. [Online]. Available: http://cvxr.com/cvx

[3] S. Sivrioglu and K. Nonami, "Lmi approach to gain scheduled h_∞ control beyond pid control for gyroscopic rotor-magnetic bearing system," in *Proc. Decision and Control (CDC), 1996 IEEE 35th Annual Conference*, Kobe, Japan, 1996, pp. 3694–3699.

[4] M. Ge, M.-S. Chiu, and Q.-G. Wang, "Robust PID controller design via LMI approach," *Journal of Process Control*, vol. 12, no. 1, pp. 3–13, 2002.

[5] M. Sadabadi and A. Karimi, "An lmi formulation of fixed-order h infinity and h2 controller design for discrete-time systems with polytopic uncertainty," in *Proc. Decision and Control (CDC), 2013 IEEE 52nd Annual Conference*, Firenze, 2013, pp. 2453 – 2458.

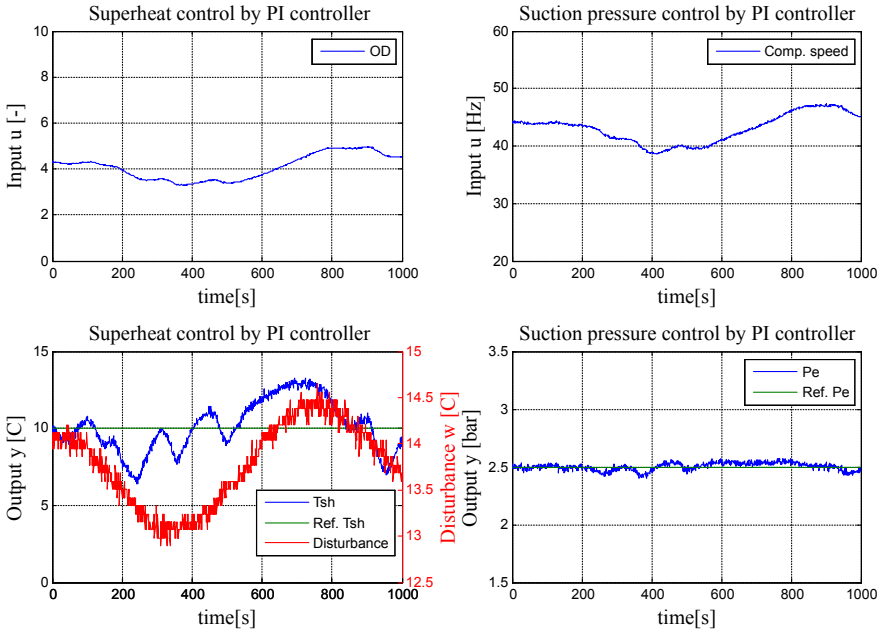

Fig. 12: Swing disturbance response with PI control without DFC gain.

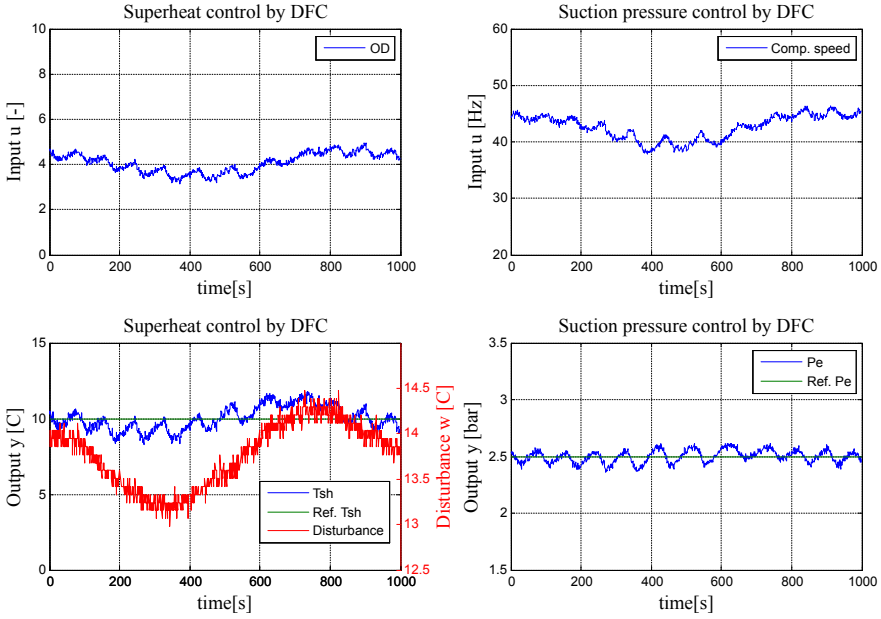

Fig. 13: Swing disturbance response with PI control with DFC gain.

[6] S. Boyd, M. Hast, and K. J. Åström, "MIMO PID Tuning via Iterated LMI Restriction," *International Journal of Robust and Nonlinear Control, DOI: 10.1002/rnc.3376*, 2015.

[7] F. Kawai, K. Vinther, P. Andersen, and J. D. Bendtsen, "Pid control with robust disturbance feedback control," in *The 2015 IEEE Multi-Conference on Systems and Control (MSC)*, Sydney, 2015, pp. 1223–1229.

[8] K. Ohishi, K. Ohnishi, and K. Miyachi, "Torque - speed regulation of dc motor based on load torque estimation method," in *Proc. International Power Electronics Conference (IPEC)*, Tokyo, 1983, pp. 1209 – 1218.

[9] T. Hoshino, J.-I. Itoh, and T. Kaneko, "Dead-time voltage error correction with parallel disturbance observers for high performance v/f control," in *Proc. Industry Applications Conference*, New Orleans, LA, 2007, pp. 2038 – 2044.

[10] Carsten Scherer and Siep Weiland. (2004) Linear matrix inequalities in control. [Online]. Available: http://www.dcsc.tudelft.nl/~cscherer/lmi/notes05.pdf

[11] C. Scherer, P. Gahinet, and M. Chilali, "Multiobjective Output-Feedback Control via LMI Optimization," *IEEE Transactions on Automatic Control*, vol. 42, no. 7, pp. 896–911, 1997.

[12] P. M. Gahinet and P. Apkarian, "A Linear Matrix Inequality Approach to H_∞ Control," *International Journal of Robust and Nonlinear Control*, vol. 4, no. 4, pp. 421–448, 1994.

[13] R. W. Cottle, "Manifestations of the Schur complement," *Linear Algebra and its Applications*, vol. 8, no. 3, pp. 189–211, 1974.

[14] M. Chilali, P. Gahinet, and P. Apkarian, "Robust pole placement in LMI regions ," *IEEE Transactions on Automatic Control*, vol. 44, no. 12, pp. 2257 – 2270, 1999.

[15] R. Izadi-Zamanabadi, K. Vinther, H. Mojallali, H. Rasmussen, and J. Stoustrup, "Evaporator unit as a benchmark for plug and play and fault tolerant control," in *Proc. 8th IFAC Symposium on Fault Detection, Supervision and Safety of Technical Processes*, Mexico City, Mexico, 2012, pp. 701–706.

Paper C

Robust & Anti-Windup Disturbance Feedback Control for Water Chiller Systems

Fukiko Kawai, Kasper Vinther, Palle Andersen, and Jan D. Bendtsen

The paper has been published in the
2017 IEEE Conference on Control Technology and Applications (CCTA),
IEEE, 2017. p. 1472 - 1479.

Abstract

Disturbance Feedback Control (DFC) is a technique in which an existing controller is augmented with an additional loop. It was originally proposed by Fuji Electric in 1980, and has been applied in Factory Automation (FA). This paper proposes a robust DFC including the anti-windup controllers for process control. The proposed method is designed in two steps; firstly, the robust DFC without saturation is designed by Linear Matrix Inequality (LMI) approach, and then LMI technique are used again for stabilizing the closed loop system with anti-windup compensator. The simulation results for the water chiller system shows the improvements of control performances, and keeps stability of the system when the saturation blocks are introduced.

1 Introduction

Disturbance Feedback Control (DFC) was originally developed by Fuji Electric in 1980. DFC has been applied in industrial systems for attenuating disturbances, such as speed control for steel factories. This control structure has an additional *feedback* loop L to compensate for disturbance and model uncertainties as shown in Fig. 1. we can see that the control structure is categorized as two-degree-of-freedom (2DOF) controllers.

In a previous study, the authors proposed a low-order robust DFC for a refrigeration system, to address the control issues of performance degradation due to non-linearities and load disturbances [1]. The robust DFC improved the performance compared to conventional PI control. However, for a more general control design in practical use, anti-windup is needed to handle the limitations in the device and actuators.

A tutorial on modern anti-windup design is presented by Galeani et al. [2], and the tutorial introduced two approaches, namely direct linear anti-windup and model recovery anti-windup. In addition, the authors described that the most of the anti-windup design can be formulated by LMIs.

An LMI approach to H_∞ control has been proposed by Gahinet and Apkarian [3] and they applied a lemma for turning H_∞ suboptimal constraints into an LMI proved by Scherer [4]. As for low order controllers as a practical control, LMIs have been proposed for satisfying stability and robustness of systems controlled by PID controllers [5, 6]. In addition, LMI-based anti-windup synthesis methods has been proposed for considering the robustness of linear systems [7].

Another approach in which a dead-zone is introduced, and a local control design technique is proposed in [8]. In general, anti-windup designs are considered for one-degree-of freedom (1DOF) controllers for closed loop systems. However, many industrial applications are applied in 2DOF controllers because

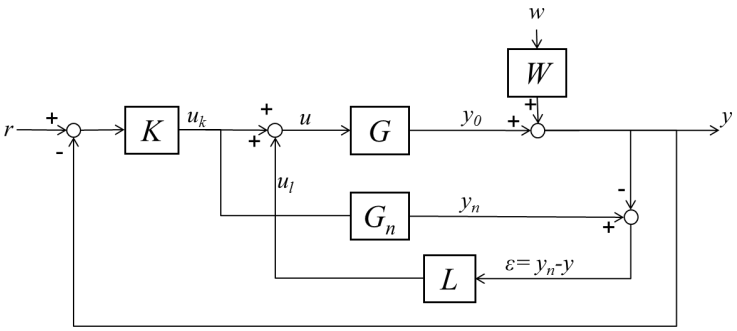

Fig. 1: Block diagrams of disturbance feedback control.

the systems need to guarantee of both the set point and disturbance responses. Therefore, it could be useful for industrial applications to find a design methods for anti-windup 2DOF controllers. Moreover, numerical analysis is necessary to find out whether the previous studies can be applied for 2DOF systems as well.

For these reasons, this paper introduces an anti-windup compensator for 2DOF controllers, one for existing controller and another for DFC. The proposed design method is applied in the superheat control and the suction pressure control for a water chiller system, and both set point and disturbance responses are investigated through simulation.

The rest of the paper first explains the problem definition and the parametric uncertainty model in Section 2. Next, Section 3 and Section 4 show the LMIs formulations for DFC design with anti-windup compensation. After that, numerical examples are demonstrated in Section 4 for the water chiller system. Finally, discussion and conclusions are given in Section 5.

2 Problem Definition

2.1 Design Concepts for Disturbance Feedback Control

Fig. 1 shows a block diagram of a closed-loop system with DFC, where r is the reference input, $u = u_k + u_l$ is the control input, w is the disturbance, W is a weighting function, G is the plant, G_n is the nominal plant model, K is an existing feedback controller, L is the transfer function of the disturbance feedback, y_n is the output of the nominal plant, and ϵ is the error between y_n and y. The block diagram indicates that the DFC compensates for the disturbance using u_l. Fig. 4 shows a general closed-loop system with two input, two output formulation (Left) and the closed-loop system for DFC (Right). In general, when designing controllers, the transfer function T from w to z, where

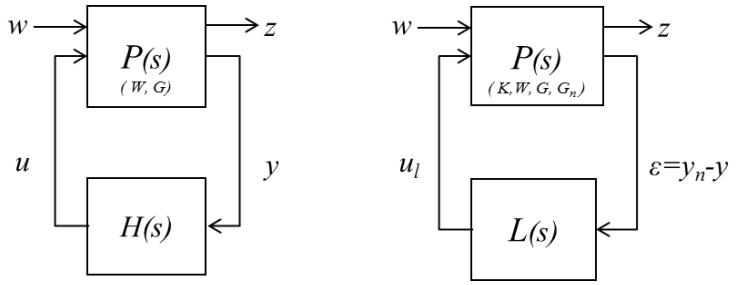

Fig. 2: A closed-loop system for design of an H_∞ controller $H(s)$ (Left), and a closed-loop system for design of DFC $L(s)$ (Right).

z is the output for evaluating the performance of the controlled systems and y are the measurements. Note that the motivation of the DFC design is to improve the existing system. We assume that the existing controller K is fixed, meaning we can deal with K as a part of the plant P. Thus, P includes G, G_n, W, and K in the DFC design.

2.2 Parametric Uncertainty Model

The plant model is transformed from the s-domain shown in Fig. 1 to a time domain representation;

$$\begin{aligned} \dot{\boldsymbol{x}} &= \boldsymbol{A}\boldsymbol{x} + \boldsymbol{B}\boldsymbol{u} \\ \boldsymbol{y_0} &= \boldsymbol{C}\boldsymbol{x}, \end{aligned} \tag{1}$$

where $\boldsymbol{A} \in \mathbb{R}^{n\times n}$, $\boldsymbol{B} \in \mathbb{R}^{n\times m}$, and $\boldsymbol{C} \in \mathbb{R}^{m\times n}$. The plant parameters are affected by parametric uncertainties [9]) expressed by

$$\boldsymbol{A} = \boldsymbol{A_n} + \sum_{i=1}^{p} \delta_{a,i}\boldsymbol{A_i}, \quad \delta_{a,i} \in [-1, +1], \tag{2}$$

$$\boldsymbol{B} = \boldsymbol{B_n} + \sum_{i=1}^{q} \delta_{b,i}\boldsymbol{B_i}, \quad \delta_{b,i} \in [-1, +1], \tag{3}$$

$$\boldsymbol{C} = \boldsymbol{C_n} + \sum_{i=1}^{r} \delta_{c,i}\boldsymbol{C_i}, \quad \delta_{c,i} \in [-1, +1], \tag{4}$$

where $\boldsymbol{\delta_a} = (\delta_{a,i}, \ldots, \delta_{a,p})$, $\boldsymbol{\delta_b} = (\delta_{b,i}, \ldots, \delta_{b,q})$, $\boldsymbol{\delta_c} = (\delta_{c,i}, \ldots, \delta_{c,r})$ are unknown vectors, which express the ensemble of all uncertainty quantities in a given dynamics and $\boldsymbol{A_n}$, $\boldsymbol{B_n}$, and $\boldsymbol{C_n}$ are the nominal state space representation using G_n and $\boldsymbol{A_i}$, $\boldsymbol{B_i}$, and $\boldsymbol{C_i}$ describe the uncertainty.

2.3 PI Controller

We consider a PI controller as the existing controller $\boldsymbol{K}$;

$$\begin{aligned} \dot{\boldsymbol{x}}_{\boldsymbol{k}} &= \boldsymbol{A}_{\boldsymbol{k}}\boldsymbol{x}_{\boldsymbol{k}} + \boldsymbol{B}_{\boldsymbol{k}}(\boldsymbol{r}-\boldsymbol{y}), \\ \boldsymbol{u}_{\boldsymbol{k}} &= \boldsymbol{C}_{\boldsymbol{k}}\boldsymbol{x}_{\boldsymbol{k}} + \boldsymbol{D}_{\boldsymbol{k}}(\boldsymbol{r}-\boldsymbol{y}), \end{aligned} \tag{5}$$

where $\boldsymbol{A}_{\boldsymbol{k}} \in \mathbb{R}^{m\times m}$, $\boldsymbol{B}_{\boldsymbol{k}} \in \mathbb{R}^{m\times m}$, $\boldsymbol{C}_{\boldsymbol{k}} \in \mathbb{R}^{m\times m}$, and $\boldsymbol{D}_{\boldsymbol{k}} \in \mathbb{R}^{m\times m}$ are the state space representation of $\boldsymbol{K}$.

2.4 Disturbance Weighting Function

The weighting function for the disturbance $\boldsymbol{w}$ is defined as

$$\begin{aligned} \dot{\boldsymbol{x}}_{\boldsymbol{w}} &= \boldsymbol{A}_{\boldsymbol{w}}\boldsymbol{x}_{\boldsymbol{w}} + \boldsymbol{B}_{\boldsymbol{w}}\boldsymbol{w}, \\ \boldsymbol{y}_{\boldsymbol{w}} &= \boldsymbol{C}_{\boldsymbol{w}}\boldsymbol{x}_{\boldsymbol{w}} + \boldsymbol{D}_{\boldsymbol{w}}\boldsymbol{w}, \end{aligned} \tag{6}$$

where $\boldsymbol{A}_{\boldsymbol{w}} \in \mathbb{R}^{m\times m}$, $\boldsymbol{B}_{\boldsymbol{w}} \in \mathbb{R}^{m\times m}$, $\boldsymbol{C}_{\boldsymbol{w}} \in \mathbb{R}^{m\times m}$, and $\boldsymbol{D}_{\boldsymbol{w}} \in \mathbb{R}^{m\times m}$ are the state space representation of the weighting function.

2.5 Disturbance Feedback Controller

The Disturbance Feedback Controller (DFC) is chosen as

$$\begin{aligned} \dot{\boldsymbol{x}}_{\boldsymbol{ul}} &= \boldsymbol{A}_{\boldsymbol{l}}\boldsymbol{x}_{\boldsymbol{ul}} + \boldsymbol{B}_{\boldsymbol{l}}\boldsymbol{\epsilon} \\ \boldsymbol{u}_{\boldsymbol{l}} &= \boldsymbol{C}_{\boldsymbol{l}}\boldsymbol{x}_{\boldsymbol{ul}} + \boldsymbol{D}_{\boldsymbol{l}}\boldsymbol{\epsilon}, \end{aligned} \tag{7}$$

where $\boldsymbol{A}_{\boldsymbol{l}} \in \mathbb{R}^{2(n+m)\times 2(n+m)}$, $\boldsymbol{B}_{\boldsymbol{l}} \in \mathbb{R}^{2(n+m)\times m}$, $\boldsymbol{C}_{\boldsymbol{l}} \in \mathbb{R}^{m\times 2(n+m)}$, and $\boldsymbol{D}_{\boldsymbol{l}} \in \mathbb{R}^{m\times m}$.

3 Disturbance Feedback Control Design

In this section, we present a MIMO robust DFC design method based on output feedback control via an LMI approach. Firstly, the closed loop system $T(s)$ is obtained by the extended state space representation. Next, two constraints are introduced to design DFC. Here, we make use of the Bounded Real Lemma and regional pole placement for continuous time systems [10]. The Bounded Real Lemma is used to guarantee a robust performance, and regional pole placement is introduced to specify the control performance. The DFC is categorized as an output feedback control. Therefore, a linearizing change of variable is needed to formulate the problem in terms of LMI.

3.1 The Extended State Space Representation for Robust DFC

The extended state space representation of the overall system can be written as follows[1];

$$
\begin{aligned}
\dot{\boldsymbol{x}_p} &= \boldsymbol{A}_p\boldsymbol{x}_p + \boldsymbol{B}_{w1}\boldsymbol{w} + \boldsymbol{B}_p\boldsymbol{u}_l \\
\boldsymbol{z} &= \boldsymbol{C}_z\boldsymbol{x}_p + \boldsymbol{D}_z\boldsymbol{u}_l \\
\boldsymbol{\epsilon} &= \boldsymbol{C}_p\boldsymbol{x}_p + \boldsymbol{D}_{w1}\boldsymbol{w},
\end{aligned}
\tag{8}
$$

where

$$
\begin{aligned}
\boldsymbol{x}_p &= \begin{pmatrix} \boldsymbol{x}^{\mathrm{T}} & \boldsymbol{x}_n{}^{\mathrm{T}} & \boldsymbol{x}_k{}^{\mathrm{T}} & \boldsymbol{x}_w{}^{\mathrm{T}} \end{pmatrix}^{\mathrm{T}}, \\
\boldsymbol{A}_p &= \begin{pmatrix} \boldsymbol{A}-\boldsymbol{B}\boldsymbol{D}_k\boldsymbol{C} & \boldsymbol{0} & \boldsymbol{B}\boldsymbol{C}_k & -\boldsymbol{B}\boldsymbol{D}_k\boldsymbol{C}_w \\ -\boldsymbol{B}_n\boldsymbol{D}_k\boldsymbol{C} & \boldsymbol{A}_n & \boldsymbol{B}_n\boldsymbol{C}_k & -\boldsymbol{B}_n\boldsymbol{D}_k\boldsymbol{C}_w \\ -\boldsymbol{B}_k\boldsymbol{C} & \boldsymbol{0} & \boldsymbol{A}_k & -\boldsymbol{B}_k\boldsymbol{C}_w \\ \boldsymbol{0} & \boldsymbol{0} & \boldsymbol{0} & \boldsymbol{A}_w \end{pmatrix}, \\
\boldsymbol{B}_{w1} &= \left(\begin{array}{cccc} \boldsymbol{0} & \boldsymbol{0} & \boldsymbol{0} & \boldsymbol{0} \\ \hline -(\boldsymbol{B}\boldsymbol{D}_k\boldsymbol{D}_w)^{\mathrm{T}} & -(\boldsymbol{B}_n\boldsymbol{D}_k\boldsymbol{D}_w)^{\mathrm{T}} & -(\boldsymbol{B}_k\boldsymbol{D}_w)^{\mathrm{T}} & (\boldsymbol{B}_w)^{\mathrm{T}} \end{array}\right)^{\mathrm{T}}, \\
\boldsymbol{B}_p &= \begin{pmatrix} \boldsymbol{B}^{\mathrm{T}} & \boldsymbol{0} & \boldsymbol{0} & \boldsymbol{0} \end{pmatrix}^{\mathrm{T}}, \\
\boldsymbol{C}_z &= \left(\begin{array}{cccc} -\boldsymbol{C} & \boldsymbol{C}_n & \boldsymbol{0} & -\boldsymbol{C}_w \\ \hline \boldsymbol{0} & \boldsymbol{0} & \boldsymbol{0} & \boldsymbol{0} \end{array}\right), \\
\boldsymbol{C}_p &= \begin{pmatrix} -\boldsymbol{C} & \boldsymbol{C}_n & \boldsymbol{0} & -\boldsymbol{C}_w \end{pmatrix}, \\
\boldsymbol{D}_z &= \left(\begin{array}{c} \boldsymbol{0} \\ \hline \rho_z\boldsymbol{I} \end{array}\right), \quad \boldsymbol{D}_{w1} = \left(\begin{array}{c|c} \rho_w\boldsymbol{I} & \boldsymbol{0} \end{array}\right),
\end{aligned}
$$

$\boldsymbol{w}$ is an output disturbance, and ρ_z and ρ_w are small numbers which are introduced to maintain full rank and to avoid numerical issues if $\boldsymbol{D}_z$ and $\boldsymbol{D}_{w1}$ are zero matrices. Note that $\boldsymbol{z} = (\boldsymbol{\epsilon}_z, \boldsymbol{D}_z\boldsymbol{u}_l)^{\mathrm{T}}$ is defined in order to distinguish each performance, where $\boldsymbol{\epsilon}_z = \boldsymbol{y}_n - (\boldsymbol{C}\boldsymbol{x} + \boldsymbol{D}\boldsymbol{u} + \boldsymbol{C}_w\boldsymbol{x}_w)$, and $\boldsymbol{\epsilon}_z$ is defined without the direct-thorough of disturbance $\boldsymbol{D}_w\boldsymbol{w}$.

The closed loop transfer function $T(s)$ from $\boldsymbol{w}$ to $\boldsymbol{z}$ is defined as follows;

$$
\begin{aligned}
\dot{\boldsymbol{x}_{cl}} &= \boldsymbol{\mathcal{A}}\boldsymbol{x}_{cl} + \boldsymbol{\mathcal{B}}\boldsymbol{w} \\
\boldsymbol{z} &= \boldsymbol{\mathcal{C}}\boldsymbol{x}_{cl} + \boldsymbol{\mathcal{D}}\boldsymbol{w},
\end{aligned}
\tag{9}
$$

where

$$
\left(\begin{array}{c|c} \boldsymbol{\mathcal{A}} & \boldsymbol{\mathcal{B}} \\ \hline \boldsymbol{\mathcal{C}} & \boldsymbol{\mathcal{D}}, \end{array}\right) =
$$

[1] Corrigendum corrected in (8) compared to original publication

$$\left(\begin{array}{cc|c} \boldsymbol{A_p + B_p D_l C_p} & \boldsymbol{B_p C_l} & \boldsymbol{B_{w1} + B_p D_l D_{w1}} \\ \boldsymbol{B_l C_p} & \boldsymbol{A_l} & \boldsymbol{B_l D_{w1}} \\ \hline \boldsymbol{C_z + D_z D_l C_p} & \boldsymbol{D_z C_l} & \boldsymbol{D_z D_l D_{w1}} \end{array}\right).$$

3.2 Optimization Problem for DFC Design

The optimization problem after the change of variables is given by

$$\text{minimize } \gamma, \tag{10}$$

$$\text{subject to;} \tag{11}$$

$$\left(\begin{array}{ccc} \hat{\boldsymbol{\mathcal{A}}}^{\mathrm{T}}\hat{\boldsymbol{\mathcal{P}}} + \hat{\boldsymbol{\mathcal{P}}}\hat{\boldsymbol{\mathcal{A}}} & \hat{\boldsymbol{\mathcal{P}}}\hat{\boldsymbol{\mathcal{B}}} & \hat{\boldsymbol{\mathcal{C}}}^{\mathrm{T}} \\ \hat{\boldsymbol{\mathcal{B}}}^{\mathrm{T}}\hat{\boldsymbol{\mathcal{P}}} & -\gamma \boldsymbol{I} & \hat{\boldsymbol{\mathcal{D}}}^{\mathrm{T}} \\ \hat{\boldsymbol{\mathcal{C}}} & \hat{\boldsymbol{\mathcal{D}}} & -\gamma \boldsymbol{I} \end{array}\right) < 0, \quad \gamma > 0,$$

$$\hat{\boldsymbol{\mathcal{P}}} = \left(\begin{array}{cc} \boldsymbol{X} & \boldsymbol{I} \\ \boldsymbol{I} & \boldsymbol{Y} \end{array}\right), \quad \hat{\boldsymbol{\mathcal{P}}} > 0,$$

$$[\alpha_{ij}\boldsymbol{\mathcal{P}} + \beta_{ij}\boldsymbol{\mathcal{A}}^{\mathrm{T}}\boldsymbol{P} + \beta_{ji}\boldsymbol{\mathcal{P}}\boldsymbol{\mathcal{A}}]_{i,j} < 0,$$

where

$$\hat{\boldsymbol{\mathcal{A}}}^{\mathrm{T}}\hat{\boldsymbol{\mathcal{P}}} + \hat{\boldsymbol{\mathcal{P}}}\hat{\boldsymbol{\mathcal{A}}} =$$

$$\left(\begin{array}{c} \boldsymbol{A_p X} + \boldsymbol{X A_p}^{\mathrm{T}} + \boldsymbol{B_p}\hat{\boldsymbol{C}} + (\boldsymbol{B_p}\hat{\boldsymbol{C}})^{\mathrm{T}} \\ \hat{\boldsymbol{A}} + (\boldsymbol{A_p} + \boldsymbol{B_p}\hat{\boldsymbol{D}}\boldsymbol{C_p})^{\mathrm{T}} \end{array}\right.$$

$$\left.\begin{array}{c} \hat{\boldsymbol{A}}^{\mathrm{T}} + (\boldsymbol{A_p} + \boldsymbol{B_p}\hat{\boldsymbol{D}}\boldsymbol{C_p}) \\ \boldsymbol{A_p}^{\mathrm{T}}\boldsymbol{Y} + \boldsymbol{Y}\boldsymbol{A_p} + \hat{\boldsymbol{B}}\boldsymbol{C_p} + (\hat{\boldsymbol{B}}\boldsymbol{C_p})^{\mathrm{T}} \end{array}\right),$$

$$\hat{\boldsymbol{\mathcal{P}}}\hat{\boldsymbol{\mathcal{B}}} = \left(\begin{array}{c} \boldsymbol{B_j} + \boldsymbol{B_p}\hat{\boldsymbol{D}}\boldsymbol{F_j} \\ \boldsymbol{Y}\boldsymbol{B_j} + \hat{\boldsymbol{B}}\boldsymbol{F_j} \end{array}\right),$$

$$\hat{\boldsymbol{\mathcal{C}}} = \left(\begin{array}{cc} \boldsymbol{C_j X} + \boldsymbol{E_j}\hat{\boldsymbol{C}} & \boldsymbol{C_j} + \boldsymbol{E_j}\hat{\boldsymbol{D}}\boldsymbol{C_p} \end{array}\right),$$

$$\hat{\boldsymbol{\mathcal{D}}} = \boldsymbol{E_j}\hat{\boldsymbol{D}}\boldsymbol{F_j},$$

$$\boldsymbol{B_j} := \boldsymbol{B_w}\boldsymbol{R_j}, \quad \boldsymbol{C_j} := \boldsymbol{L_j}\boldsymbol{C_z},$$

$$\boldsymbol{E_j} := \boldsymbol{L_j}\boldsymbol{D_z}, \quad \boldsymbol{F_j} := \boldsymbol{D_w}\boldsymbol{R_j},$$

and $\boldsymbol{L_j}, \boldsymbol{R_j}$ are input/output channel for $T(s)$ from w to z;

$$\boldsymbol{T_j} = \boldsymbol{L_j}\boldsymbol{T}\boldsymbol{R_j}. \tag{12}$$

4 Anti-Windup Control Design

This section describes anti-windup control design for the existing PI controller $\boldsymbol{K}$ and the robust DFC $\boldsymbol{L}$. The anti-windup control design method using the dead zone function is presented by Wada and Saeki [8, 11], and the formulation

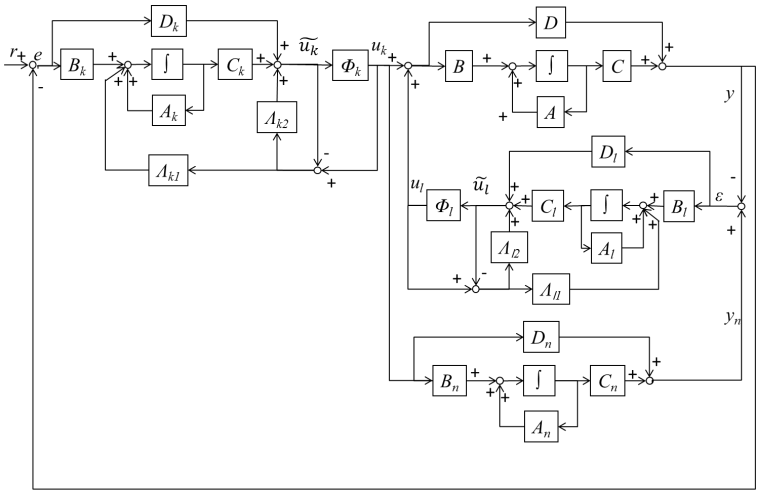

Fig. 3: A state space representation of the PI control with robust DFC including the anti-windup controllers.

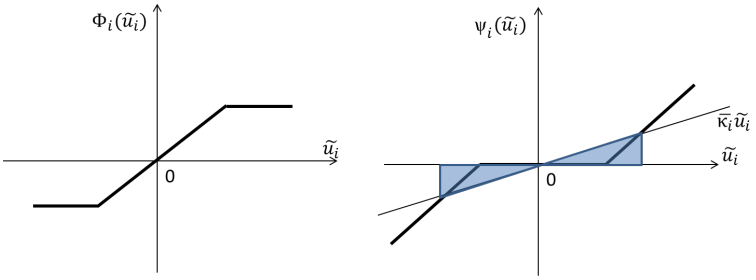

Fig. 4: A saturation function (left) and a dead zone function (right).

and numerical example are derived for 1DOF control systems. As mentioned in Section 1, DFC is categorized as a 2DOF controller, and therefore, the method will be reshaped for DFC.

4.1 The Extended State Space Representation for Anti-Windup Controllers

Now the extended state space representation including the anti-windup controllers are considered in Fig. 5. The nonlinearity is introduced by the actuator constraints. The dead zone function can be described by

$$\boldsymbol{d} = \boldsymbol{\Psi}(\tilde{\boldsymbol{u}}) = \tilde{\boldsymbol{u}} - \boldsymbol{\Phi}(\tilde{\boldsymbol{u}}) \tag{13}$$

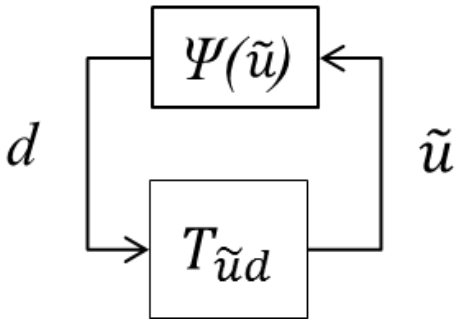

Fig. 5: A simplified feedback system for anti-windup control design.

where $\boldsymbol{\Phi}(\tilde{\boldsymbol{u}})$ is a saturation function, $\boldsymbol{\Psi}(\tilde{\boldsymbol{u}})$ is a dead zone function, and $\tilde{\boldsymbol{u}}$ is a control output vector before saturation block. These two functions are shown in Fig. 6, and $\bar{\kappa} \in [0, 1]$ is a sector parameter to represent the sector bounded nonlinearity [11]. The anti-windup controllers $\boldsymbol{\Lambda_{k1}}$ and $\boldsymbol{\Lambda_{k2}}$ for PI control are described as follows:

$$\begin{aligned} \dot{\boldsymbol{x_k}} &= \boldsymbol{A_k x_k} + \boldsymbol{B_k}(\boldsymbol{r} - \boldsymbol{y}) + \boldsymbol{\Lambda_{k1}}(\boldsymbol{u_k} - \tilde{\boldsymbol{u_k}}) \\ \tilde{\boldsymbol{u_k}} &= \boldsymbol{C_k x_k} + \boldsymbol{D_k}(\boldsymbol{r} - \boldsymbol{y}) + \boldsymbol{\Lambda_{k2}}(\boldsymbol{u_k} - \tilde{\boldsymbol{u_k}}). \end{aligned} \tag{14}$$

Next, the anti-windup controllers $\boldsymbol{\Lambda_{l1}}$ and $\boldsymbol{\Lambda_{l2}}$ for DFC are derived by

$$\begin{aligned} \dot{\boldsymbol{x_l}} &= \boldsymbol{A_l x_l} + \boldsymbol{B_l}(\boldsymbol{r} - \boldsymbol{y}) + \boldsymbol{\Lambda_{l1}}(\boldsymbol{u_l} - \tilde{\boldsymbol{u_l}}) \\ \tilde{\boldsymbol{u_l}} &= \boldsymbol{C_l x_k} + \boldsymbol{D_l}(\boldsymbol{r} - \boldsymbol{y}) + \boldsymbol{\Lambda_{l2}}(\boldsymbol{u_l} - \tilde{\boldsymbol{u_l}}). \end{aligned} \tag{15}$$

The last term of the controllers in (18) and (19), $(\boldsymbol{u_k} - \tilde{\boldsymbol{u_k}})$ and $(\boldsymbol{u_l} - \tilde{\boldsymbol{u_l}})$ can be assumed as disturbance $\boldsymbol{d}$ to consider the internal stability. The system in Fig. 5 can be simplified as Fig. 7[2].

$$\begin{aligned} \dot{\boldsymbol{x}} &= \tilde{\boldsymbol{\mathcal{A}}}\boldsymbol{x} + \tilde{\boldsymbol{\mathcal{B}}}\boldsymbol{d} \\ \tilde{\boldsymbol{u}} &= \tilde{\boldsymbol{\mathcal{C}}}\boldsymbol{x} + \tilde{\boldsymbol{\mathcal{D}}}\boldsymbol{d} \end{aligned} \tag{16}$$

where

$$\begin{pmatrix} \boldsymbol{d_1} \\ \boldsymbol{d_2} \end{pmatrix} = \begin{pmatrix} \tilde{\boldsymbol{u_k}} \\ \tilde{\boldsymbol{u_l}} \end{pmatrix} - \begin{pmatrix} \boldsymbol{u_k} \\ \boldsymbol{u_l} \end{pmatrix}, \tag{17}$$

$$\tilde{\boldsymbol{\mathcal{A}}} = \begin{pmatrix} \boldsymbol{A} - \boldsymbol{B}\boldsymbol{D_k}\boldsymbol{C} - \boldsymbol{B}\boldsymbol{D_l}\boldsymbol{C} & \boldsymbol{B}\boldsymbol{D_l}\boldsymbol{C_n} \\ -\boldsymbol{B_n}\boldsymbol{D_k}\boldsymbol{C} & \boldsymbol{A_n} \\ -\boldsymbol{B_k}\boldsymbol{C} & \boldsymbol{0} \\ -\boldsymbol{B_l}\boldsymbol{C} & \boldsymbol{B_l}\boldsymbol{C_n} \end{pmatrix}$$

[2]Corrigendum corrected in (17) compared to original publication

$$\begin{pmatrix} \boldsymbol{BC_k} & \boldsymbol{BC_l} \\ \boldsymbol{B_nC_k} & \boldsymbol{0} \\ \boldsymbol{A_k} & \boldsymbol{0} \\ \boldsymbol{0} & \boldsymbol{A_l} \end{pmatrix},$$

$$\tilde{\boldsymbol{\mathcal{B}}} = \begin{pmatrix} -\boldsymbol{B}(\boldsymbol{\Lambda_{k2}} + \boldsymbol{I}) & -\boldsymbol{B}(\boldsymbol{\Lambda_{l2}} + \boldsymbol{I}) \\ -\boldsymbol{B_n}(\boldsymbol{\Lambda_{k2}} + \boldsymbol{I}) & \boldsymbol{0} \\ -\boldsymbol{\Lambda_{k1}} & \boldsymbol{0} \\ \boldsymbol{0} & -\boldsymbol{\Lambda_{l1}} \end{pmatrix},$$

$$\tilde{\boldsymbol{\mathcal{C}}} = \begin{pmatrix} -\boldsymbol{D_kC} & \boldsymbol{0} & \boldsymbol{C_k} & \boldsymbol{0} \\ -\boldsymbol{D_lC} & \boldsymbol{D_lC_n} & \boldsymbol{0} & \boldsymbol{C_l} \end{pmatrix},$$

$$\tilde{\boldsymbol{\mathcal{D}}} = \begin{pmatrix} -\boldsymbol{\Lambda_{k2}} & \boldsymbol{0} \\ \boldsymbol{0} & -\boldsymbol{\Lambda_{l2}} \end{pmatrix}.$$

4.2 LMIs for Anti-windup Controllers

This subsection describes how to formulate the optimization problem for the robust DFC with anti-windup controllers. First, recall the LMI of positive-real lemma [12], the lemma yields a frequency-domain interpretation for a certain LMI. A transfer function $G(s) := \boldsymbol{C}(sI - \boldsymbol{A})^{-1}\boldsymbol{B} + \boldsymbol{D}$ is positive real, which means that

$$G(j\omega) + G(j\omega)^* > 0, \forall\omega, \tag{18}$$

if the following LMI has a solution $\boldsymbol{P}$ that satisfies

$$\begin{pmatrix} \boldsymbol{PA} + \boldsymbol{A}^{\mathrm{T}}\boldsymbol{P} & \boldsymbol{PB} - \boldsymbol{C}^T \\ \boldsymbol{B}^T\boldsymbol{P} - \boldsymbol{C} & -\boldsymbol{D} - \boldsymbol{D}^T \end{pmatrix} \leq 0,$$

$$\boldsymbol{P} = \boldsymbol{P}^{\mathrm{T}} > 0. \tag{19}$$

This positive real is equivalent to the passivity, and the LMI (19) is feasible if and only if the linear system $G(j\omega)$ is *passive*. Next, the multi-variable circle theorem [13] is applied in (18), and we obtain

$$(I - \bar{\kappa}G(j\omega)) + (I - \bar{\kappa}G(j\omega))^* > 0, \forall\omega. \tag{20}$$

Now consider the anti-windup DFC design about (20). The stability condition for the closed loop system $T_{ud}(s) := \tilde{\boldsymbol{\mathcal{C}}}(sI - \tilde{\boldsymbol{\mathcal{A}}})^{-1}\tilde{\boldsymbol{\mathcal{B}}} + \tilde{\boldsymbol{\mathcal{D}}}$ is given by

$$(I - \bar{\kappa}T_{ud}(j\omega)) + (I - \bar{\kappa}T_{ud}(j\omega))^* > 0, \forall\omega, \tag{21}$$

if the following LMI has a solution $\tilde{\boldsymbol{\mathcal{P}}}$ that satisfies

$$\begin{pmatrix} \tilde{\boldsymbol{\mathcal{P}}}\tilde{\boldsymbol{\mathcal{A}}} + \tilde{\boldsymbol{\mathcal{A}}}^{\mathrm{T}}\tilde{\boldsymbol{\mathcal{P}}} & \tilde{\boldsymbol{\mathcal{B}}} + \tilde{\boldsymbol{\mathcal{P}}}\tilde{\boldsymbol{\mathcal{C}}}^{\mathrm{T}}\bar{\kappa} \\ \tilde{\boldsymbol{\mathcal{B}}}^{\mathrm{T}} + \bar{\kappa}\tilde{\boldsymbol{\mathcal{C}}}\tilde{\boldsymbol{\mathcal{P}}} & \bar{\kappa}\tilde{\boldsymbol{\mathcal{D}}} + \tilde{\boldsymbol{\mathcal{D}}}^{\mathrm{T}}\bar{\kappa} - 2\boldsymbol{I} \end{pmatrix} \leq 0,$$

$$\tilde{\boldsymbol{\mathcal{P}}} = \tilde{\boldsymbol{\mathcal{P}}}^{\mathrm{T}} > 0. \tag{22}$$

5 Numerical Examples

This section demonstrates the proposed design on a model of a MIMO water chiller system, which has model uncertainty and slow time constant and delay. Especially the superheat control is challenging to design because the refrigerant has non-linearity which comes from two-phase vapor-liquid refrigerant at the evaporator. This non-linearity can be represented by model uncertainties. Practical results indicate that the dominant uncertainty is the process gain of the superheat model [1, 14].

The system includes four main components; a compressor, a condenser, an expansion valve, and an evaporator. In a basic refrigeration system, one control device is installed for each component as shown in Fig. 10. These controllers regulate pressure or temperature based on operating conditions. A hot water tank is set as heat load. For example, the rotational speed of the compressor is controlled to keep a constant refrigerant suction pressure P_e. The opening degree of the expansion valve maintains a suitable refrigerant superheat T_{sh} (difference between the temperature at the outlet of the evaporator and the evaporation temperature inside the evaporator). The speed of the evaporator fan is controlled to keep the temperature on the load side T_r constant. The speed of the condenser fan is controlled in order to keep the condensing pressure P_c constant.

5.1 Modeling of the Water Chiller System

A simple superheat model and a suction pressure model is chosen for the MIMO control design and these models can be described by a first order plus dead time system, e.g., see [15]. The model is created using experimental data obtained from step response tests conducted at different operating conditions.

$$\begin{aligned} \mathcal{G}_{ij} &= \frac{k_{ij}}{1+\tau_{ij}s}e^{-\theta_{ij}s}; \\ k_{ij} &\in [k_{min,ij}, k_{max,ij}], \tau_{ij} \in [\tau_{min,ij}, \tau_{max,ij}], \\ \theta_{ij} &\in [\theta_{min,ij}, \theta_{max,ij}], \\ i &= 1,2, j = 1,2. \end{aligned} \tag{23}$$

Next, the nominal model is computed using average parameter values of $\mathcal{G}$.

$$G_{n,ij} = \frac{k_{n,ij}}{1+\tau_{n,ij}s}e^{-\theta_{n,ij}s}. \tag{24}$$

For more simple DFC design, the time delay is approximated by a second order system. In addition, only one parameter k_{11} is chosen as main uncertainty because a plant gain of the superheat k_{11} is the most dominant part of the

Fig. 6: A layout of the water chiller system with basic control structure.

Table 1: Estimation results of parameter uncertainty.

	k	τ	θ
g_{11}	[-10.00 -9.00]	[34.73 62.46]	[14 29]
g_{21}	[0.061 0.22]	[2.01 21.40]	[0 2]
g_{12}	[-0.55 -0.36]	[8.37 15.50]	[0 3]
g_{22}	[-0.073 -0.047]	[5.43 15.29]	[0 3]

uncertainty and nonlinearity, shown in Table 1. Therefore, G and G_n are approximated as follows:

$$\mathcal{G}_{11} = \frac{k_{11}}{(1+\tau_{n,11}s)(1+\theta_{n,11}s)}; \qquad (25)$$
$$k_{11} \in [k_{min,11}, k_{max,11}],$$

and the rest of the subsystems are expressed by the nominal model.

$$\mathcal{G}_{ij} = \frac{k_{n,ij}}{(1+\tau_{n,ij}s)(1+\theta_{n,ij}s)}; \qquad (26)$$
$$i = 1,2, j = 1,2, except \quad ij = 11.$$

A PI controller K and a disturbance weighting function W are designed by parameter values in Table 1 and Table 2.

5.2 Robust DFC with Anti-windup control

This subsection demonstrates the robust DFC with anti-windup control by two types of LMIs. First, the robust DFC without saturation are designed, and then the anti-windup controllers are solved for both of the PI and robust DFC controllers.

Table 2: Primary parameter uncertainty and nominal parameters for LMI design.

	k	τ	θ
g_{11}	[-10.00 -9.00]	[48.60]	[21.5]
$g_{n,21}$	[0.141]	[11.71]	[1]
$g_{n,12}$	[-0.455]	[11.93]	[1.5]
$g_{n,22}$	[-0.060]	[10.36]	[1.5]

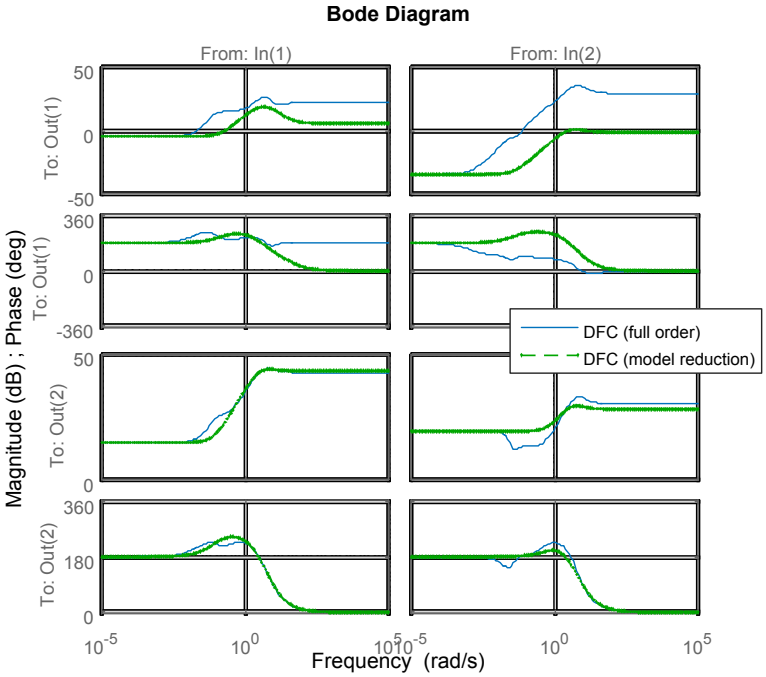

Fig. 7: Bode plots of DFC from ϵ to u_l, before and after model reduction.

The optimal H_∞ performance was $\gamma = 0.8255$ with full order DFC without saturation, and the DFC was a 20th order system because $dim(A_l) = 2(n + m), n = 8, m = 2$. It would be more useful for industrial systems if a lower order DFC can be obtained. Therefore, model reduction of DFC is considered, and the second order DFC $\boldsymbol{L}$ is given by the Matlab command `modred`.

$$\begin{aligned} \boldsymbol{A_l} &= \begin{pmatrix} -8.77 & 4.013 \\ -4.001 & -0.269 \end{pmatrix}, \boldsymbol{B_l} = \begin{pmatrix} -50.73 & -8.971 \\ -5.897 & -1.963 \end{pmatrix} \\ \boldsymbol{C_l} &= \begin{pmatrix} 1.829 & 0.1461 \\ 51.49 & -6.214 \end{pmatrix}, \boldsymbol{D_l} = \begin{pmatrix} 1.921 & 0.856 \\ 149.8 & 25.77 \end{pmatrix}. \end{aligned} \tag{27}$$

Fig. 11 shows bode-plots in comparison with DFCs before/after the model reduction. The figure indicates that the second order DFC can maintain the main feature of the original DFC. Next anti-windup controllers are designed for both of PI and robust DFC controllers. The sector parameter $\bar{\kappa}$ is set as $0.9\boldsymbol{I}$ from a result of a line search. The anti-windup controllers to stabilize MIMO

Table 3: Simulation conditions.

Items	Values	Unit	Remarks
Set point r_1	10.0	[C]	
Set point r_2	0.0	[bar]	
Disturbance w_1	-1.0	[C]	
Disturbance w_2	0.0	[bar]	
Step time of set points	1.0	[sec]	
Step time of disturbances	500	[sec]	
Simulation time T	1000	[sec]	
Control output u_{k1}	[-2.5, 2.5]	[-]	input constraint
Control output u_{l1}	[-1.0, 1.0]	[-]	input constraint
Control output u_{k2}	[-2.5, 2.5]	[Hz]	input constraint
Control output u_{l2}	[-1.0, 1.0]	[Hz]	input constraint

system was solved by (23), and then we obtained the results as

$$\begin{aligned}
\boldsymbol{\Lambda_{k1}} &= \begin{pmatrix} -7.2632 & -82.1123 \\ -11.2030 & -611.2147 \end{pmatrix}, \\
\boldsymbol{\Lambda_{k2}} &= \begin{pmatrix} 99.6055 & -4.9722 \\ -11.6266 & 669.6095 \end{pmatrix}, \\
\boldsymbol{\Lambda_{l1}} &= \begin{pmatrix} 4.6105 & -45.6700 \\ 0.4424 & 28.3426 \end{pmatrix}, \\
\boldsymbol{\Lambda_{l2}} &= \begin{pmatrix} -1.0010 & 9.1893 \\ -12.1928 & 571.5409 \end{pmatrix}.
\end{aligned} \tag{28}$$

Now simulation tests are examined, and step response and load disturbance response are evaluated for PI with/without robust DFC and with/without anti-windup controller as shown as Fig. 15 and Fig. 16. The each design method simulates three cases about g_{11}, where $k_{min} = -10.0$ as case 1, $k_{max} = -9.0$ as case 2, $k_n = -9.5$ as case 3.

Table 4 shows the evaluation results of each design method. Five design methods are examined, and then evaluated by six items. Item number 1, 2 evaluate the robustness of controllers from model uncertainties δ as shown in Fig. 17. These items calculate the absolute values $|y_{case_i}(t) - y_{case_i}(t)|,\ i = 1,2,3,\ t = [0,T]$, then choose the maximum values from the results. In addition, Item number 3, 4 evaluate the control performance using mean values of Integral Absolute Error (IAE). Moreover, Yes/No questions are prepared in item number 5 and 6. The item number 5 checks whether the each design can keep the limiter of input u_2 or not, and the item number 6 checks whether the each design can track the set point y_2.

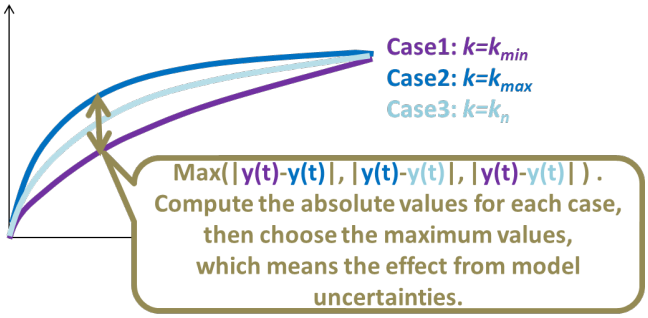

Fig. 8: An explanation of the item number 1 and 2, the robustness of controllers from model uncertainties.

Note that the bold values in Table 4 indicate the best (minimum) value for all design methods, which values are determined by the logical product; *minimum value* $\wedge$ *two sets of Yes*. Moreover, the minimum values excluding *two sets of Yes* are described superscript $*$ at the right side of the values.

Design method number one, PI + robust DFC with anti-windup controller obtains the best values for all items. On the other hand, design method number two, PI + robust DFC *without* anti-windup degrades the performance due to the integral windup phenomenon as shown in Table 4 and Fig. 15. Design method number three, four, and five cannot secure *two sets of Yes*. The number three and five can track the set point y_2. However, these design breach the input constraint u_2. Conversely, the number four cannot achieve the tracking the set point y_2 due to saturation of u_2 as shown in Fig. 16. Therefore, these methods do not work at real systems.

As results of the simulation, the design method number one, PI control + robust DFC with anti-windup controller, demonstrates the best control performance while keeping the input constraints.

6 Discussion and Conclusions

This paper proposed a control design method for anti-windup disturbance feedback control. The control design is derived by formulating two sets of LMIs, one for solving the robust DFC problem, and a second for stabilizing the closed loop system with anti-windup controllers. Simulation of a water chiller system demonstrates the effectiveness of the proposed method. In the future, we will try another type of systems such as mechanical systems for the Factory Automation (FA).

Table 4: Evaluations of each control design.

	Design method number	1	2	3	4	5
Item number	Description	PI + Robust DFC with AW	PI + Robust DFC without AWC	PI + Robust DFC no saturation	PI control without AWC	PI control no saturation
1	Robustness from δ_{y_1}	**0.1677***	0.1677*	0.2011	0.5455	0.4996
2	Robustness from δ_{y_2}	**0.0193**	0.0201	0.0065	0.0172	0.0026*
3	Mean value of IAE of y_1	**764.3183**	771.5813	763.9305*	820.6928	806.37
4	Mean value of IAE of y_2	**4.8645**	5.8291	4.7221	5.9216	3.9264*
5	Keep the limiter of u_2?	Yes	Yes	No	Yes	No
6	Track the set point of y_2?	Yes	Yes	Yes	No	Yes

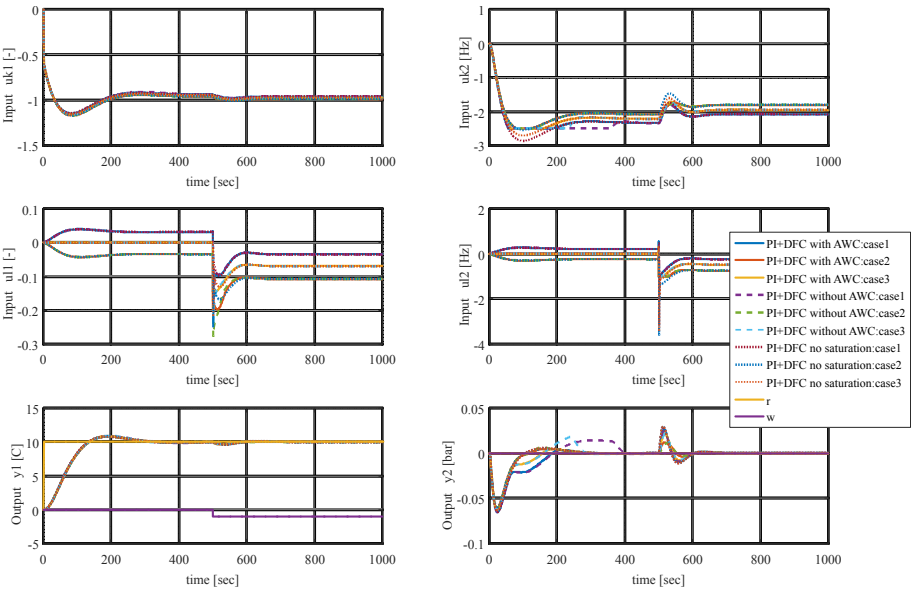

Fig. 9: Simulation results of the PI control + robust DFC.

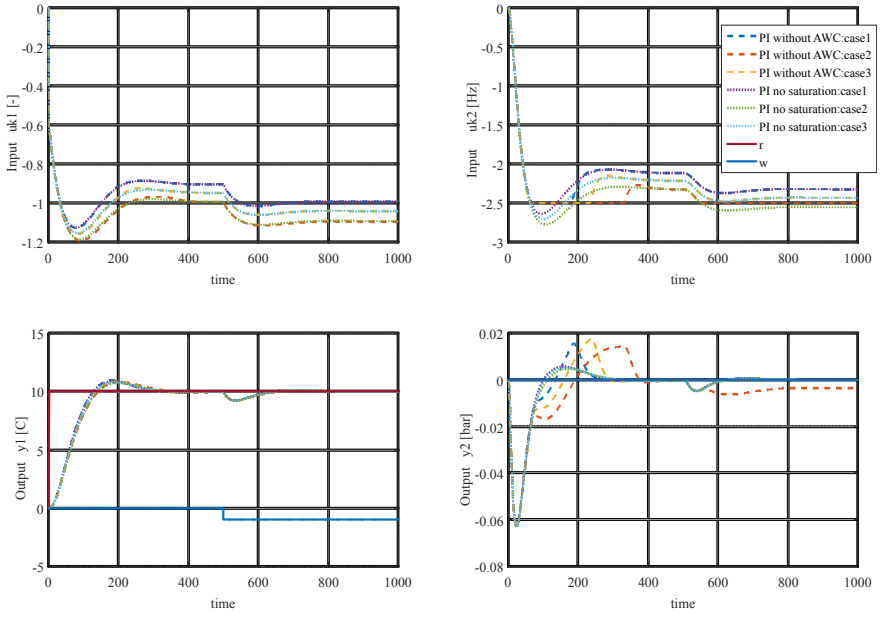

Fig. 10: Simulation results of the PI control.

References

[1] F. Kawai, K. Vinther, P. Anderson, and J. D. Bendtsen, "Mimo robust disturbance feedback control for refrigeration systems via an lmi approach," in *Proc. IFAC 2017*, Toulouse, Jul. 2017, pp. 14 525 – 14 532.

[2] A. T. on Modern Anti-windup Design, "Automatic tuning and adaptation for PID controllers-a survey," *European Journal of Control*, vol. 15, no. 3-4, pp. 418–440, 2009.

[3] P. M. Gahinet and P. Apkarian, "A Linear Matrix Inequality Approach to H_∞ Control," *International Journal of Robust and Nonlinear Control*, vol. 4, no. 4, pp. 421–448, 1994.

[4] R. W. Cottle, "Manifestations of the Schur complement," *Linear Algebra and its Applications*, vol. 8, no. 3, pp. 189–211, 1974.

[5] M. Ge, M.-S. Chiu, and Q.-G. Wang, "Robust PID controller design via LMI approach," *Journal of Process Control*, vol. 12, no. 1, pp. 3–13, 2002.

[6] M. Sadabadi and A. Karimi, "An lmi formulation of fixed-order h infinity and h2 controller design for discrete-time systems with polytopic uncertainty," in *Proc. Decision and Control (CDC), 2013 IEEE 52nd Annual Conference*, Firenze, 2013, pp. 2453 – 2458.

[7] G. Grimm, A. R. Teel, and L. Zaccarian, "Robust linear anti-windup synthesis for recovery of unconstrained performance," *Int. J. Robust Nonlinear Control,*, vol. 14, no. 13-14, pp. 1133—1168, 2004.

[8] U. Wasiwitono and M. Saeki, "Fixed-Order Output Feedback Control and Anti-Windup Compensation for Active Suspension Systems," *Journal of System Design and Dynamics*, vol. 5, no. 2, pp. 264–278, 2011.

[9] Carsten Scherer and Siep Weiland. (2004) Linear matrix inequalities in control. [Online]. Available: http://www.dcsc.tudelft.nl/~cscherer/lmi/notes05.pdf

[10] C. Scherer, P. Gahinet, and M. Chilali, "Multiobjective Output-Feedback Control via LMI Optimization," *IEEE Transactions on Automatic Control*, vol. 42, no. 7, pp. 896–911, 1997.

[11] N. Wada and M. Saeki, "Synthesis of a static anti-windup compensator via linear matrix inequalities," in *the 3rd IFAC Symposium on Robust Control Design*, Prague.

[12] S. Boyd, L. E. Ghaoui, E. Feron, and V. Balakrishnan, *Linear Matrix Inequalities in System and Control Theory*. Society for Industrial and Applied Mathematics (SIAM), 1994.

[13] H. Rosenbrock, *Multivariable circle criterion in recent Mathematical Development in Control*. D.J. Bell, Ed., 1973.

[14] K. Vinther, R. J. Nielsen, K. M. Nielsen, P. Andersen, T. S. Pedersen, and J. D. Bendtsen, "Absorption Cycle Heat Pump Model for Control Design," in *2015 European Control Conference (ECC)*, 2015.

[15] R. Izadi-Zamanabadi, K. Vinther, H. Mojallali, H. Rasmussen, and J. Stoustrup, "Evaporator unit as a benchmark for plug and play and fault tolerant control," in *Proc. 8th IFAC Symposium on Fault Detection, Supervision and Safety of Technical Processes*, Mexico City, Mexico, 2012, pp. 701–706.

Paper D

Anti-windup Disturbance Feedback Control: Practical Design with Robustness

Fukiko Kawai, Kasper Vinther, Palle Andersen, and Jan D. Bendtsen

The paper has been published in the
Journal of Process Control, Vol. 69, 09.2018, p. 30-43.

The layout has been revised.

Abstract

This paper presents a practical design method of robust Disturbance Feedback Control (DFC) along with an application to industrial refrigeration systems. DFC is a controller configuration in which an existing controller is augmented with an additional loop. The design method for DFC is proposed in two steps; firstly, the robust DFC without saturation is designed by a Linear Matrix Inequality (LMI) approach, and then LMI techniques are used again for designing an anti-windup compensator to accommodate actuator saturation. The proposed method is compared to a conventional design on a water chiller system, both in simulation and through practical experiments. The test results indicate that both robustness and performance can be improved in the presence of model uncertainties, and the proposed method can avoid wind-up phenomena when the control inputs are saturated.

1 Introduction

Disturbance Feedback Control (DFC) was originally developed by Fuji Electric in 1980 [1]. DFC has been applied in industrial systems for attenuating disturbances, such as motor drive systems [2]. In addition to a standard reference-following regulator, this control structure incorporates an additional *feedback* loop to compensate for disturbance and model uncertainties. The control structure can thus be categorized as a two-degree-of-freedom (2DOF) controller. Especially, a 2DOF control, composed of a stand PID control and DFC, can be chosen for practical design of industrial applications.

As for practical design with robustness, various tuning methods for PID control or low order controllers have been proposed, see e.g.,[3], [4], [5], [6]. In addition, methods for PID control design relying on optimization via Linear Matrix Inequalities (LMIs) to satisfy certain stability and robustness requirements have been proposed [7]. Moreover, combinations of robust control and Internal Model Control (IMC) have been proposed as new challenges in the literature [8].

Note that DFC is not the same as IMC [9] because DFC has two feedback signals, which means two degrees of freedom. Basic IMC has only one feedback signal, which will be zero when there is no modeling error. Also, DFC allows for a two-step design in which a classical controller is designed first, and then subsequently augmented by the extra feedback for better disturbance rejection.

In addition, the IMC structure and the classical feedback structure are equivalent representations [10]. Here, IMC and PI control as a classical feedback control can be equivalent, and therefore PI control with or without DFC will be compared in Section 3, instead of IMC. The challenges of adding new controllers and new subsystems to a plant are treated in related research on

the plug & play control, see [11, 12].

In a previous study, the authors presented a low order robust DFC for a water chiller system, to address the control issues of performance degradation due to non-linearities and load disturbances [13]. The robust DFC was found to improve the performance compared to conventional PI control. However, for a more practical design, an anti-windup scheme is necessary to handle the constraints of the control devices and actuators.

A tutorial on modern anti-windup design can be found in [14], in which two approaches, namely direct linear anti-windup and model recovery anti-windup, are presented. In addition, the authors state that most anti-windup designs can be formulated by LMIs. LMI-based anti-windup synthesis methods have been proposed for robust control of linear systems [15]. Another approach in which a dead-zone is introduced for anti-windup control design, and a local control design technique is proposed, is presented in [16]. Anti-windup schemes for discrete time system using LMI based design were proposed by Rohman et al [17] in order to address the issues of the algebraic loops of anti-windup controllers.

In general, anti-windup designs are considered for one-degree-of freedom (1DOF) controllers for closed loop systems. However, 2DOF controllers are used for many industrial applications because the systems need to guarantee both set point following and disturbance rejection responses.

Therefore, it could be useful for industrial applications to find a design methods for anti-windup 2DOF controllers for discrete time systems. In addition, numerical analysis including experimental test is necessary to find out whether the previous studies can be applied for 2DOF systems as well.

For these reasons, this paper introduces an anti-windup compensator for 2DOF controllers, one for an existing controller and another for DFC, in a discrete time systems. The proposed design method is applied to superheat control and suction pressure control in a refrigeration system. Both simulations and experimental tests are examined to evaluate the robustness of DFC and the effectiveness of the anti-windup scheme, and clear performance improvements can be observed by the addition of DFC.

The rest of the paper first explains the DFC design method in Section 3, providing LMI formulations for DFC design with anti-windup compensation. After that, experimental results of refrigeration system control are demonstrated in Section 3. Finally, conclusions are given in Section 4.

2 DFC Design

Fig. 1 shows block diagrams of an existing control system (Left) and the same system augmented with DFC (Right). The existing controller K is assumed to be a 1DOF controller, a PID controller for instance, and it may be designed

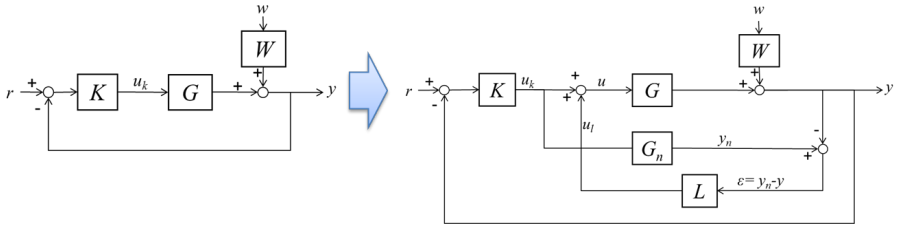

Fig. 1: Block diagrams of existing control systems(Left), and the existing control with DFC(Right).

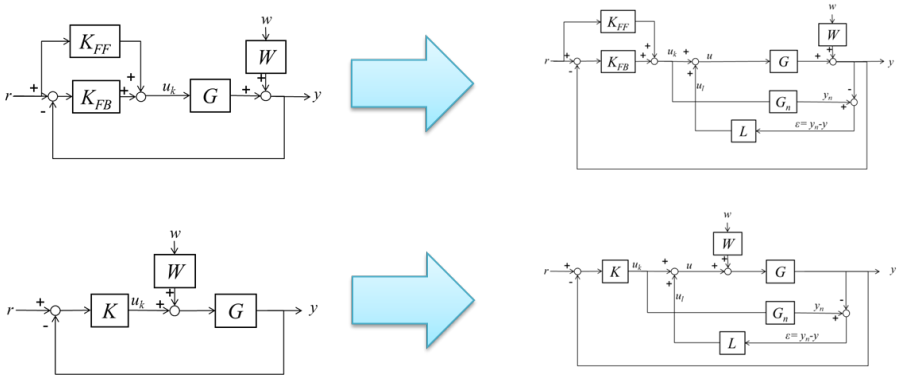

Fig. 2: Block diagrams of other variations about existing control systems(Left), and the existing control with DFC(Right).

by traditional methods; IMC, pole placement, or similar. W is a disturbance weighting transfer matrix.

On the right side, DFC is added to the existing control system to improve the robustness against disturbances. In addition, DFC can work to compensate for model uncertainties if there are modeling errors between the nominal model G_n and the actual plant G. Notice how the DFC control signal is added to the existing control signal after the u_k branch; this configuration makes DFC different from IMC [9].

Other variations of DFC can be described as shown in Fig. 2. In one variant, the existing controller is composed of a feedback and a feedforward part. In another variant, a weighting function W places more emphasis on certain disturbance frequency ranges. The method presented in the following applies to these variants as well with minor modifications.

This section presents a method to design the DFC to meet certain stability and robustness requirements. Firstly, the existing control systems are defined. Next, LMIs for the DFC synthesis are presented, and finally the controller is discretized and augmented with anti-windup.

2.1 Existing Control Systems

The plant model G in Fig. 1 is assumed given as a time domain representation in state space;

$$\begin{aligned} \dot{x} &= Ax + Bu \\ y - d &= Cx, \end{aligned} \tag{1}$$

where $A \in \mathbb{R}^{n\times n}$, $B \in \mathbb{R}^{n\times m}$, and $C \in \mathbb{R}^{m\times n}$ are real constant matrices. $x \in \mathbb{R}^n$ is the plant state, $u \in \mathbb{R}^m$ is the control input and $y \in \mathbb{R}^m$ is the output. The plant parameters are affected by parametric uncertainties [18]) expressed by

$$A = A_n + \sum_{i=1}^{p} \delta_{a,i} A_i, \quad \delta_{a,i} \in [-1, +1], \tag{2}$$

$$B = B_n + \sum_{i=1}^{q} \delta_{b,i} B_i, \quad \delta_{b,i} \in [-1, +1], \tag{3}$$

$$C = C_n + \sum_{i=1}^{r} \delta_{c,i} C_i, \quad \delta_{c,i} \in [-1, +1], \tag{4}$$

where $\delta_a = (\delta_{a,1}, \ldots, \delta_{a,p})$, $\delta_b = (\delta_{b,1}, \ldots, \delta_{b,q})$, $\delta_c = (\delta_{c,1}, \ldots, \delta_{c,r})$ are unknown vectors, which express the ensemble of all uncertainty quantities in a given dynamics, A_n, B_n, and C_n are the nominal state space representation corresponding to G_n, and A_i, B_i, and C_i describe the uncertainties.

The existing control K is given by

$$\begin{aligned} \dot{x}_k &= A_k x_k + B_k(r - y), \\ u_k &= C_k x_k + D_k(r - y), \end{aligned} \tag{5}$$

where $r \in \mathbb{R}^m$ is a reference signal, and $A_k \in \mathbb{R}^{n_K\times n_K}$, $B_k \in \mathbb{R}^{n_K\times m}$, $C_k \in \mathbb{R}^{m\times n_K}$, and $D_k \in \mathbb{R}^{m\times m}$ comprise the state space representation of K.

The weighting function W for the disturbance d is defined as

$$\begin{aligned} \dot{x}_w &= A_w x_w + B_w w, \\ d &= C_w x_w + D_w w, \end{aligned} \tag{6}$$

where $A_w \in \mathbb{R}^{n_W\times n_W}$, $B_w \in \mathbb{R}^{n_W\times m}$, $C_w \in \mathbb{R}^{m\times n_W}$, and $D_w \in \mathbb{R}^{m\times m}$ are the state space representation of the weighting function. $w \in \mathbb{R}^m$ is an external bounded signal. Note that this weight function W is designed as weighting filter using classical H_∞ theory [19].

2.2 DFC Design for Existing Control Systems

We now consider adding the DFC block L in the right part of Fig. 1. This is done using the well-known configuration shown in Fig. 3, where the vector

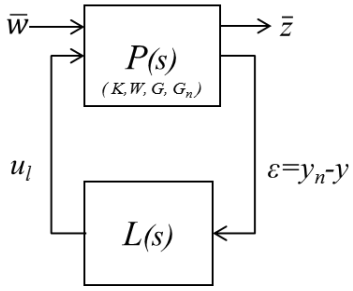

Fig. 3: A closed-loop system for design of DFC $L(s)$.

signal $\bar{w}$ contains the external inputs, disturbance w and measurement noise w_n, and $\bar{z}$ denotes outputs for evaluating performance. Note that the motivation of the DFC design is to improve the disturbance rejection of existing system since the existing controller already stabilizes the plant. Therefore, r is disregarded as an external input, and removed away from DFC design.

We assume that the existing controller K is fixed, meaning we can deal with K as a part of the plant P. Thus, P includes G, G_n, W, and K in the DFC design.

The DFC is designed by classical and modern robust control theory, where W is chosen with weighting filter scheme of classical H_∞ theory, and the robust DFC is designed via LMI optimization using modern robust control theory.

The Disturbance Feedback Controller (DFC) is chosen as

$$\begin{aligned} \dot{x}_{ul} &= A_l x_{ul} + B_l \epsilon \\ u_l &= C_l x_{ul} + D_l \epsilon, \end{aligned} \tag{7}$$

where $A_l \in \mathbb{R}^{(2n+n_K+n_W)\times(2n+n_K+n_W)}$, $B_l \in \mathbb{R}^{(2n+n_K+n_W)\times m}$, $C_l \in \mathbb{R}^{m\times(2n+n_K+n_W)}$, and $D_l \in \mathbb{R}^{m\times m}$.

Note that DFC, as presented in this paper, is a full order output feedback controller, and thus the scheme proposed in [20], can be applied in the DFC design. Firstly, the closed loop transfer matrix $T(s) : \bar{w} \mapsto \bar{z}$ is obtained by way of an extended state space representation. Next, two constraints are introduced in order to design L. Here, we make use of the Bounded Real Lemma and regional pole placement for continuous time systems [20, 21]. The Bounded Real Lemma is used to guarantee robust performance, and regional pole placement is introduced to specify the control performance. Then, a linearizing change of variable is needed to formulate the problem in terms of LMIs.

The extended state space representation of the overall system shown in Fig. 4, can be written as follows;

$$\begin{aligned}
\dot{x}_p &= A_p x_p + B_{pw}\bar{w} + B_p u_l \\
\bar{z} &= C_z x_p + D_z u_l \\
\epsilon &= C_p x_p + D_{pw}\bar{w},
\end{aligned} \tag{8}$$

where

$$x_p = \begin{pmatrix} x^{\mathrm{T}} & {x_n}^{\mathrm{T}} & {x_k}^{\mathrm{T}} & {x_w}^{\mathrm{T}} \end{pmatrix}^{\mathrm{T}},$$

$$A_p = \begin{pmatrix} A - BD_kC & 0 & BC_k & -BD_kC_w \\ -B_nD_kC & A_n & B_nC_k & -B_nD_kC_w \\ -B_kC & 0 & A_k & -B_kC_w \\ 0 & 0 & 0 & A_w \end{pmatrix},$$

$$B_{pw} = \left(\begin{array}{cccc} 0 & 0 & 0 & 0 \\ \hline -(BD_kD_w)^{\mathrm{T}} & -(B_nD_kD_w)^{\mathrm{T}} & -(B_kD_w)^{\mathrm{T}} & {B_w}^{\mathrm{T}} \end{array}\right)^{\mathrm{T}},$$

$$B_p = \begin{pmatrix} B^{\mathrm{T}} & 0 & 0 & 0 \end{pmatrix}^{\mathrm{T}},$$

$$C_z = \left(\begin{array}{cccc} -C & C_n & 0 & -C_w \\ \hline 0 & 0 & 0 & 0 \end{array}\right),$$

$$C_p = \begin{pmatrix} -C & C_n & 0 & -C_w \end{pmatrix},$$

$$D_z = \left(\begin{array}{c} 0 \\ \hline \rho_z I \end{array}\right), \quad D_{pw} = \left(\begin{array}{c|c} \rho_w I & 0 \end{array}\right),$$

In the above, ρ_z and ρ_w are small scalars which are introduced to maintain full rank and to avoid numerical issues if D_z and D_{pw} are zero matrices. Note that $\bar{z} = ({\epsilon_z}^{\mathrm{T}}, (\bar{D}_z u_l)^{\mathrm{T}})^{\mathrm{T}}$ where $\epsilon_z = y_n - (Cx + C_w x_w)$, $\bar{D}_z = \rho_z I$, and $\bar{D}_{pw} = \rho_w I$.

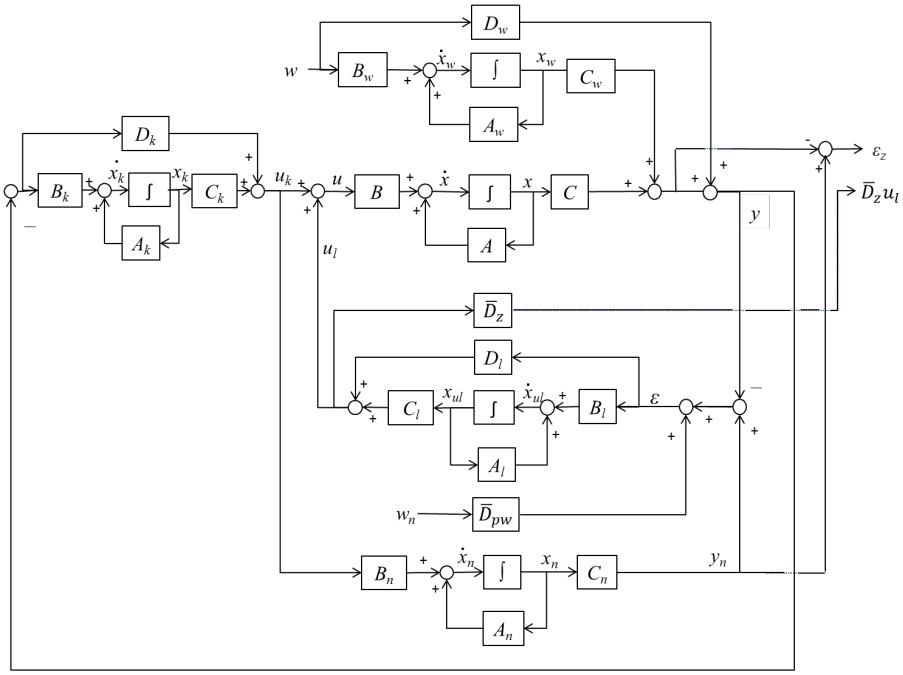

Fig. 4: State space representation of the DFC design.

The closed loop transfer function $T(s)$ from $\bar{w}$ to $\bar{z}$ becomes;

$$\begin{aligned} \dot{x_{cl}} &= \mathcal{A}x_{cl} + \mathcal{B}\bar{w} \\ \bar{z} &= \mathcal{C}x_{cl} + \mathcal{D}\bar{w}, \end{aligned} \tag{9}$$

where

$$\left(\begin{array}{c|c} \mathcal{A} & \mathcal{B} \\ \hline \mathcal{C} & \mathcal{D} \end{array}\right) = \left(\begin{array}{cc|c} A_p + B_p D_l C_p & B_p C_l & B_{pw} + B_p D_l D_{pw} \\ B_l C_p & A_l & B_l D_{pw} \\ \hline C_z + D_z D_l C_p & D_z C_l & D_z D_l D_{pw} \end{array}\right),$$

which has to be stabilized for all possible values of $\delta_{a,i}$, $\delta_{b,i}$, $\delta_{c,i}$. Using the Bounded Real Lemma [20] and regional pole placement [21], we formulate the following optimization problem.

$$\underset{X,Y,\hat{A},\hat{B},\hat{C},\hat{D}}{\text{minimize}} \qquad \gamma_1, \tag{10}$$

$$\text{subject to;} \tag{11}$$

$$\begin{pmatrix} \hat{\mathcal{A}}_\circ{}^{\mathrm{T}}\hat{\mathcal{P}} + \hat{\mathcal{P}}\hat{\mathcal{A}}_\circ & \hat{\mathcal{P}}\hat{\mathcal{B}}_\circ & \hat{\mathcal{C}}_\circ{}^{\mathrm{T}} \\ \hat{\mathcal{B}}_\circ{}^{\mathrm{T}}\hat{\mathcal{P}} & -\gamma_1 I & \hat{\mathcal{D}}^{\mathrm{T}} \\ \hat{\mathcal{C}} & \hat{\mathcal{D}} & -\gamma_1 I \end{pmatrix} < 0, \quad \gamma_1 > 0,$$

$$\hat{\mathcal{P}} = \begin{pmatrix} X & I \\ I & Y \end{pmatrix}, \quad \hat{\mathcal{P}} > 0,$$

$$2\alpha\hat{\mathcal{P}} + \hat{\mathcal{A}}_\circ{}^{\mathrm{T}}\hat{\mathcal{P}} + \hat{\mathcal{P}}\hat{\mathcal{A}}_\circ < 0,$$

where (12)

$$\hat{\mathcal{A}}_\circ{}^{\mathrm{T}}\hat{\mathcal{P}} + \hat{\mathcal{P}}\hat{\mathcal{A}}_\circ =$$

$$\begin{pmatrix} A_pX + XA_p{}^{\mathrm{T}} + B_p\hat{C} + (B_p\hat{C})^{\mathrm{T}} & \hat{A} + (A_p + B_p\hat{D}C_p)^{\mathrm{T}} \\ \hat{A}^{\mathrm{T}} + (A_p + B_p\hat{D}C_p) & A_p{}^{\mathrm{T}}Y + YA_p + \hat{B}C_p + (\hat{B}C_p)^{\mathrm{T}} \end{pmatrix}_\delta,$$

$$\hat{\mathcal{P}}\hat{\mathcal{B}}_\circ = \begin{pmatrix} B_c + B_p\hat{D}F_c \\ YB_c + \hat{B}F_c \end{pmatrix}_\delta,$$

$$\hat{\mathcal{C}}_\circ = \begin{pmatrix} C_cX + E_c\hat{C} & C_c + E_c\hat{D}C_p \end{pmatrix}_\delta,$$

$$\hat{\mathcal{D}} = E_c\hat{D}F_c,$$

$$B_c := B_{pw}R_c, \quad C_c := N_cC_z,$$

$$E_c := N_cD_z, \quad F_c := D_{pw}R_c,$$

In the above, the subscript δ notation should be understood as requiring the LMIs to be satisfied for all extremal points of δ as defined in (2)-(4). That is, the LMIs must be satisfied everywhere on the convex hull defined by the permissible values of the uncertainties; i.e., one LMI has to be solved for every vertex of the hypercube $(\delta_a, \delta_b, \delta_c) \in [-1, 1]^{p+q+r}$ to yield one common $\hat{\mathcal{P}}$. The scaling parameter $\alpha > 0$ is included to provide extra tuning freedom; essentially, the permitted pole locations are to the left of $s = -\alpha$. N_c, R_c are given input/output channel for $T(s)$ from $\bar{w}$ to $\bar{z}$;

$$T_c = N_cTR_c. \tag{13}$$

2.3 Disctretization and Anti-windup Control

Assuming the minimization problem (10)-(11) can be solved, this section describes an anti-windup control design for the discretized PI controller K and the robust DFC L for practical implementation. The anti-windup control design for discrete time systems proposed by Syaichu-Rohman and Middleton [17], and was originally derived for 1DOF control systems. As mentioned in Section 1, DFC is categorized as a 2DOF controller, and therefore, the method will be reshaped for DFC.

Firstly, discretization of the closed loop system including G, G_n, W, and L is done by bilinear method [22]. With $H_c(s)$ denoting the continuous time transfer function and $H(z)$ the discrete time transfer function, the bilinear transformation corresponds to replacing s by

$$s = \frac{2}{T_d}\left(\frac{1-z^{-1}}{1+z^{-1}}\right), \tag{14}$$

that is,

$$H_z = H_c\left[\frac{2}{T_d}\left(\frac{1-z^{-1}}{1+z^{-1}}\right)\right], \tag{15}$$

where T_d is a sampling time.

Next, the extended state space representation including the anti-windup controllers in Fig. 5 is considered. Unit delay blocks for wind-up gains Λ_{k2} and Λ_{l2} are introduced to avoid algebraic loops.

The vector $v(k)$, the saturation function Φ, and the dead zone function Ψ can be described by

$$v(k) = \tilde{u}(k) - u(k) = \tilde{u}(k) - \Phi(\tilde{u}(k)) \tag{16}$$

$$\Psi(\tilde{u}(k)) = I - \Phi(\tilde{u}(k)) \tag{17}$$

where $\tilde{u}$ is a control output before a saturation block, $\Phi : \mathbb{R}^m \to \mathbb{R}^m$ is a saturation function, $\Psi : \mathbb{R}^m \to \mathbb{R}^m$ is a deadzone function, and $\tilde{u}(k)$ is a control output vector before saturation block. These two functions are illustrated in Fig. 6. PI control is discretized with bilinear method, and the anti-windup gains Λ_{k1} and Λ_{k2} for discrete PI control are described as follows:

$$\begin{aligned} x_k(k+1) &= A_{kd}x_k(k) + B_{kd}(r(k) - y(k)) - \Lambda_{k1}(\tilde{u}_k(k) - u_k(k)) \\ \tilde{u}_k(k) &= C_{kd}x_k(k) + D_{kd}(r(k) - y(k)) + x_{ek}(k) \\ x_{ek}(k+1) &= -\Lambda_{k2}(\tilde{u}_k(k) - u_k(k)). \end{aligned} \tag{18}$$

Similarly, the anti-windup gains Λ_{l1} and Λ_{l2} for the discrete DFC are included in the controller equations as follows:

$$x_l(k+1) = A_{ld}x_l(k) + B_{ld}(r(k) - y(k)) - \Lambda_{l1}(\tilde{u_l}(k) - u_l(k)) \tag{19}$$

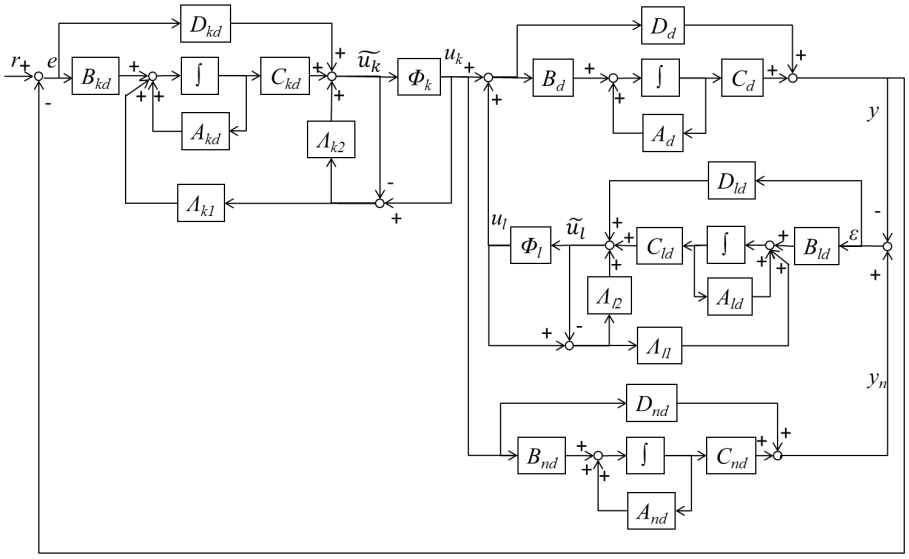

Fig. 5: A state space representation of the PI control with robust DFC including the anti-windup controllers.

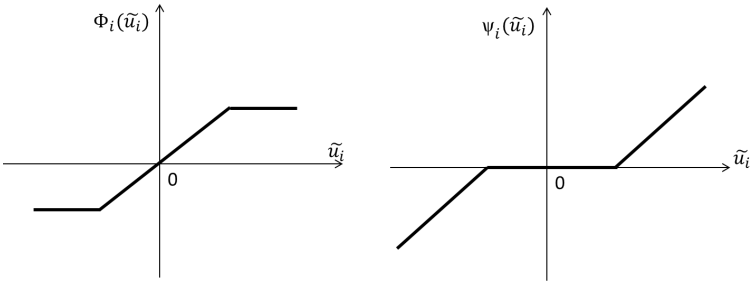

Fig. 6: A saturation function (left) and a dead zone function (right).

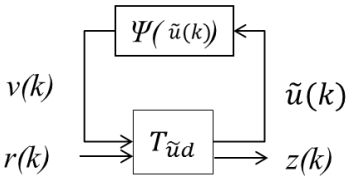

Fig. 7: A simplified feedback system for anti-windup control design.

$$\tilde{u_l}(k) = C_{ld}x_k(k) + D_{ld}(r(k) - y(k)) + x_{el}(k)$$
$$x_{el}(k+1) = -\Lambda_{l2}(\tilde{u_l}(k) - u_l(k)).$$

The last terms of the controller equations in (18) and (19), $(\tilde{u_k}(k) - u_k(k))$ and $(\tilde{u_l}(k) - u_l(k))$ can be seen as a disturbance in terms of stability and performance. The system in Fig. 5 can be simplified in Fig. 7, giving rise to the system equations

$$\begin{aligned} \tilde{x}(k+1) &= \tilde{\mathcal{A}}\tilde{x}(k) + \tilde{\mathcal{B}}v(k) + \tilde{\mathcal{B}}_r r(k) \\ \tilde{u}(k) &= \tilde{\mathcal{C}}_u\tilde{x}(k) + \tilde{\mathcal{D}}_u v(k) + \tilde{\mathcal{D}}_{ur} r(k) \\ z(k) &= \tilde{\mathcal{C}}_z\tilde{x}(k) + \tilde{\mathcal{D}}_z v(k) + \tilde{\mathcal{D}}_{zr} r(k) \end{aligned} \tag{20}$$

where

$$\begin{pmatrix} v_1(k) \\ v_2(k) \end{pmatrix} = \begin{pmatrix} \tilde{u_k}(k) \\ \tilde{u_l}(k) \end{pmatrix} - \begin{pmatrix} u_k(k) \\ u_l(k) \end{pmatrix}, \tag{21}$$

$$\tilde{x}(k) = \begin{pmatrix} x(k)^{\mathrm{T}} & x_n(k)^{\mathrm{T}} & x_k(k)^{\mathrm{T}} & x_{ek}(k)^{\mathrm{T}} & x_l(k)^{\mathrm{T}} & x_{el}(k)^{\mathrm{T}} \end{pmatrix}^{\mathrm{T}},$$

$$\tilde{\mathcal{A}}_\delta = \begin{pmatrix} A_d - B_d D_{kd} C_d - B_d D_{ld} C_d & B_d D_{ld} C_{nd} & B_d C_{kd} & B_d & B_d C_{ld} & B_d \\ -B_{nd} D_{kd} C_d & A_{nd} & B_{nd} C_{kd} & B_{nd} & 0 & 0 \\ -B_{kd} C_d & 0 & A_{kd} & 0 & 0 & 0 \\ 0 & 0 & 0 & 0 & 0 & 0 \\ -B_{ld} C_d & B_{ld} C_{nd} & 0 & 0 & A_{ld} & 0 \\ 0 & 0 & 0 & 0 & 0 & 0 \end{pmatrix}_\delta,$$

$$\tilde{\mathcal{B}}_\delta = \begin{pmatrix} -B_d & -B_d \\ -B_{nd} & 0 \\ -\Lambda_{k1} & 0 \\ -\Lambda_{k2} & 0 \\ 0 & -\Lambda_{l1} \\ 0 & -\Lambda_{l2} \end{pmatrix}_\delta, \tilde{\mathcal{B}}_{v,\delta} = \begin{pmatrix} -B_d & -B_d \\ -B_{nd} & 0 \\ 0 & 0 \\ 0 & 0 \\ 0 & 0 \\ 0 & 0 \end{pmatrix}_\delta,$$

$$\tilde{\mathcal{B}}_e = \begin{pmatrix} 0 & 0 \\ 0 & 0 \\ I & 0 \\ I & 0 \\ 0 & I \\ 0 & I \end{pmatrix}, \tilde{\mathcal{B}}_{r,\delta} = \begin{pmatrix} -B_d D_{kd} \\ -B_{nd} D_{kd} \\ B_{kd} \\ 0 \\ 0 \\ 0 \end{pmatrix}_\delta,$$

$$\tilde{\mathcal{C}}_{u,\delta} = \begin{pmatrix} -D_{kd} C_d & 0 & C_{kd} & I & 0 & 0 \\ -D_{ld} C_d & D_{ld} C_{nd} & 0 & 0 & C_{ld} & I \end{pmatrix}_\delta,$$

$$\tilde{\mathcal{C}}_{z,\delta} = \begin{pmatrix} -C_d & 0 & 0 & 0 & 0 & 0 \end{pmatrix}_\delta,$$

$$\tilde{\mathcal{D}}_u = \begin{pmatrix} 0 \\ 0 \end{pmatrix}, \tilde{\mathcal{D}}_{ur} = \begin{pmatrix} D_k \\ 0 \end{pmatrix}, \tilde{\mathcal{D}}_z = \begin{pmatrix} 0 & 0 \end{pmatrix}, \tilde{\mathcal{D}}_{zr} = I. \tag{22}$$

The explicit static anti-windup scheme proposed by Rohman [17] is reshaped for conventional controller K and DFC L as follows:

$$\underset{\tilde{\mathcal{Q}},V,M,\kappa}{\text{minimize}}\ \gamma_2 \tag{23}$$

$$\text{subject to;} \tag{24}$$

$$\begin{pmatrix} \tilde{\mathcal{Q}} & * & * & * & * & * \\ 0 & -\gamma_2 I & * & * & * & * \\ \tilde{\mathcal{C}_{u,\delta}}\tilde{\mathcal{Q}} & \tilde{\mathcal{D}_{ur}} & -2M & * & * & * \\ \tilde{\mathcal{C}_{z,\delta}}\tilde{\mathcal{Q}} & \tilde{\mathcal{D}_{zr}} & 0 & -\gamma_2 I & * & * \\ \tilde{\mathcal{A}}_\delta\tilde{\mathcal{Q}} & \tilde{\mathcal{B}_{r,\delta}} & \tilde{\mathcal{B}}_{r,\delta}M - \tilde{\mathcal{B}}_e V & 0 & -\tilde{\mathcal{Q}} & * \\ 0 & 0 & M & 0 & 0 & \kappa I \end{pmatrix} \leq 0,$$

$$\tilde{\mathcal{Q}} = \tilde{\mathcal{Q}}^{\mathrm{T}} > 0, \quad \gamma_2 > 0, \quad \kappa > 0,$$

where $M > 0 \in \mathbb{R}^{2m\times 2m}$ is a diagonal matrix, $V := \Lambda M \in \mathbb{R}^{2m\times 2m}$ is an arbitrary matrix, γ_2 and κ are scalars. Similarly to (11)-(13), subscript $(\cdot)_\delta$ in (21)-(24) indicates that one LMI has to be solved for every extremal point of $(\delta_a, \delta_b, \delta_c) \in [-1, 1]^{p+q+r}$ to yield one common $\tilde{\mathcal{Q}}$.

3 Experimental Results

This section demonstrates the proposed design on a model of a MIMO water chiller system at Aalborg University (AAU) shown in Fig. 8. The system is challenging to control due to model uncertainties, changing system gains, and time delays. Conventional control designs tend to exhibit poor performance away from nominal operating conditions due to these effects.

Especially the superheat control is challenging to design, because the refrigerant exhibits strong nonlinear characteristics due to the two-phase (vapor-liquid) state in the evaporator.

Due to nonlinearities, the gains of linearizations in different operating points very significantly, for instance.

These model variations are dealt with in the following by means of robust design. The application is inspired by Fuji Electric's business case of refrigerant applications such as vending machine and air conditioning units (two examples are shown in Fig. 9). These applications exhibit the same control issues as the laboratory system, and the applications need robustness against changes in heat load and outside air temperature.

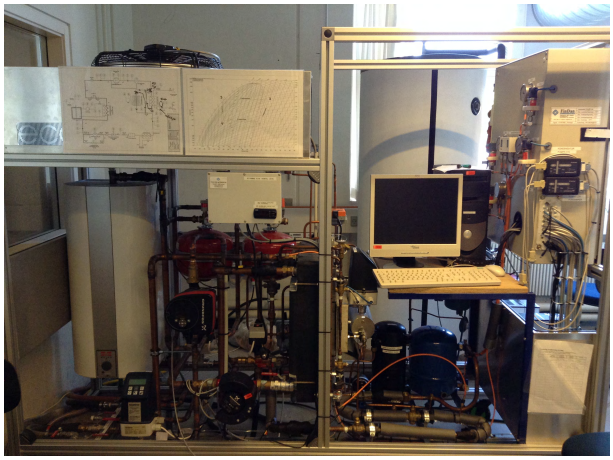

Fig. 8: The refrigeration system test setup at Aalborg University.

Fig. 9: The refrigeration applications by Fuji Electric, Vending machines (Left), and Hybrid indirect air conditioning unit F-COOL NEO (Right).

3.1 Lab system setup

The lab system includes four main components; a compressor, a condenser, an expansion valve, and an evaporator. In a basic refrigeration system, one control device is installed for each component as shown in Fig. 10. These controllers regulate pressure or temperature to maintain specified operating conditions. For example, the rotational speed of the compressor is controlled to keep a constant refrigerant suction pressure P_e. The opening degree of the expansion valve maintains a suitable refrigerant superheat T_{sh} (difference between the temperature at the outlet of the evaporator and the evaporation temperature inside the evaporator). The speed of the evaporator fan is controlled to keep the temperature on the load side T_r constant. The speed of the condenser fan is controlled in order to keep the condensing pressure P_c constant. A hot water

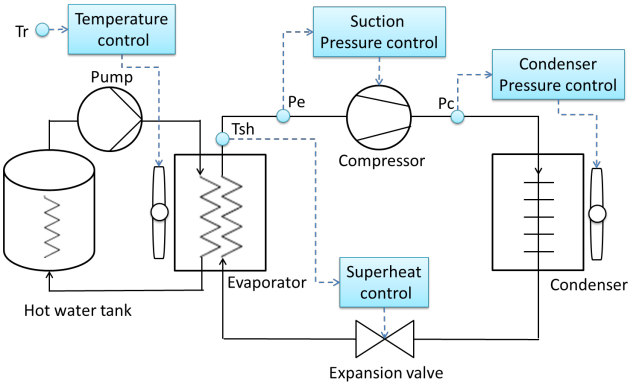

Fig. 10: A layout of the water chiller system with basic control structure.

tank is set as heat load.

3.2 Model

In the following, a simple 2 input and 2 output model is considered for MIMO control design of the water chiller system. A simple superheat model and a suction pressure model is chosen for the MIMO control design, and these models can be described by a first order plus dead time system, see e.g., [23]. Practical results in previous studies furthermore also indicate that the dominant uncertainty is the gain of the superheat model [13, 24].

The model is created using experimental data obtained from step-up and step-down responses conducted at two operating conditions, which means that four sets of step responses are used for model identification.

We assume a model of the form as follows:

$$\begin{pmatrix} y_1(s) \\ y_2(s) \end{pmatrix} = \begin{pmatrix} G_{11}(s) & G_{12}(s) \\ G_{21}(s) & G_{22}(s) \end{pmatrix} \begin{pmatrix} u_1(s) \\ u_2(s) \end{pmatrix}, \tag{25}$$

where y_1 is a superheat temperature, y_2 is a suction pressure of the compressor, G_{11}, G_{12}, G_{21}, G_{22} are subsystems of the 2 input 2 output system, u_1 is the opening degree of the expansion valve, and u_2 is a compressor speed.

That is, scalar gains k_{ij}, time constants τ_{ij}, and time delay θ_{ij} in the following first-order plus time delay models are fitted to measurement data using straightforward least-squares methods.

$$G_{ij} = \frac{k_{ij}}{1+\tau_{ij}s} e^{-\theta_{ij}s}; \tag{26}$$
$$k_{ij} \in [k_{min,ij}, k_{max,ij}], \tau_{ij} \in [\tau_{min,ij}, \tau_{max,ij}],$$

$$\theta_{ij} \in [\theta_{min,ij}, \theta_{max,ij}],$$
$$i = 1,2, j = 1,2.$$

Next, the nominal model is computed using average parameter values of $\mathcal{G}$, i.e.,

$$G_{n,ij} = \frac{k_{n,ij}}{1 + \tau_{n,ij}s} e^{-\theta_{n,ij}s}. \tag{27}$$

where

$$k_{n,ij} = \frac{k_{max,ij} + k_{min,ij}}{2}, \tau_{n,ij} \quad = \frac{\tau_{max,ij} + \tau_{min,ij}}{2}, \theta_{n,ij} = \frac{\theta_{max,ij} + \theta_{min,ij}}{2},$$

We focus on the worst case of model, which is the corner points of the model sets. That is the reason why average values of minimum and maximum parameters are used for nominal model.

To keep the design simple, the time delay is approximated by a first order filter. In addition, only one parameter, k_{11}, is considered uncertain because it represents the strongest uncertainty (nonlinearity). Therefore, G and G_n are approximated as follows:

$$G_{11} = \frac{k_{11}}{(1 + \tau_{n,11}s)(1 + \theta_{n,11}s)}; \tag{28}$$
$$k_{11} \in [-10.64, -8.71],$$

and the rest of the subsystems are expressed by the nominal model.

$$G_{ij} = \frac{k_{n,ij}}{(1 + \tau_{n,ij}s)(1 + \theta_{n,ij}s)}; \tag{29}$$
$$i = 1,2, j = 1,2, except \quad ij = 11.$$

and nominal parameters of the subsystems are shown in Table 1.

Table 1: Nominal parameters of the subsystems.

	k	τ	θ
$g_{n,11}$	-9.68	44.83	20.50
$g_{n,21}$	0.28	10.32	5.50
$g_{n,12}$	0.74	42.03	18.50
$g_{n,22}$	-0.046	7.20	4.0

3.3 Control Design

This subsection demonstrates the robust DFC with anti-windup control by two types of LMIs. First, the robust DFC without saturation are designed, and then the anti-windup controllers are solved for both of the PI and robust DFC controllers.

The PI controllers are tuned based on the parameters of each corner point of the plant of the subsystems in order to maintain nominal stability for all parameter values. Each corner point was chosen from largest absolute gain, minimum time constant, and largest time delay respectively. In addition, Betraqs method proposed by Fuji Electric, was chosen for PI control design [25].

$$K = \begin{pmatrix} K_{11}(s) & 0 \\ 0 & K_{22}(s) \end{pmatrix}, \tag{30}$$

where

$$K_{11} = \frac{-0.0675s - 0.00229}{s},\ K_{22} = \frac{-6.439s - 0.7013}{s}.$$

The disturbance weight function is chosen as a first order system, and designed using the nominal time constants $\tau_{n,11}, \tau_{n,22}$. In addition, the weight of superheat W_{11} is given priority in terms of disturbance rejection.

$$W = \begin{pmatrix} W_{11}(s) & 0 \\ 0 & W_{22}(s) \end{pmatrix}. \tag{31}$$

where

$$W_{11} = \frac{1}{14.95s + 1},\ W_{22} = \frac{0.1}{7.208s + 1}. \tag{32}$$

The artificial parameters in (8) for DFC are chosen as follows:

$$\rho_z = 10^{-1},\ \ \rho_w = 10^{-6}. \tag{33}$$

The optimal H_∞ performance obtained by solving the first LMIs (10)-(12) was $\gamma_1 = 0.4000$ with full order DFC without saturation, and the DFC was a 20th order system because $dim(A_l) = 2n + n_K + n_W, n = 8, n_K = 2, n_W = 2$. It would be more useful for industrial systems if a lower order DFC can be obtained. Therefore, model reduction is applied to reduce the DFC to a simple gain. The Matlab command `modred` yields

$$D_l = \begin{pmatrix} -0.2835 & 0.2860 \\ 1.6681 & -7.0684 \end{pmatrix}. \tag{34}$$

Fig. 11 shows bode-plots in comparison with DFCs before/after the model reduction. The figure indicates that the DFC gain matrix can maintain the response of the original DFC in the frequency range of interest.

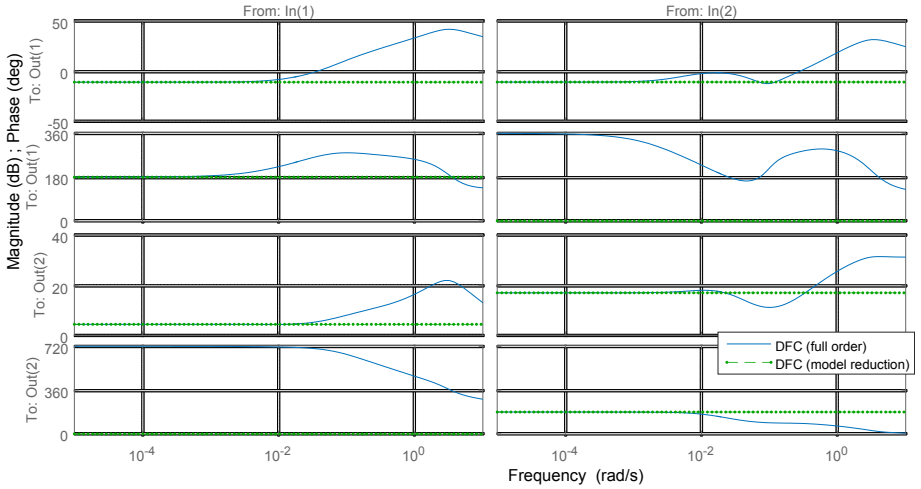

Fig. 11: Bode plots of DFC from ϵ to u_l, before and after model reduction.

Fig. 12 shows a pole-zero map in the s-plane of closed loop system with DFC gain matrix. The mapping shows that all the poles for all model corner points are in the left half plane, and therefore the system with DFC gain matrix guarantees the stability. In addition, the norm γ_1 with DFC gain was 0.7960. Thus the system can maintain $\gamma_1 < 1$.

Table 2 and Fig. 13 show the simulation results for comparing PI control with or without DFC. The set-point r and disturbance w were changed for the superheat control. Simulation results indicate that a simple DFC gain improves the disturbance rejection more than 35 %. Moreover, the DFC gain matrix exhibits similar robustness against model uncertainties for the step response as the full order DFC. As a result, we choose the DFC gain for practical design.

Table 2: IAE of the simulation results.

	PI	PI + DFC (full order)	PI + DFC (gain)
Superheat control	744.53	447.37	483.08
Suction pressure control	14.67	15.02	18.48

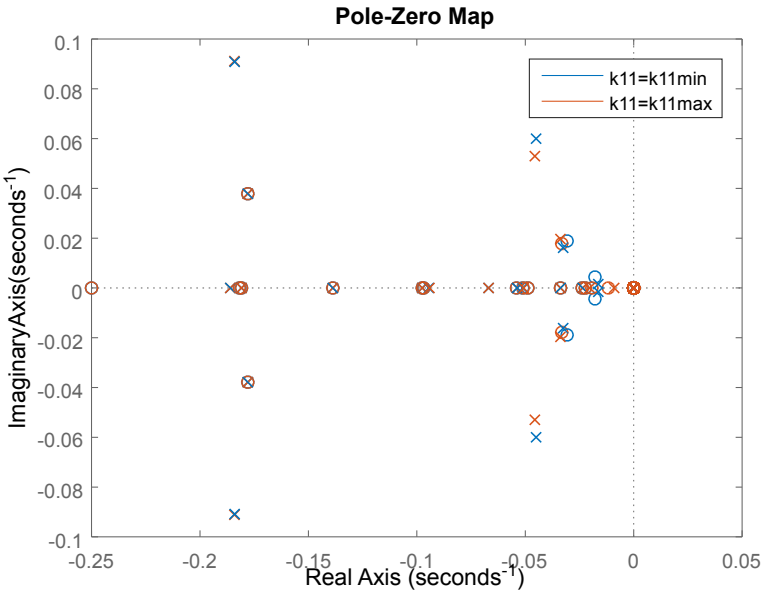

Fig. 12: Pole-zero map of closed loop system with DFC gain matrix.

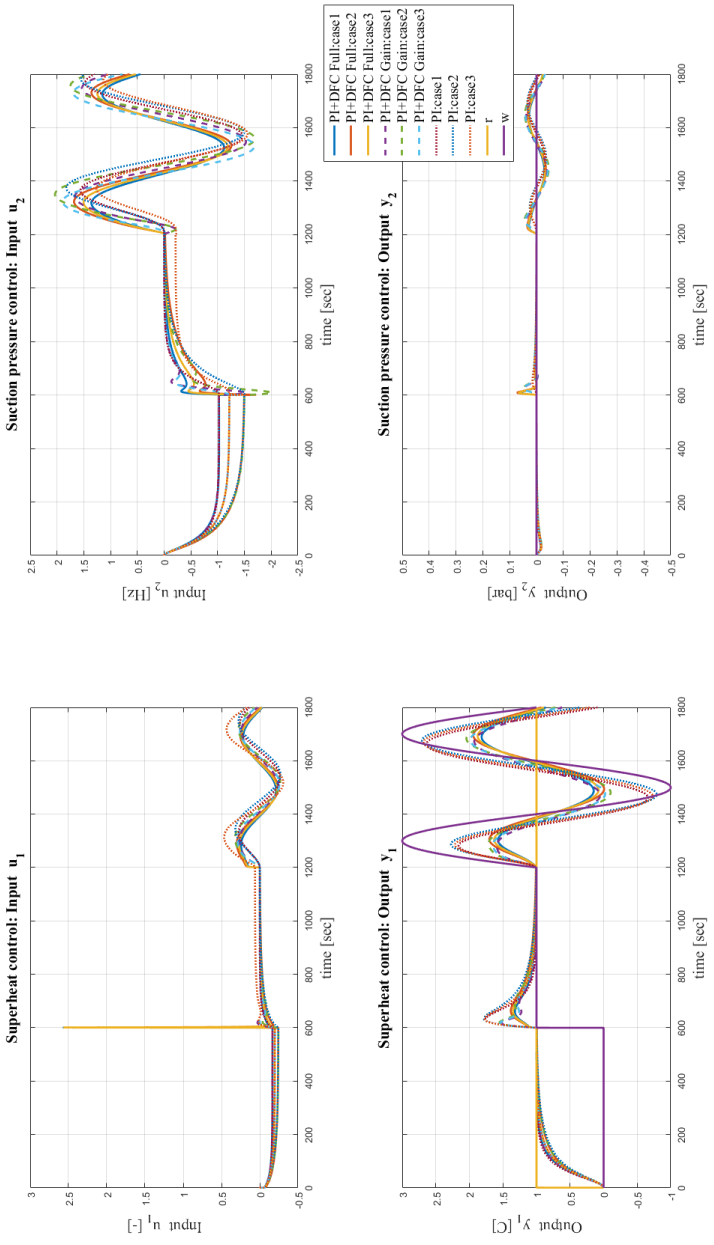

Fig. 13: Simulation results using PI control with or without DFC.

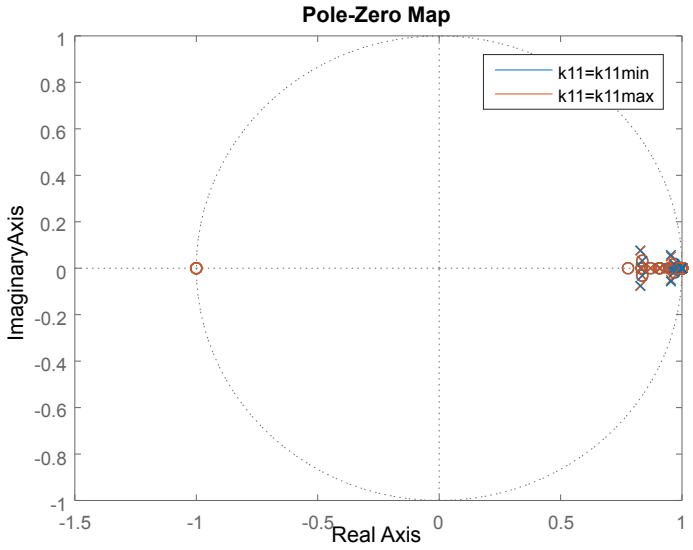

Fig. 14: Pole-zero map of discretized system with DFC gain matrix.

Next, discrete anti-windup controllers are designed for the PI controller.

The system is dicretized, and poles and zeros in the z-plane of closed loop system are computed as shown in Fig. 14; the mapping shows that the discretized system still satisfies the stability and pole placement requirements.

Solving (23)-(24), from which we obtained the results

$$\Lambda_{k1} = \begin{pmatrix} -0.8546 & -0.0288 \\ -0.3146 & -0.0575 \end{pmatrix}, \tag{35}$$

$$\Lambda_{k2} = \begin{pmatrix} 0.1136 & 0.0678 \\ -2.9893 & -0.1257 \end{pmatrix}.$$

3.4 Simulation Results

Now simulation tests are examined on simulation conditions in Table 3. The simulation results are obtained with linear transfer function models, which are identified from experimental data. Step response and load disturbance response are evaluated for PI with/without robust DFC and with/without anti-windup controller as shown as Fig. 15 and Fig. 16 . Each design method is evaluated for three cases, where the actual superheat gain is set to $k_{min} = -10.64$ as case 1, $k_{max} = -8.71$ as case 2, $k_n = -9.68$ as case 3.

The results show that both sets of limiters, Λ_{k1} and Λ_{k2}, work correctly and wind-up phenomea can be avoided with the proposed method, PI+DFC

Table 3: Simulation conditions.

Items	Values	Unit	Remarks
Set point r_1	5.0	[C]	
Set point r_2	0.0	[bar]	
Disturbance w_1	$16.0\sin(\frac{\pi}{400})t$	[C]	
Disturbance w_2	0.0	[bar]	
Step time of set points	1.0	[sec]	
Step time of disturbances	600	[sec]	
Simulation time T	1600	[sec]	
Control output u_{k1}	[-4.0, 4.0]	[-]	input constraint
Control output u_{l1}	[-1.0, 1.0]	[-]	input constraint
Control output u_{k2}	[-10.0, 15.0]	[Hz]	input constraint
Control output u_{l2}	[-5.0, 5.0]	[Hz]	input constraint

with anti-windup control. In addition, the proposed method can follow the no saturation behaviour whenever the signals are unsaturated. In other word, the proposed method can achieve improved performance compared to the controller with saturation block only.

It can also be confirmed that DFC yields the intended disturbance attenuation, even after the system is discretized and anti-windup gains are introduced.

Table 4 shows the evaluation results of each design. Five designs are examined, and then evaluated by four performance items. Item number 1 and 2 evaluate the robustness against model uncertainties δ. For these items, we compute the performances $\max_{t\in[0,T]} |y_{case_i}(t) - y_{case_j}(t)|,\ i = 1,2,3, j = 1,2,3$ as shown in Fig. 17. Items number 3 and 4 are simply the maximum values of y_1 and y_2 to evaluate the wind-up phenomena. Design number one, PI + robust DFC with anti-windup controller obtains the best values (minimum values) for all items within the control limiters. On the other hand, design number two, PI + robust DFC *without* anti-windup exhibits worse the performance due to the windup phenomena as shown in Table 4 and Fig. 15.

Design number three, PI + robust DFC with no saturation obtains smaller values than design number one. However, design number three does not take saturation into account, which means that this design will not work in many real applications.

In design numbers four and five, the PI control alone shows poorer control performance compared to the PI + robust DFC. To conclude, the proposed design, PI control + robust DFC with anti-windup controller, exhibits the best simulation performance while respecting the input constraints.

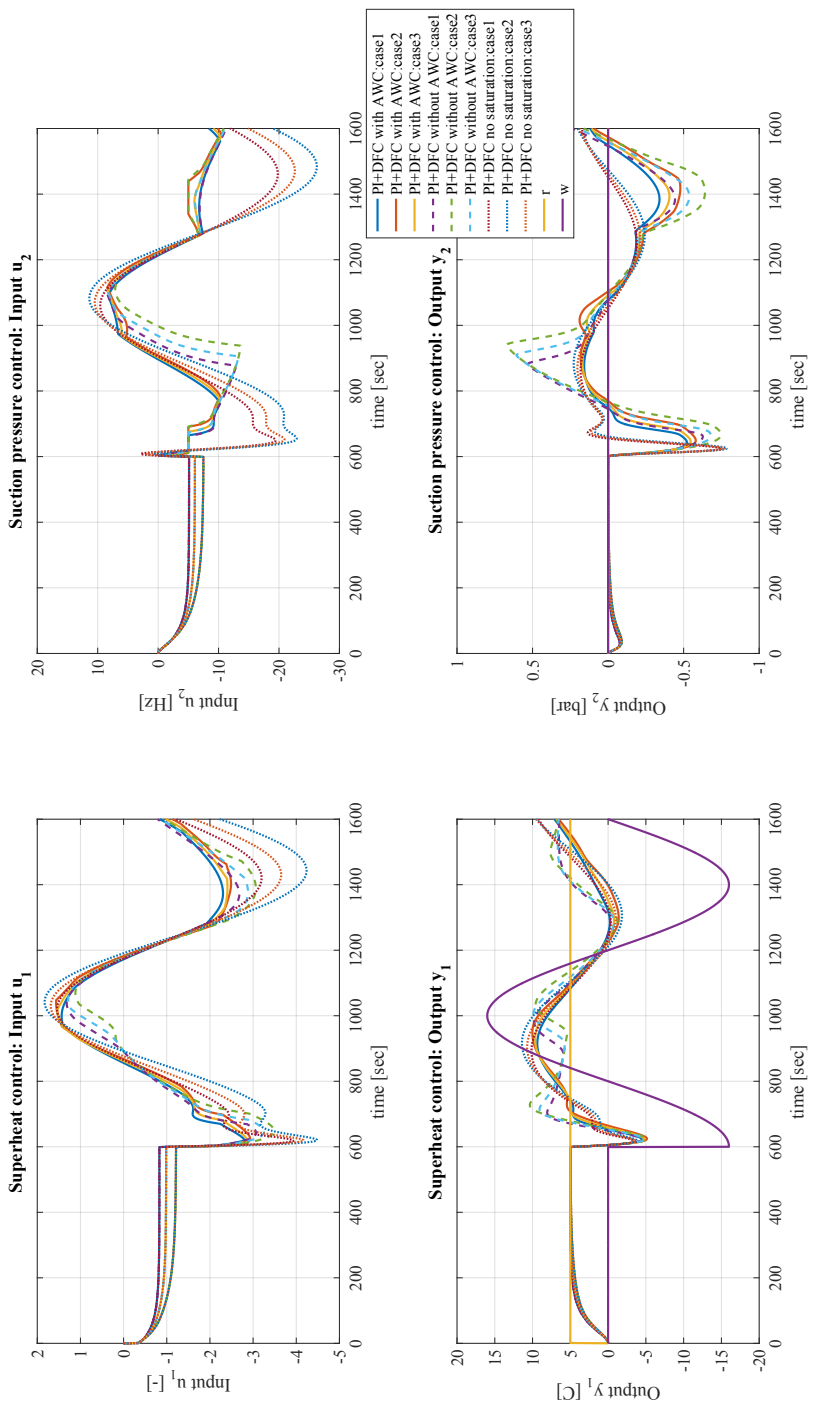

Fig. 15: Simulation results of the PI control + robust DFC.

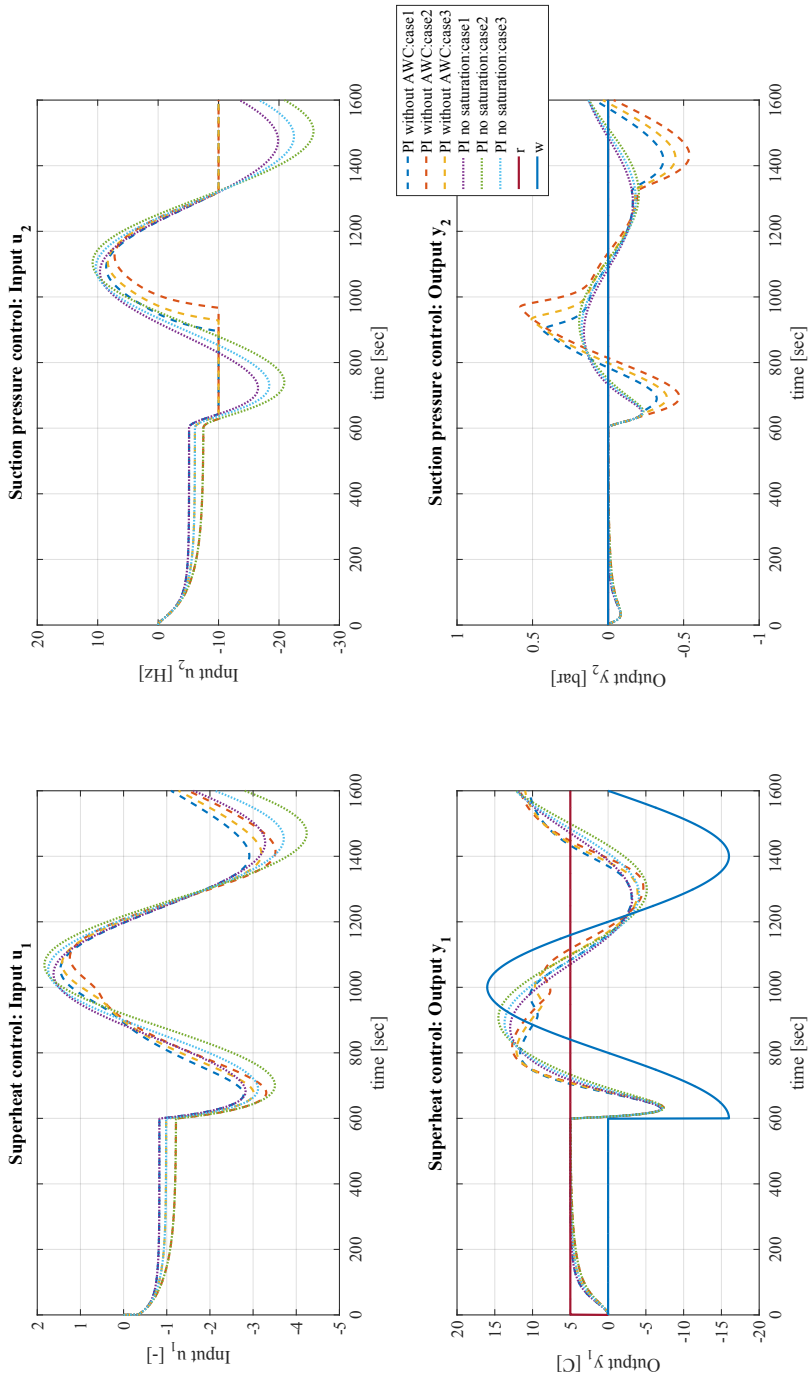

Fig. 16: Simulation results of the PI control.

Table 4: Evaluations of each control design.

	Design method number	1	2	3	4	5
Item number	Description	PI + Robust DFC with AW	PI + Robust DFC without AWC	PI + Robust DFC no saturation	PI control without AWC	PI control no saturation
1	Robustness from δ_{y_1}	**1.9114**	3.6732	*1.8311*	2.5681	2.8069
2	Robustness from δ_{y_2}	**0.3405**	0.4905	*0.1016*	0.4365	*0.0565*
3	Maximum value y_1	**10.0221**	10.3608	11.4051	12.7000	14.5240
4	Maximum value y_2	**0.1887**	0.6709	0.2278	0.5811	0.1915

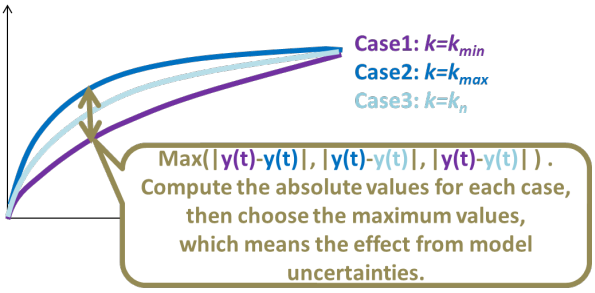

Fig. 17: An explanation of the item number 1 and 2, the robustness of controllers from model uncertainties.

3.5 Experimental Results

Table 5 and Table 6 show set point values of the test system and the experimental conditions, respectively. The temperature of the water tank is set at 14 degrees for the initial condition. Then the set point is changed to 15.0 degrees, and kept there for the first 500 seconds for making a load disturbance response. Next, the set point is changed to 16.0 degrees from 501 to 1000 seconds in order to test that the anti-windup controllers work correctly. The set point is changed back to 14 degrees after 1000 seconds, and kept there for additional 1000 seconds. Experimental data is sampled each second, and the data is evaluated for 2000 seconds in total.

Fig. 18 shows PI control without anti-windup controllers. Fig. 19 and 20 show a disturbance response of PI control + robust DFC with/without anti-windup controllers. The test results show that both control configurations, PI+DFC with and without anti-windup, can improve the performance of the superheat control.

In addition, PI control + robust DFC with anti-windup can avoid wind-up phenomena from 1000 - 1200 seconds, and demonstrates more accurate regulation compared to PI control + robust DFC without anti-windup controllers.

We also confirmed that the windup phenomenon during 1000-1200 seconds affects the cross-coupled output (superheat y_1), when the suction pressure speed (u_2) is saturated in the design without anti-windup controller. This result indicates that the anti-windup design is also effective for MIMO systems.

Table 7 shows Integral Absolute Error (IAE) of the superheat control and suction pressure control for the three control design methods.

The IAE of suction pressure with PI + robust DFC without anti-windup obtained 104.9, which was a poorer performance than the PI without anti-windup, IAE=84.2, due to the lower priority of the weighting function W.

However, the IAE of proposed method, PI + robust DFC with anti-windup, amounted to 89.7, which means that the proposed method can recover the performance.

The superheat control with PI + DFC with/without anti-windup control obtained IAE=1966.4 and IAE=2220.5 respectively. The IAE of PI control without anti-windup control amounted to 3472.7, which means that the proposed method achieved 43 % better performance than only PI control alone without anti-windup.

Table 5: Set point values of the test system.

Set point	Value	Controlled by
Superheat	10.0 [C]	PI with/without DFC
Suction pressure	2.8 [bar]	PI with/without DFC
Condenser	9.0 [bar]	PI
Water tank (initial condition)	14.0 [C]	PI

Table 6: Experimental conditions.

Items	Values	Unit	Remarks
Load disturbance by changing	14.0 $\rightarrow$ 15.0	[C]	
the setpoint of water tank w_1	$\rightarrow$ 16.0 $\rightarrow$ 14.0		
Experimental time T	2000	[sec]	
Control output u_{k1}	[-5.0, 5.0]	[-]	input constraint
Control output u_{l1}	[-2.5, 2.5]	[-]	input constraint
Control output u_{k2}	[-10.0, 15.0]	[Hz]	input constraint
Control output u_{l2}	[-5.0, 7.5]	[Hz]	input constraint

Table 7: IAE of the experimental results.

	PI + robust DFC with AWC	PI + robust DFC without AWC	PI without AWC
The superheat control	1966.4	2220.5	3472.7
The suction pressure control	89.7	104.9	84.2

4 Conclusions

In this paper, anti-windup controllers were designed for the 2DOF controllers, K and L, and we introduced modified LMIs for discretized antiwindup control. The control design is derived by formulating two sets of LMIs, one for solving the robust DFC problem, and a second for designing the discrete anti-windup controllers. Both simulation and experimental results of the refrigeration system demonstrated the effectiveness of the proposed method. In the future, we will try applying the design method for other types of systems, such as mechanical systems for Factory Automation.

References

[1] Fuji Electric Co., Ltd. (1981) Fuji electric journal 54, (1), pp.33 in industry application, *in Japanese*,. [Online]. Available: http://www.fujielectric.co.jp/company/jihou_archives/pdf/54-01/FEJ-54-01-024-1981.pdf

[2] H. Umida and M. Ohara, "A digital observer for impact drop compensations," in *Proc. SPIE 0858, Signal Acquisition and Processing*, Cambridge, CA, 1987, pp. 1004 – 1010.

[3] V. M. Alfaro and R. Vilanova, "Model reference based robust tuning of five-parameter 2dof pid controllers for first-order plus dead-time models," in *Proc. European Control Conference (ECC2013)*, Zurich, Switzerland, 2013, pp. 3931–3936.

[4] T. Emami and R. J. Hartnett, "Discrete time robust stability design of pid controllers autonomous sailing vessel application," in *Proc. the American Control Conference (ACC2014)*, Portland, OR, 2014, pp. 1993–1998.

[5] M. Saeki and M. Ogawa, "Partial numerical optimization of low order h inf controller on the frequency domain," in *Proc. IEEE International Conference on Control Applications*, San Antonio, TX, 2008, pp. 804–809.

[6] H. Bevrani, T. Hiyama, and H. Bevrani, "Robust PID based power system stabiliser: Design and real-time implementation," *International Journal of Electrical Power and Energy Systems*, vol. 33, no. 2, pp. 179–188, 2011.

[7] M. Ge, M.-S. Chiu, and Q.-G. Wang, "Robust PID controller design via LMI approach," *Journal of Process Control*, vol. 12, no. 1, pp. 3–13, 2002.

[8] S. Alcantara, W. Zhang, C. Pedret, R. Vilanova, and S. Skogestad, " IMC-like analytical H inf design with S/SP mixed sensitivity consideration: Utility in PID tuning guidance," *Process Control*, vol. 21, no. 4, pp. 554–563, 2011.

[9] D. E. Rivera, M. Morari, and S. Skogestad, "Internal model control: PID controller design," *Industrial & engineering chemistry process design and development*, vol. 25, no. 1, pp. 252–265, 1986.

[10] D. E. Rivera and M. E. Flores, *CONTROL SYSTEMS, ROBOTICS AND AUTOMATION - Vol.II Internal Model Control -*. EOLSS Publications, 2009.

[11] J. Stoustrup, "Plug Play Control: Control Technology towards new Challenges," *European Journal of Control*, vol. 15, no. 3-4, pp. 311–330, 2009.

[12] J. Bendtsen, K. Trangbaek, and J. Stoustrup, "Plug-and-Play Control—Modifying Control Systems Online," *IEEE Transactions on Control Systems Technology*, vol. 21, no. 1, pp. 79–93, 2013.

[13] F. Kawai, K. Vinther, P. Anderson, and J. D. Bendtsen, "Mimo robust disturbance feedback control for refrigeration systems via an lmi approach," in *Proc. IFAC 2017*, Toulouse, Jul. 2017, pp. 14 525 – 14 532.

[14] A. T. on Modern Anti-windup Design, "Automatic tuning and adaptation for PID controllers-a survey," *European Journal of Control*, vol. 15, no. 3-4, pp. 418–440, 2009.

[15] G. Grimm, A. R. Teel, and L. Zaccarian, "Robust linear anti-windup synthesis for recovery of unconstrained performance," *Int. J. Robust Nonlinear Control,*, vol. 14, no. 13-14, pp. 1133—1168, 2004.

[16] U. Wasiwitono and M. Saeki, "Fixed-Order Output Feedback Control and Anti-Windup Compensation for Active Suspension Systems," *Journal of System Design and Dynamics*, vol. 5, no. 2, pp. 264–278, 2011.

[17] A. Syaichu-Rohman and R. Middleton, "Anti-windup schemes for discrete time systems: an lmi-based design," in *Proc. 5th Asian Control Conference*, Melbourne, 2004, pp. 554 – 561.

[18] Carsten Scherer and Siep Weiland. (2004) Linear matrix inequalities in control. [Online]. Available: http://www.dcsc.tudelft.nl/~cscherer/lmi/notes05.pdf

[19] S. Skogestad and I. Postlethwaite, *Multivariable Feedback Control.* John Wiley & Sons, Ltd, 2005.

[20] C. Scherer, P. Gahinet, and M. Chilali, "Multiobjective Output-Feedback Control via LMI Optimization," *IEEE Transactions on Automatic Control*, vol. 42, no. 7, pp. 896–911, 1997.

[21] M. Chilali, P. Gahinet, and P. Apkarian, "Robust pole placement in LMI regions ," *IEEE Transactions on Automatic Control*, vol. 44, no. 12, pp. 2257 – 2270, 1999.

[22] A. V. Oppenheim and R. W. Schafer, *Discrete-time signal processing.* Englewood Cliffs, N.J. : Prentice Hall, 1989.

[23] R. Izadi-Zamanabadi, K. Vinther, H. Mojallali, H. Rasmussen, and J. Stoustrup, "Evaporator unit as a benchmark for plug and play and fault tolerant control," in *Proc. 8th IFAC Symposium on Fault Detection, Supervision and Safety of Technical Processes*, Mexico City, Mexico, 2012, pp. 701–706.

[24] K. Vinther, R. J. Nielsen, K. M. Nielsen, P. Andersen, T. S. Pedersen, and J. D. Bendtsen, "Absorption Cycle Heat Pump Model for Control Design," in *2015 European Control Conference (ECC)*, 2015.

[25] Mitsuhashi Shigetaka and Tatsuo Inoue. (1965) Fuji electric journal 38, (4), pp.257-266 , *in Japanese*),. [Online]. Available: https://www.fujielectric.co.jp/company/jihou_archives/pdf/38-04/FEJ-38-04-257-1965.pdf

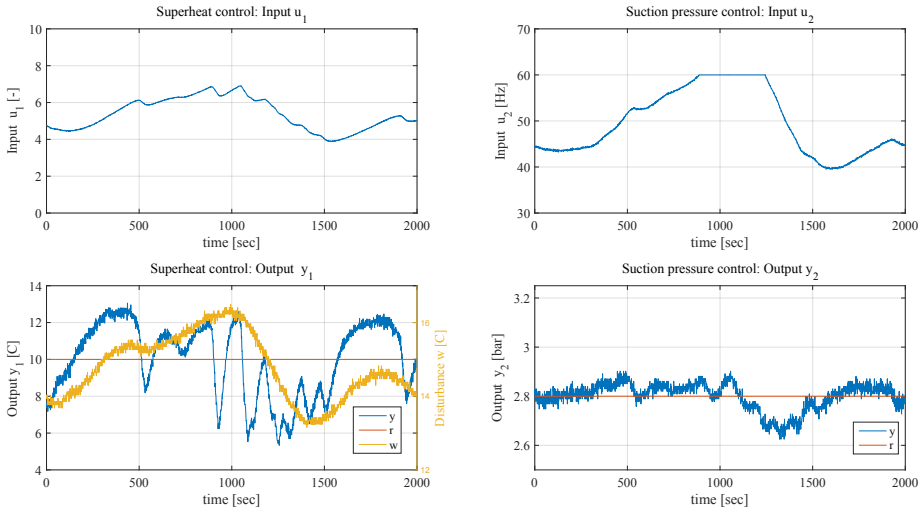

Fig. 18: Experimental results of PI control without anti-windup controllers.

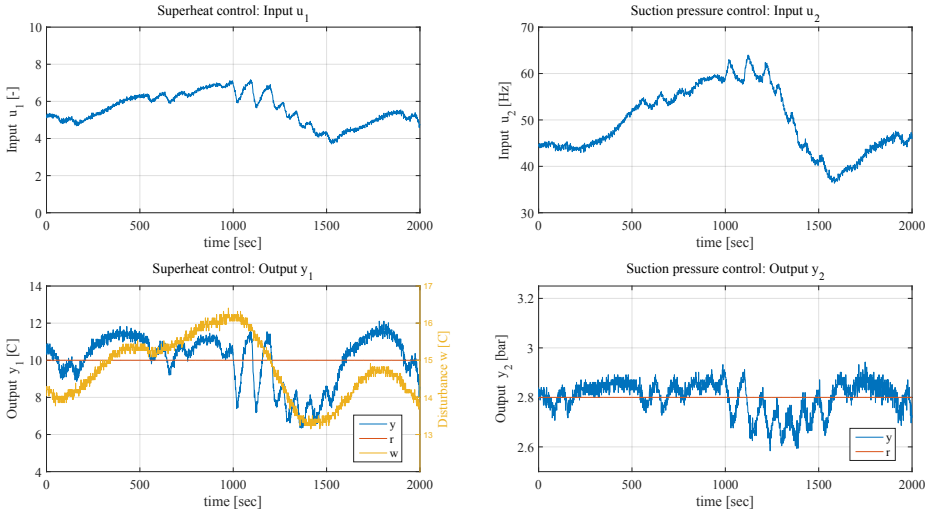

Fig. 19: Experimental results of PI control + robust DFC without anti-windup controllers.

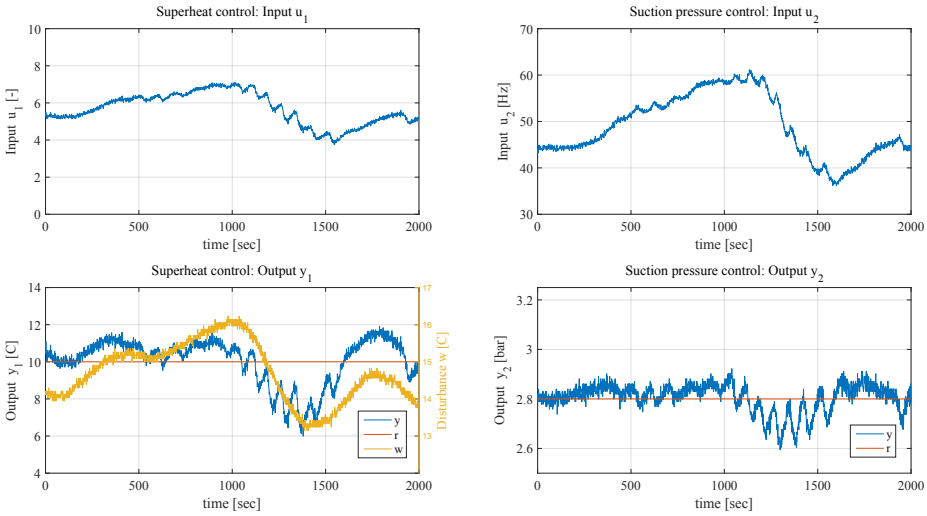

Fig. 20: Experimental results of PI control + robust DFC with anti-windup controllers.

Paper E

Anti-Sway Control for Crane Systems: Robust Design with LMI Optimization

Fukiko Kawai, Takashi Hayashi, Takayuki Kaneko, Palle Andersen, and Jan Dimon Bendtsen

The paper has been published in the
2018 IEEE Conference on Control Technology and Applications (CCTA),
IEEE, 2018.

The layout has been revised.

Abstract

Disturbance Feedback Control (DFC) is a control concept in which an existing controller is augmented with an additional feedback in order to achieve better disturbance rejection performance. This paper proposes an anti-sway control scheme for crane systems using robust DFC designed to minimize the sway angle and trolley position errors via Linear Matrix Inequality optimization. The robust DFC is added to an existing crane control system composed of a feed forward and state feedback control. Simulation results for the gantry crane system shows improvements in control performance when the gantry load is subjected to impulse force disturbances.

1 Introduction

Gantry cranes are of immense importance in shipping applications and can be found in container harbors all over the world. Traditionally, gantry crane systems have been controlled by means of feedforward control, taking motor torque and trolley speed limitations into account [1, 2]. Feedback control is also necessary to remove errors between references and measurement values; this is typically achieved by PID control of the gantry crane trolley [3].

Over the years, Fuji Electric has developed various anti-sway control schemes for crane systems, including an observer based control scheme. Subsequently, this anti-sway control scheme was further improved to combine feed forward control and state feedback control, and applied in commercial gantry cranes like the one shown in Fig. 1 [4]. This controller exhibits sufficient performance in terms of tracking control; however, better stability and performance could be obtained if robustness against external disturbances and model parameter uncertainties were taken into account.

Several results on robust gantry crane control have been published in the literature. For example, a robust iterative learning control scheme is proposed and validated experimentally in [5]. A Linear Matrix Inequality (LMI)-based H_∞ design was proposed in [6], and a robust fuzzy H_∞ control scheme for nonlinear systems was presented in [7].

The aforementioned robust designs are all constructed as one-degree-of freedom (1DOF) controllers, in which case the existing controllers already in place have to be removed and replaced by the new, more advanced controllers. However, many industrial practitioners prefer to keep existing controllers, because they embody extensive tuning and domain-specific know-how by customers and experienced engineers. In case a new control design for a system that has already been commissioned is desired, for example for improved closed-loop performance, it is thus often advantageous to maintain the original controller [8]. This is certainly the case in gantry crane applications, where a trolley

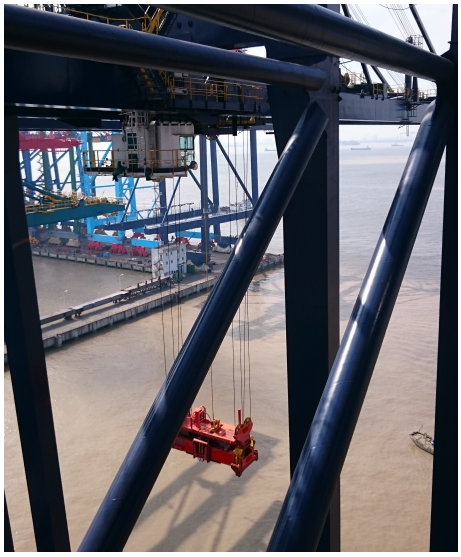

Fig. 1: A gantry crane system [11].

position controller is typically designed rather conservatively to ensure basic positioning functionality, but where an extra anti-sway mechanism could improve the exact positioning of the load in the presence of disturbances such as wind gusts.

In this paper one such add-on control configuration, known as Disturbance Feedback Control (DFC), is discussed – see Fig. 2. It was originally developed for drop impact attenuation in steel rolling mills by Fuji in 1980 [9]. This control structure has an additional feedback L to compensate for disturbance and model uncertainties as shown in the figure.

Note that although it might superficially look like Internal Model Control (IMC) [10], DFC is different since it involves two feedback signals, one for the existing control K and one for the disturbance feedback. IMC has only one feedback signal, which will be zero when there is no modeling error.

In a previous study, the authors proposed a robust DFC scheme for a refrigeration system in [12], and presented an anti-windup modification for the scheme in [13]. Among other things, gantry cranes differ from the refrigeration application by having a feedforward term in the existing control, as well as very different nonlinear dynamics, however. To illustrate the versatility of the design method, this paper thus proposes a robust anti-sway DFC scheme for gantry cranes based on LMI optimization. The proposed method is applied to velocity control of the trolley in a gantry crane system such as the one shown in Fig. 1. Both set point and disturbance responses are examined with and

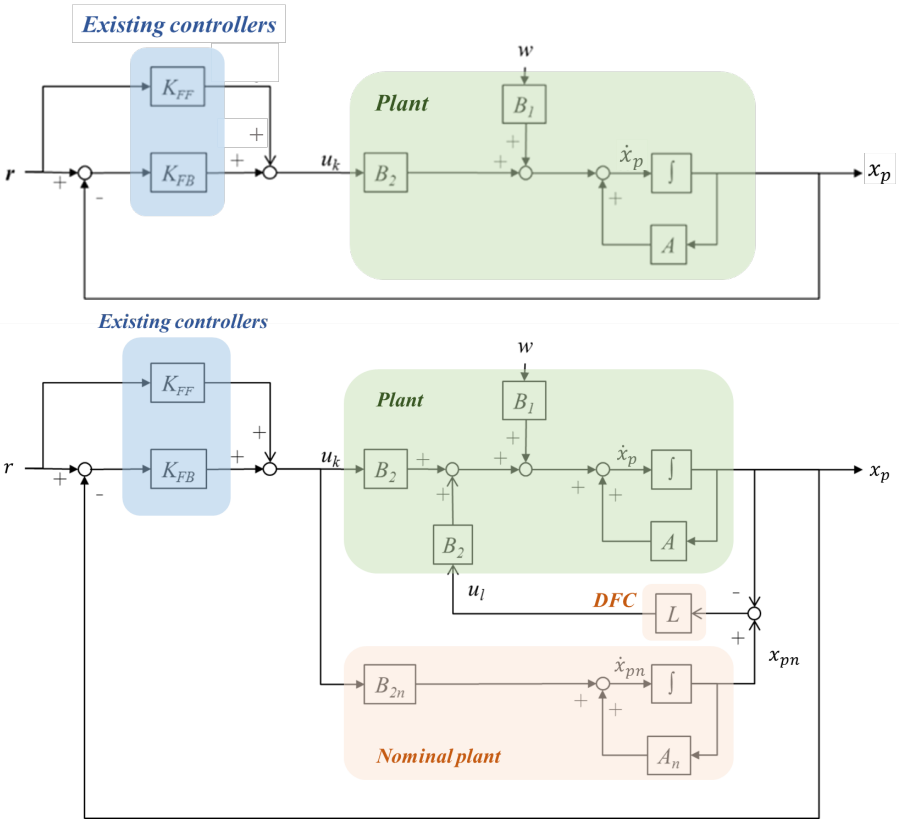

Fig. 2: Top: Block diagram of an existing crane control system. Bottom: The control system augmented with Disturbance Feedback Control.

without robust DFC through simulations on a non-linear model. Noticeable disturbance rejection performance improvements are observed, with no impact on the reference following capabilities of the existing controller.

The outline of the rest of the paper is as follows. Section 2 first briefly presents the nonlinear crane model used for simulation along with a linearized version used for conventional design. Next, Section 3 formulates the robust design problem and the LMIs used to solve it. After that, numerical examples of a gantry crane system are demonstrated in Section 4. Finally, discussion and conclusions are given in Section 5.

2 Problem Definition

2.1 Crane System Model

The crane system model considered in this work is taken from [1]. It is described by the nonlinear coupled differential equations

$$(m_T + m_L)\ddot{x}_T + m_L l\ddot{\theta}\cos\theta - m_L l\dot{\theta}^2 \sin\theta = F \tag{1}$$

$$\ddot{x}_T \cos\theta + l\ddot{\theta} + g\sin\theta = 0 \tag{2}$$

where m_T and m_L are masses of trolley and load, x_T is the trolley position along the supporting rail, θ is the angle of the load from vertical, l is the length of the suspension rope, g is the gravitational acceleration and F is the force applied to the trolley via the drive train (command input); see also Fig. 3.

For the sake of both the conventional design and the subsequent LMI-based DFC design, the model has to be linearized in an operating point. Assuming θ to be small, we can make the simplifications[1]

$$\sin\theta \approx \theta,\ \cos\theta \approx 1,\ \sin^2\theta \approx 0,\ \dot{\theta}^2 \approx 0 \text{ , and } x \approx l\theta$$

where x is the position of the load along the x_T-axis. These approximations yield the linear model[2]

$$m_T\ddot{x} = F + m_L g\theta \tag{3}$$

$$m_L(\ddot{x}_T + \ddot{x}) = -m_L g\theta, \tag{4}$$

which will be used for control design.

The motor force to the trolley F is given by a inverter, which regulates the trolley speed:

$$F = G_{asr}(u_T - \dot{x}_T), \tag{5}$$

where G_{asr} is the Auto Speed Regulator (ASR) gain, u_T is the reference of trolley speed, and $\dot{x}_T$ is the trolley speed.

Equations (3)–(5) are combined into the LTI description

$$\dot{x}_p = Ax_p + B_2 u_T,$$

where $x_p = (\dot{x}_T \ \ \dot{x} \ \ x_T \ \ x)^{\mathrm{T}}$ is the state vector, and

$$A = \begin{pmatrix} \frac{-G_{ASR}}{m_T} & 0 & 0 & \frac{g}{l}(\frac{m_L}{m_T}) \\ \frac{G_{ASR}}{m_T} & 0 & 0 & \frac{-g}{l}(\frac{m_L}{m_T}+1) \\ 1 & 0 & 0 & 0 \\ 0 & 1 & 0 & 0 \end{pmatrix}, \tag{6}$$

[1] Corrigendum corrected in the simplifications compared to original publication

[2] Corrigendum corrected in (4) compared to original publication

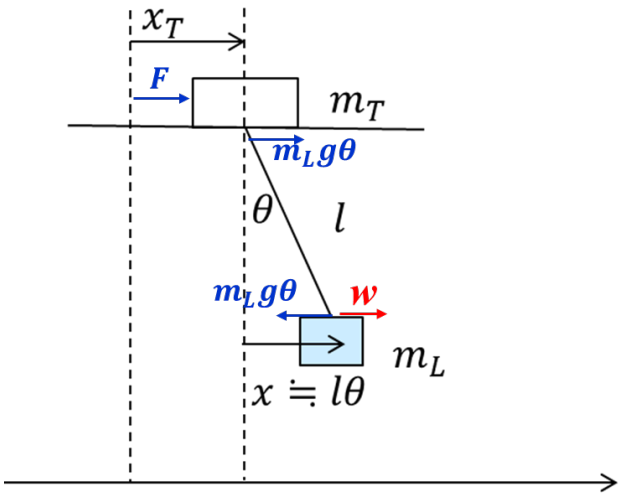

Fig. 3: A crane model for control design.

$$B_2 = \begin{pmatrix} \frac{G_{ASR}}{m_T} \\ \frac{-G_{ASR}}{m_T} \\ 0 \\ 0 \end{pmatrix} \tag{7}$$

are the system dynamics and input matrices, respectively.

2.2 Existing controller

The feedforward controller K_{FF} is designed by reference data set based on the oscillation cycle of hoisting loads. The data set of acceleration and deceleration was obtained from measurements of the trolley speed carried out on an actual gantry crane [14]. A reference trajectory for the trolley velocity $\dot{x_T}$ was designed to avoid oscillations in the load to the greatest degree possible. The rest of the state variable trajectories, i.e., trolley position x_T, load position $x = l\theta$, and horizontal load velocity $\dot{x}$, are calculated with control input data $u_T = x_T$.

The state feedback control K_{FB} is defined as

$$u_k = K_{FB} x_p, \tag{8}$$

where $K_{FB} \in \mathbb{R}^{m \times n}$ is a standard state feedback gain matrix, in this case designed via pole placement.

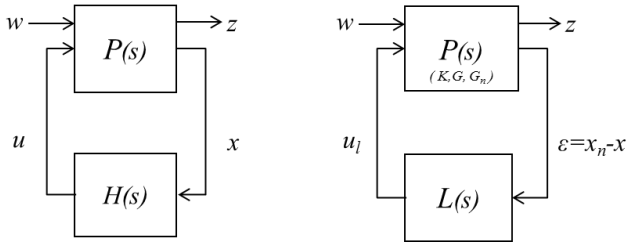

Fig. 4: Closed-loop setup for design of an H_∞ controller $H(s)$ (Left), and the corresponding setup for design of DFC $L(s)$ (Right).

3 Disturbance Feedback Control design

This section presents a robust DFC design method for state feedback control using LMI optimization.

The bottom diagram in Fig. 2 shows the closed-loop system with DFC, where r is the reference input, $u_T = u_k + u_l$ is the control input, w is the disturbance, B_1 is a gain matrix for w, A and B_2 are matrices of the plant model. The existing controller is specified by a feedforward term K_{FF} and a feedback term K_{FB}. The DFC comprises a nominal plant model specified by parameter matrices A_n and B_{2n} along with the disturbance feedback L. The true states of the plant are denoted x_p, while x_{pn} contains the state values of the nominal plant.

Fig. 4 shows a general closed-loop system in a two input, two output formulation (left) and the closed-loop DFC design configuration (right). As per usual, the design consists of choosing L such that the transfer function T from w to z, where z is the output for evaluating the performance of the controlled systems, becomes small in some sense. We assume that K_{FF} and K_{FB} are fixed; that is, the existing controller is considered as part of the plant P. Thus, P includes the true plant G, the nominal model G_n, and the existing controller K in the robust DFC design setup.

3.1 Parametric Uncertainty Model

To achieve a robust design, parametric uncertainties in the crane system model must be considered. Let the true plant be

$$\dot{x}_p = Ax_p + B_2 u_T, \tag{9}$$

with the plant parameters $A \in \mathbb{R}^{n\times n}$, $B \in \mathbb{R}^{n\times m}$ being affected by parametric uncertainties of the form [15])

$$A = A_n + \sum_{i=1}^{p} \delta_{a,i} A_i, \quad \delta_{a,i} \in [-1, +1]^p. \tag{10}$$

Here, A_n is the nominal state space representation, while $\delta_a = (\delta_{a,1}, \ldots, \delta_{a,p})$ are unknown vectors multiplied by known (constant) matrices A_i that express the ensemble of all uncertain quantities in the model. The design will have to ensure stability and performance for all possible values of the unknown parameters $\delta_{a,i}$.

The Disturbance Feedback Controller (DFC) is chosen as

$$u_l = L\epsilon, \tag{11}$$

where $L \in \mathbb{R}^{m\times n}$ is the disturbance feedback gains, $\epsilon = x_{pn} - x_p$, and $x_{pn} = \begin{pmatrix} \dot{x}_{Tn} & \dot{x}_n & x_{Tn} & x_n \end{pmatrix}^{\mathrm{T}} \in \mathbb{R}^{n\times 1}$ is the state vector of the nominal plant model.

The extended state space representation of the overall system can be written as follows;

$$\begin{aligned} \dot{x}_{pp} &= A_{pp} x_{pp} + B_{pp1} w + B_{pp2} u_l \\ z &= C_z x_{pp} + D_z u_l \end{aligned} \tag{12}$$

where

$$\begin{aligned} x_{pp} &= \begin{pmatrix} \dot{x}_T & \dot{x} & x_T & x & \dot{x}_{Tn} & \dot{x}_n & x_{Tn} & x_n \end{pmatrix}^{\mathrm{T}}, \\ A_{pp} &= \begin{pmatrix} A_\delta - B_2 K_{FB} & 0 \\ 0 & A_n - B_2 K_{FB} \end{pmatrix}, \\ B_{pp1} &= \begin{pmatrix} B_1 \\ 0 \end{pmatrix}, B_{pp2} = \begin{pmatrix} B_2 \\ 0 \end{pmatrix}, \\ C_z &= \begin{pmatrix} -I & 0 \end{pmatrix}, D_z = 0, \end{aligned}$$

and w is an input disturbance, and A_δ can be any extremal value of A in (6).

The closed loop transfer function T from w to z is computed as follows:

$$\begin{aligned} \dot{x}_{pp} &= \mathcal{A}_\delta x_{pp} + \mathcal{B} w \\ z &= \mathcal{C} x_{pp} + \mathcal{D} w, \end{aligned} \tag{13}$$

where

$$\left(\begin{array}{c|c} \mathcal{A}_\delta & \mathcal{B} \\ \hline \mathcal{C} & \mathcal{D}, \end{array}\right) =$$

$$\left(\begin{array}{cc|c} A_\delta - B_2 K_{FB} - B_2 L & B_2 L & B_1 \\ 0 & A_n - B_2 K_{FB} & 0 \\ \hline -I & 0 & 0 \end{array}\right).$$

3.2 Optimization Problem of robust DFC Design

The optimization problem of robust DFC design is given as follows[3]:

$$\underset{X_1,X_2,Y,W}{\text{minimize}} \quad \gamma, \tag{14}$$

$$\text{subject to;} \tag{15}$$

$$\begin{pmatrix} \mathcal{A}_\delta{}^{\mathrm{T}}\mathcal{X} + \mathcal{X}\mathcal{A}_\delta & \mathcal{B} & \mathcal{X}\mathcal{C}^{\mathrm{T}} \\ \mathcal{B}^{\mathrm{T}} & -\gamma I & \mathcal{D}^{\mathrm{T}} \\ \mathcal{C}\mathcal{X} & \mathcal{D} & -\gamma I \end{pmatrix} < 0,$$

$$\mathcal{X} = \begin{pmatrix} X_1 & 0 \\ 0 & X_2 \end{pmatrix}, \quad \mathcal{X} > 0, \quad \gamma > 0,$$

$$\begin{pmatrix} X_1 & Y \\ Y & \mu^2 I \end{pmatrix} > 0, \begin{pmatrix} X_2 & W \\ W & \mu^2 I \end{pmatrix} > 0,$$

where $Y := LX_1$ and $W := LX_2$, and μ is the upper limit of the control signal, i.e., the trolley velocity. In the above, the subscript-δ notation should be understood as requiring the LMIs to be satisfied for all extremal points of δ_a as defined in (6). That is, the LMIs must be satisfied everywhere on the convex hull defined by the permissible values of the uncertainties, implying that one LMI has to be solved for every vertex of the hypercube $\delta_a \in [-1, 1]^p$ to yield one common $\mathcal{X}$.

4 Numerical Examples

This section demonstrates the robust DFC design for an example gantry crane system.

4.1 Modeling of the Crane Systems

The nonlinear system (1)–(2) is simulated in Matlab using the built-in fixed-step `automatic solver selection` solver with the parameter values given in Table 1. The existing controller and the DFC are designed based on the linearized model with parameter matrices (6)-(7). The DFC is furthermore allowed knowledge about the permitted changes in the parameter l (shown in the table). The nominal model G_n is thus given by

$$A_n = \begin{pmatrix} -6.25 & 0 & 0 & 1.960 \\ 6.25 & 0 & 0 & -2.352 \\ 1.00 & 0 & 0 & 0 \\ 0 & 1.0 & 0 & 0 \end{pmatrix}, B_{2n} = \begin{pmatrix} 6.25 \\ -6.25 \\ 0 \\ 0 \end{pmatrix}$$

[3]Corrigendum corrected in (15) compared to original publication

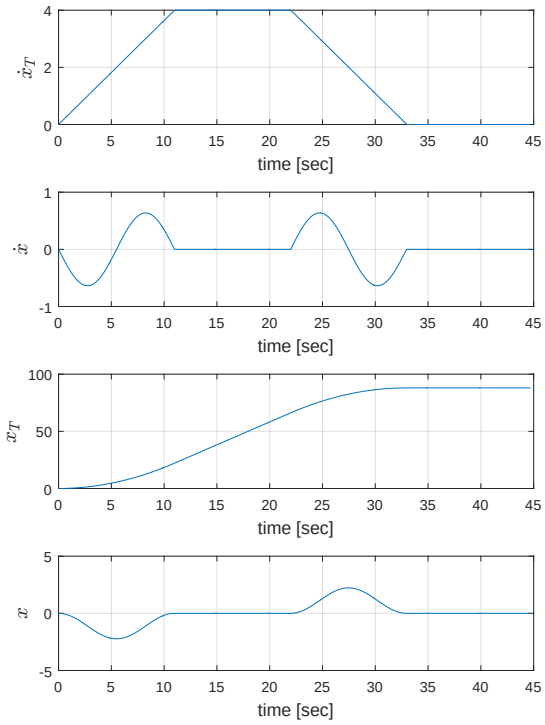

Fig. 5: A reference data set r for state $\dot{x}_T$, $\dot{x}$, x_T, and x ($x := \theta l$).

where A_n is the nominal model with rope length set to 25 m.

Fig. 5 shows the reference data set r for state $\dot{x}_T$, $\dot{x}$, x_T, and x. This data set is created in advance according to the following rules:

- The acceleration/deceleration of the trolley should be piecewise constant.
- The trolley position profile must match the fundamental load oscillation period.
- The angle θ and $\dot{\theta}$ should be zero when the acceleration and deceleration phases are finished.

Table 1: Parameter values of the crane system model.

Parameter	Value	Unit
m_T	10×10^3	kg
m_L	50×10^3	kg
l	[5, 45]	m
g	9.8	m/s^2
G_{asr}	62.5	-

The state feedback controller K_{FB} is designed by standard pole placement[4]:

$$K_{FB} = \begin{pmatrix} 3.8708 & 3.5494 & 1.5625 & -0.6732 \end{pmatrix}. \tag{16}$$

4.2 Robust DFC Design

The optimal H_∞ performance achieved by solving the optimization problem in (11)-(15), was $\gamma = 0.5052$, and the robust DFC gain is obtained as follows,

$$L = \begin{pmatrix} 14.2388 & 11.9464 & 2.5123 & -10.7141 \end{pmatrix}. \tag{17}$$

The design may for example be analyzed in the frequency domain. Bode plots of T are shown in Fig. 6, where it is seen that the proposed design is able to achieve better disturbance attenuation for all state variables than the conventional control, especially for frequencies less than 20 [rad/sec].

4.3 Simulation Results

The system's response to position set point changes and disturbances are then examined to compare the conventional control and proposed control. A summary of the simulation conditions are shown in Table 2.

Fig. 7 and Fig. 8 show simulation results of Fuji's existing control (left), and Fuji's control with robust DFC (right). The robust DFC did not disturb the original control during the set point change, and thus $\dot{x}_T$, $\dot{x}$, x_T, and x, are almost identical for both control methods for the first minute. On the other hand, as can be seen, the robust DFC went into action to attenuate the load sway when an impulse force was applied to the load. Impulse disturbances could for instance represent sudden gusts of wind or collisions during the operation of the gantry crane system.

The simulation in case 3, which has the shortest rope length with l=5m, exhibits the worst sway for both control methods. Here, the proposed method

[4]Corrigendum corrected in (16) compared to original publication

Table 2: Simulation conditions.

Item	Value	Unit
Sampling time	10^{-3}	s
Set point of trolley	88	m
Upper limit of trolley velocity	6.0	m/s
Simulation time	100	s
Time of impulse disturbance	60	s
Pulse width of disturbance	2	s
Pulse amplitude of disturbance	2×10^5	N

Table 3: Simulation results of the disturbance responses.

Item	Conventional method $(K_{FF} + K_{FB})$	Proposed method $(K_{FF} + K_{FB} + DFC)$
Maximum angle	0.68 rad	0.64 rad
Minimum angle	-0.16 rad	-0.12 rad
Maximum settling time	89.49 s	88.27 s
Minimum settling time	66.12 s	64.04 s

shows noticeably better performance than the conventional method, but in fact one can notice better attenuation in all three cases. Table 3 shows evaluation values in simulation results of the disturbance responses. The proposed method improved the maximum and minimum load angle θ by 0.04 and 0.08 radians, respectively, which means DFC decreased the sway by 4.58 degrees in total. In addition, the settling time was improved by between 1.22 seconds (case 2, $l = 45$m) and 2.07 seconds (case 3, $l = 5$m). As a result, the proposed method demonstrated the improvement of anti-sway control when an impulse disturbance is applied. Also, while 4.6 degrees may not sound like much, it is worth noting that the simulation considers a 50-ton load.

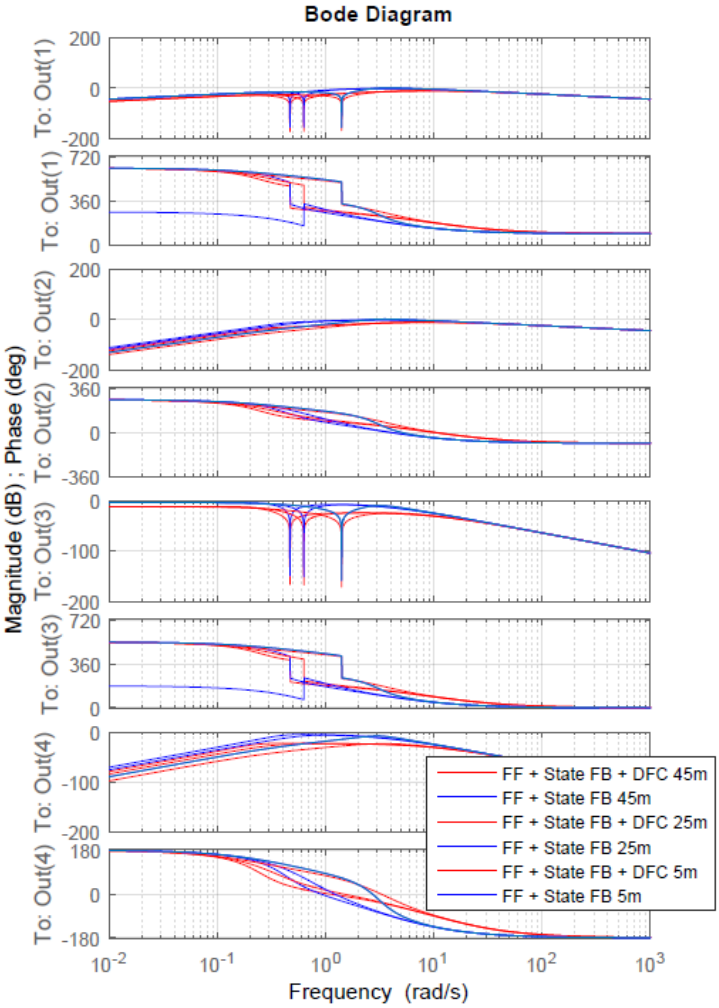

Fig. 6: Bode plots of closed loop system transfer function from w to z.

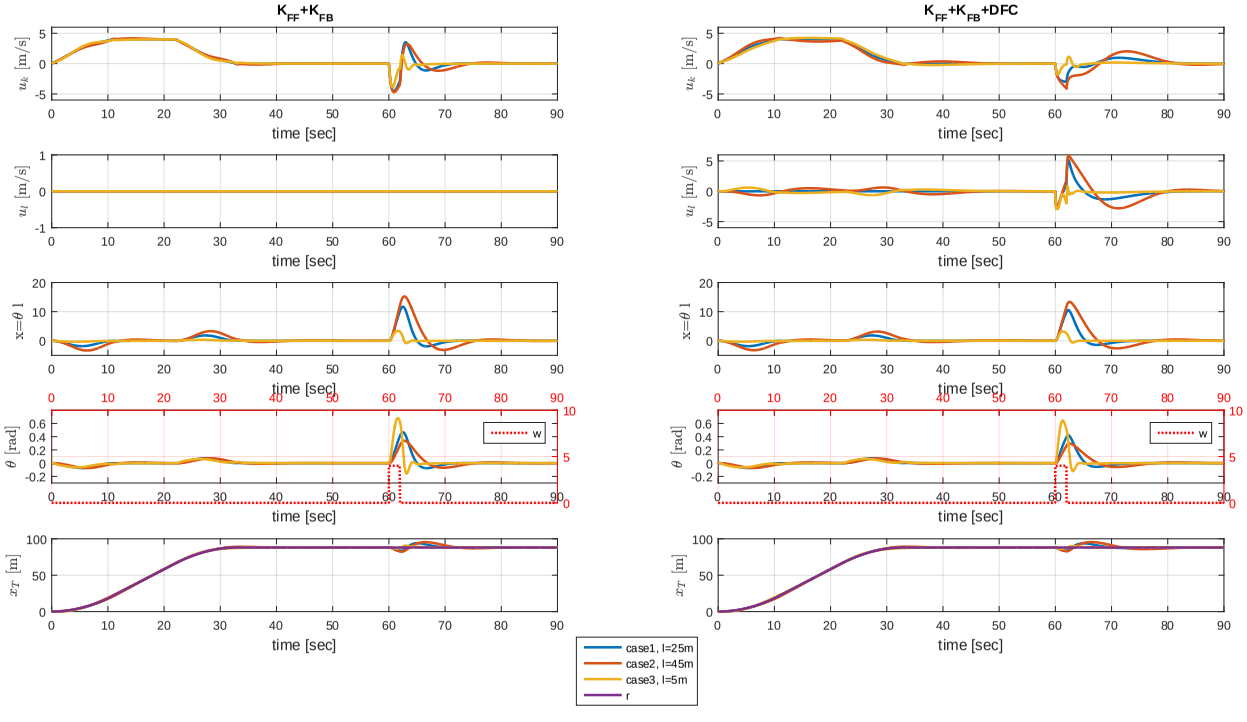

Fig. 7: Simulation results of Fuji's conventional control (left), and Fuji's control with robust DFC (right).

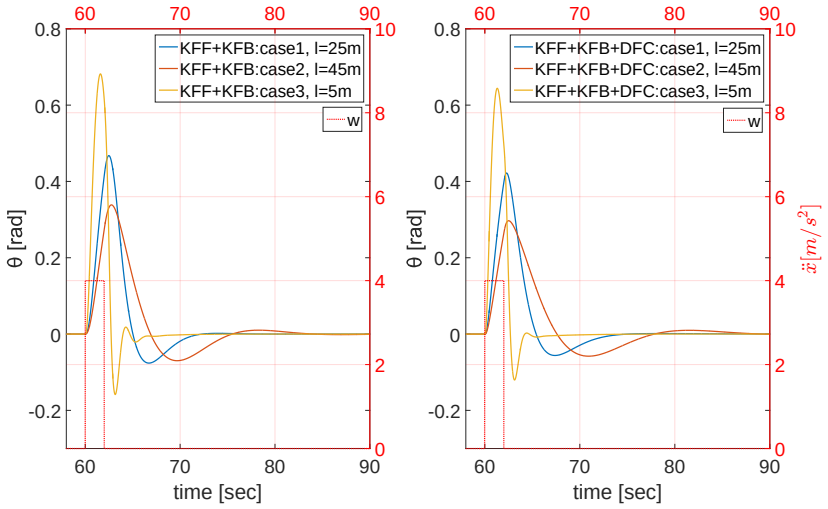

Fig. 8: Zoom on the sway angle in the disturbance responses.[5]

5 Discussion and Conclusions

This paper proposed an anti-sway control design for crane systems based on robust Disturbance Feedback Control (DFC). The robust DFC design is formulated in such a way that it can be added on to existing conventional control loops without affecting feedforward positioning profiles. The design is made robust by way of LMI optimization; assuming the optimization problem can be solved, the solution is guaranteed to respect robust performance and input constraints. The design method was tested in simulation against a realistic nonlinear gantry crane system model. The conventionally designed system response was left unaffected during a position set point change, whereas the DFC was able to attenuate an impulse disturbance response better than the conventional feedback control, thus exhibiting better anti-sway control performance.

In future work, we will attempt to verify the design on a laboratory-scale gantry crane setup using Hardware In the Loop (HIL) simulation and Programmable Logic Controllers (PLCs) under more realistic circumstances.

References

[1] J. Ackermann, *Robust Control The Parameter Space Approach.* Springer, 2002.

[5] The font size is enlarged in this figure compared to original publication

[2] M. Ahmad, R. Raja Ismail, M. Ramli, N. Abd Ghani, and N. Hambali, "Investigations of feed-forward techniques for anti-sway control of 3-d gantry crane system," in *Proc. 2009 IEEE Symposium on Industrial Electronics & Applications*, Kuala Lumpur, Malaysia, Oct. 2009, pp. 265–270.

[3] H. I. Jaafar, Z. Mohamed, A. F. Z. Abidin, and Z. A. Ghani, "Pso-tuned pid controller for a nonlinear gantry crane system," in *Proc. 2012 IEEE International Conference on Control System, Computing and Engineering*, Penang, Malaysia, Mar. 2012, pp. 515–519.

[4] H. Sano, K. Ohishi, T. Kaneko, and H. Mine, "Anti-sway crane control based on dual state observer with sensor-delay correction," in *Proc. Advanced Motion Control, 2010 11th IEEE International Workshop*, Niigata, Japan, March 2010, pp. 679 – 684.

[5] T. D. Son, G. Pipeleers, and J. Swevers, "Experimental validation of robust iterative learning control on an overhead crane test setup," in *Proc. IFAC 2014*, Cape Town, Aug. 2014, pp. 5981 – 5986.

[6] M. Z. M. Tumari, M. S. Saealal, M. R. Ghazali, and Y. A. Wahab, "H∞ controller with graphical lmi region profile for gantry crane system," in *Proc. SCIS-ISIS 2012*, Kobe, Japan„ Nov. 2012, pp. 1398 – 1402.

[7] K. R. Lee, E. T. Jeung, and H. B. Park, "Robust fuzzy H∞ control for uncertain nonlinear systems via state feedback: an LMI approach," *Fuzzy Sets and Systems*, vol. 120, pp. 123–134, 2001.

[8] J. Stoustrup, "Plug Play Control: Control Technology towards new Challenges," *European Journal of Control*, vol. 15, no. 3-4, pp. 311–330, 2009.

[9] Fuji Electric Co., Ltd. (1981) Fuji electric journal 54, (1), pp.33 in industry application, *in Japanese*,. [Online]. Available: http://www.fujielectric.co.jp/company/jihou_archives/pdf/54-01/FEJ-54-01-024-1981.pdf

[10] D. E. Rivera, M. Morari, and S. Skogestad, "Internal model control: PID controller design," *Industrial & engineering chemistry process design and development*, vol. 25, no. 1, pp. 252–265, 1986.

[11] T. Hayashi, *A gantry crane system.* [photograph], (Hayashi's own private collection), 2015.

[12] F. Kawai, K. Vinther, P. Anderson, and J. D. Bendtsen, "Mimo robust disturbance feedback control for refrigeration systems via an lmi approach," in *Proc. IFAC 2017*, Toulouse, Jul. 2017, pp. 14 525 – 14 532.

[13] Kawai, Fukiko and Vinther, Kasper and Anderson, Palle and Bendtsen, Jan Dimon, "Robust and anti-windup disturbance feedback control for

water chiller systems," in *Proc. 2017 IEEE Conference on Control Technology and Applications (CCTA2017)*, Hawaii, United States, Aug. 2017, pp. 1472 – 1479.

[14] T. MIYOSHI, K. TERASHIMA, and M. MORITA, "Study of Feedforward Control Input without Residual Vibration for the Time-Variant Vibration Mechanism and Its Application to the Crane System," *Transactions of the Japan Society of Mechanical Engineers Series C*, vol. 64, no. 624, pp. 2859–2866, 1998.

[15] Carsten Scherer and Siep Weiland. (2004) Linear matrix inequalities in control. [Online]. Available: http://www.dcsc.tudelft.nl/~cscherer/lmi/notes05.pdf

Paper F

Robustness against Uncertainties in Frequency Domain for Crane Control Systems Designed by Polytopic Approach

Fukiko Kawai, Palle Andersen, and Jan D. Bendtsen

The paper has been published in the
SICE Annual Conference 2018 (SICE 2018).

The layout has been revised.

Abstract

This paper examines additional model uncertainties in frequency domain for robust Disturbance Feedback Control (DFC) which was designed with parametric uncertainties for crane control systems. A gantry crane model is represented by state space model with parametric uncertainties. Robust DFC is solved by Linear Matrix Inequality (LMI) optimization in order to minimize the sway angle of the load against external disturbance. Robust stability of the robust DFC in frequency domain is analysed in order to verify the robustness against uncertainties in frequency domain. The results of analysis shows that the proposed method can cut off the uncertainties in high frequency domain.

1 Introduction

Traditionally, gantry crane systems have been controlled by means of feedforward control, taking the limited motor torque and constraints of trolley speed into account [1, 2]. Feedback control is also necessary to remove errors between references and measurement values, which is typically achieved by PID control of the gantry crane trolley [3].

Over the years, Fuji Electric (Fuji) has developed various anti-sway control schemes for crane systems, amongst others an observer based control scheme [4]. Subsequently, the anti-sway control scheme was further improved to combine feed forward control and state feedback control, and applied in commercial gantry cranes as shown in Fig. 1. This controller shows sufficient performance when tracking control is examined, however, it could improve the stability and performance if the robustness against external uncertainties (disturbances) and internal uncertainties (perturbations of model parameters) is taken into account.

Robust control scheme for crane systems is proposed, and an experimental validation of robust iterative learning control is investigated in [5]. In addition, H_∞ control via LMI approach for crane systems are proposed in [6], and robust fuzzy H_∞ control for nonlinear systems are presented with state feedback via LMI in [7].

These robust designs in previous studies are considered for one-degree-of freedom (1DOF) controllers for closed loop systems. Conventional or existing controller has to be replaced if the new controllers are introduced above. However, many industrial applications prefer to keep existing control because control specification and know-how are contained by customers and engineers with a lot of experience.

Disturbance Feedback Control (DFC), which can argument the existing control system, was originally developed as impact drop observer by Fuji in 1980 [8]. This control structure has an additional *feedback L* to compensate for

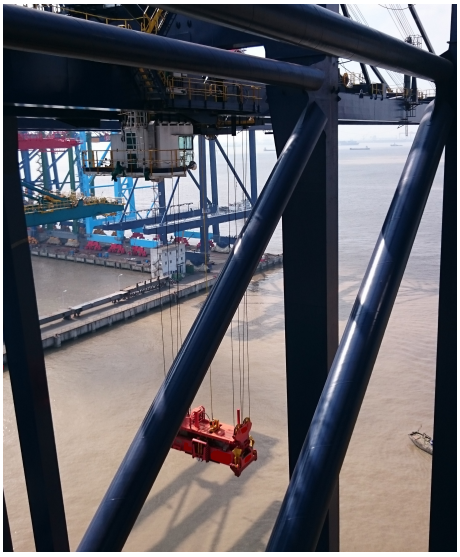

Fig. 1: A gantry crane system [10].

disturbance and model uncertainties as shown in Fig. 2. This control system can maintain existing control K and augment the system by DFC L. Note that DFC is not the same as Internal Model Control (IMC) [9] because DFC has two feedback signals, which means two degrees of freedom (2DOF). On the other hand, IMC has only one feedback signal, which will be zero when there is no modeling error.

In a previous study, we proposed a robust DFC for a refrigeration system in [11], and presented the relevant works about anti windup design for the robust DFC in [12]. The robust DFC improved the performance compared to conventional control. Thus, there may be advantage for crane applications to maintain conventional control and augment the system by DFC L instead of replace the entire control design. For these reasons, this paper proposes a robust anti-sway DFC scheme based on LMI optimization.

The proposed method is applied in velocity control of the trolley for the gantry crane systems as shown in Fig. 1, and the conventional control scheme is augmented by proposed robust DFC, and both set point and disturbance responses are examined with or without robust DFC through simulations.

The rest of the paper firstly describes the problem definition, and crane system model including parametric uncertainty model is considered. Then proposed method and conventional method are explained in Section 2. Next, Section 3 formulates the LMIs used for optimization of the robust DFC design for crane systems. After that, numerical examples of a gantry crane system

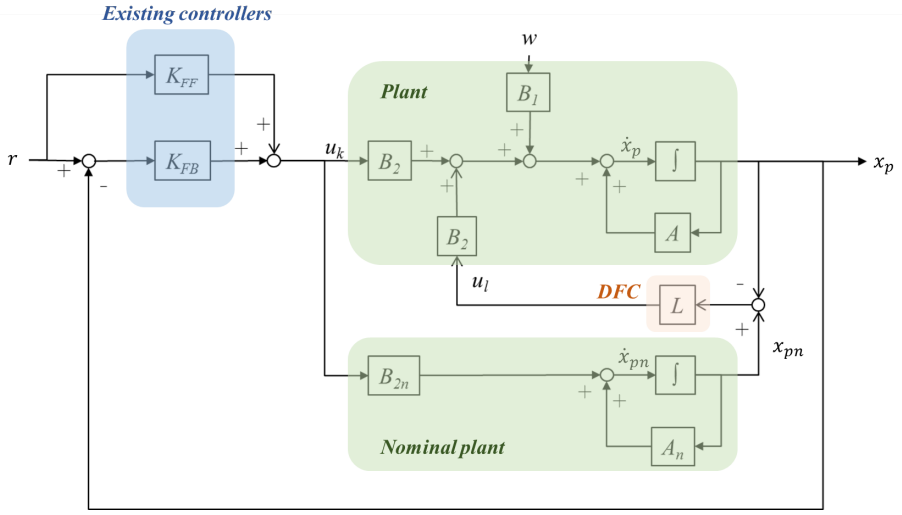

Fig. 2: Block diagrams of a crane control system with disturbance feedback control.

are demonstrated in Section 4. Finally, discussion and conclusions are given in Section 5.

2 Problem Definition

2.1 Crane System Model

Crane system model is given by a principle of the pendulum as shown in Fig. 3 [1].

$$m_T\ddot{x} = F + m_L g\theta \tag{1}$$

$$m_L(\ddot{x}_T + \ddot{x}) = -m_L g\theta, \tag{2}$$

which will be used for control design.

where m_T is the trolley mass, m_L is the load mass, F is the force exerted on the trolley by the drive train, g is the gravitational acceleration, θ is the angle of the suspension rope from vertical, l is the rope length, and x_T is the position of trolley. Assuming θ to be small, we can make the linearizing simplifications $x \approx l\theta$ and $\sin\theta \approx \theta$.

The motor force to the trolley F is given by a inverter which regulates the trolley speed.

$$F = G_{asr}(u_T - \dot{x}_T), \tag{3}$$

[1] Corrigendum corrected in (1)-(2) compared to original publication

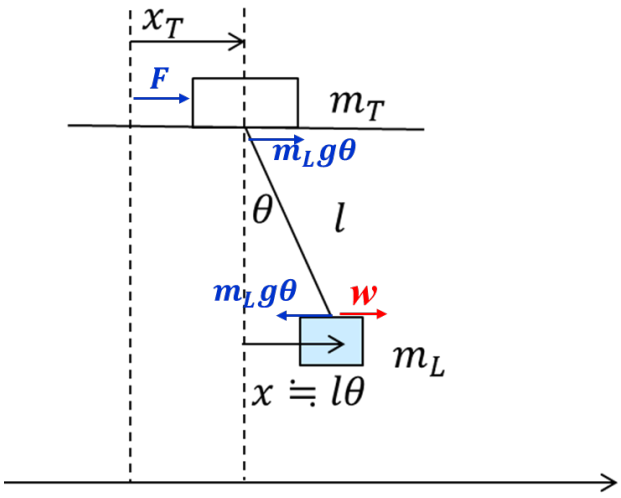

Fig. 3: A crane model for control design.

where G_{asr} is the Auto Speed Regulator (ASR) gain, u_T is the reference of trolley speed, and $\dot{x}_T$ is the state of trolley speed.

State space representation for by crane system model is yielded in (1) - (3).

$$\dot{x}_p = Ax_p + B_2 u_T,$$

where $x_p = (\dot{x}_T \;\; \dot{x} \;\; x_T \;\; x)^{\mathrm{T}} \in \mathbb{R}^{n\times 1}$ is the state vector, and

$$A = \begin{pmatrix} \frac{-G_{ASR}}{m_T} & 0 & 0 & \frac{g}{l}(\frac{m_L}{m_T}) \\ \frac{G_{ASR}}{m_T} & 0 & 0 & \frac{-g}{l}(\frac{m_L}{m_T}+1) \\ 1 & 0 & 0 & 0 \\ 0 & 1 & 0 & 0 \end{pmatrix} \tag{4}$$

$$B_2 = \begin{pmatrix} \frac{G_{ASR}}{m_T} \\ \frac{-G_{ASR}}{m_T} \\ 0 \\ 0 \end{pmatrix},$$

and $A \in \mathbb{R}^{n\times n}$, $B_2 \in \mathbb{R}^{n\times m}$.

2.2 Design Concepts for Disturbance Feedback Control

Fig. 2 shows a block diagram of a closed-loop system with DFC, where r is the reference input, $u_T = u_k + u_l$ is the control input, w is the disturbance, B_1

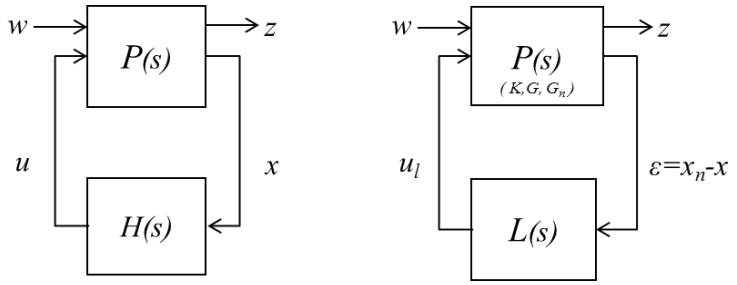

Fig. 4: A closed-loop system for design of an H_∞ controller $H(s)$ (Left), and a closed-loop system for design of DFC $L(s)$ (Right).

is a matrix for w, A and B_2 are matrices of the plant model, A_n and B_{2n} are matrices of the nominal plant model, K_{FF} is an existing feed forward controller, K_{FB} is an existing feedback controller, L is the disturbance feedback controller, x_p is the state values of the plant, x_{pn} is the state values of the nominal plant.

Fig. 4 shows a general closed-loop system with two input, two output formulation (left) and the closed-loop system for DFC (Right). In general, when designing controllers, the transfer function T from w to z, where z is the output for evaluating the performance of the controlled systems. Note that the motivation of the robust DFC design is to improve the existing system. We assume that the existing controller K, which is K_{FF} and K_{FB} in the crane application, is fixed. This means we can deal with K as a part of the plant P. Thus, P includes plant model G, nominal model G_n, and conventional controller K for the robust DFC design.

2.3 Parametric Uncertainty Model

Now parametric uncertainties of the crane system model is considered;

$$\dot{x}_p = Ax_p + B_2 u_T, \tag{5}$$

where $A \in \mathbb{R}^{n\times n}$, $B \in \mathbb{R}^{n\times m}$. The plant parameters are affected by parametric uncertainties [13]) expressed by

$$A = A_n + \sum_{i=1}^{p} \delta_{a,i} A_i, \quad \delta_{a,i} \in [-1, +1], \tag{6}$$

where $\delta_a = (\delta_{a,1}, \ldots, \delta_{a,p})$ are unknown vectors, which express the ensemble of all uncertainty quantities in a given dynamics, A_n is the nominal state space representation, and A_i describe the uncertainty.

2.4 Feed Forward Controller

The feed forward controller K_{FF} is designed by reference data set based on the oscillation cycle of hoisting loads. The data set of acceleration and deceleration for trolley speed is considered by [14]. State value of the trolley speed $\dot{x_T}$ is created in order to attenuate residual oscillation for the time-variant oscillation mechanism. The rest of data set for state variables, position of trolley x_T, $x = l\theta$ is a rope length l times angle θ, and $\dot{x}$, are calculated with control input data $u_T = x_T$.

2.5 State Feedback Controller

The state feedback control for K_{FB} is defined as

$$u_k = K_{FB} x_p, \tag{7}$$

where $K_{FB} \in \mathbb{R}^{m \times n}$ is the state feedback gains, and $x_p = (\dot{x_T} \;\; \dot{x} \;\; x_T \;\; x)^{\mathrm{T}} \in \mathbb{R}^{n \times 1}$ is the state vector.

2.6 Disturbance Feedback Controller

The Disturbance Feedback Controller (DFC) is chosen as

$$u_l = L\epsilon, \tag{8}$$

where $L \in \mathbb{R}^{m \times n}$ is the disturbance feedback gains, $\epsilon = x_{pn} - x_p$, and $x_{pn} = \begin{pmatrix} \dot{x}_{Tn} & \dot{x}_n & x_{Tn} & x_n \end{pmatrix}^{\mathrm{T}} \in \mathbb{R}^{n \times 1}$ is the state vector of nominal plant model.

3 Disturbance Feedback Control Design

This section presents a robust DFC design method for state feedback control using an LMI optimization. Firstly, the closed loop system $T_{zw}(s)$ is obtained by the extended state space representation. Next, two constraints are introduced to design the robust DFC. Here, we make use of the Bounded Real Lemma (BRL) and the input constraints [15]. The BRL is applied to guarantee a robust performance, and the input constraint is introduced to consider limitation of the control devices.

3.1 The Extended State Space Representation for Robust DFC

The extended state space representation of the overall system can be written as follows;

$$\dot{x}_{pp} = A_{pp} x_{pp} + B_{pp1} w + B_{pp2} u_l \tag{9}$$

$$
\begin{aligned}
z &= C_z x_{pp} + D_z u_l \\
\text{where} & \\
x_{pp} &= \left(\begin{array}{cccccccc} \dot{x}_T & \dot{x} & x_T & x & \dot{x}_{Tn} & \dot{x}_n & x_{Tn} & x_n \end{array} \right)^{\mathrm{T}}, \\
A_{pp} &= \left(\begin{array}{cc} A_\delta - B_2 K_{FB} & 0 \\ 0 & A_n - B_2 K_{FB} \end{array} \right), \\
B_{pp1} &= \left(\begin{array}{c} B_1 \\ 0 \end{array} \right), B_{pp2} = \left(\begin{array}{c} B_2 \\ 0 \end{array} \right), \\
C_z &= \left(\begin{array}{cc} -I & 0 \end{array} \right), D_z = 0,
\end{aligned}
$$

and w is an input disturbance, and A_δ can be any extremal value of A in (6). The closed loop transfer function T from w to z is computed as follows:

$$
\begin{aligned}
\dot{x}_{pp} &= \mathcal{A}_\delta x_{pp} + \mathcal{B} w \\
z &= \mathcal{C} x_{pp} + \mathcal{D} w,
\end{aligned}
\tag{10}
$$

where

$$
\left(\begin{array}{c|c} \mathcal{A}_\delta & \mathcal{B} \\ \hline \mathcal{C} & \mathcal{D}, \end{array} \right) =
\left(\begin{array}{cc|c} A_\delta - B_2 K_{FB} - B_2 L & B_2 L & B_1 \\ 0 & A_n - B_2 K_{FB} & 0 \\ \hline -I & 0 & 0 \end{array} \right).
$$

3.2 Optimization Problem of robust DFC Design

The optimization problem of robust DFC design is given as follows:

$$
\underset{X_1, X_2, Y, W}{\text{minimize}} \quad \gamma, \tag{11}
$$

$$
\text{subject to;} \tag{12}
$$

$$
\left(\begin{array}{ccc} \mathcal{A}_\delta{}^{\mathrm{T}} \mathcal{X} + \mathcal{X} \mathcal{A}_\delta & \mathcal{B} & \mathcal{X} \mathcal{C}^{\mathrm{T}} \\ \mathcal{B}^{\mathrm{T}} & -\gamma I & \mathcal{D}^{\mathrm{T}} \\ \mathcal{C} \mathcal{X} & \mathcal{D} & -\gamma I \end{array} \right) < 0,
$$

$$
\mathcal{X} = \left(\begin{array}{cc} X_1 & 0 \\ 0 & X_2 \end{array} \right), \quad \mathcal{X} > 0, \quad \gamma > 0,
$$

$$
\left(\begin{array}{cc} X_1 & Y \\ Y & \mu^2 I \end{array} \right) > 0, \left(\begin{array}{cc} X_2 & W \\ W & \mu^2 I \end{array} \right) > 0,
$$

where $Y := L X_{11}$ and $W := L X_{22}$, and μ is the upper limit of control output, which is the trolley speed. In the above, the subscript δ notation should be

understood as requiring the LMIs to be satisfied for all extremal points of δ_a as defined in (6). That is, the LMIs must be satisfied everywhere on the convex hull defined by the permissible values of the uncertainties; i.e., one LMI has to be solved for every vertex of the hypercube $\delta_a \in [-1, 1]^p$ to yield one common $\mathcal{X}$.

4 Numerical Examples

This section demonstrates the robust DFC design for gantry crane systems.

4.1 Modeling of the Crane Systems

Numerical model for crane system is obtained by parameter values in Table 1 and the state space equation in (2.1)-(6).

$$A_n = \begin{pmatrix} -6.2500 & 0 & 0 & 1.6333 \\ 6.2500 & 0 & 0 & -1.9600 \\ 1.0000 & 0 & 0 & 0 \\ 0 & 1.0 & 0 & 0 \end{pmatrix} \tag{13}$$

$$A_1 = \begin{pmatrix} 0 & 0 & 0 & -0.5444 \\ 0 & 0 & 0 & 0.6533 \\ 0 & 0 & 0 & 0 \\ 0 & 0 & 0 & 0 \end{pmatrix}$$

$$A_2 = \begin{pmatrix} 0 & 0 & 0 & 1.6333 \\ 0 & 0 & 0 & -1.9600 \\ 0 & 0 & 0 & 0 \\ 0 & 0 & 0 & 0 \end{pmatrix}$$

$$B_1 = \begin{pmatrix} 1 \\ 1 \\ 1 \\ 1 \end{pmatrix} B_{2n} = \begin{pmatrix} 6.2500 \\ -6.2500 \\ 0 \\ 0 \end{pmatrix},$$

where A_n is the nominal model with rope length set to 30 m, A_1 and A_2 are parametric uncertainties when rope length reaches the corner points 45 m and 15 m respectively, B_{2n} is the nominal matrix of B_2, and $B_2 = B_{2n}$ in this examples.

Fig. 5 shows a reference data set r for state $\dot{x}_T$, $\dot{x}$, x_T, and x, $(x := \theta l)$. This data set is created in advance, and designed by following policies:

- The speed variation of trolley is constant during acceleration and deceleration.

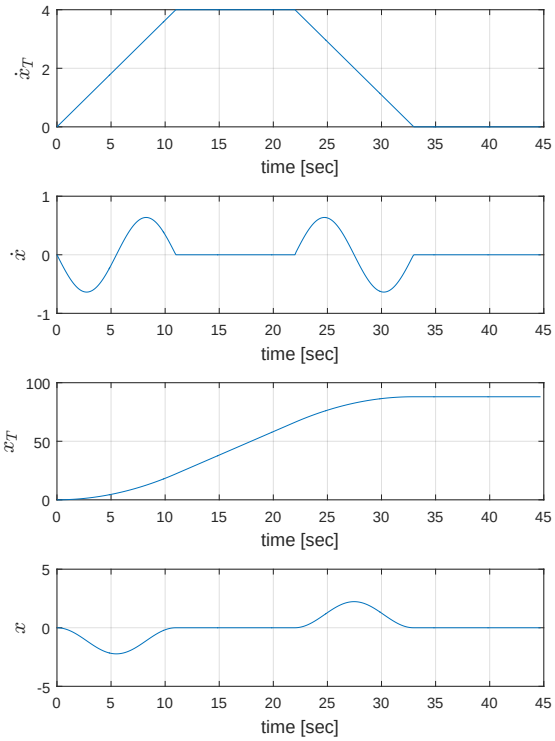

Fig. 5: A reference data set r for state $\dot{x}_T$, $\dot{x}$, x_T, and x ($x := \theta l$).

- The travelling plan is made by using period of the oscillation on load.
- The angle θ and $\dot{\theta}$ should be zero when the acceleration and deceleration are finished.

Note that the control signal from the feed forward control K_{FF} is equivalent to reference data of trolley speed, $x_{T,ref}$ on the top of the graphs at Fig. 5. Next, state feedback controller K_{FB} is designed by pole placement scheme.

$$K_{FB} = \begin{pmatrix} 4.1603 & 3.8579 & 1.5625 & -0.5320 \end{pmatrix}. \tag{14}$$

Table 1: Parameter values of the crane system model.

Parameter	Value	Unit
m_T	10	$ton\ (10^3kg)$
m_L	50	$ton\ (10^3kg)$
l	[15, 45]	m
g	9.8	m/s^2
G_{asr}	62.5	-

4.2 Robust DFC Design

The optimal H_∞ performance, solved by the optimization problem in (11)-(12), was $\gamma = 0.3864$, and the robust DFC is obtained as follows,

$$L = \begin{pmatrix} 8.3127 & 5.4399 & 1.9572 & -5.0353 \end{pmatrix}. \tag{15}$$

Now the result of robust DFC L is analysed in the frequency domain. Bode plots of T_{zw}, which is a transfer function from w to z in Fig. 4, are shown in Fig. 6. Proposed method can cut off the disturbance for all state variables better than conventional control, especially frequencies less than 30[rad/sec]. Fig. 7 shows enlarged figures of the sway angle on the disturbance responses with nonlinear system model. The simulation in case 3, which has the shortest rope length with l=15m, exhibits the worst sway in both control methods. More importantly, the proposed method shows better performance than conventional method in the all three case.

4.3 Verification of Robustness against Internal Uncertainty in Frequency Domain

Robust stability against internal uncertainties in frequency domain is considered for robust DFC L which was solved in 4.2. Multiplicative uncertainties Δ and its weight function W_u are added to the plant model set G which includes the parametric uncertainties in 2.3. Transfer function from $\tilde{u}$ to u in Fig. 8 is represented by

$$T_{\tilde{u}u} = -(LG_nK_{FB}G + LG + K_{FB}G) \tag{16}$$

where G is plant model set, G_n is nominal plant model represented by transfer function, K_{FB} is state feedback controller which is given in (14), and L is robust DFC which is solved in (15).

The model of weight function W_u is chosen as first order systems.

$$W_u = \kappa\frac{s+\beta}{s+\alpha} \tag{17}$$

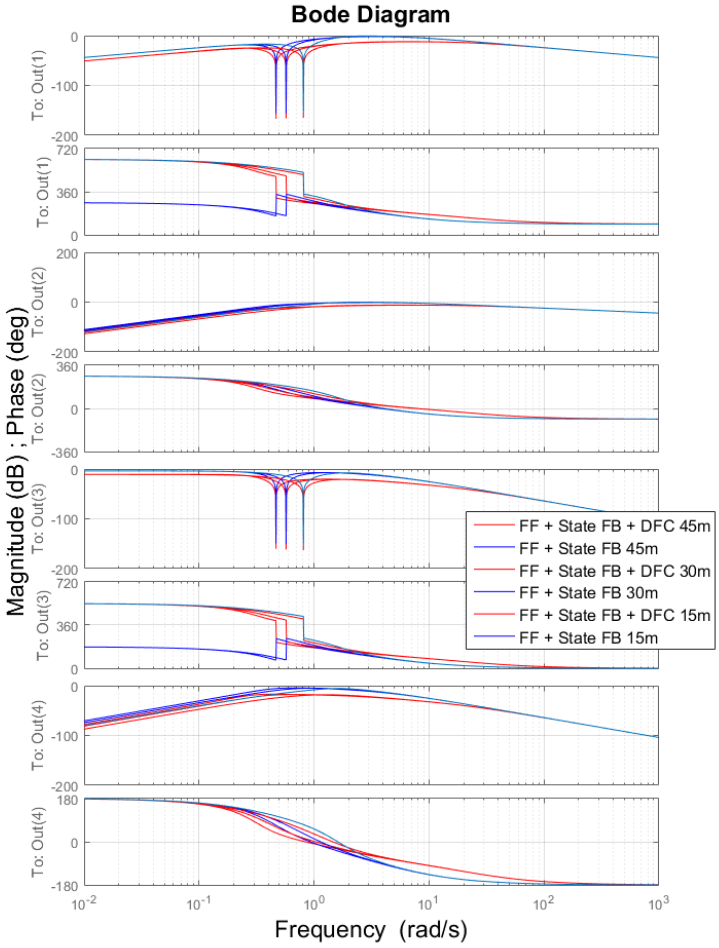

Fig. 6: Bode plots of a closed loop system T_{zw}.

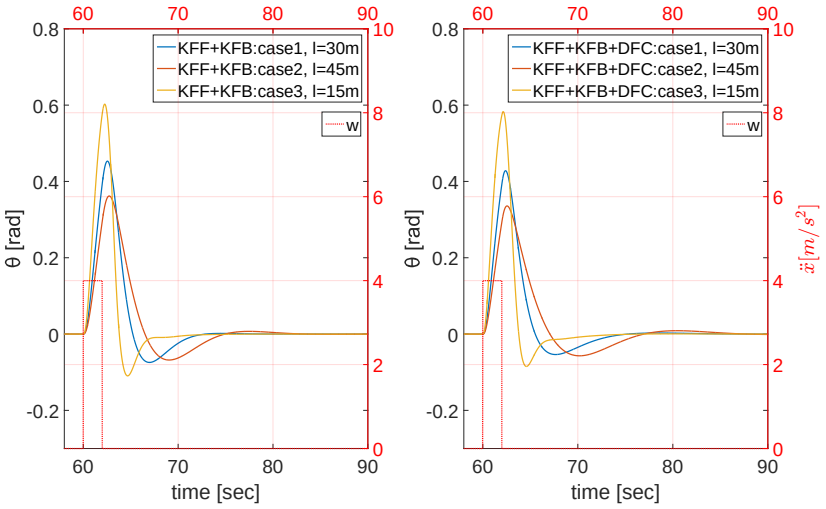

Fig. 7: Sway angle on the disturbance responses.

where κ, α, and β are tuning parameters in order to find the worst case of $|W_u||T_{\tilde{u}u}| < 1$

An example of the worst case of W_u is given with κ=2.27210523, α=1000, and β=0.0001. W_u gives magnitude more than 0 [dB] in the high frequency area 500-10000 [rad/sec]. The peak gain G_p = -0.975 [dB] and peak frequency f_p = 0.457 [rad/sec] respectively.

The figure shows that the optimized DFC L including parametric uncertainties can be robust against the high frequency domain.

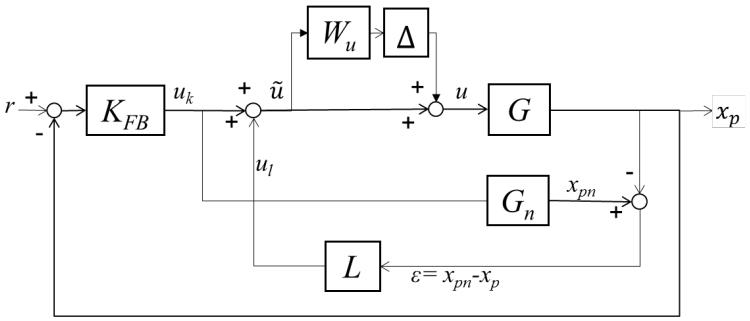

Fig. 8: Block diagrams of a crane control system with DFC, and multiplicative uncertainty $W_u\Delta$ is added to the plant set G.

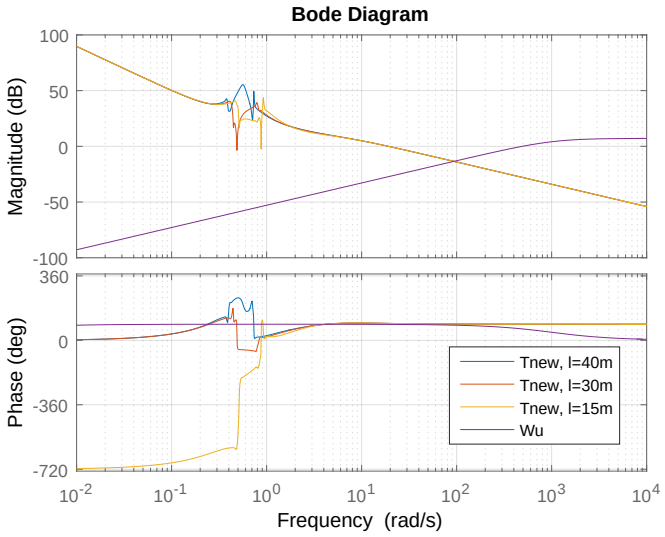

Fig. 9: Bode diagram of weight function W_u, and transfer function from $\tilde{u}$ to u, $T_{\tilde{u}u}$ with each corner points of parametric uncertainties.

5 Discussion and Conclusions

This paper examines additional model uncertainties in frequency domain for robust Disturbance Feedback Control (DFC) which was designed with parametric uncertainties for crane control systems. Robust stability of the robust DFC in frequency domain is analysed in order to verify the robustness against uncertainties in frequency domain. The results of analysis shows that the proposed method can cut off the uncertainties in high frequency domain. The simulation results demonstrate the effectiveness of the proposed design methods.

References

[1] J. Ackermann, *Robust Control The Parameter Space Approach*. Springer, 2002.

[2] M. Ahmad, R. Raja Ismail, M. Ramli, N. Abd Ghani, and N. Hambali, "Investigations of feed-forward techniques for anti-sway control of 3-d gantry crane system," in *Proc. 2009 IEEE Symposium on Industrial Electronics & Applications*, Kuala Lumpur, Malaysia, Oct. 2009, pp. 265–270.

[3] H. I. Jaafar, Z. Mohamed, A. F. Z. Abidin, and Z. A. Ghani, "Pso-tuned

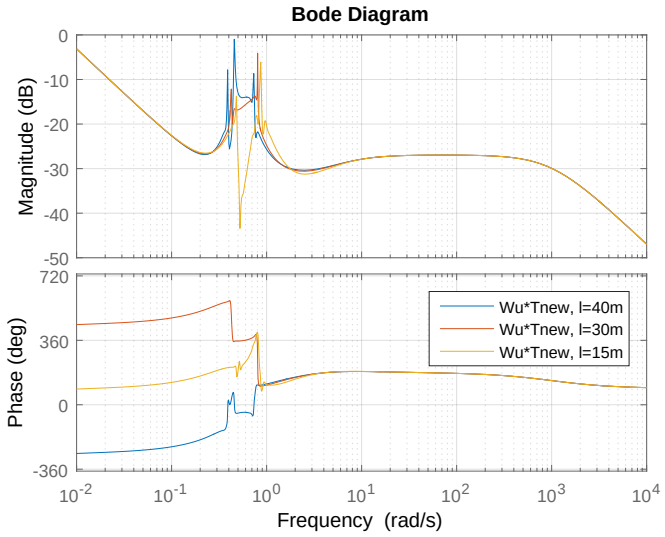

Fig. 10: Bode diagram of $W_u T_{\tilde{u}u}$ for verification of the robustness against additional frequency domain uncertainties.

pid controller for a nonlinear gantry crane system," in *Proc. 2012 IEEE International Conference on Control System, Computing and Engineering*, Penang, Malaysia, Mar. 2012, pp. 515–519.

[4] H. Sano, K. Ohishi, T. Kaneko, and H. Mine, "Anti-sway crane control based on dual state observer with sensor-delay correction," in *Proc. Advanced Motion Control, 2010 11th IEEE International Workshop*, Niigata, Japan, March 2010, pp. 679 – 684.

[5] T. D. Son, G. Pipeleers, and J. Swevers, "Experimental validation of robust iterative learning control on an overhead crane test setup," in *Proc. IFAC 2014*, Cape Town, Aug. 2014, pp. 5981 – 5986.

[6] M. Z. M. Tumari, M. S. Saealal, M. R. Ghazali, and Y. A. Wahab, "H∞ controller with graphical lmi region profile for gantry crane system," in *Proc. SCIS-ISIS 2012*, Kobe, Japan,, Nov. 2012, pp. 1398 – 1402.

[7] K. R. Lee, E. T. Jeung, and H. B. Park, "Robust fuzzy H∞ control for uncertain nonlinear systems via state feedback: an LMI approach," *Fuzzy Sets and Systems*, vol. 120, pp. 123–134, 2001.

[8] Fuji Electric Co., Ltd. (1981) Fuji electric journal 54, (1), pp.33 in industry application, *in Japanese*,. [Online]. Available: http://www.fujielectric.co.jp/company/jihou_archives/pdf/54-01/FEJ-54-01-024-1981.pdf

[9] D. E. Rivera, M. Morari, and S. Skogestad, "Internal model control: PID controller design," *Industrial & engineering chemistry process design and development*, vol. 25, no. 1, pp. 252–265, 1986.

[10] T. Hayashi, *A gantry crane system.* [photograph], (Hayashi's own private collection), 2015.

[11] F. Kawai, K. Vinther, P. Anderson, and J. D. Bendtsen, "Mimo robust disturbance feedback control for refrigeration systems via an lmi approach," in *Proc. IFAC 2017*, Toulouse, Jul. 2017, pp. 14 525 – 14 532.

[12] Kawai, Fukiko and Vinther, Kasper and Anderson, Palle and Bendtsen, Jan Dimon, "Robust and anti-windup disturbance feedback control for water chiller systems," in *Proc. 2017 IEEE Conference on Control Technology and Applications (CCTA2017)*, Hawaii, United States, Aug. 2017, pp. 1472 – 1479.

[13] Carsten Scherer and Siep Weiland. (2004) Linear matrix inequalities in control. [Online]. Available: http://www.dcsc.tudelft.nl/~cscherer/lmi/notes05.pdf

[14] T. MIYOSHI, K. TERASHIMA, and M. MORITA, "Study of Feedforward Control Input without Residual Vibration for the Time-Variant Vibration Mechanism and Its Application to the Crane System," *Transactions of the Japan Society of Mechanical Engineers Series C*, vol. 64, no. 624, pp. 2859–2866, 1998.

[15] S. Boyd, L. E. Ghaoui, E. Feron, and V. Balakrishnan, *Linear Matrix Inequalities in System and Control Theory.* Society for Industrial and Applied Mathematics (SIAM), 1994.

ISSN (online): 2446-1628
ISBN (online): 978-87-7210-321-1

AALBORG UNIVERSITY PRESS